THE UNIVERSITY OF MICHIGAN
COLLEGE OF LITERATURE, SCIENCE, AND THE ARTS
Department of Astronomy

Technical Note No. 2

ABUNDANCES OF ELEMENTS IN STARS AND NEBULAE

(The Abundance of Certain Elements in the Solar Atmosphere)

L. H. Aller

ORA Project 03719

under contract with:

AIR FORCE OFFICE OF SCIENTIFIC RESEARCH
AIR RESEARCH AND DEVELOPMENT COMMAND
CONTRACT NO. AF 49(638)-807
Washington, D. C.

administered through:

OFFICE OF RESEARCH ADMINISTRATION ANN ARBOR

June 1962

PREFACE

Studies of chemical compositions of stars, the sun, and gaseous nebulae are dependent on knowledge of basic atomic parameters such as collision cross-sections and transition probabilities. This report is concerned with application of the transition probabilities measured by C. Corliss at the National Bureau of Standards to the composition of the sun. Applications of these gf-values to stellar problems will be made in other reports in this series.

I am grateful to Dr. Corliss for sending me his results in advance of publication.

L. H. Aller
The University of Michigan Observatory

June 7, 1962

TABLE OF CONTENTS

LIST OF ILLUSTRATIONS

LIST OF ILLUSTRATIONS (Concluded)

ABSTRACT

The solar abundances of 21 elements (Na, Sc, Cu, Zn, Ga, Ge, Sr, Y, Zr, Nb, Mo, Ru, Rh, Pd, Ag, Cd, In, Sn, Sb, Ba, and Yb) are revised with the aid of new gf-values obtained by C. Corliss of the National Bureau of Standards. Some implications of the new measurements are discussed and it is emphasized that a comprehensive reconsideration of solar abundances should be undertaken, in which ions as well as neutral atoms and a new model solar atmosphere are used.

I. INTRODUCTION

One of the persistent problems of interest to geochemists and others concerned with the chemistry of meteorites and planets has been the original composition of the solar systems. It is generally accepted that the surface layers of the sun provide the best sample now available. The influence of thermal diffusion in modifying the chemical composition of the solar atmosphere may have been appreciable over long intervals of time,[1] but its exact amount is difficult to assess until we know more about the structure of the sub-photospheric layers of the solar envelope. In any event, the loss of heavier elements from the upper layers depends smoothly on the atomic number in the sense that the heavier the atom, the greater the amount of depletion.

Analysis of the chemical composition of the sun's atmosphere requires that we extract from the intensity (equivalent width) of a spectral line the abundance of the element acting to produce it. Now the intensity of an absorption line in the solar spectrum depends on a number of factors, only one of which is the abundance (see, for example Refs. 2,3,4,5,6, and 7). These other factors include (a) the transition probability of the line in question or Ladenburg f ; (b) the sources of line broadening (Doppler widening, natural damping, and collisional damping); and (c) the number of atoms in the right stage of excitation and ionization. (The latter depends on the stratification of the solar atmosphere; i.e., it is determined by the dependence of temperature and density with depth.)

The equivalent width of a line (defined as the energy removed from the continuous spectrum expressed in equivalent angstroms thereof), can be measured for weak as well as for strong lines in the solar spectrum. A comprehensive collection of reliable data has been given by workers at the Utrecht Observatory. The infrared region of the solar spectrum has been surveyed by Mohler[9] and by Mohler *et al.*[10] In addition, many individual observers have made measurements of particular lines in the solar spectrum.

II. THEORY

In Pecker's theory,[11] the equivalent width of a line at a particular point on the solar disk is given by [12,13,14]

$$\frac{W_{\mu,\lambda}}{\lambda} = \int_{-\infty}^{+\infty} \frac{M}{\mu} Z(x)\ \psi - \left(\frac{Y}{\mu}, a\right)\ g_{\lambda}^{\mu}(x)\ \left(1 - e^{-h\nu/kT}\right)\ dx \qquad (1)$$

At the center of the disk,

$$\mu = \cos\Theta = 1 \qquad (2)$$

Here M involves the abundance of the element in question, the factor $gf\lambda$, and certain known numerical factors. In the factor $gf\lambda$, g is the statistical weight of the lower level of the transition in question, f is the Ladenburg "f" or "oscillator strength," and λ, of course, is the wavelength of the line. We define

$$x = \log \tau_{o} \qquad (3)$$

where τ_{o} is the optical depth at the selected standard wavelength.

The factor Z(x) allows for the variation of ionization and thermal excitation with depth[15] ψ is Pecker's saturation function. It expresses the well-known phenomenon that a strong line is formed higher in the star's atmosphere than is a weaker line. The "weighting function" $g_{\lambda}(x)$ depends only on the structure of the atmosphere. It expresses the fact that for a weak line, different layers contribute different amounts to the line intensity. The last factor allows for the atimulated emissions (negative absorptions). The intensity of a weak line is given by

$$\frac{W_{\lambda}}{\lambda} = \int_{-\infty}^{+\infty} MZ(x)\ g_{\lambda}(x)\ \left(1 - e^{-h\nu/kT}\right)\ dx = ML_{\lambda} \qquad (4)$$

since $\psi = 1$. Let us define

$$\log C = \log gf\lambda + \Delta x\Theta_{o} + L_{\lambda} + \text{const.} \qquad (5)$$

where we set $\Theta_{o} = \frac{5040}{T_{o}} = 1.0$ for the sun. The constant is known. The curve of growth consists of a plot of $\log W_{\lambda}/\lambda$ against $\log C$. It is clear that this relationship will differ not only for a given element in different stages of ion-

ization, but for different lines of different excitation potential or for lines of the same excitation potential which fall in different regions of the spectrum. The latter effects are generally small, however.

Equivalent widths of weak or medium intensity lines as observed at the center of the sun's disk are connected to the abundance of the element in question by the relation

$$\log \frac{W_\lambda}{\lambda} = \log C + \log \frac{N_i}{N_H} \qquad (6)$$

For any given line, we know $\Delta\chi$, the difference between the excitation and ionization potentials of the line in question; the f-value from laboratory measurements; and L_λ from the structure of the solar atmosphere. The latter also influences the shape of the curve of growth.

For each element we plot log W_λ/λ against log C and fit these empirical plots to the proper theoretical curves. For the neutral lines of most metals we can use the iron curve, although for these elements for which the data are good, special curves can be calculated.

A systematic study of the abundances of elements in the sun was undertaken by Goldberg, Müller, and Aller,[17] using an empirical solar model atmosphere and f-values derived from various sources. The observational data were taken mostly from the Utrecht[8] and Michigan[10] work, but additional observations were also secured at the McMath-Hulbert Observatory.

III. FACTORS INFLUENCING THE DETERMINATION OF ELEMENTAL ABUNDANCES IN THE SOLAR ATMOSPHERE

Determinations of the composition of the sun may be improved in 3 ways:

(1) Consideration of the formulation of each spectral line under its own particular circumstances.

(2) Improvements in the model solar atmosphere.

(3) Improvements in the transition probabilities.

For the abundant metals it is nearly always possible to find enough lines which are unaffected by blends for one to carry out an analysis based on unblended lines. Usually the strongest lines of an abundant metal are affected by collisional damping; hence one must use either lines of moderate strength or weak lines.

The rarer metals, on the other hand, are represented (if at all) by weak lines. These weak lines are sometimes totally blended with other lines—in which event they are useless for abundance studies. In other existences they fall on the edges or "wings' of stronger lines, in which event one should consider first the problem of the formation of the stronger line and then that of the weak line of the element of interest. In the ultraviolet part of the spectrum, the wings of strong or moderately strong lines overlap so thoroughly that one never sees the "continuum" that would have been defined by the negative hydrogen ion, which is the principal source of continuous absorption throughout most of the solar spectrum. Hence the calculation for each line has to be undertaken as a separate problem.[18] The computations attain a fairly high level of complexity but are being undertaken for a few particularly important elements in the solar atmosphere—lead, berylluim, and lithium.[19] Likewise, the question of the model atmosphere influences the results. Some lines, such as these of sodium and potassium, are formed almost entirely in the shallowest layers. Hence it is of the utmost importance to know the temperature and pressures in these strata very accurately. Other lines such as those of oxygen, all formed primarily in very deep layers—hence the model atmosphere must be accurate there also. These problems are being investigated by Mutschlecner (particularly for shallow layers) and by Mugglestone for the deeper layers. We shall not consider these general problems here but shall limit ourselves to the third question, that of the transition probabilities.

IV. THE ROLE OF TRANSITION PROBABILITIES IN ABUNDANCE DETERMINATION

Uncertainties in the f-values enter directly into stellar abundance determinations, and indirectly insofar as they are employed to fix the level of ionization of a stellar atmosphere by comparing lines arising from two different stages of ionization. In the comprehensive Michigan study of solar abundances[17], transition probabilities were derived from many sources -both observational and experimental.

Since this investigation was published, C. H. Corliss at the Bureau of Standards has obtained relative -values for 24,000 lines of 70 elements between λ2000A and λ9000A.[20] By calibrating this scale with known, absolute gf-values, Corliss has been able to put it on an absolute basis. The technique he used was the following: An arc was struck between copper electrodes to which a single element was added in the ratio of one atom of the element to 1000 atoms of copper. Hence the operating condition of the arc is not influenced by the trace substance. Corliss then photographed the resultant spectrum in the usual way, calibrating the plates with the aid of standard lamps. In this fashion he could obtain a set of arc line intensities corresponding to uniform conditions of temperature and pressure.[21] Next he used lines for which relative gf-values had been obtained in order to get the temperature of the arc, 5100°K ± 110°K. He then compared intensities of lines of 11 elements which appeared in two stages of ionization and for which relative gf-values were known. In this way it is possible to find the relative numbers of neutral atoms and ions and then, with the aid of the Saha ionization equation, to deduce the electron density in the arc. Corliss thus found an electron density of 2.4×10^{14} cm^{-3}. With both temperature and electron density known, it is possible to determine the relative numbers of ions and neutral atoms for each of the 70 elements in the arc. It is necessary to make a small correction for the thermal diffusion of atoms from the arc stream. Thus, when the ionization in the arc (i.e., the relative numbers of atoms and ions) is known, one can calculate the absolute gf-values for lines of all 70 elements, provided absolute gf-values for some of them are known. Of course, the arc must have a unique excitation temperature; i.e., the relative populations of the levels must be given by Boltzmann's law. Corliss checked this question carefully and came to the conclusion that the Boltzmann equation was sufficiently well satisfied. Note that a small error in the temperature would cause the gf-values for high-level lines to be systematically in error compared with gf-values for low-level lines! A similar method has been employed by C. W. Allen and his associates[22] for a more limited series of elements.

The copper arc method is a relative rather than a fundamental method, and is still dependent on absolute methods for the basic calibration. Therefore, the accuracy of the procedure is ultimately limited by the accuracy of the basic

f-values which can be obtained experimentally with the aid of (a) lifetime measurements of excited levels, (b) the atomic-beam method, (c) the electric furnace, (d) anomalous dispersion, and (e) the luminous shock tube. Transition probabilties can also be calculated by theory; relative f-values are usually easier to get than absolute f-values. In some instances, it is possible to derive working gf-values from measurements of stellar spectral lines. We shall describe this procedure in a separate report.

V. SOLAR ABUNDANCES OF PARTICULAR ELEMENTS

The great advantage of Corliss' gf-data is that they constitute a set of transition probabilities measured in a uniform way. If the line strength are systematically in error, they are likely to be so in a manner which is probably roughly comparable for different atoms. An error in the arc temperature, for example, would introduce an error depending only on the excitation of the levels involved.

Accordingly, we have re-examined the solar abundances of a number of elements. Most of the elements of the iron group are being studied by Miss Edith Müller, who is taking advantage of the great number of solar lines of these elements to investigate not only abundances but also such questions as deviations from local thermodynamic equilibrium. She is also examining the influence of changes in the model atmosphere. Paul Mutschlecner is studying lead, beryllium, and lithium—all of which are of interest in connection with nucleogenesis problems.

In the present work we have simply derived new values of log C with the Corliss gf-values and constructed curves of growth with the log W/λ-values previously obtained. Individual curves of growth have been obtained for only a few elements; hence the FeI curve of growth[17] has been employed for most of the heavier metals.

Table I gives the basic data for curve-of-growth plots. Successive columns give for each element the wavelength, the multiplet number, log gf, the abscissa of the curve-of-growth log C, and log W/λ. (W/λ is the equivalent width divided by the wavelength).

Table II summarizes the abundance determinations. Column 3 gives the value of log N obtained in the present work; column 4 gives previously published results[17] based on the same solar line intensities.

Transition probabilities are available for only a few lines of sodium and potassium. The sodium abundance is based on multiplets (5) and (6) alone. Notice that the scatter is rather large (Fig. 2); hence the determination is rather shaky. The derived abundance is an order of magnitude smaller than the old determination.

The potassium abundance is based on only 3 lines. Two of them belonging to multiplet (3), λ4044 and λ4047, give a potassium abundance log N = 3.61 on the scale log N (hydrogen) = 12, whilst λ7699 of multiplet (1) gives log N = 3.66.

Thus the NBS f-values do not define as good a curve of growth as did the

previously employed data. We are inclined to accept the value given by λ7699. Figure 3 shows the curve of growth fitted to both multiplets (1) and (3). It should be compared with Fig. 10 of Ref. 17. The problem of potassium needs further investigation.

Figure 4 shows the results for neutral scandium, and the caption to Fig. 4 lists the multiplets used. Hence $\Delta\chi$ is the distance of the energy level below ionization level (expressed in electron volts), the wavelength region denotes the part of the spectrum in which the lines appear, and the multiplet number gives the number of the multiplet according to the Revised Multiplet Table.[23] For scandium we use the average iron curve of growth (Ref. 17, p. 63). We derive the same abundance for scandium as had been found from the f-sum rule and from use of the Bates-Damgaard Tables.[24]

The plot for copper is given in Fig. 5. The scatter appears to be somewhat larger than with the older f-values; on the other hand, use of the Corliss f-values seems to remove the apparent discrepancy between the solar[17] and Suess-Urey[25] abundance. The theoretical curve is the FeI curve of growth.

For ZnI (Fig. 6), λ6362 (multiplet 6) and the lines of multiplet (2) give discordant results. The adopted zinc abundance is somewhat smaller than that obtained earlier, but is very uncertain. More work needs to be done on this element.

The abundance of gallium (Fig. 7) is raised and that of germanium (Fig. 8) is lowered as a consequence of revising the f-values. Notice that the results are in any event uncertain because of the nature of the solar data. The single gallium line is blended and has an uncertain intensity. The GeI λ4226 line is seriously blended with the strong CaI λ4226.74 line. Clearly, one should treat these lines from the point of view of the blended line theory.[18]

The spectrum of SrI (Fig. 9) is characterized by one strong line, λ4607, which falls on the transition region of the curve of growth, and a number of weak lines which fall on the linear part of the curve of growth. Two lines, λ4876 and λ5486, fall some distance to the left of the straight line defined by the others; possibly they are affected by blends. The final abundance derived from SrI is somewhat larger than that found previously, whereas the abundance found from λ4161 SrII (Fig. 10) is slightly smaller. Hence the discrepancy between the strontium abundance found from SrI and SrII is increased. This element needs further investigation.

The abundance of yttrium previously derived[17] was very uncertain because of the unsatisfactory status of the f-values. Most of the lines are weak and fall on the straight part of the curve of growth. Even with the Corliss f-values, the scatter remains very bad. This element is an example of that group whose abundance can be derived much better from the ionic lines than from the lines of the neutral element (see Fig. 11).

The lines of neutral zirconium and of neutral niobium likewise all fall on the straight part of the curve of growth. The abundances derived with the aid of the NBS gf-values are somewhat more than twice those previously obtained[17] with approximate estimates of the f-values (see Figs. 12 and 13).

Molybdenum is represented in our analysis by three lines of MoI which fall on the straight-line part of the curve of growth (see Fig. 14). Rhodium and particularly ruthenium show a considerable scatter, probably as a consequence of blends and difficulties in the measurement of these extremely weak lines (see Figs. 15 and 16). For all of these elements Nb, Mo, Ru, and Rh, use of the Corliss f-values results in an increase of the abundance determined.

On the other hand, the palladium abundance is hardly changed by the new -values (see Fig. 17). The scatter is less severe than for ruthenium, although for all these elements the weakness of the lines makes it impossible to obtain really reliable abundance.

The abundance of silver is raised by nearly an order of magnitude when the new f-values are employed (see Fig. 18). The new value is much more closely in line with the Suess-Urey compilation. Cadmium and indium are represented by single lines that are affected by blends or by an uncertain position of the continuum. The new abundances are only slightly increased.

Neutral tin is represented by two rather weak lines which yield an uncertain abundance about three times greater than that previously published (see Fig. 19). On the other hand the abundance of antimony is decreased by more than an order of magnitude (see Fig. 20). It must be remarked however, that the Sb abundance depends on extremely weak and uncertain solar lines.

The curve of growth for ionized barium is shown in Fig. 31. The dotted curve gives the theoretical relation according to the calculations by Elste. The same general features are shown in Fig. 21 as in Fig. 48 of Ref. 13 but the derived abundance is increased by about a factor of 2.5.

The lanthanide rare earth ytterbium (see Fig. 22) would appear to have an abundance considerably in excess of that expected for this group of elements.[26] Note that this estimate depends on a single line, which may be affected by a blend with an unknown contributor. Now that the necessary gf-values are available, it will be important to measure the abundances of other lanthanide elements.

In Fig. 23 we compare the new solar abundances with a previously suggested abundance scale for the solar system[27] which was based partly on meteoritic data, the older solar data,[17] a semi-empirical compilation by Suess and Urey,[25] and a semi-theoretical treatment by Cameron.[28] In some instances the discrepancy between the solar and "standard" abundances is decreased; in other instances it is increased. For most elements we are tempted to conclude that a definite improvement in the abundances has been achieved!

We want to emphasize that in this particular investigation we have not attempted to improve the basic solar model atmosphere, nor generally to make use of lines of ionized metals. Availability of the National Bureau of Standards transitions probabilities has made it possible to use many more lines than could be used before. Hence a comprehensive new treatment of this problem would entail the following steps:

(1) Construction of a new model for the solar atmosphere, in which the best available data is used to improve the temperature distribution in both the shallowest and deepest layers. Such a model has been devised by Paul Mutschlecner.[19]

(2) With the aid of the new model one would calculate curves of growth and other required data not only for the lines that have been used in the previous work but also for a host of lines arising from different levels and from ions for which gf-values are now available.

(3) At least for the few available lines of the rarer elements, one would treat the problem of their formation on an individual basis, taking into account blends, etc.

REFERENCES

1. S. Chapman and L. H. Aller, Astrophysical Journal, Vol. 132, 1960, p. 461.

2. L. H. Aller, Atmospheres of the Sun and Stars, Ronald, New York, 1953.

3. V. A. Ambarzumian (ed.), Theoretical Astrophysics, J. B. Sykes (tr.), Pergamon, London, 1958.

4. J. L. Greenstein (ed.), Stellar Atmospheres (Compendium of Stars and Stellar Systems, Vol. 6), University of Chicago Press, 1960.

5. J. C. Pecker and E. Schatzman, Astrophysique Generale, Masson, Paris, 1959.

6. A. Unsöld, Physik der Sternatmosphären, Springer, Berlin, 1955.

7. R. Woolley and D. W. Stibbs, Outer Layers of a Star, Oxford University Press, 1953.

8. "Preliminary Photometric Catalogue of Fraunhofer Lines λ3164-λ8770," Astronomical Researches of the Utrecht Observatory, Vol. 15, 1960.

9. O. C. Mohler, A Table of Solar Spectrum Wavelengths, 11984A to 25578A, University of Michigan Press, 1955.

10. O. C. Mohler, A. K. Pierce, R. McMath, and L. G. Goldberg, Photometric Atlas of Near-Infrared Solar Spectrum λ8465 to λ25242, University of Michigan Press, 1950.

11. J. C. Pecker, Annales d'Astrophysique, Vol. 14, 1951, p. 383.

12. See Ref. 4, p. 156.

13. L. H. Aller, G. Elste, and J. Jugaku, Astrophysical Journal Supplement, Vol. 3, 1957, p. 1.

14. L. G. Goldberg and A. K. Pierce, Handbuch der Physik, Vol. 52, 1958.

15. See Ref. 4, p. 172, Eq. (41).

16. See Ref. 4, p. 173, Eq. (53).

17. L. G. Goldberg, E. A. Müller, and L. H. Aller, Astrophysical Journal Supplement, Vol. 5, 1960, p. 1.

18. L. H. Aller in Physics and Chemistry of the Earth, Vol. 4, Pergamon, London, 1961, p. 1.

19. P. Mutschlecner, Unpublished Thesis, The University of Michigan, 1962.

20. C. H. Corliss, National Bureau of Standards Monograph (in press, 1962).

21. W. F. Meggers, C. H. Corliss, and B. F. Scribner, Tables of Spectral-Line Intensities, National Bureau of Standards Monograph No. 32, 1961.

22. C. W. Allen and A. S. Asaad, Monthly Notices of the Royal Astronomical Society, Vol. 117, 1957, p. 36; C. W. Allen, ibid, Vol. 117, 1957, p. 622; and Vol. 121, 1960, p. 299.

23. C. E. Moore, Multiplet Table of Astrophysical Interest, Princeton Observatory Contributions, No. 20, 1945.

24. D. R. Bates and A. Damgaard, Philosophical Transactions of the Royal Society (London), sers. A, Vol. 242, 1949, p. 101.

25. H. Suess and H. C. Urey, Reviews of Modern Physics, Vol. 28, 1956, p. 53.

26. R. A. Schmitt, A. W. Mosen, C. S. Suffredini, J. E. Lasch, R. A. Sharp, and D. A. Olehy, Nature, Vol. 186, 1960, p. 863.

27. L. H. Aller, Abundance of the Elements, Interscience, New York, 1961.

28. A. G. Cameron, Astrophysical Journal, Vol. 129, 1959, p. 656; and Vol. 131, 1960, p. 521.

TABLE I

CURVE OF GROWTH DATA FOR VARIOUS ATOMS

λ	Mult. No.	log gf	log C	log W/λ
		Sodium NaI		
6160.76	5	-0.50	1.65	-5.15
6154.24	5	-0.80	1.36	-5.36
5282.65	6	-0.37	1.80	-4.74
5688.22	6	-0.07	2.09	-4.67
5153.42	6	-0.82	1.36	-5.33
		Potassium KI		
7698.98	1	-0.16	3.23	-4.70
4044.15	3	-0.63	2.77	-5.57
4047.19	3	-0.93	2.47	-6.01
		Scandium ScI		
4054.57	6	-0.18	4.13	-5.49
3996.61	7	-0.16	4.15	-5.56
4020.40	7	+0.39	4.70	-4.95
4023.69	7	+0.41	4.70	-4.91
4047.81	7	-0.48	3.81	-5.57
3911.83	8	+0.52	4.80	-4.83
5671.84	12	+0.35	3.28	-5.68
5708.67	12	-0.54	2.38	-6.28
5686.85	12	+0.26	3.20	-5.91
5717.31	12	-0.48	2.46	-6.53
5724.10	12	-0.60	2.33	-6.76
5081.59	13	+0.61	3.53	-5.80
5083.71	13	+0.37	3.30	-5.86
5085.50	13	+0.30	3.23	-5.67
5086.94	13	+0.14	3.08	-6.23
4743.83	14	+0.39	3.31	-5.83
5520.52	15	+0.44	2.96	-5.90
5514.22	15	+0.36	2.90	-6.44
5482.00	16	+0.50	3.02	-6.26
5484.65	16	+0.33	2.87	-6.34
5356.09	17	+0.37	2.89	-6.43
5349.29	17	+0.18	2.72	-6.43
4709.33	22	+0.25	2.35	-6.67
		Copper CuI		
5105.55	2	-1.70	3.45	-4.79
5700.30	2	-2.16	2.74	-5.61
5782.10	2	-1.57	3.33	-5.25
7933.16	6	+0.09	2.91	-5.56
8092.64	6	+0.41	3.20	-5.33
5218.21		+0.99	3.82	-5.04
5220.09		+0.19	3.02	-5.57
		Zinc ZnI		
4810.54	2	0.86	4.32	-4.76
4722.16		0.69	4.20	-4.88
4680.14		0.28	3.80	-5.05
6362.36	6	0.44	2.32	-5.53
		Gallium GaI		
4172.05	1	-0.27	4.60	-5.08
		Germanium GeI		
4226.567	4	-0.08	4.19	-5.37
		Strontium SrI		
4607.34	2	-0.57	3.77	-5.05
7070.07	3	-0.18	2.37	-6.62
6878.32	3	-0.28	2.31	-6.84
4876.09	4	-0.90	1.72	-6.57
4962.29	4	+0.25	2.83	-6.00
4872.51	4	-0.20	2.42	-6.51
4811.89	5	+0.07	2.64	-6.51
4722.29	5	-0.13	2.49	-6.37
6408.48	8	+0.50	2.66	-6.36
6504.01	8	+0.26	2.43	-6.64
5486.12	9	-0.31	1.89	-6.59
5521.79	9	+0.05	2.24	-6.70
		Strontium SrII		
4161.80		-0.28	4.23	-5.28
		Yttrium YI		
6191.75	2	-1.56	2.76	-6.32
6222.61	2	-2.18	2.14	-6.75
4128.31	5	+0.06	4.27	-5.88
4142.85	5	-0.09	4.18	-5.78
4102.39	7	+0.11	4.30	-6.00
3620.97	8	+0.09	4.27	-5.78
5630.10	12	-0.43	2.55	-6.15
4781.02	13	-0.80	2.14	-6.57
4819.65	13	-0.77	2.21	-6.24
4839.89	13	+0.03	2.94	-5.62
4477.45	14	-0.55	2.42	-5.90
4487.52	14	-0.28	2.70	-5.87
4475.72	14	-0.48	2.46	-6.51
4505.93	14	-0.04	2.92	-6.48

TABLE I (Concluded)

λ	Mult. No.	log gf	log C	log W/λ
		Zirconium ZrI		
4815.64	43	-0.69	+2.97	-6.36
4772.32		-0.56	3.08	-6.07
4710.08		-0.16	3.41	-6.04
4687.81		-0.01	3.51	-5.81
4739.45		-0.32	3.29	-5.99
4805.89		-1.04	2.54	-6.57
4241.71	45	-0.20	3.39	-6.23
4282.22		-0.56	3.02	-6.23
4072.20	46	+0.11	3.66	-5.89
4027.25		-0.23	3.37	-6.16
4030.03		-0.56	3.07	-6.49
		Niobium (Columbium) NbI		
4100.92	1	-0.20	+3.85	-5.84
4137.12		-0.72	3.39	-6.32
4139.73		-0.53	3.45	-6.22
4168.12		-0.56	3.55	-6.14
3713.10	3	-0.25	3.70	-6.27
3697.87		-0.65	3.37	-6.17
		Molybdenum MoI		
5506.51	4	-0.05	+3.83	-6.01
5533.04		-0.23	3.65	-6.14
5570.40		-0.56	3.32	-6.20
		Ruthenium RuI		
3799.35	1	-0.21	+4.66	-5.68
3798.91	1	-0.06	4.66	-5.54
3742.28	2	-0.19	4.35	-5.87
3498.95	4	+0.05	4.89	-5.13
3435.75	4	+0.11	4.83	-5.63
3589.22	4	+0.25	4.73	-6.09
3301.58	4	-1.17	3.65	-5.84
4554.54	5	+0.15	4.25	-6.06
3984.84	9	-0.25	3.63	-6.30
4709.51	14	-0.20	3.58	-6.20
		Rhodium RhI		
3692.36	1	-0.24	+4.82	-5.75
3507.31	2	-0.33	4.40	-6.15
3434.90		-0.14	4.90	-5.66
3396.83	3	-0.28	4.76	-5.91
3470.64		+0.02	4.64	-6.39
3583.11		-0.29	4.58	-6.20
3462.08		+0.02	4.74	-6.26
		Palladium PdI		
3516.95	1	+0.07	+5.43	-5.37
3404.59	2	+0.30	+5.80	-5.06
3460.74	2	-0.22	+5.28	-5.34
3609.56	2	+0.25	+5.61	-5.44
3372.97	3	-0.21	+5.14	-5.68
3342.72	3	+0.08	+5.56	-5.23
3553.10	9	+0.54	+5.41	-5.95
3433.46	11	+0.24	+5.10	-5.76
		Silver AgI		
3382.90	1	-0.89	+5.66	-5.39
3380.68	1	-0.83	+6.01	-5.12
8273.48	2	+0.49	+3.06	-5.92
		Cadmium CdI		
3261.05	1	-2.84	+4.00	-6.34
		Indium InI		
4511.34	1	-0.18	+4.32	-6.40
		Tin SnI		
3801.03	2	-0.37	+4.04	-6.10
3330.62	2	-0.49	+3.89	-5.92
		Antimony SbI		
3332.55	2	0.54	4.91	-6.73
3267.54	2	0.26	4.89	-6.61
3029.83	2	0.16	4.76	-6.18
		Barium BaII		
4554.04	1	-0.55	6.59	-4.45
4934.08	1	-1.17	5.92	-4.49
6141.73	2	-0.67	5.55	-4.67
5853.69	2	-1.59	4.70	-5.01
6496.92	2	-1.03	5.31	-4.84
4524.95	3	-0.76	3.78	-5.18
4130.66	4	+0.66	4.93	-5.09
3891.78	4	+0.52	4.35	-5.19
		Ytterbium YbI		
3987.97	2	-0.42	4.43	-5.35

TABLE II

SUMMARY OF ABUNDANCE DETERMINATIONS

Element	Ion	Log N NBS gf	Log N Ref. 17	Element	Ion	Log N NBS gf	Log N Ref. 17
Sodium	NaI	5.44:	6.30	Molybdenum	MoI	2.30	1.90
Potassium	KI	4.66:	4.70	Ruthenium	RuI	1.82	1.43
Scandium	ScI	2.80	2.82	Rhodium	RhI	1.37	0.78
Copper	CuI	3.50	5.04	Palladium	PdI	1.27	1.21
Zinc	ZnI	3.52	4.40	Silver	AgI	1.04	0.14
Gallium	GaI	2.51	2.36	Cadmium	CdI	1.66	1.46
Germanium	GeI	2.49	3.29	Indium	InI	1.28	1.16
Strontium	SrI	3.10	2.53	Tin	SnI	2.05	1.54
	SrII	2.56	2.60				
				Antimony	SbI	0.42	1.94
Strontium-Adopted		2.70	2.60				
				Barium	BaII	2.50	2.10
Yttrium	YI	3.20	2.25:				
				Ytterbium	YbI	2.28	1.53
Zirconium	ZrI	2.65	2.23				
Niobium (Columbium)	NbI	2.30	1.95				

: indicates a highly uncertain result.

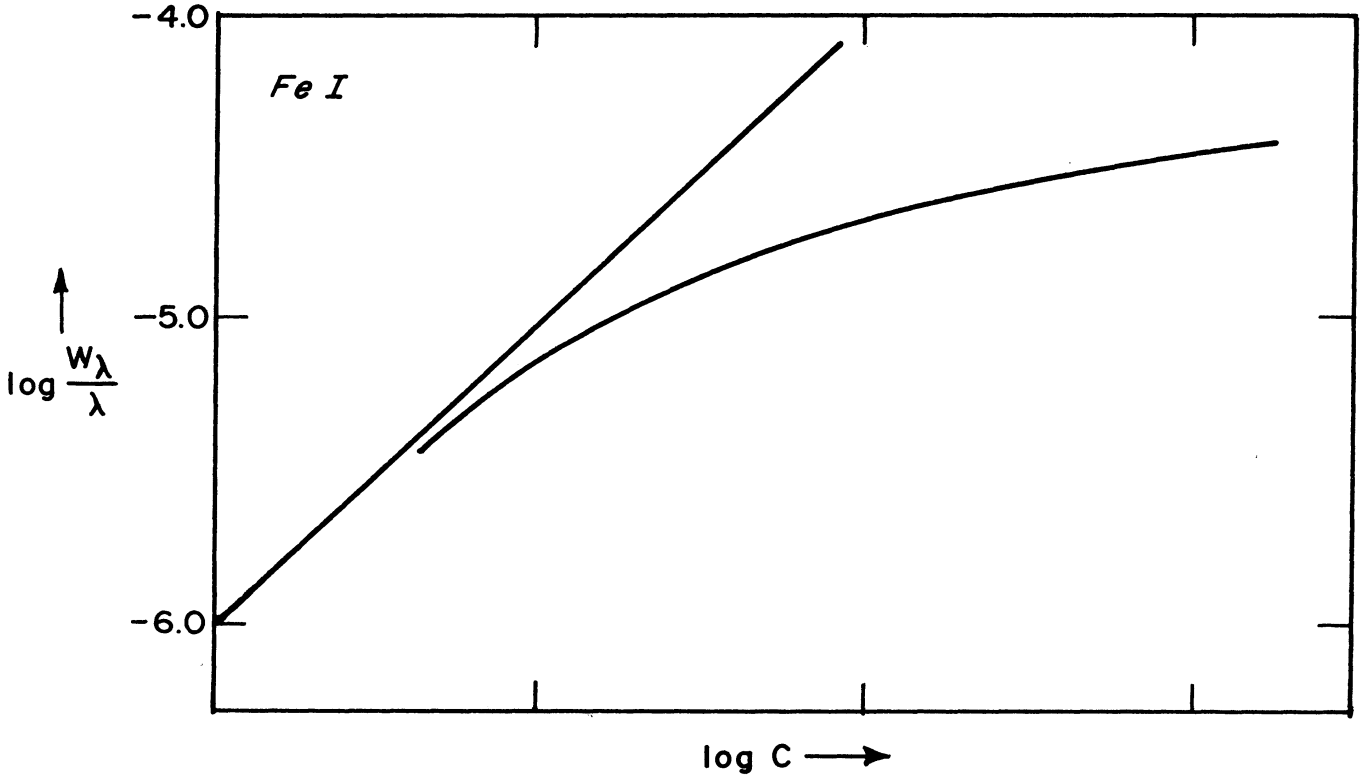

Fig. 1. The theoretical curve of growth for iron. (Abscissae are log C; the zero point of the scale depends on the abundance.)

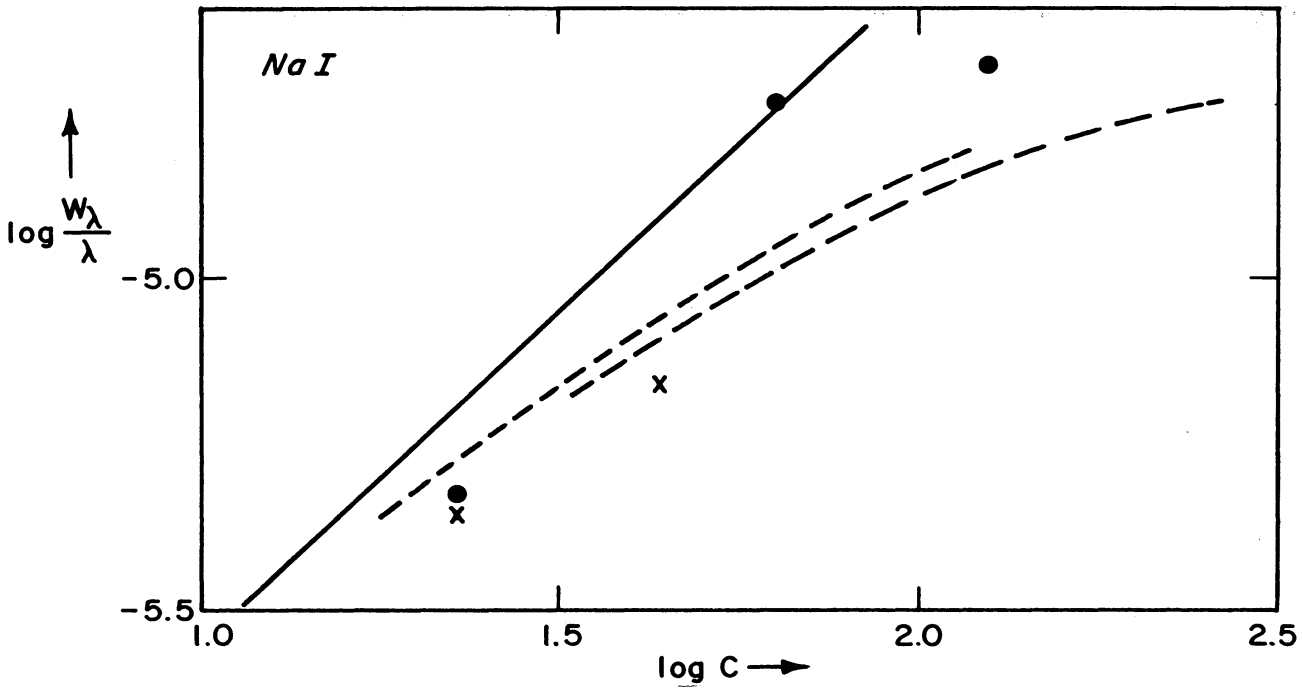

Fig. 2. Curve of growth for sodium.

x = Multiplet[5] ● = Multiplet[6]

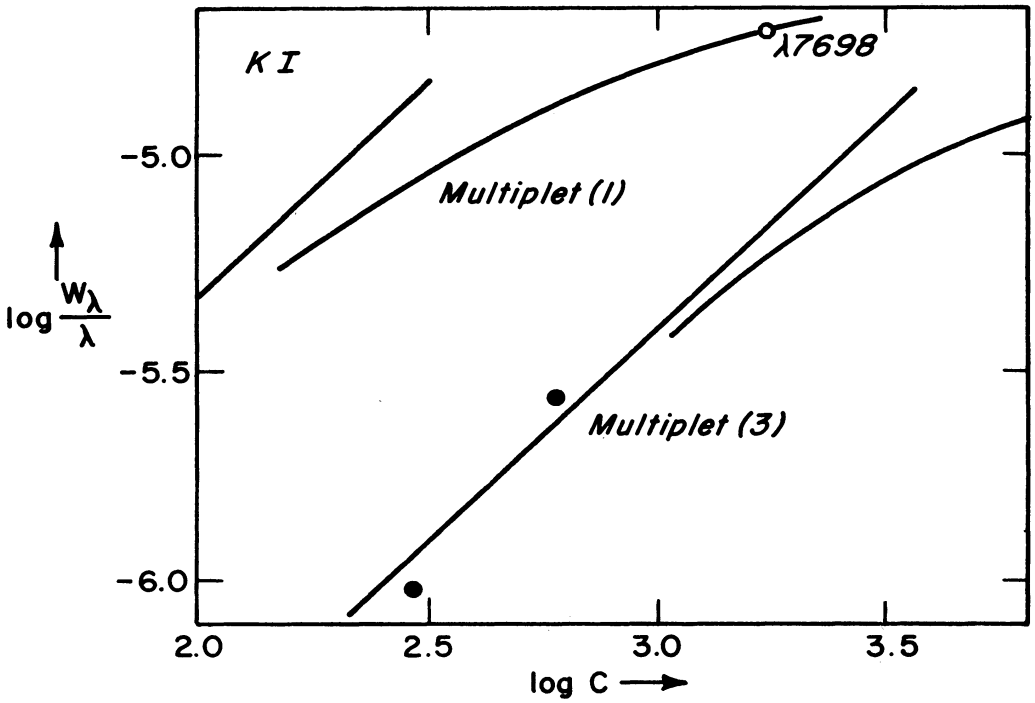

Fig. 3. Curve of growth of potassium.

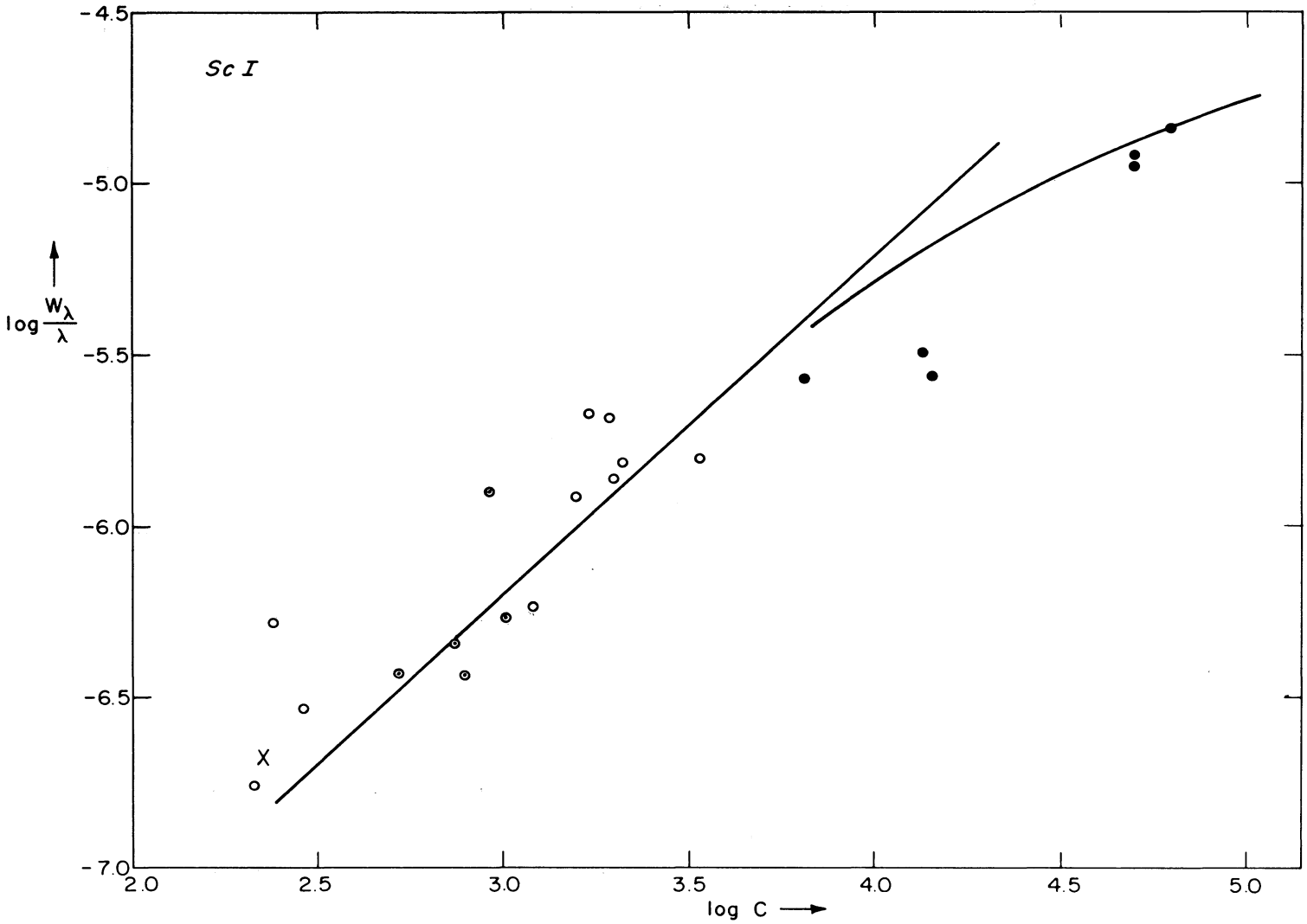

Fig. 4. Curve of growth for scandium.

Symbol	$\Delta\chi$	Wavelength Region, ft	Multiplet Number
●	6.7	4000	6, 7, 8
o	5.3	4700-5700	12, 13, 14
⊙	4.8	5300-5600	15, 16, 17
x	4.4	4709	22

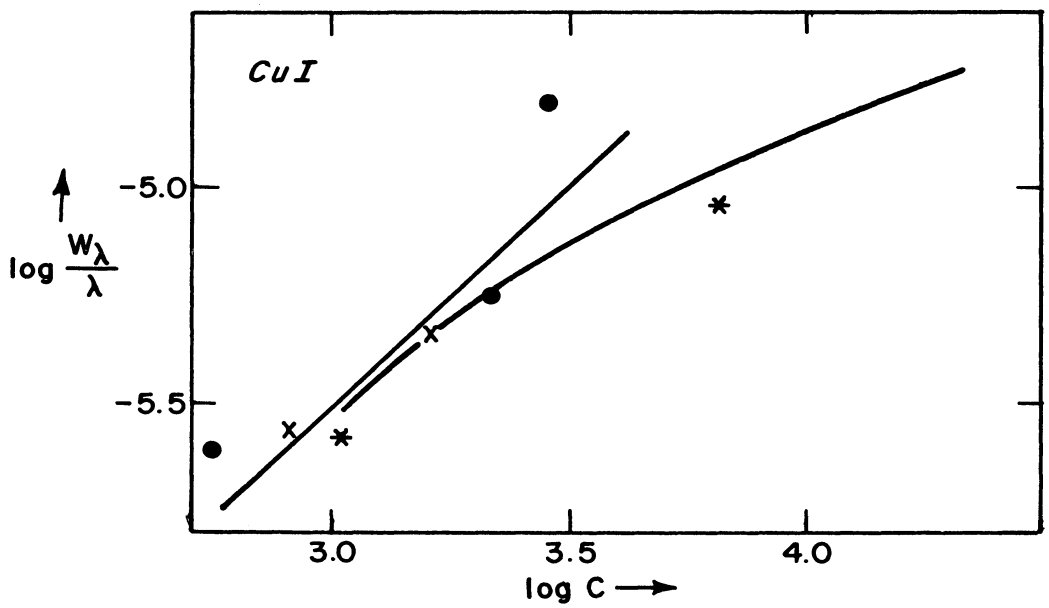

Fig. 5. Curve of growth for copper.

$\Delta\chi$	λ
• 6.3	5105, 5700, 5782
x 3.9	7933, 8093
* 3.4	5220

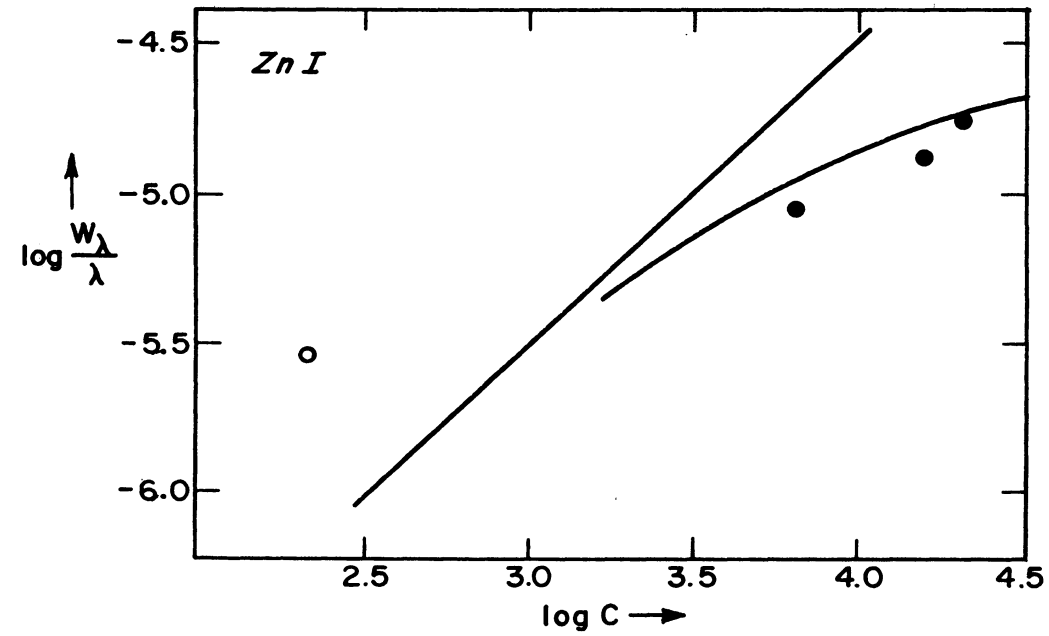

Fig. 6. Curve of growth for zinc.

• 4680, 4722, 4810
o 6362

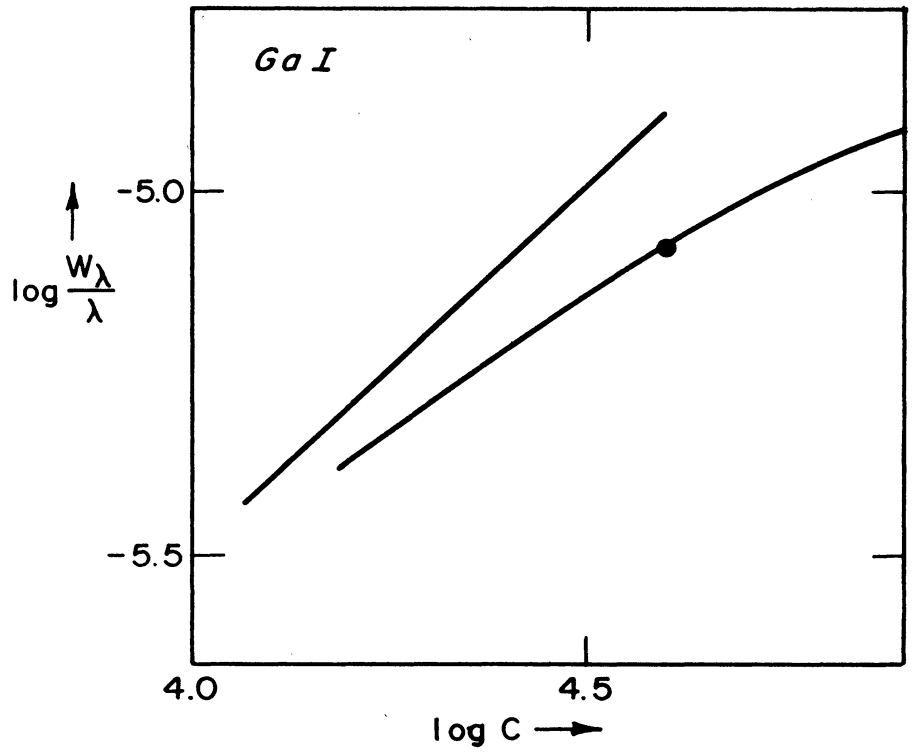

Fig. 7. Curve of growth for gallium.

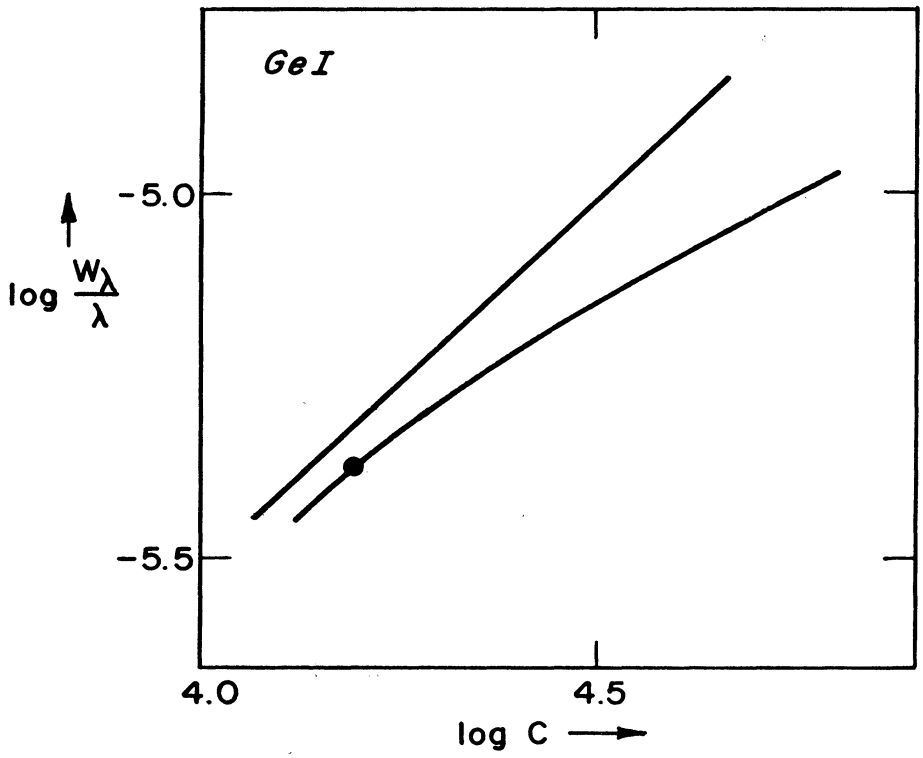

Fig. 8. Curve of growth for germanium.

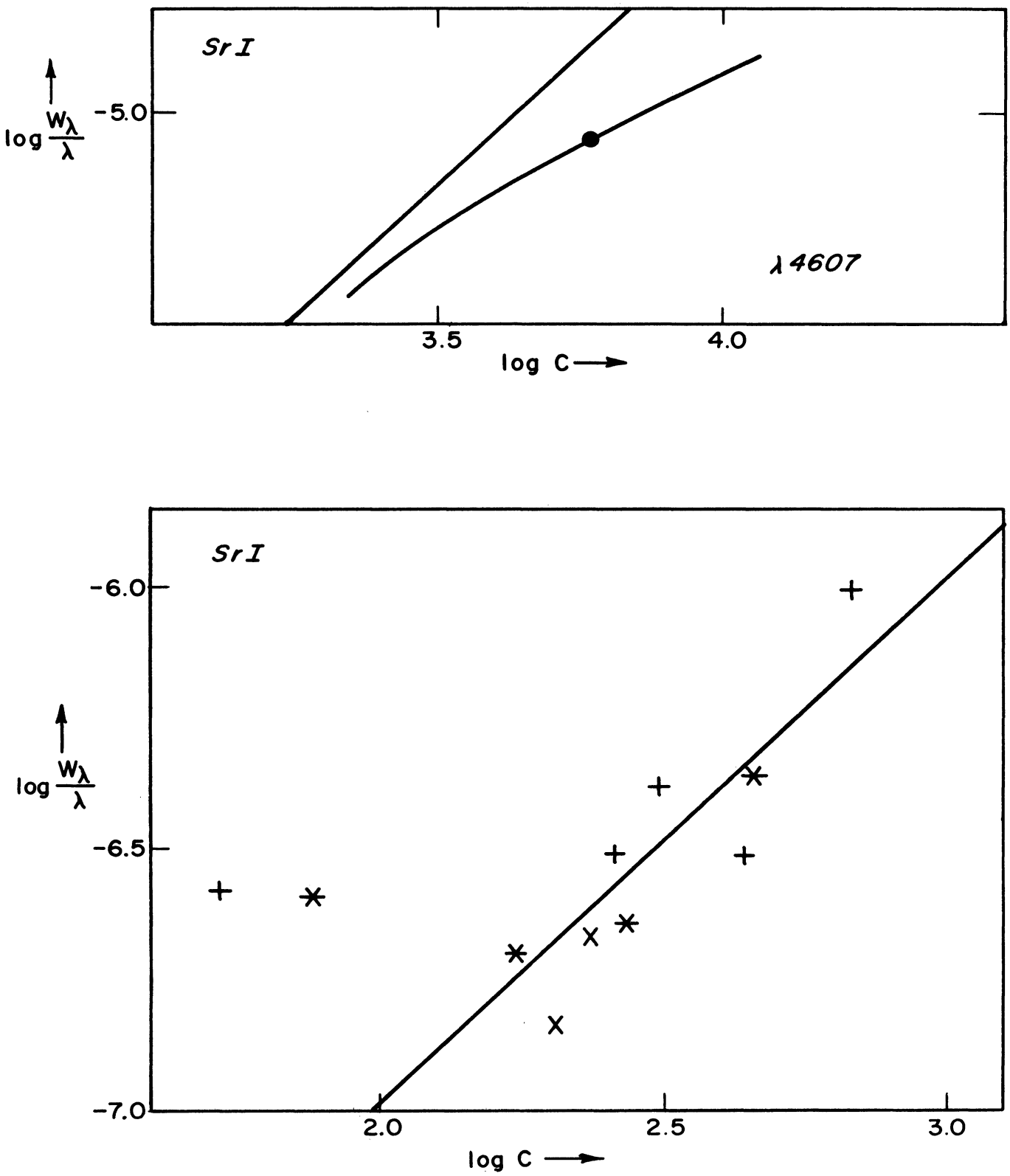

Fig. 9. Curve for growth for neutral strontium. (The portions of the curve for the strong and weak lines are shown separately.)

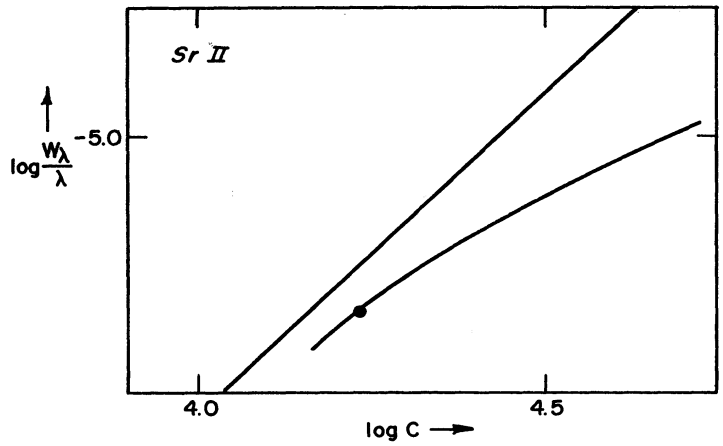

Fig. 10. Curve of growth for ionized strontium.

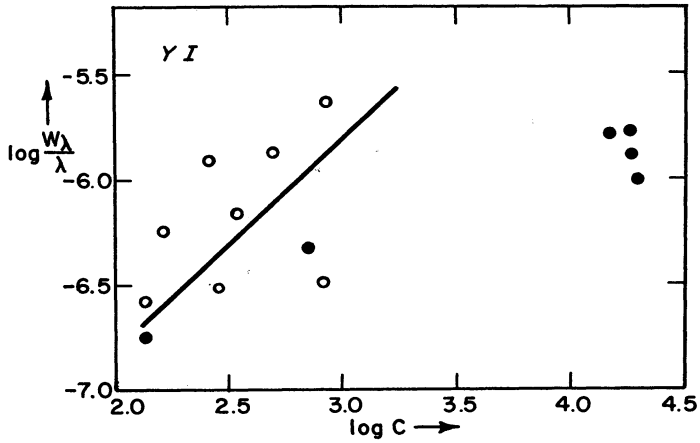

Fig. 11. Curve of growth for neutral yttrium.

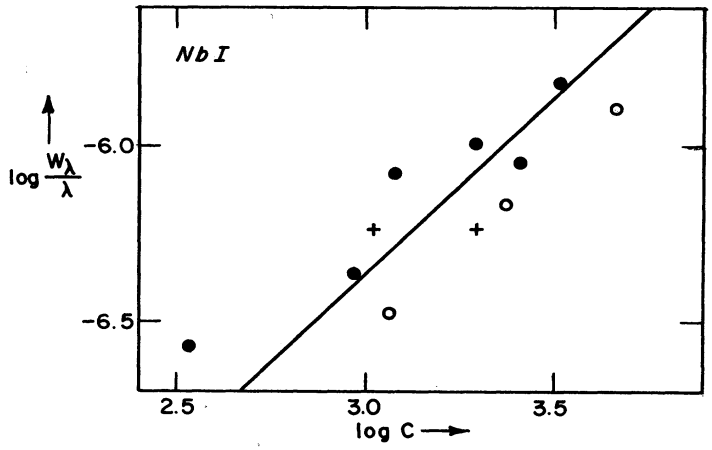

Fig. 12. Curve of growth for strontium.

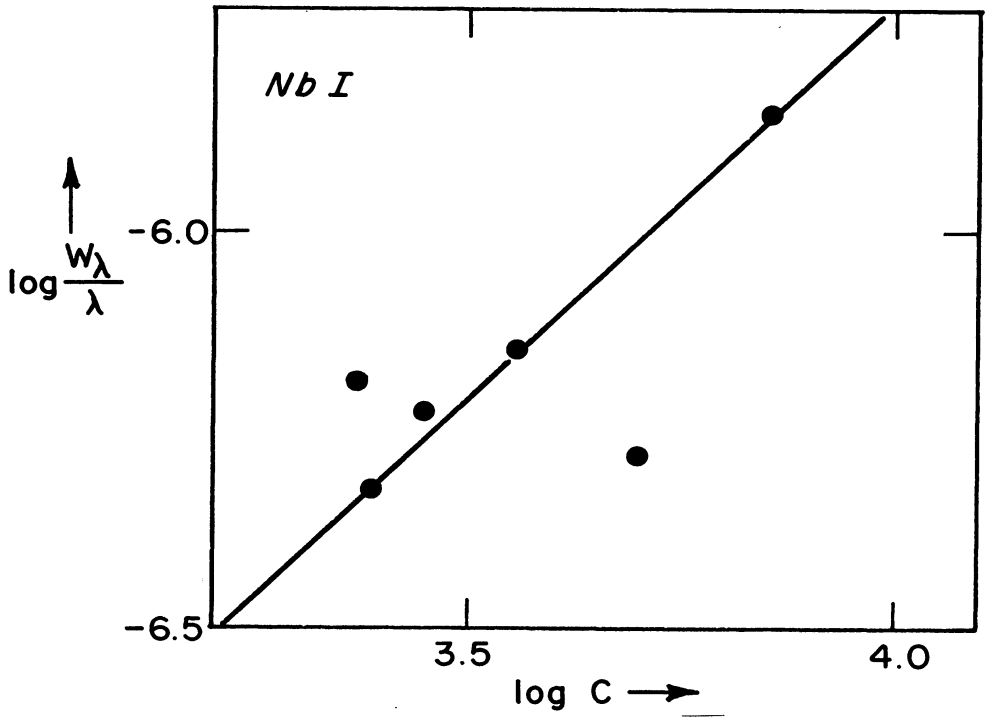

Fig. 13. Curve of growth for niobium (columbium).

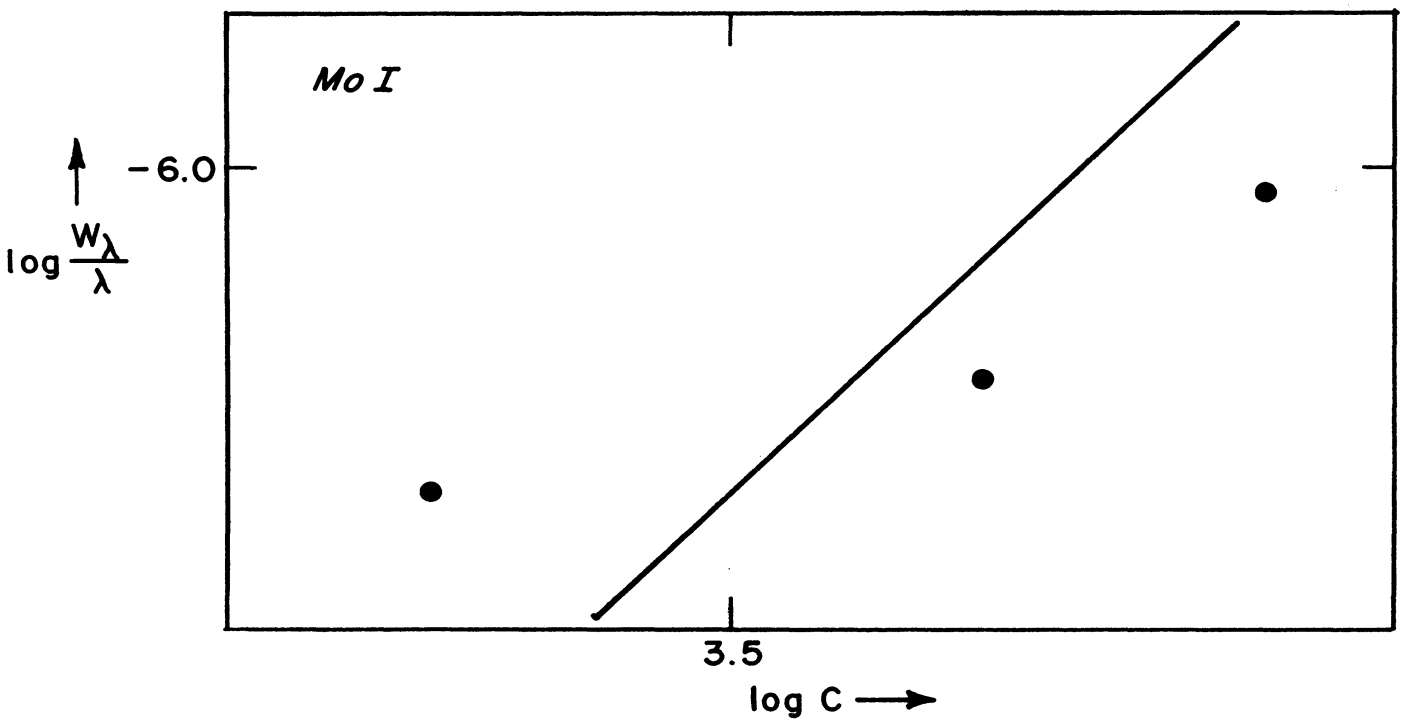

Fig. 14. Curve of growth for molybdenum.

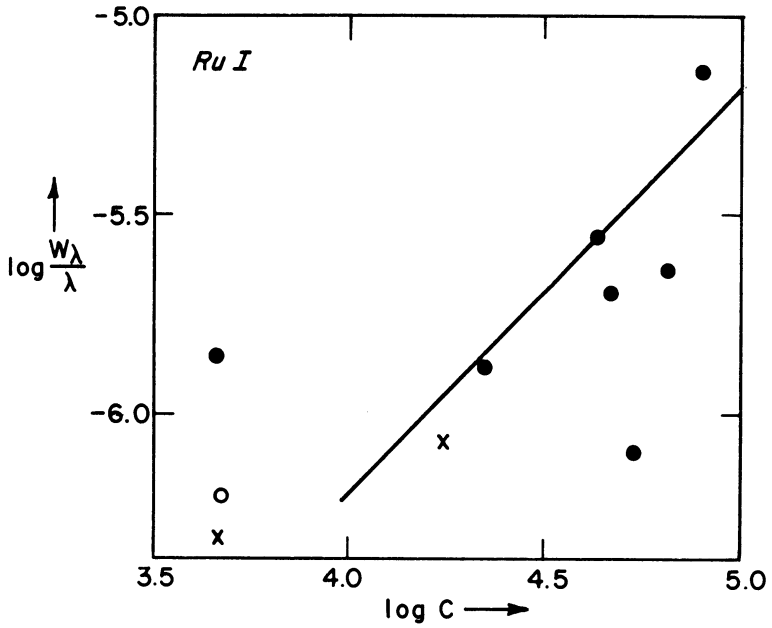

Fig. 15. Curve of growth for ruthenium.

	Δχ	Multiplet
●	7.4	(1), (2), (4)
x	6.60	(5), (9)
o	6.37	(14)

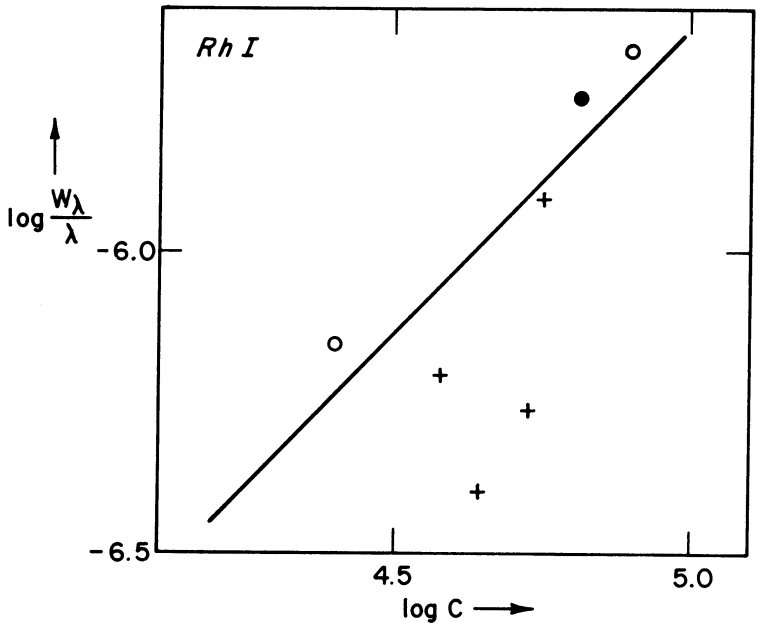

Fig. 16. Curve of growth for rhodium.

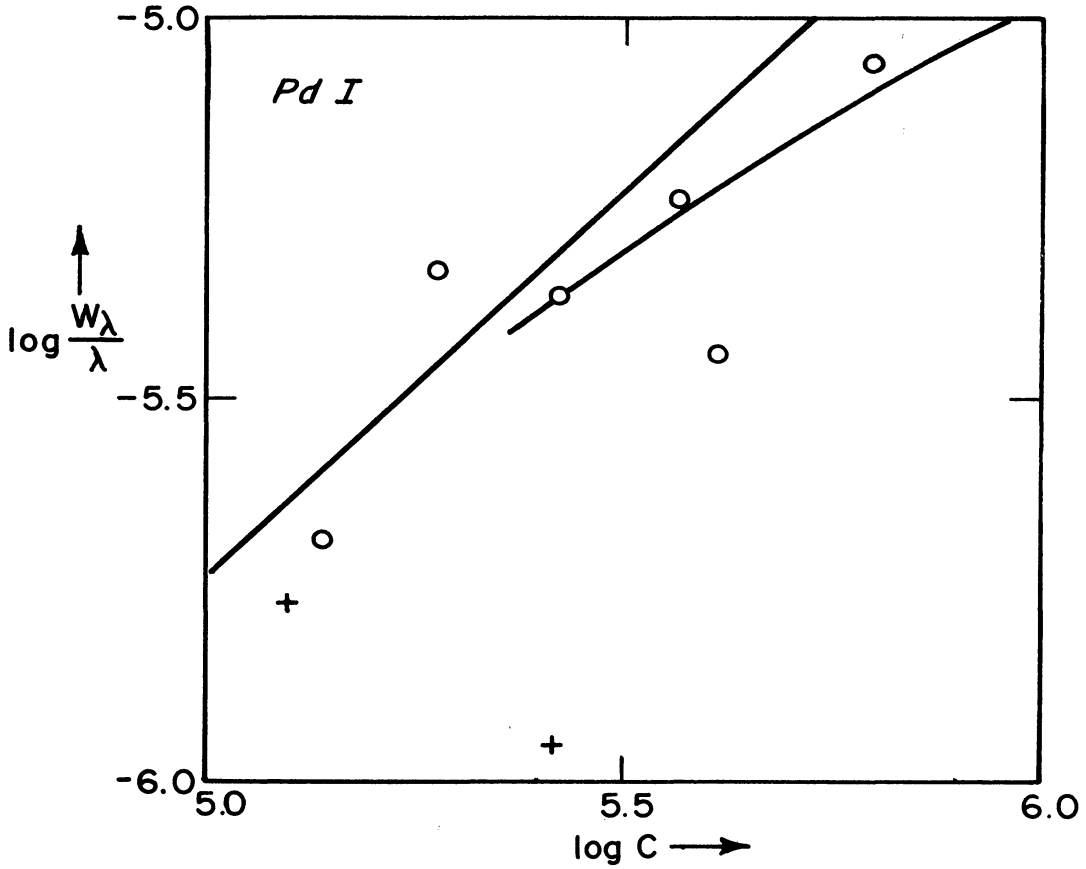

Fig. 17. Curve of growth for palladium.

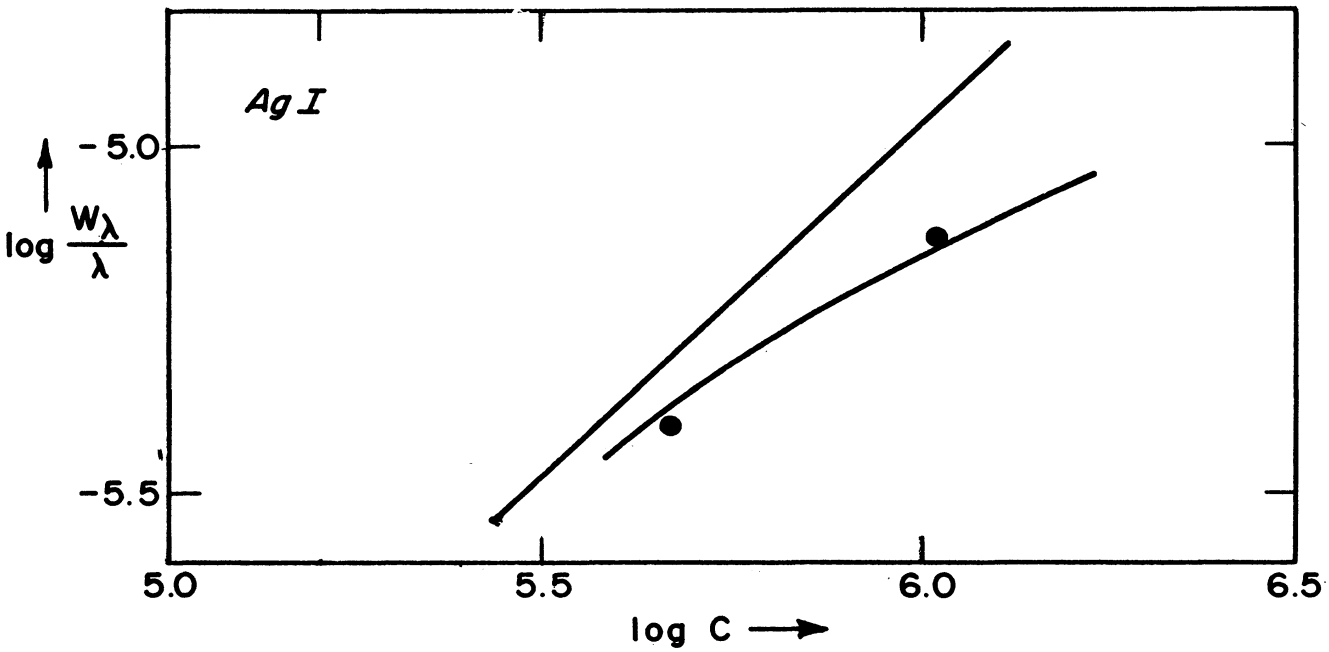

Fig. 18. Curve of growth for silver.

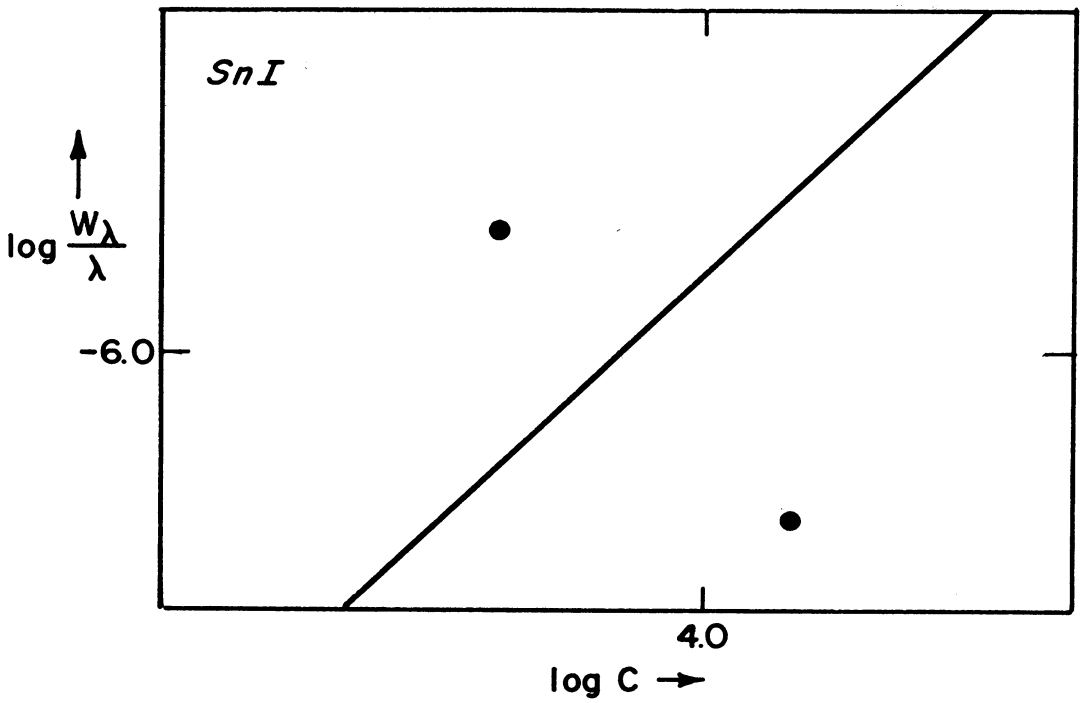

Fig. 19. Curve of growth for tin.

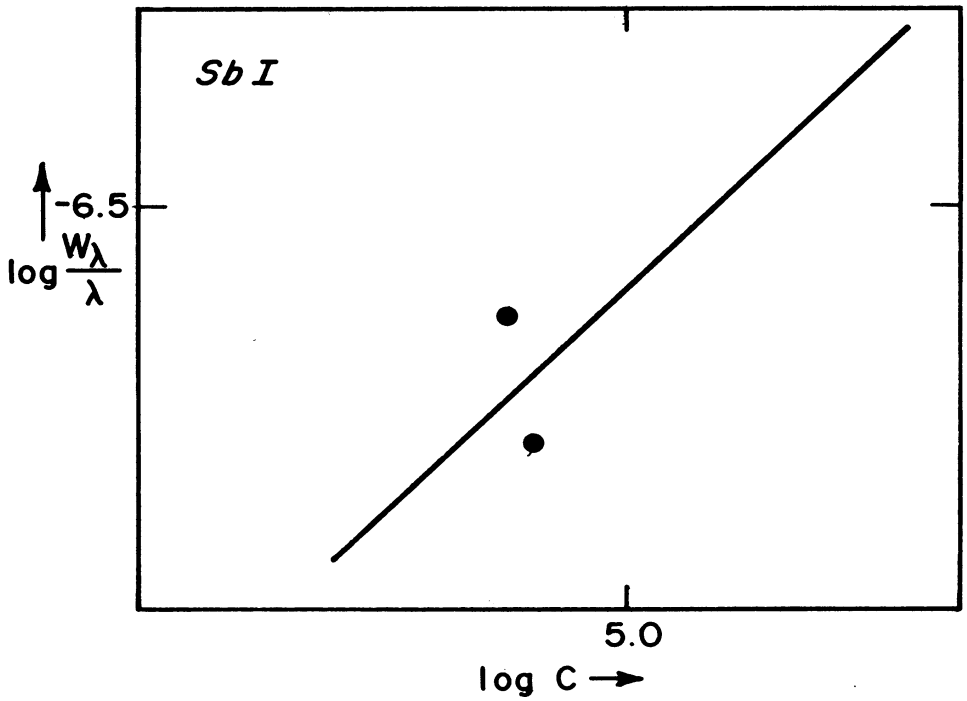

Fig. 20. Curve of growth for antimony.

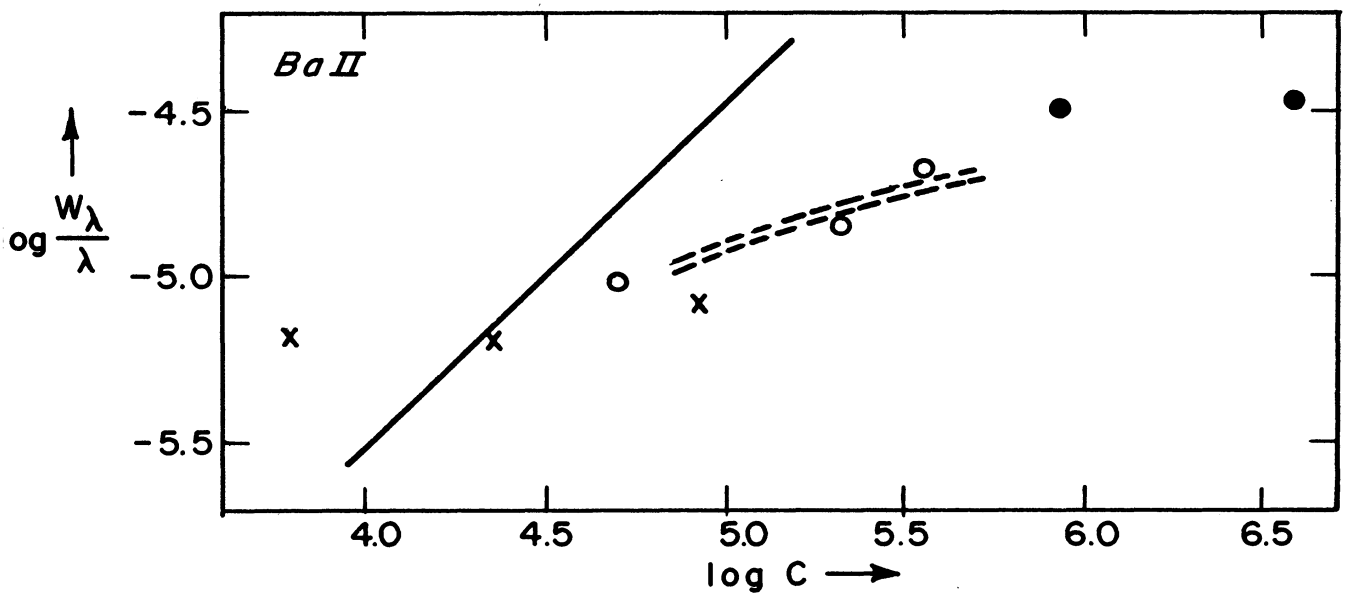

Fig. 21. Curve of growth for ionized barium.

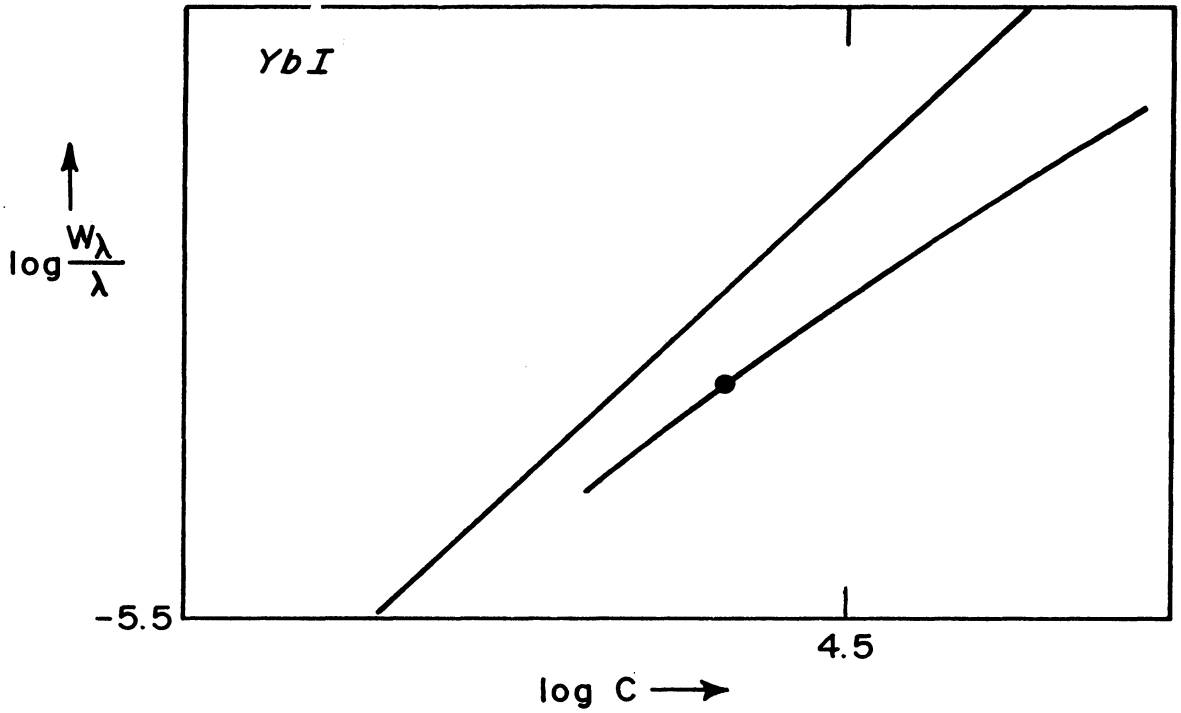

Fig. 22. Curve of growth for ytterbium.

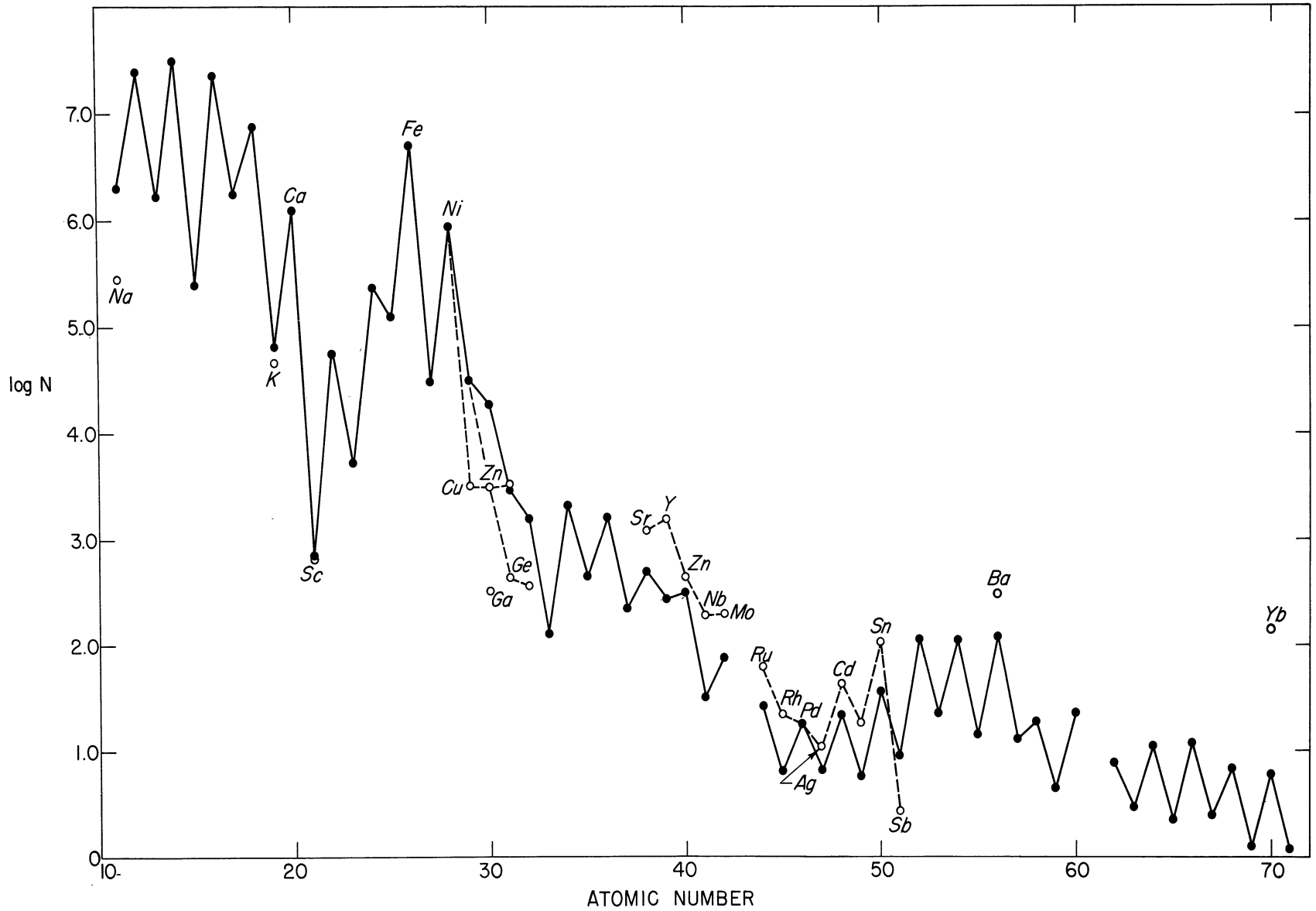

Fig. 23. Comparison of solar abundances with "standard" abundances prepared for solar systems.

T H E U N I V E R S I T Y O F M I C H I G A N

COLLEGE OF LITERATURE, SCIENCE, AND THE ARTS
Department of Astronomy

Technical Note No. 3

ABUNDANCES OF ELEMENTS I N STARS AND NEBULAE

(Spectral Line Strengths from Astrophysical Data)

L. H. Aller

ORA Project 03719

under contract with:

AIR FORCE OFFICE OF SCIENTIFIC RESEARCH
AIR RESEARCH AND DEVELOPMENT COMMAND
CONTRACT NO. AF 49(638)-807
WASHINGTON, D. C.

administered through:

OFFICE OF RESEARCH ADMINISTRATION ANN ARBOR

July 1962

PREFACE

In order to carry out studies of the chemical compositions of stars, good oscillator strength must be available. Although such data are available for lines of neutral atoms, no comparable data are available for FeII, CrII and MnII in spectral regions of astrophysical interest. It is the aim of the present study to partly fill this need with line strengths obtained from stellar spectral line data. It is hoped that these $gf\lambda$-values may be useful in laboratory as well as in astrophysical applications.

Thanks are due to Charles Corliss of the National Bureau of Standards for supplying us with gf-data for many atoms in advance of publication. I am also grateful to Prof. Lochte Holtgreven for sending us the FeII and TiII gf-measurements secured in his laboratory at Kiel. Assistance in the reduction and assessment of data was supplied by J. Bergey, W. Dent, J. Dickel, J. Ehman, J. Kirk, H. Graboske, D. Gray, G. Withbroe, Miss. C. Parks and Miss. Nancy Houk. Helpful discussions with Dr. K. O. Wright of Dominion Astrophysical Observatory are also gratefully acknowledged.

L. H. Aller
The University of Michigan Observatory
June 18, 1962

TABLE OF CONTENTS

LIST OF ILLUSTRATIONS

ABSTRACT

An attempt is made to compile empirical $\log(gf\lambda)$'s for lines of metallic ions of FeII, FeIII, CrII, TiII, and MnII. Here f is the Landenburg f, or oscillator strength, g is the statistical weight of the lower level, and λ is the wavelength of the line. The curve of growth relates the equivalent width of a spectral line to the number of atoms capable of absorbing it and to the f-value of the transition involved. If the electron pressure and temperature in the stellar atmosphere are known, relative $\log gf\lambda$'s can be determined. Furthermore, if laboratory absolute gf's are available for a few of these lines, then relative $gf\lambda$'s can all be converted to absolute $gf\lambda$'s.

The advantages and limitations of these "astrophysical" gf's are described, and it is emphasized that in order to secure adequate line strength data, one must

(a) secure good line-intensity data
(b) interpret these with the aid of a model atmosphere, taking into account effects of the stratification in the atmosphere.

The $gf\lambda$-values herein tabulated may be useful in analyzing the spectra of incandescent gases in laboratory or experimental sources of unknown temperature and pressure.

I. INTRODUCTION

Quantitative interpretation of the spectra of stars and nebulae or of the properties of an incandescent laboratory gas requires a knowledge of the transition probabilities of the observed lines. The transition probability of a line may be expressed in various ways, some of which are more convenient than others, for a particular problem. If we are concerned with emission line spectra it is most appropriate to work with the Einstein coefficient for spontaneous emission,[1,2,3] viz.,

$$A_{nn'} = \frac{g_{n'}}{g_n} \frac{8\pi^2 \epsilon^2 \nu^2}{mc^3} f_{n'n} \qquad (1)$$

Here n is the upper level of the transition involved; n' is the lower level. The symbols π, ϵ, m, and c have their usual significance; g_n and $g_{n'}$ are the statistical weights of the upper and lower levels respectively. The frequency of the transition $n \to n'$ is ν, and $f_{n'n}$ is the Landenburg f, or oscillator strength.

In working with absorption lines, as in the interpretation of stellar spectra, it is easiest to think in terms of the oscillator strength, since

$$\int \alpha_\nu \, d\nu = \frac{\pi e^2}{mc} f_{n'n} \qquad (2)$$

where α_ν is the coefficient of absorption and the integration is carried out over the line.

Since the other Einstein coefficients can be calculated immediately if one of them is known, the essential problem is to obtain either by theory or by experiment, the A-value of the f-value. In addition to these quantities, we frequently define a number S, called the strength of a transition by means of the expression

$$A(\alpha J;\alpha' J') \qquad \frac{1}{2J+1} \frac{64\pi^4 \nu^3}{3hc^3} S_1(\alpha J;\alpha' J') \qquad (3)$$

where J denotes the total quantum number of the upper level, and J' that of the lower level. Here α and α' are the designations of the upper and lower terms respectively, i.e., the quantum numbers $n\ell Ls$ and $n'\ell' L' S'$. The total strength S_1 contains two factors

$$S_1 = S(\alpha J;\alpha' J')\ \sigma^2(n\ell;n'\ell') \qquad (4)$$

where S depends only on the angular factors in the wave function. For a given type of coupling (e.g., LS or jj) it can be tabulated once and for all.[4,5] The σ^2 factor depends on the radial quantum integral involving the radial wave functions for both the upper and the lower level. For certain atoms and ions for which good wave functions are available, σ can be computed to adequate accuracy.

Inserting numerical values, we can write Eq. (1) in the form[6]

$$f_{n'n} = 1.5 \times 10^{-8}\ \lambda^2_{(\mu)}\ \frac{g}{g'}\ A_{nn'} \qquad (5)$$

where the wavelength λ is expressed in microns. Here $g = 2J+1$ and $g' = 2J'+1$ denote the statistical weights of the upper and lower levels respectively. Similarly, Eq. (3) can be written in the form

$$f = \frac{304}{g'\lambda_A} S_1 \qquad (6)$$

where λ_A denotes the wavelength expressed in angstrom units.

The spectral lines observed in the stars are legion and absolute f- or A-values have been measured for only a few of them. The experimental techniques are difficult, but by utilizing absolute measurements for a few lines of a few elements to establish the electron pressure and temperature in an incandescent gas, it is possible to convert relative f-values to tolerably good absolute gf-values. Thus, quite recently Corliss[7] has obtained gf-values for a large number of lines observed in a copper arc, to the electrodes of which small quantities of the metal under consideration had been added. This study has added a vast wealth of data which is badly needed for astrophysical investigations.

Unfortunately, however, even this valuable collection of gf-determinations does not supply enough data for certain metallic ions which are of great astrophysical importance. We refer in particular to the ions FeII, NiII, CrII, MnII, and TiII, which characterize the spectra of stars of spectral classes F, A, and late B whose surface temperatures lie between about 7500°K and 13,000°K.

Of these elements, iron would appear to be the most important. In almost every incandescent astrophysical source it appears as FeI and FeII in the solar photospheric spectrum, and as FeIII in the spectra of hotter stars such as the B2V star γ Pegasi. Emission lines of iron, both permitted and forbidden have been observed in the solar chromosphere and corona—nearly all stages from FeII to

[FeXIV]. Certain stars such as XX Ophiuchi in its emission-line phase, η Carinae, and RR Telescopii show strong lines of FeII and [FeII] (see Figs. 1 and 2). Other stars with extended envelopes and high levels of excitation show lines of [FeIII], [FeV], [FeVII], and even [FeX]! These stars include BF Cygni, CI Cygni, Z Andromedae, and T Coronae Borealis.[8] Only hydrogen ranks with iron in spectroscopic importance.

Transition probabilities for the forbidden lines of iron have been calculated theoretically. In particular, in recent years one may mention the efforts of Garstang[9] and the program recently initiated by S. Czyzak at Wright Patterson Air Force Base.

In stellar spectra and in the envelopes of the nova-like stars η Carinae and XX Ophiuchi we are particularly concerned with the permitted lines of FeII. Even with the great advances already made in the theory of atomic spectra, particularly by Racah[10] and with the possibilities opened up by modern computing techniques, reliable theoretical calculations of transition probabilities for FeII appear intractable. Similar remarks apply to the lines of NiII and CrII.

Experimental methods, notably the wall-stabilized arc and eventually the luminous shock tube, promise to give us considerable help, but at the present time, data for only a relatively few lines of FeII and TiII are available. We shall see that by using the Corliss gf-values, the above mentioned FeII gf-values obtained by Roder,[11] and a few other measurements in connection with equivalent widths of metallic ion lines measured in the sun and other stars, we can assemble a body of gf-values for lines of CrII, TiII, FeII, etc., that may be useful for the interpretation of the spectra of hotter stars. Such astrophysical gf-values may be used for comparisons of stellar atmospheres, abundance determination, etc., but they should not be taken as definitive. Efforts should be continued to obtain good laboratory and theoretical transition probabilities for all ions of astrophysical interest.

II. EMPIRICAL ASTROPHYSICAL TRANSITION PROBABILITIES

Attempts have been made to derive relative gf-values from both emission and absorption stellar spectra. For example, W. Petrie attempted to get empirical f-values from the spectrum of the sollar Chromosphere observed by the Harvard eclipse expedition.[12] Some years later[13] the present writer and his associates attempted to get relative f-values for FeII from the rich emission line spectrum of the "iron star," XX Ophiuchi.

The energy emitted per unit volume in a monochromatic line of frequency ν in an incandescent gas is proportional to the number of atoms in the upper level N_J multiplied by the Einstein A coefficient for the transition and the energy per quantum, $h\nu$, viz.,

$$E \sim N_J A h\nu \tag{7}$$

If an excitation temperature can be found so that the relative populations of the excited levels can be represented by Boltzmann's equation with a unique temperature, T_e, then relative A-values can be found in principle from measurements of the emission line intensities.

In practice, A or gf-value determinations by this method are beset by a number of severe difficulties. Since the emitting column is optically thick, self-absorption will occur and the intensity of the observed bright line will no longer be strictly proportional to the number of emitting atoms per unit volume. Second, the radiating volume may consist of strata of several different temperatures and densities. Third, within a given radiating volume there may exist substantial departures from local thermodynamic equilibrium, so that Boltzmann's formula does not represent the relative populations of the exicted levels. All of these difficulties seem to exist both in the solar chromosphere and in the envelopes of stars such as η Carinae or XX Ophiuchi. Hence the emission lines are probably useless for gf-values determinations, except perhaps for relative strengths within a multiplet.

Absorption line intensities appear to offer much better possibilities. Extensive measurements of relative gf-values were made a number of years ago by K. O. Wright[14] and by Barbara Bell.[15] Since then, many other determinations have been made in which not only solar but also stellar data were used. The studies yield relative gf-values unless the structure of the stellar atmosphere and its composition are sufficiently well known to permit one to obtain absolute gf-values.

Consider, first of all, the simplest model for a stellar atmosphere—a photosphere which radiates a continuous spectrum overlaid by a "reversing layer" which produces absorption by discrete spectral lines. For this Schuster-Schwarzschild Model, Menzel,[16] Unsöld,[2] Wrubel,[17] and others have calculated theoretical curves of growth.

The ordinate of the curve of growth is log W/λ c/v where W is the equivalent width expressed (as is λ) in Angstroms, c is the velocity of light, and v is the most probable velocity of the absorbing atoms. If there is no turbulence this will be the most probable gas kinetic velocity, but if microturbulence is present, then

$$v^2 = \frac{2kT}{M} + \xi^2 \tag{8}$$

where ξ is the most probable velocity of the turbulent elements, M is the mass of the atom, and T is the gas kinetic temperature.

The abscissa of the curve of growth (in Menzel's notation) is

$$\log X_o = \log N_r + \log g_{r,s} f\lambda - \theta\chi_{r,s} - \log v\, U_r(T) + \log \frac{\sqrt{\pi\epsilon^2}}{mc} \tag{9}$$

where

N_r = number of atoms above the photosphere in the r^{-th} stage of ionization. For neutral atoms r = 0.

$\chi_{r,s}$ = is the excitation potential (in electron volts) of the level (r,s) of statistical weight $g_{r,s}$.

θ = 5040/T where T is the excitation temperature.

v is defined by Eq. (8).

$U_r(T)$ is the partition function for the atom in the r^{-th} state of ionization. The constant $\log \sqrt{\pi\epsilon^2/mc} = -1.826$.

If, as is usually true, the coefficient of continuous absorption varies with wavelength, we must replace log N_r by log $N_r\, \kappa(\lambda_o)/\kappa(\lambda)$ where $\kappa(\lambda_o)$ is the continuous absorption coefficient at wavelength λ_o. Hence N_r refers to the number of atoms above the photosphere at λ_o.

Let us suppose that the spectrum of a given star is analyzed by curve-of-growth techniques using lines whose gf-values are known.[14,15] Then one obtains

the velocity of v and a good enough estimate of the temperature T to compute $U_r(T)$. If we are willing to suppose that the same excitation temperature, T, holds for the ions whose gf-values are unknown as for the atoms whose gf-values are known, we may use the curve of growth to derive empirical gf-values. The equivalent width, W_1, of a line λ_1 is measured in the spectrum of the star. We then calculate log W/λ c/v and enter the curve of growth (see Fig. 3), to read off the value of log X_o. From this value one can then obtain the quantity log N_r+log $gf\lambda$. It is clear that we cannot obtain the absolute value of log gf unless log N_r is known. Sometimes we can make a good estimate of log N_r if the temperature and electron pressure are known.

For example, we possess tolerably good estimates of the mean temperature and electron pressure in the solar atmosphere; T = 5700°K, $P_\epsilon \cong 11$ dynes/cm^2 are reasonable values to use. These estimates are obtained for those elements which are observed in two stages of ionization and for which gf-values are known. Suppose that we have gf-values for a neutral atom, e.g., FeI, and wish to determine gf-values for the ion FeII. We can determine the excitation temperature from the FeI lines in the following way. First we sort out the lines in groups according to their excitation potentials. For each line we have the value of log W/λ c/v and we read the value of log X_o from the curve of growth. Hence for each group of lines of a given value of lower excitation potential χ_1 we can write from Eq. (9)

$$Y_1 = \log X_o - \log gf\lambda = \log C_r - \theta\chi_1 \qquad (10)$$

Similarly, for lines of lower excitation potential χ_2,

$$Y_2 = \log X_o - \log gf\lambda = \log C_r - \theta\chi_2 \qquad (11)$$

Hence by plotting Y against χ we can determine $\theta = 5040/T_{ex}$ and log C_r. From log C_r we can compute log N_r, since v is known and $U_r(T_{ex})$ can be calculated. With the electron pressure and temperature known, the ionization level of the metal can be found, i.e., we get log N_{r+1}/N_r. For the ionic lines the process is repeated, but we now know N_{r+1}, θ, v, U(T), etc., so we can derive log $gf\lambda$ for the transitions of interest.

It is clear that any uncertainity in the abundance of the element involved, in the theory, or in the P_ϵ and T adopted will enter directly into the absolute gf's. Hence such empirical gf's are likely to be useful in comparing the spectra of similar stars, since the effects of atmospheric structure and inadequacies in the theory are likely to enter in the same direction in each instance. However, they might be less useful in the interpretation of emission spectra observed in the laboratory.

Essentially the same procedure is employed if we use the Milne-Eddington approximation, except that in place of log X_o as abscissa, one uses log η_o where

$$\eta_o = N_{r,s}\, \alpha_o / \kappa_\lambda \tag{12}$$

$N_{r,s}$ is the number of atoms per gram of stellar material in the level (r,s) capable of absorbing the line in question, α_o is essentially the coefficient of monochromatic absorption at the center of the line, and κ_λ is the coefficient of continuous absorption (defined per gram of material). The form of the curve of growth is slightly different; Wrubel[18] has published a number of such curves.

The conventional curve-of-growth approach assumes that the same curve applies to both neutral atoms and ions. In a more detailed treatment we take into account the stratification of temperature and density in the stellar atmosphere. Then each atom in each stage of ionization and excitation has its own curve of growth. Usually it is possible to use a single curve for atoms in a given stage of ionization. For example, most of the neutral metals in the sun follow rather well the curve of growth for neutral iron. The ionized metals probably require a different curve of growth.

In the version of the theory proposed by Pecker[19] and applied by Aller, Elste, and Jugaku,[20] the abscissa of the curve of growth is

$$\log C = \log g_{r,s}\, f\lambda + \Delta\chi_{r,s}\, \theta_o + \log L^*_\lambda + \log K \tag{13}$$

where K is a numerical constant that depends on the mean molecular weight of the stellar material, $\theta_o = 5040/T_o$ (where T_o may be taken as the mean temperature of the stellar atmosphere), and

$$\begin{aligned} \Delta\chi_{r,s} &= I - \chi_{r,s} \text{ (neutral atoms)} \\ &= -\chi_{r,s} \text{ (ions)} \end{aligned} \tag{14}$$

where I is the ionization potential.

Now L^*_λ is defined by an integral which involves the weighting function for the stellar atmosphere and the distribution of absorbing atoms as a function of depth.

The ordinate of the curve of growth is log W/λ. For any given line, L^*_λ can be calculated, $\Delta\chi_{r,s}\ \theta_o$ is readily computed, K is known, and log C is read from the curve of growth. Hence $\log gf\lambda$ can be determined directly. The resultant value is subject to uncertainties caused by inadequacies in the model atmosphere and by inaccuracies in the f-values.

A procedure similar to that which we have described was employed by Groth[21] to get gf-values for FeII. Instead of the Pecker theory, however, he used Unsölds curve of growth, which is similar in form to Menzel's.

The empirical method is useful for getting relative gf-values for many ions. Then, if an absolute calibration for a few lines of a given ion is known, these relative f-values can be converted to absolute f-values. This program has been carried out for CrII, FeII, and TiII, but for MnII it was necessary to use entirely empirical gf's.

III. EMPIRICAL gf-VALUES FOR FeII

We are primarily interested in obtaining gf-values for lines of ions which appear in stars of spectral classes F, A, and late B.

Among available sources of line-intensity data I have chosen the following:

K. O. Wright's compilation of data for the solar spectrum.[14]

The Utrecht catalogue of equivalent widths in the solar spectrum.[22]

W. Buscombe's measurements of equivalent widths in the A stars, α Cygni (Deneb) and γ Geminorum.[23]

Unpublished measurements in the spectrum of α Cygni secured by the writer at the Lick Observatory in 1937.

In addition to these data we have Groth's determination[21] of $\log gf$-values based on his study of the spectrum of α Cygni. With the aid of a model atmosphere for this star and Unsöld's curve of growth, he attempted to derive absolute line strengths.

Although the solar spectrum exhibits numerous lines of FeII, many of which are prominent in the spectra of hotter stars, here they are blended with neutral metal lines. Furthermore, although most iron atoms in the sun are singly ionized, the observable FeII lines arise from high levels for which the Boltzmann factor is unfavorable. Since the sun is often used as a standard for comparison with other stars, it seems worthwhile to see what information can be obtained from solar FeII lines.

The spectra of A stars would appear to offer better possibilities for determinations of gf-values. The ionic lines are still strong but blending is much less severe. The chief difficulty is that ionic lines tend to fall on the straight-line part of the curve of growth; hence a small error in the measured intensity can produce a large error in $\log gf$. Buscombe measured equivalent widths in the spectra of the dwarf γ Geminorum and the supergiant α Cygni using coudé plates secured with the 100-inch telescope at Mt. Wilson. He used Wrubel's curves of growth to obtain $\log \eta_o$'s from which $\log gf\lambda$'s could be calculated when the excitation temperature and electron pressure were determined. The Lick data consisted of equivalent widths of lines measured on Mills spectrograph plates obtained by G. F. Paddock. They covered only the region λ4300-λ4630, but many plates of excellent quality were available. Groth used Mt. Wilson coudé data.

The first step was to reduce all $\log gf\lambda$-data to Groth's system and to the

system of the solar line-strengths. In order to do this, one must know the excitation temperature, which is not necessarily the same as the ionization temperature. In fact, $\theta_{ex} \simeq 0.75$ for γ Geminorum—corresponding to a temperature somewhat lower than the ionization temperature for this star. We assumed $\theta_{ex} \simeq 1.04$ for the FeII lines in the sun—a value derived from the FeI data. It would have been better to have analyzed the solar FeII data with the aid of a model atmosphere and properly calculated contribution functions.

Figure 4 shows a plot of $\log(gf\lambda)_\alpha$ -[α Cygni - Lick data] vs. $\log(gf\lambda)$. [solar data - due mostly to Wright]. Here λ is given in Angstroms. The zero points have yet to be adjusted. We prepared a similar plot of $\log(gf\lambda)_\alpha$ vs. $\log(gf\lambda)_{Groth}$ as well as corresponding diagrams comparing the Buscombe data with those of Groth and with solar data.

In this fashion, we could reduce all our $\log gf\lambda$'s to the same system, i.e., to the same zero point—either that of Groth or the solar gf-system for which we adopted an iron abundance and a mean electron pressure and temperature for the solar atmosphere.

Although the solar-based and Deneb-based (Groth model) relative gf-values agreed reasonably will with one another, there occurred appreciable differences in the corresponding absolute gf-values. Hence the adopted atmospheric parameters and iron abundance for one star or the other (or both) must be a fault.

Hence it is most urgent to seek absolute gf-measurements for FeII. The extensive Bureau of Standards gf-value determinations[7] do not help much here, as little data are available for the spectral regions accessible to observation.

Fortunately, some absolute oscillator strengths have been measured by Roder[11] working with a wall-stabilized arc in the laboratory of Lochte-Holtgreven in Kiel. The measured transition probabilities were obtained for lines belonging to multiplets (27), 37, 38, 42, and 49 of FeII, but the absolute gf-values were obtained by calibrating these with respect to just one multiplet of FeI, multiplet 41. The gf-values for this multiplet were taken from the work of King[24] as calibrated by Bell, Davis, King, and Routly.[25]

In Figs. 5 and 6 we plot $\log gf\lambda$ as measured by Roder at Kiel against the $\log gf\lambda$-values obtained from the sun and from α Cygni (Groth). In this way we find the reduction factors necessary to express all our $\log gf\lambda$-values on the same absolute scale. Table I gives the results: we have expressed λ in centimeters. The columns headed B, A, and G refer to the $\log(gf\lambda)$ values found from the spectrum of α Cygni with data obtained by Buscombe, the present writer, and by Groth. Buscombe's γ Geminorum data supply the data for the next column; the solar data are in the next column; and the last column gives the adopted mean value. It would probably be just as satisfactory to use Groth's gf-values.

Several obvious improvements can be made. Additional stars should be ob-

served; we may mention Traving's investigation of Sirius, wherein accurate equivalent widths were measured. A reliable model atmosphere can be constructed since the temperature and surface gravity of this star are accurately known. Several other late B and A stars could be similarly investigated.

IV. ESTIMATES OF TRANSITION PROBABILITIES FOR FeIII

Lines of FeIII are often visible in the spectra of B stars. In the later subdivisions they are sometimes seen with lines of FeII—or, in the case of HR6870, are present along with lines of both FeII and FeI. These lines could be very useful in fixing the excitation tempurature of a stellar atmosphere.

In order to get empirical $\log gf\lambda$'s we shall use line-intensity measurements for γ Pegasi.[26] Jugaku, Sargent, and Greenstein[27] suggest that the excitation level of the spectrum of this star can be represented by T = 18,000°K, $\log P_\epsilon = 0.234$. We shall use Wrubel's curve of growth[19] for $B_1/B_0 = 4/3$. His curves were calculated for the Milne-Eddington approximation and the assumption

$$B = B_0 + B_1\tau \tag{15}$$

where τ is the optical depth in the continuum in the neighborhood of the line. The ordinate of the theoretical curve of growth is

$$\log \frac{W}{\lambda}\frac{c}{v} = \log \frac{W}{\lambda}\frac{c}{\sqrt{\frac{2kT}{M} + \xi_t^2}} \tag{16}$$

and the abscissa is

$$\log \frac{\eta_c}{N_r} = \log \frac{\sqrt{\pi\epsilon^2}}{mc^2} - \log v - \log U(T)$$

$$+ \log gf\lambda - \theta\chi_{r,s} - \log \kappa_\lambda(T,P_\epsilon) \tag{17}$$

The turbulent velocity ξ_t, is 4.5 km sec^{-1} according to Struve and Mrs. Böhm-Vitense.[28] We interpolate the coefficient of continuous absorption from Allen's[29] tables for $\log P_\epsilon = 2.34$, $\theta = 5040/T = 0.278$. Putting in numerical values, $\log v = 5.70 \log U(\text{FeIII}) = 1.73$, $\log \kappa$ varies from 0.04 at λ4000 to 0.225 at λ5000. The abundance of iron in γ Pegasi is not known *a priori*, so we have assumed it to be the same as in the sun; each gram of stellar material is presumed to contain 1.42×10^{18} iron atoms. By application of the ionization equation we find $N(\text{FeIII})/N(\text{Fe}_{\text{total}}) \cong 0.83$.

Details of this calculation are given in Table II. Successive columns give the wavelength of the line, the multiplet number according to the Revised Multiplet Table,[30] the excitation potential χ (in e.v.), the equivalent width of the lines in mA (B indicates a blend), $W/\lambda \times 10^6$, log W/λ c/v (of Eq. 16), log κ_λ, and log η_0. The last two columns give the quantities: $-\theta\chi$ + log $gf\lambda$ and log $gf\lambda$ (calculated for $\theta = 0.278$). Notice the marked increase of log $gf\lambda$ with excitation potential. The probable explanation of this phenomenon is as follows: In the atmosphere of γ Pegasi the high excitation lines arise in the deeper layers where the Boltzmann correction $-\theta\chi$ is smaller, whilst the low excitation lines originate in the cooler, shallower layers where $\theta\chi$ is larger. The curve of growth procedure uses the same value of θ for <u>all</u> levels; hence a systematic error in log $gf\lambda$ is introduced. When we compare two stars, the same approximation is employed in both, and the errors tend to cancel out. Hence the numbers in the last column are in error, if they are interpreted strictly as log $gf\lambda$ values.

V. TRANSITION PROBABILITIES FOR TiII, CrII, AND MnII

A. IONIZED TITANIUM

Experimental transition probabilities for TiII in the astrophysically important range from 3000A to 8000A has been measured by R. B. King and A. S. King,[31] by J. B. Tatum[32] by K. H. Wobig,[33] and by C. Corliss.[7] For many lines not measured by these authors we can use empirical $gf\lambda$'s from the solar curve of growth, calibrating them with the laboratory gf-values. Both Tatum and Wobig calibrated the gf-values from the sum rules, whereas Corliss interpreted his relative gf-values with aid of the measured temperature and electron density in the arc.

Since gf-values are available for both TiI and TiII we can solve for the ionization equilibrium in the sun. Assuming $T_{ion} = 5700°K$, we get $\log P_e \cong 1.12$. This (P_e,T) combination can then be used to get rough estimates of absolute $\log gf\lambda$-values for other ions, such as NiII or MnII, for which no other data are available.

For getting the solar $\log gf\lambda$-values, we employed Menzel's curve of growth as revised by Wright, and read off $\log X_o$ values corresponding to the observed $\log W/\lambda$'s. The lines whose $gf\lambda$-values were known permitted calculation of the quantity

$$Y = \log X - \log gf\lambda = \log C_r - \theta\chi \qquad (18)$$

Then, by plotting Y for each multiplet against χ, the excitation potential of the lower term, we obtained $\log C_r$ and θ_r. Two independent solutions in which different weights were used for different lines gave $\theta_{ex} = 1.03$ and 1.12, corresponding to excitation temperatures of 4500°K and 4900°K respectively.

Table III gives the final results. The first three columns give the wavelength of the line, the multiplet number, and the excitation potential. The next three columns give $\log gf$ as measured by Corliss, Tatum, and Wobig. The seventh column gives

$$F = \left(\frac{W}{\lambda}\right) \times 10^6 \qquad (19)$$

noting important blends, and the last column gives the finally adopted value of $\log gf\lambda$. Where laboratory data are available they are used; where they are not we have resorted to empirical solar $\log gf\lambda$'s.

B. IONIZED CHROMIUM

Ionized chromium represents a more difficult problem. Our treatment is similar to that for FeII in that we employ data from both the sun and α Cygni, including Groth's empirical log gf-values for Deneb. Absolute gf-values are available for only a few CrII lines in the astrophysically important region λ3800-λ5000A. The data for the calibration are given in Table IV. The columns headed "Theory and Laboratory" consist of relative strengths for multiplet 44 (CrII) computed for LS coupling calibrated with Corliss' measurement for λ4558.68. For other lines, laboratory gf-determinations are available.

Table V gives the finally adopted log $gf\lambda$-values for CrII, based on both solar and α Cygni equivalent widths and calibrated with the aid of the data in Table IV. Since the absolute calibration depends on very few lines, additional measurements of gf-values for CrII are urgently needed.

A plot of log $gf\lambda$-values obtained from solar line intensities against corresponding quantities obtained by Groth from his study of α Cygni show a considerable scatter, probably partly due to blends. These blends are likely to be much more serious in the sun then in the hotter star, whose spectrum is much less crowded with lines and consists mostly of lines of ions. Accordingly, we have given greater weight to Groth's data in forming the final means in Table V.

C. IONIZED MANGANESE

The A-star 53 Tauri is characterized by strong lines of Manganese, particularly those of MnII. The stronger lines of MnI are also observed in this star; the f-values for the resonance lines have been measured by a number of experimenters.

Determination of log $gf\lambda$ for MnII lines from solar of stellar curves of growth are beset with a number of severe difficulties. In most A-stars the MnII lines are few and weak; lines of this ion appear in the sun (cf. Table VI). In Table VI the first three columns give the lines, multiplet numbers, and excitation potentials. The fourth column gives the intensity of the line divided by the wavelength, i.e., W/λ, multiplied by 10^6. These lines are all extremely weak, with Rowland intensities of 0, -1, and -2. We have selected only those lines that are believed to be reasonably free of blends. In any event, the intensities are subject to large, random, observational errors. This cause alone would disqualify them from consideration as reliable sources of line-strength data.

Column 5 gives the quantity log $S/\Sigma s$ (where s denotes the strength of the line, and Σs the total strength of the whole multiplets). These quantities are calculated for LS coupling. Unfortunately MnII does not follow LS coupling, so theoretical calculations of even relative f-values will not be possible unless

an intermediate coupling theory along with other refinements are used. Multiplet (2) represents an intercombination, $a^5D - z^7P$, while multiplets (7) violate the LS coupling scheme because the initial and final terms arise from different parents, i.e., a^4F and a^4P of MnIII. We would expect the gf-values for multiplet (2) to be smaller than those for multiplets (6), (7), and (8)—a prediction that seems to be substantiated by the data.

The last column gives $\log gf\lambda - \theta\chi$ as derived from the solar MnII lines. We assumed a solar $\log P_e$ and T, as described above. The MgI lines were used to fix the constants in the abscissa of the curve of growth. The ionization equilibrium and adopted M_n abundance permits one to calculate $\log gf\lambda - \theta\chi$. Notice that most of the available lines have a rather high excitation potential; only the levels of multiplet (2) lie within 2 volts of the ground level. It is unlikely that the same value of θ applies to both these levels since the 5.37-volt lines must originate, on the average, in deeper layers than the 1.8-volt lines.

We conclude therefore that the solar data give us no help in establishing usable $\log gf\lambda$-values for MnII; it would be better to invert the procedure and obtain $\log gf\lambda$-values from the MnII lines in 53 Tauri and other Manganese stars, using preferably a model atmosphere technique. In the meantime, laboratory investigations should be pushed further in an effort to obtain absolute gf-values for at least a few lines of MnII. Perhaps the luminous shock tube can yield satisfactory results.

REFERENCES

1. E. Condon and G. Shortley, Theory of Atomic Spectra, Cambridge University Press, 1935.

2. A Unsöld, Physik der Sternatmosphären, Springer-Verlag, Berlin, 1955.

3. L. H. Aller, Atmospheres of the Sun and Stars, (Chapter 5), Ronald, New York, 1953.

4. L. Goldberg, Astrophysical Journal, Vol. 82, 1935, p. 1; and Vol. 84, 1936, p. 11.

5. H. E. White, Introduction to Atomic Spectra, McGraw-Hill, New York, 1934, p. 439.

6. D. R. Bates and A. Damgaard, Philosophical Transactions of the Royal Society of London, Series A, Vol. 242, 1949, p. 101.

7. C. Corliss, National Bureau of Standards (in press).

8. See e.g., J. Sahade, "Composite and Combination Spectra," and D. B. McLaughlin, "Spectra of Novae" in Stars and Stellar Systems, ed. by J. L. Greenstein, University of Chicago Press, 1960.

9. R. Garstang, Monthly Notices of the Royal Astronomical Society (in press).

10. G. Racah, Physical Review, Vol. 61, 1942, p. 186; Vol. 62, 1942, p. 438; Vol. 63, 1943, p. 367; Vol. 76, 1949, p. 1352.

11. O. Roder, Zeitschrift für Astrophysik (in press).

12. W. Petrie, Unpublished Thesis, Harvard University, 1942.

13. L. H. Aller in Proceedings of the Indiana National Science Foundation: Conference on Stellar Atmospheres, ed. by M. Wrubel, 1954.

14. K. O. Wright, Publications of the Dominion Astrophysical Observatory, Vol. 8, 1948, p. 1.

15. B. Bell, Special Report 25, AMC Contract W19-122ac-17, Harvard University Observatory, 1949.

16. D. H. Menzel, Astrophysical Journal, Vol. 84, 1936, p. 462.

17. M. Wrubel, Astrophysical Journal, Vol. 119, 1954, p. 51.

18. M. Wrubel, Astrophysical Journal, Vol. 109, 1949, p. 66; Vol. 111, 1950, p. 157. (See also the curve of growth for pure absorption quoted in Greenstein (Ref. 8), p. 199.)

19. J. C. Pecker, Annales d'Astrophysique, Vol. 14, 1951, p. 383.

20. L. H. Aller, G. Elste, and J. Jugaku, Astrophysical Journal Supplement, Vol. 3, No. 25, 1957, p. 1.

21. H. G. Groth, Zeitschrift für Astrophysik, Vol. 51, 1961, p. 206.

22. Utrecht Observatory Publications, Vol. 12, 1960.

23. W. Buscombe, Astrophysical Journal, Vol. 114, 1951, p. 73.

24. R. B. King and A. S. King, Astrophysical Journal, Vol. 87, 1938, p. 24.

25. G. D. Bell, M. H. Davis, R. B. King, and P. M. Routly, Astrophysical Journal, Vol. 127, 1958, p. 775.

26. L. H. Aller and J. Jugaku, Astrophysical Journal Supplement, Vol. 4, 1959, p. 109; Astrophysical Journal, Vol. 127, 1958, p. 125.

27. J. Jugaku, W. L. Sargent, and J. L. Greenstein, Astrophysical Journal, Vol. 134, 1961, p. 783.

28. O. Struve and E. Bohm-Vitense, Astrophysical Journal, Vol. 123, 1956, p. 288.

29. C. W. Allen, Astrophysical Quantities, Athlone Press, London, 1955.

30. C. Moore, "Revised Multiplet Table," Princeton University Observatory Contribution No. 20, 1945.

31. R. B. King and A. S. King, Astrophysical Journal, Vol. 94, 1941, p. 27; Vol. 95, 1942, p. 78.

32. J. B. Tatum, Monthly Notices of the Royal Astronomical Society, Vol. 112, 1961, p. 311.

33. K. H. Wobig, Zeitschrift für Astrophysik (in press).

TABLE I

EMPIRICAL LOG $gf\lambda$-VALUES FOR SINGLY IONIZED IRON FeII

	Deneb			γ		Adopted
λ	B	A	G	Geminorum	Sun	Mean
3762.94			-5.99			-5.99
3781			-7.22		-7.25	-7.23
3783.39			-7.51		-7.24	-7.50
3824.95			-7.31		-6.58	-7.30
3827.07			-6.95		-6.43	-6.92
3845.18			-6.52			-6.52
3864			-7.03			-7.03
3935.96	-5.37		-5.65	-4.88		-5.60
3938.31	-7.95			-7.82		-7.90
3938.95	-5.27		-5.86	-5.36	-5.31	-5.80
3960.90	-4.82					
3975			-6.48		-5.52	-6.45
4024.55	-6.19			5.85		-6.00:
4044			-6.66			-6.66
4122.64	-6.88		-7.57		-7.90	-7.57
4128.74			-7.85		-7.31	-7.82
4173.48	-6.74		-6.76	-6.54		-6.75
4177.69			-7.75		-6.88	-7.75
4178.86	-6.73		-6.45	-6.91		-6.67
4233.18	-5.77		-6.10	-6.43	-6.05	-6.04
4258			-7.53			
4273.33	-7.28		-7.55	-7.36		-7.45
4296.56	-6.99	-7.24	-7.15	-7.00	-6.91	-7.03
4303.19	-6.53	-6.91	-6.70	-6.83	-6.57	-6.65
4351.76	-6.22	-6.41	-6.17			-6.25
4369			-7.66			
4385.39	-6.73	-6.79	-6.67	-6.83	-6.59	-6.66
4416.81	-6.80	-6.92	-6.74	-6.89	-6.86	-6.80
4473			-7.63			
4489.17	-6.97	-7.03	-7.04	-6.97	-7.33	-7.05
4491.42	-6.86	-6.91	-6.93	-7.02	-7.00	-6.90
4508.28	-6.53	-6.39	-6.52	-6.74	-6.77	-6.60
4515.33	-6.61	-6.71	-6.62	-6.72	-6.84	-6.67
4520.20	-6.56	-6.83	-6.68	-6.83	-6.91	-6.73
4522.60	-6.17	-6.42	-6.30	-6.44	-6.23	-6.25
4541.55	-6.89	-7.08	-7.11	-7.06	-6.54	-7.01
4555.89	-6.47	-6.52	-6.45	-6.48	-6.81	-6.52
4576.30	-6.98	-7.08	-7.02	-6.99	-7.28	-7.08
4582.85		-7.21	-7.25	-7.06	-7.44	-7.26
4583.82	-6.02	-5.93	-6.05	-6.35	-6.08	-6.06
4629.34	-6.50	-6.65	-6.54	-6.64		-6.55
4635.33	-5.00		-5.64	-5.05		-5.60:

TABLE II

EMPIRICAL LOG $gf\lambda$-VALUES FOR DOUBLY IONIZED IRON, FeIII, DERIVED FROM THE SPECTRUM OF γ PEGASI

λ	Multiplet	χ	W	$\frac{W}{\lambda} \times 10^6$	$\log \frac{W}{\lambda}\frac{c}{v}$	$\log \kappa_\lambda$	$\log \eta_o$	$-\theta\chi + \log gf\lambda$	$\log gf\lambda$*
4371.38	4	8.21	5B	1.1	-1.17	0.11	-0.98	10.68	-7.39
4382.56		8.21	10	2.3	-0.87	0.11	-0.67	9.37	-7.08
4352.58		8.21	11	2.6	-0.82	0.11	-0.62	9.33	-7.04
4415.55		8.21	30	6.8	-0.40	0.12	-0.12	8.82	-6.53
4431.03		8.21	22B	5.0	-0.53	0.12	-0.29	8.88	-6.69
4022.38	45	11.53	11	2.7	-0.79	0.04	-0.59	9.35	-6.14
4039.21		11.53	10	2.5	-0.83	0.05	-0.62	9.38	-6.17
4122.02	118	20.51	14	3.4	-0.70	0.06	-0.49	9.23	-3.53
4164.92		20.54	31B	7.4	-0.36	0.07	-0.06	8.79	-3.09
4137.71		20.52	24	5.8	-0.46	0.07	-0.21	8.94	-3.24

*See text

TABLE III

TRANSITION PROBABILITIES FOR IONIZED TITANIUM, TiII

λ	Multiplet	log χ	log C	log W	log T	F (Eq. 19)	Blend	Solar and Stellar
3679.71	75	1.57				24.7		-4.70
3706.24	73	1.56	-0.05			37.2		-4.48
3741.65	72	1.57	0.31			44.6		-4.12
3757.68	72	1.56	-0.08			46.8		-4.51
3759.29	13	0.60	0.34			115		-4.09
3761.32	13	0.57	0.24			16		-4.19
3761.87	107	2.58	0.45					-3.97
3813.39	12	0.60				38		-5.25
3814.59	12	0.57				33.6	CN	-5.41
3882.30	40	1.11				30.9	CN	-4.93
3900.54	34	1.13	-0.02		-0.08	41		-4.43
3913.48	34	1.11	-0.06		-0.20	39.4		-4.47
3932.02	34	1.13	-1.20		-1.53	34.7		-5.41
3982.01	11	0.57				20.7		-6.28
3987.60	11	0.60				14.8		-6.99
4025.14	11	0.60	-1.69			20.9		-6.08
4028.35	87	1.88	-0.42		-0.81	22.3		-4.81
4029.68	87	1.88				26.8		-4.28
4053.80	87	1.88				16.0		-5.41
4161.53	21	1.08				23.1	Fe	-5.58
4163.66	105	2.56	0.45			25.7		-3.93
4171.92	105	2.59	0.22			21.6		-4.16
4174.10	105	2.59				9.8		-6.76
4184.32	21	1.08				18.2		-6.02
4287.89	20					21.0		-5.72
4290.23	41	1.16	-0.79	-0.80	-0.68	27.3		-5.02
4294.10	20	1.08	-0.79					-5.16
4300.06	41	1.18	-0.55	-0.47	-0.40	38.6		-4.92
4301.53	41	1.16	-0.95	-1.25	-1.17	34.4		-5.32
4307.88	41	1.16		-1.15	-1.00			-4.99
4312.88	41	1.18	-0.94	-1.14	-1.14	35.5	CH	-5.30
4314.99	41	1.16		-1.15	-0.96	28.0		-5.02
4320.99	41	1.16				16.4		-6.17
4330.24	94	2.04				9.7		-5.94
4337.93	20	1.08	-0.78	-0.97	-0.89	24		-5.14
4350.84	94	2.05				14		-5.46
4367.66	104	2.38		-0.82		22.4	CH	-4.00

TABLE III (Concluded)

λ	Multiplet	log χ	log C	log W	log T	F (Eq. 19)	Blend	Solar and Stellar
4386.88	104	2.59		-0.96		13.4		-5.08
4394.07	51	1.22				18		-5.87
4395.04	19	1.08	-0.46	-0.47	-0.30	30.7		-4.82
4395.85	41	1.24				15.0		-6.34
4399.78	51	1.23	-1.06	-1.11	-1.20	26.4		-5.42
4409.25	61	1.24				6.8		-6.90
4409.51	61	1.23				7.9		-6.93
4411.90	61	1.22				12.0		-6.65
4417.72	40	1.22		-1.17	-1.15	22.4		-5.46
4418.34	51	1.23				15.8		-6.19
4421.94	93	2.05				11.5		-6.88
4443.80	19	1.08	-0.65	-0.64	-0.64	30.8		-5.00
4444.54		1.11				12.4		-6.69
4450.48		1.08		-1.46	-1.46	17.8		-5.68
4456.64	115	3.11				15.9		-4.10
4464.45	40					15.2		-6.33
4468.50	31	1.13				29.3		-4.99
4469.13						11.0		-6.74
4488.33	115	3.11	0.28	-0.44	-0.46	10.7		-4.07
4501.28	31	1.11	-0.68	-0.70	-0.79	29.1		-5.03
4518.34	18					10.0		-6.84
4529.49		1.56				13.0		-6.11
4533.97	50		-0.50	-0.46		24	Co	-5.84
4544.02	60					7.7		-6.86
4470.85	40					12.5		-6.58
4549.64	38		-0.16	-0.08	-0.14	32.5		-4.64
4563.77	50	1.22	-0.87	-0.72	-0.84	28.0		-5.21
4568.33	40	1.22				6.1		-7.17
4571.96	82	1.56	-0.18	-0.19	-0.24	29.7		-4.52
4589.92	50	1.23	-1.51	-1.43	-1.81			-5.85

TABLE IV

DATA FOR CALIBRATION OF LOG $gf\lambda$ FOR IONIZED CHROMIUM, CrII

	log $gf\lambda$			log $gf\lambda$	
λ	Theory and Laboratory	Solar	λ	Theory and Laboratory	Solar
3677.69	3.37	3.58	4634.08	2.83	3.18:
3677.91	3.55	3.97	4616.63	2.43	2.94:
3712.95	3.67	3.42	4588.21	3.52	3.44:
4012.55	4.62	4.57	4558.66	3.78	3.58
			4554.99	2.74	2.99:

TABLE V

TRANSITION PROBABILITIES FOR IONIZED CHROMIUM, CrII

λ	log $gf\lambda$	λ	log $gf\lambda$	λ	log $gf\lambda$
3677.69	-4.62	4051.97	-6.25	4284.18	-5.48
3677.91	-4.44	4070.86	-3.41	4554.99	-5.15
3712.95	-4.33	4111.00	-5.87	4558.64	-4.22
3738.38	-5.67	4145.78	-3.31	4565.74	-5.63
3765.61	-5.94	4179.43	-4.35	4588.20	-4.47
4003.30	-3.80	4252.62	-5.60	4592.08	-5.20
4012.55	-3.38	4261.92	-5.06	4616.55	-5.11
4038.00	-3.36	4269.27	-5.88	4618.81	-4.90
4049.13	-2.59	4275.58	-5.40	4634.07	-4.82

TABLE VI

DATA PERTAINING TO TRANSITIONS OF IONIZED MANGANESE, MnII

λ	Multiplet	χ	F	log S/ΣS	log gfλ -θχ
07.25	(2)	1.82	0.6		-10.69
05.37		1.80	9.8		- 9.33
38.79		1.82	5.2		- 9.69
30.47		1.84			
34.42	(6)	5.35	6.3	-1.24	- 9.60
00.20		5.36	11.9	-1.35	- 9.18
43.97		5.37	11.5	-0.55	- 9.21
45.60		5.37	2.3	-1.50	- 9.09
06.43	(7)	5.37	14.0	-0.50	- 9.00
44.27		5.35	2.1	-1.10	-10.13
06.91	(8)	5.37	5.1	-1.50	- 9.70
08.05		5.37	16.5	-0.74	- 8.67
29.50		5.37	2.4	-1.35	-10.07

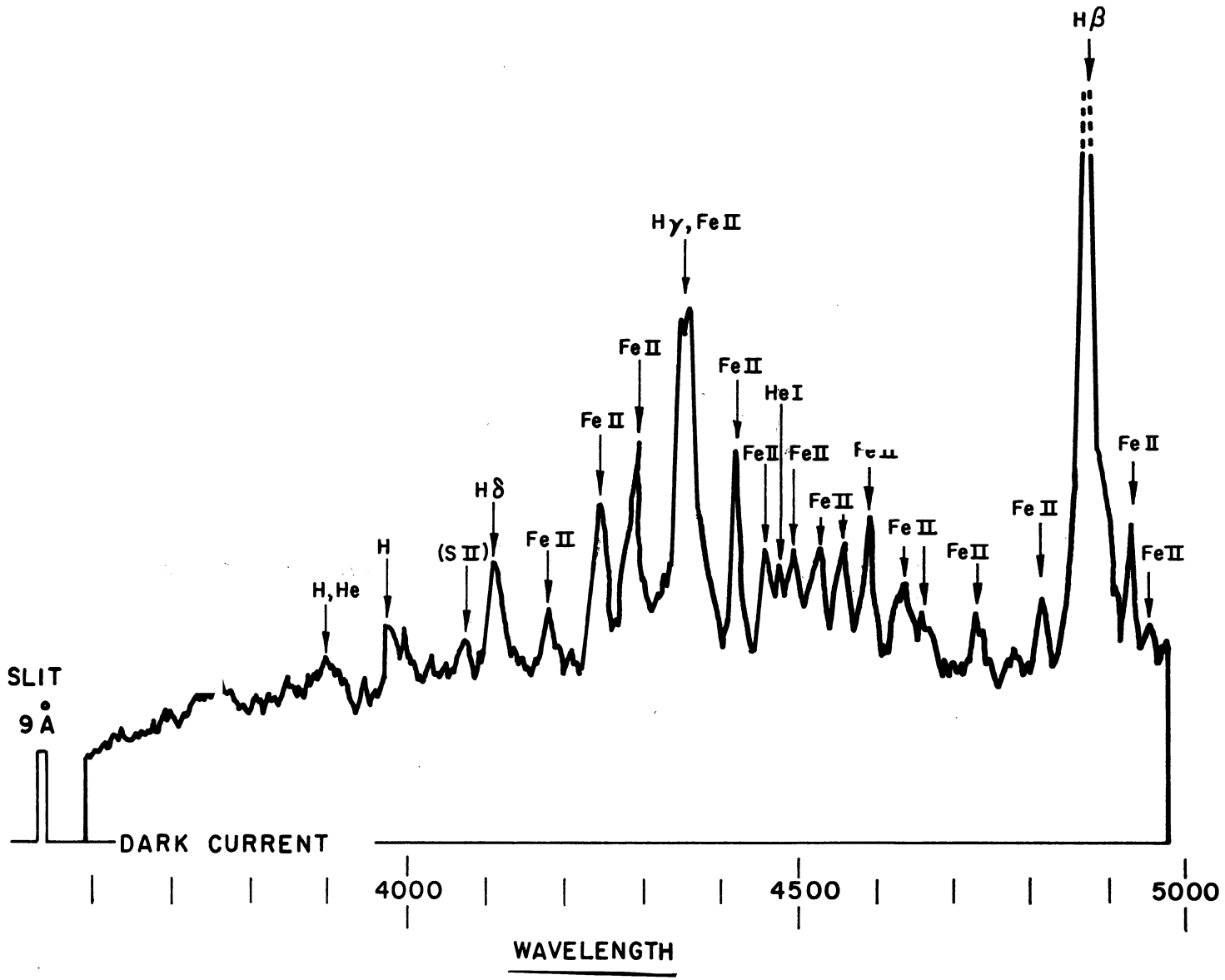

Fig. 1. Spectral scan of η Carinae. This trace was obtained with a photoelectric scanning spectrometer by D. J. Faulkner and L. H. Aller at the Mt. Bingar field station of the Mount Stromlo Observatory. The resolution is about 9A, so that many of the FeII lines are blended.

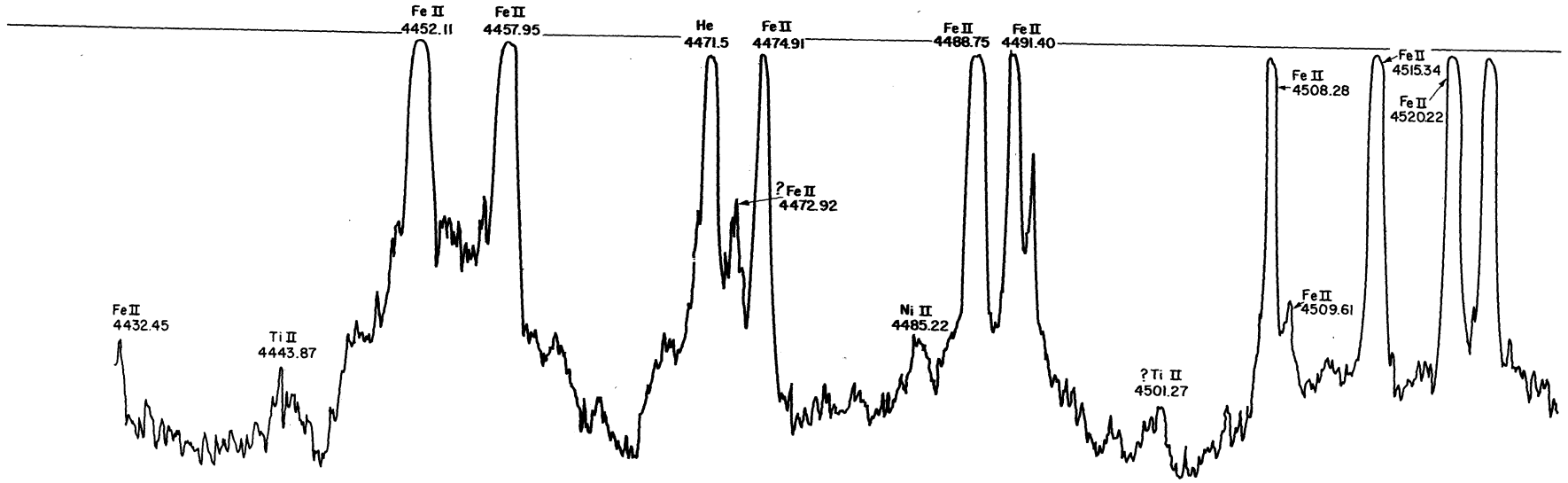

Fig. 2. Tracing of a portion of the spectrum of η Carinae. This is a part of a microphotometer tracing of a coude' spectrogram of η Carinae secured at Mt. Stromlo Observatory. Notice the dome-shaped profiles and sharp spikes of individual emission lines, indicating complicated physical conditions in the radiating gas. (Courtesy T. Dunham)

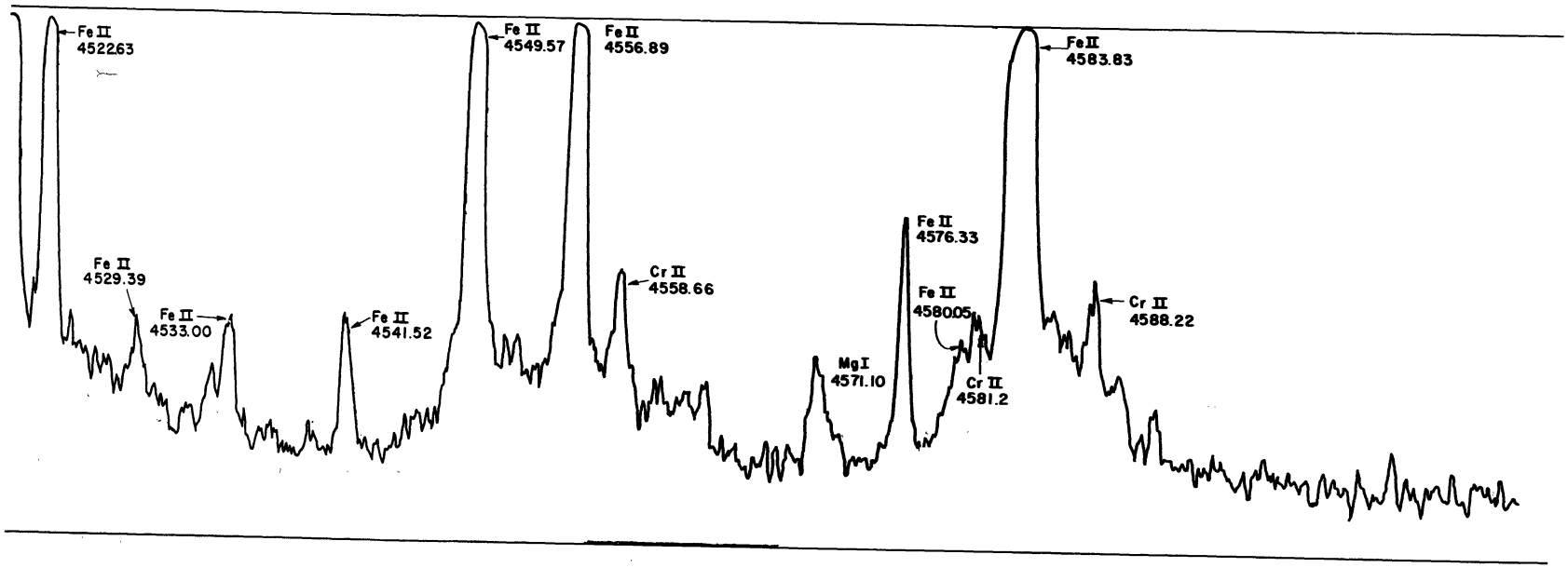

Fig. 2 concluded.

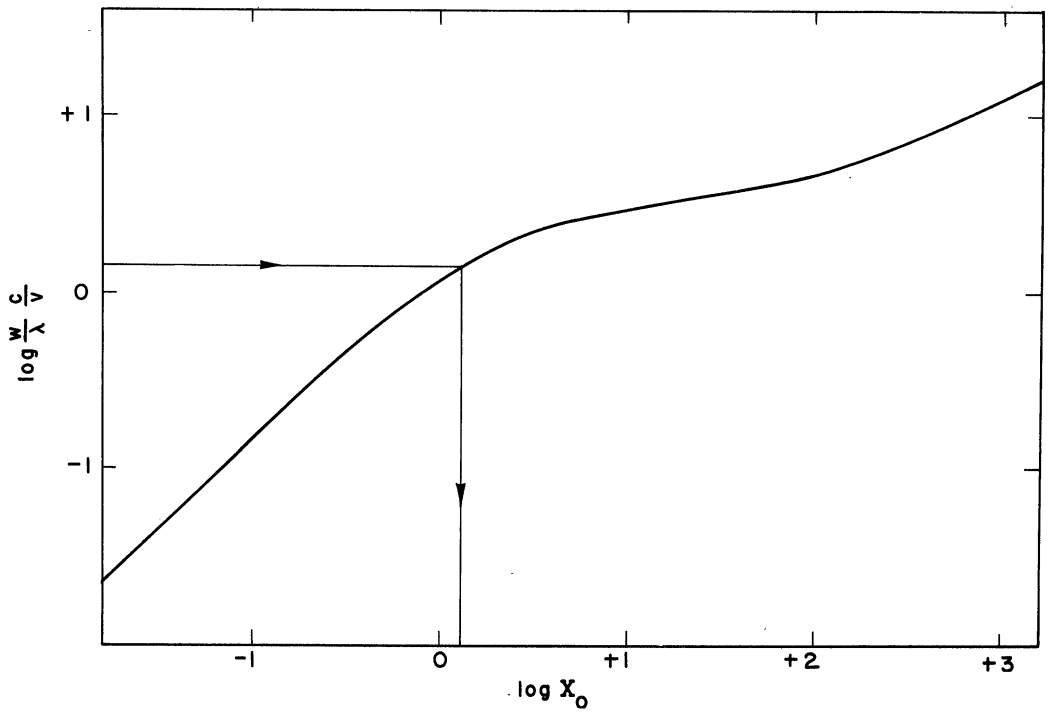

Fig. 3. Determination of $gf\lambda$ values from the curve of growth. For each line whose equivalent width W is known, one calculates log W/λ c/v and reads log X_o from the curve of growth.

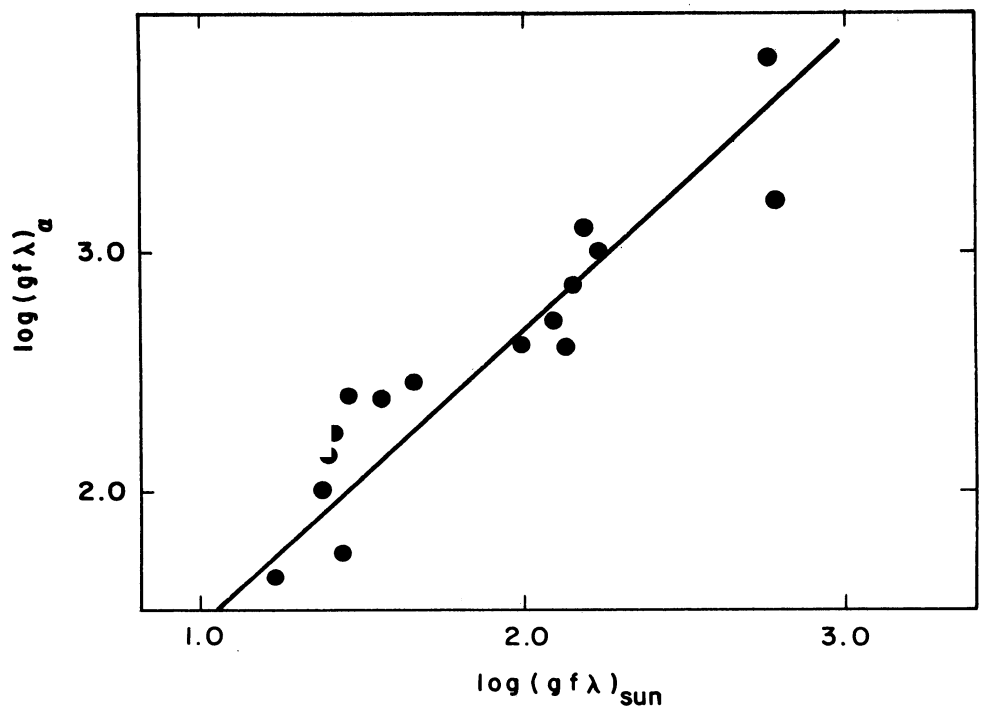

Fig. 4. Ionized iron line-strength solar data, compared with α Cygni line-strength data.

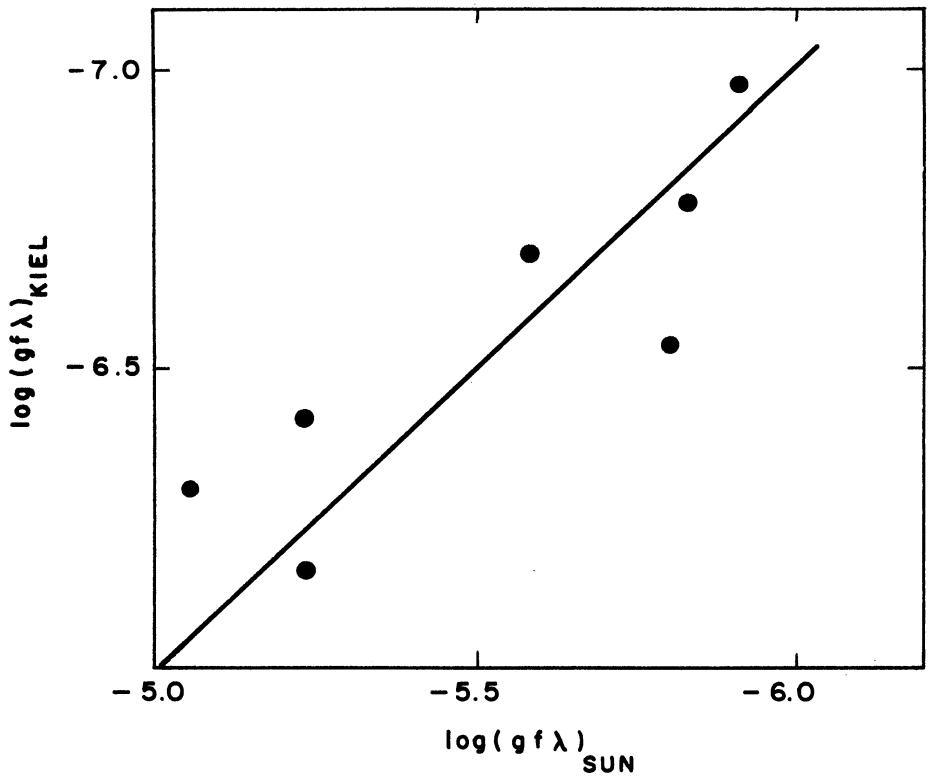

Fig. 5. Calibration of solar log $gf\lambda$ FeII data by comparison with laboratory log $gf\lambda$ data.

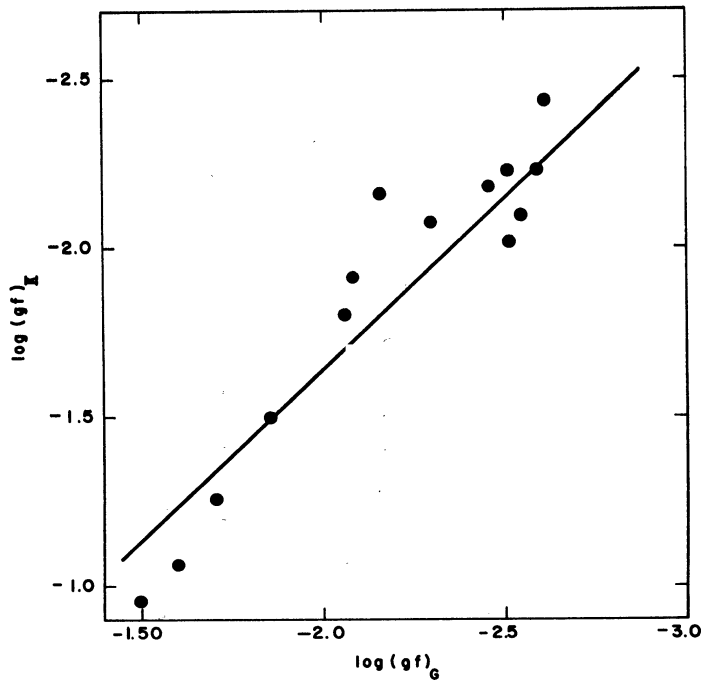

Fig. 6. Calibration of Groth's log gf's for FeII by comparison with laboratory data.

THE UNIVERSITY OF MICHIGAN
COLLEGE OF LITERATURE, SCIENCE, AND THE ARTS
Department of Astronomy

Technical Note No. 4

ABUNDANCES OF ELEMENTS IN STARS AND NEBULAE
(Determination of Ratio of Gas Pressure to Electron Pressure in Stellar Atmospheres)

C. Cowley
A. Cowley
L. Aller

ORA Project 03719

under contract with:

AIR FORCE OFFICE OF SCIENTIFIC RESEARCH
AIR RESEARCH AND DEVELOPMENT COMMAND
CONTRACT NO. AF 49(638)-807
WASHINGTON, D.C.

administered through:

OFFICE OF RESEARCH ADMINISTRATION ANN ARBOR

July 1962

ABSTRACT

The ratio of gas pressure to electron pressure has been computed over a range of temperatures by an approximate method and also by a more exact IBM 709 program. The approximate method shows large errors at low temperatures and high gas pressures. Tables I through III give the values of log P_g and log P_ϵ computed by the 709 as well as the relative abundances to which these values refer.

I. INTRODUCTION

A knowledge of the relationship between the gas and electron pressure (P_g and P_e) is necessary before one can begin to construct a model stellar atmosphere. All sources of opacity, whether discrete or continuous, depend upon the number of atoms or particles in the line of sight which are capable of absorbing a quantum of the frequency considered. For any given over-all chemical composition, the availability of a particle for the absorption of a photon of frequency will depend upon the "state" of ionization and excitation of the particle considered. Thus in general, only a fraction of the particles will be able to produce an absorption (or emission) at a given frequency, and this fraction may be determined with the aid of the Boltzmann and Saha, or ionization, equations. The purpose of the program described below is to find the relationship between the gas and electron pressures for a given chemical composition. So long as we are not concerned with the states of excitation among the various degrees of ionization, this may be done with the Saha equation alone.

The Saha equation furnishes the ratio of the number of atoms which are i+1-fold ionized to the number which are i-fold ionized in terms of the partition functions of the ith and (i+1)th states of ionization and the ionization potentials $\chi_{i,i+1}$. In addition it is necessary to specify the electron pressure and the temperature.

Stellar models are obtained by an integration of the equation of hydrostatic equilibrium which depends upon the gas pressure and not upon the electron pressure. The procedure generally followed, therefore, is to prepare a graphical relationship between the gas and electron pressures for the entire anticipated ranges of gas pressure and temperature.

The Saha equation is used in the form

$$\frac{N_{i+1}}{N_i} = \frac{1}{P_e} \frac{(2\pi m)^{3/2}}{h^3} T^{5/2} e^{-\frac{\chi_{i,i+1}}{kT}}$$

where the symbols have their usual meanings.* The ratio is then determined by the computer program described below.

*L.H. Aller, Atmospheres of the Sun and Stars, Ronald Press, N. Y., 1953.

II. METHOD OF SOLUTION BY AN IBM 709 COMPUTER PROGRAM

Ionization potentials, partition functions, abundances temperatures, and electron pressures are read into the computer as data. The machine solves the Saha equation in non-logarithmic form for each element to give ratios of the number of first-ionized to neutral atoms. This ratio (RAT) for each element is divided by one plus the same ratio to yield the number of first-ionized to first-ionized-plus-neutral atoms. The resulting quantity is then multiplied by the respective abundances and summed over all elements included in the program. The result is divided by the sum of the abundances, and from this quantity the ratio of the gas to electron pressure is determined by adding unity and dividing by the quantity.

The Fortran statements follow:

```
 1      DIMENSION  PE(14),CHI(28), PRRT(28), T(15),ABND(28)
 2      READ INPUT TAPE 7,3, (CHI(M), M=1,28)
 3      FORMAT (  6E12.3)
 4      READ INPUT TAPE 7,5, (PRRT(M), M=1,28)
 5      FORMAT (  6E12.3)
 6      READ INPUT TAPE 7,7, (T(N),N=1,15)
 7      FORMAT (  5F8.1)
 8      READ INPUT TAPE 7,9,(PE(I),I=1,14)
 9      FORMAT (  8E9.1)
31      READ INPUT TAPE 7,32,(ABND(M),M=1,28)
32      FORMAT (  6E12.3)
10      N=1
12      COF=3.3319E-01
13      BOLTEV = 8.616E-05
33      I=1
14      CONTINUE
34      DO 20 M=1,28
16      X=-CHI(M)/(BOLTEV*T(N))
35      DIMENSION RAT(28),EXI(28)
17      RAT(M)=COF*T(N)**2.5*PRRT(M)*EXP (X)/PE(I)
36      EXI(M)=RAT(M)/(RAT(M)+1.0)
20      CONTINUE
37      SEAB=0.0
38      DO 24 M=1,28
39      SEAB=SEAB+(EXI(M)*ABND(M))
24      CONTINUE
40      SAB=0.0
41      DO 29 M=1,28
42      SAB=SAB+ABND(M)
29      CONTINUE
```

```
43      EEE=SEAB/SAB
44      PGPE=(1.0+EEE)/EEE
45      WRITE OUTPUT TAPE 6,46, PGPE,N,I
46      FORMAT(7H  PGPE=1PE11.3,4H  N=I2,4H  I=I2)
47      I=I+1
48      IF(14-I)49,14,14
49      N=N+1
50      IF(15-N)51,33,33
51      CONTINUE
30      END
```

III. AN APPROXIMATE SOLUTION FOR THE RATIO P_ϵ to P_g

The original computations of the P_ϵ, P_g relations were carried out in 1959 and 1961 by hand calculations. In order to make these computations manageable, the elements of similar ionization potential were grouped together. For example, hydrogen (I.P. = 13.54), nitrogen (I.P. = 14.49) and oxygen (I.P. = 13.56) were handled together using a mean ionization potential of 13.54. Thus the solution of the ionization equation gave in this case the approximate ratio of ionized to neutral particles of H, N, and O combined. Five groups were considered:

Group I:	Helium, Neon	Mean Ionization Potential = 24.48
Group II:	Hydrogen, Nitrogen, Oxygen	Mean Ionization Potential = 13.54
Group III:	Carbon	Mean Ionization Potential = 11.20
Group IV:	Silicon, Iron, Magnesium, Nickel (other metals)	Mean Ionization Potential = 7.9
Group V:	Calcium, Aluminum, Sodium, Potassium	Mean Ionization Potential = 5.8

The resulting log P_ϵ, log P_g values for the various values of θ (where θ = 5040/T) are displayed in the Figs. 1-3 by dotted lines.

By use of The University of Michigan's IBM 709 computer we were able to solve the ionization equation exactly for each individual element, and then to determine extremely accurate log P_ϵ, log P_g relations for the same compositions which had been handled by the approximate method described above. The results of these calculations are shown in Figs. 1-3 by the solid lines and are also tabulated for each abundance. Apparently the approximate method fails most seriously at the lowest temperature and for high values of the gas pressure.

TABLE I

SOLAR-LIKE ABUNDANCE*
(IBM 709 Solution)

log P_ϵ	log P_g							
	θ=.50	θ=.60	θ=.70	θ=.75	θ=.80	θ=.85	θ=.90	θ=.95
-2.0							- .61	.07
-1.5						- .22	+ .36	1.07
-1.0				- .46	- .02	+ .63	1.34	2.04
- .5	- .17	- .16	- .05	+ .30	+ .91	1.62	2.33	2.98
0	+ .33	+ .34	+ .65	1.19	1.88	2.60	3.28	3.84
+ .5	+ .83	.87	1.48	2.15	2.87	3.57	4.19	4.58
1.0	1.34	1.45	2.41	3.12	3.84	4.51	4.99	5.26
1.5	1.84	2.14	3.38	4.11	4.81	5.38	5.72	5.94
2.0	2.37	2.96	4.36	5.08	5.72	6.16	6.43	6.66
2.5	2.94	3.89	5.35	6.03	6.56			
3.0	3.62	4.86	6.32					
	log P_g							
	θ=1.0	θ=1.1	θ=1.2	θ=1.4	θ=1.6	θ=1.8	θ=2.0	
-2.0	.78	1.92	2.22	2.65	3.27	3.64	4.20	
-1.5	1.75	2.60	2.78	3.36	3.89	4.33	5.06	
-1.0	2.65	3.20	3.39	4.08	4.53	5.09	5.95	
- .5	3.46	3.79	4.06	4.76	5.22	5.95	6.88	
0	4.14	4.42	4.76	5.41	5.97	6.85	7.85	
+ .5	4.78	5.10	5.50	6.09	6.82			
1.0	5.44	5.83	6.22	6.83				
1.5	6.14	6.58						

*As used by L. H. Aller in Stellar Atmospheres, ed. by J. L. Greenstein, University of Chicago Press, 1960, p. 234.

Relative Number of Atoms

H	= 1,000,000.	Ne	= 2,000.	Misc.	= 2.
He	= 140,000.	Si	= 40.	Ca	= 2.4
C	= 250.	Fe	= 6.	Al	= 1.6
N	= 410.	Mg	= 19.	Na	= 2.0
O	= 1,300.	Ni	= 0.6	K	= 0.09

TABLE II

ABUNDANCE A
(IBM 709 Solution)

log P_e	log P_g						
	θ=.3	θ=.4	θ=.5	θ=.6	θ=.7	θ=.8	θ=.9
-3.5							
-3.0							-2.07
-2.5						-1.89	-1.23
-2.0			-1.60	-1.45	-1.44	-1.28	- .34
-1.5			-1.03	- .95	- .93	- .56	+ .55
-1.0	- .70	- .70	- .48	- .45	- .39	+ .28	1.41
- .5	- .20	- .19	+ .04	+ .06	+ .22	1.19	2.28
0	+ .30	+ .33	.55	+ .57	.94	2.08	3.13
+ .5	+ .80	+ .83	1.06	1.11	1.79	2.98	3.89
1.0	+1.30	+1.44	1.56	1.71	2.69	3.88	4.54
1.5	+1.80	2.00	2.07	2.43	3.61	4.72	5.17
2.0	2.31	2.54	2.60	3.27	4.54	5.46	5.82
2.5	2.82	3.05	3.20	4.18	5.45	6.14	6.53
3.0	3.35	3.56	3.90	5.12	6.29	6.83	7.30
	log P_g						
	θ=1.0	θ=1.2	θ=1.4	θ=1.7	θ=2.0	θ=2.3	θ=2.6
-3.5	-1.86	- .18	+ .12	+ .93	1.48	2.22	3.44
-3.0	- .99	+ .48	.69	1.61	2.12	3.08	4.38
-2.5	- .16	1.05	1.31	2.24	2.80	3.97	5.36
-2.0	+ .67	1.59	1.97	2.86	3.58	4.88	6.35
-1.5	1.52	2.15	2.69	3.50	4.45	5.85	7.35
-1.0	2.30	2.74	3.44	4.17	5.35	6.83	8.34
- .5	2.98	3.39	4.15	4.92	6.29	7.83	9.35
0	3.58	4.09	4.82	5.77	7.26	8.82	10.34
+ .5	4.17	4.85	5.50	6.69	8.25	9.82	11.35
1.0	4.80	5.60	6.23	7.63	9.24		
1.5	5.48	6.32	7.05	8.62			
2.0	6.23	7.05	7.95	9.60			
2.5	7.02						
3.0	7.79						

Relative Number of Atoms

He	=	160,000.	C	=	1,000.	(Other metals)		2.
Ne	=	500.	Si	=	32.		Ca	= 1.6
H	=	100,000.	Fe	=	4.		Al	= 1.6
N	=	125.	Mg	=	25.		Na	= 2.0
O	=	800.	Ni	=	0.9		K	= 0.07

TABLE III

ABUNDANCE B
(IBM 709 Solution)

log P_ϵ	log P_g						
	θ=.3	θ=.4	θ=.5	θ=.6	θ=.7	θ=.8	θ=.9
-3.5							
-3.0							-1.42
-2.5						-1.24	- .66
-2.0			-1.51	- .83	- .81	- .63	+ .07
-1.5			- .81	- .32	- .29	+ .09	.76
-1.0	- .70	- .69	- .09	+ .19	+ .26	.85	1.48
- .5	- .20	- .18	+ .57	.69	.87	1.60	2.28
0	+ .30	+ .35	1.14	1.21	1.59	2.32	3.06
+ .5	.80	.94	1.67	1.75	2.36	3.10	3.77
+1.0	1.30	1.61	2.19	2.36	3.13	3.91	4.39
+1.5	1.80	2.34	2.71	3.08	3.90	4.68	5.00
+2.0	2.31	3.02	3.25	3.86	4.72	5.35	5.64
+2.5	2.83	3.63	3.85	4.66	5.54	5.99	6.35
+3.0	3.38	4.18	4.55	5.47	6.28	6.66	7.12
	log P_g						
	θ=1.0	θ=1.2	θ=1.4	θ=1.7	θ=2.0	θ=2.3	θ=2.6
-3.5	-1.45	- .35	- .06	.75	1.30	2.04	3.25
-3.0	- .79	+ .30	+ .51	1.42	1.93	2.90	4.19
-2.5	- .12	.87	1.13	2.06	2.62	3.79	5.18
-2.0	+ .62	1.41	1.79	2.68	3.40	4.70	6.16
-1.5	1.43	1.96	2.51	3.32	4.26	5.67	7.17
-1.0	2.17	2.56	3.25	3.99	5.17	6.65	8.16
- .5	2.82	3.21	3.96	4.74	6.11	7.65	9.17
0	3.40	3.91	4.64	5.59	7.08	8.64	10.16
+ .5	3.99	4.67	5.32	6.50	8.07	9.64	11.16
+1.0	4.61	5.42	6.05	7.45	9.06		
1.5	5.30	6.14	6.87	8.43			
2.0	6.05	6.87	7.77	9.42			
2.5	6.83						
3.0	7.61						

Relative Number of Atoms

He =	160,000.	C =	1,000.	(Other metals)	2.
Ne =	500.	Si =	32.	Ca =	1.6
H =	10,000.	Fe =	4.	Al =	1.6
N =	125.	Mg =	25.	Na =	2.0
O =	800.	Ni =	00.9	K =	0.07

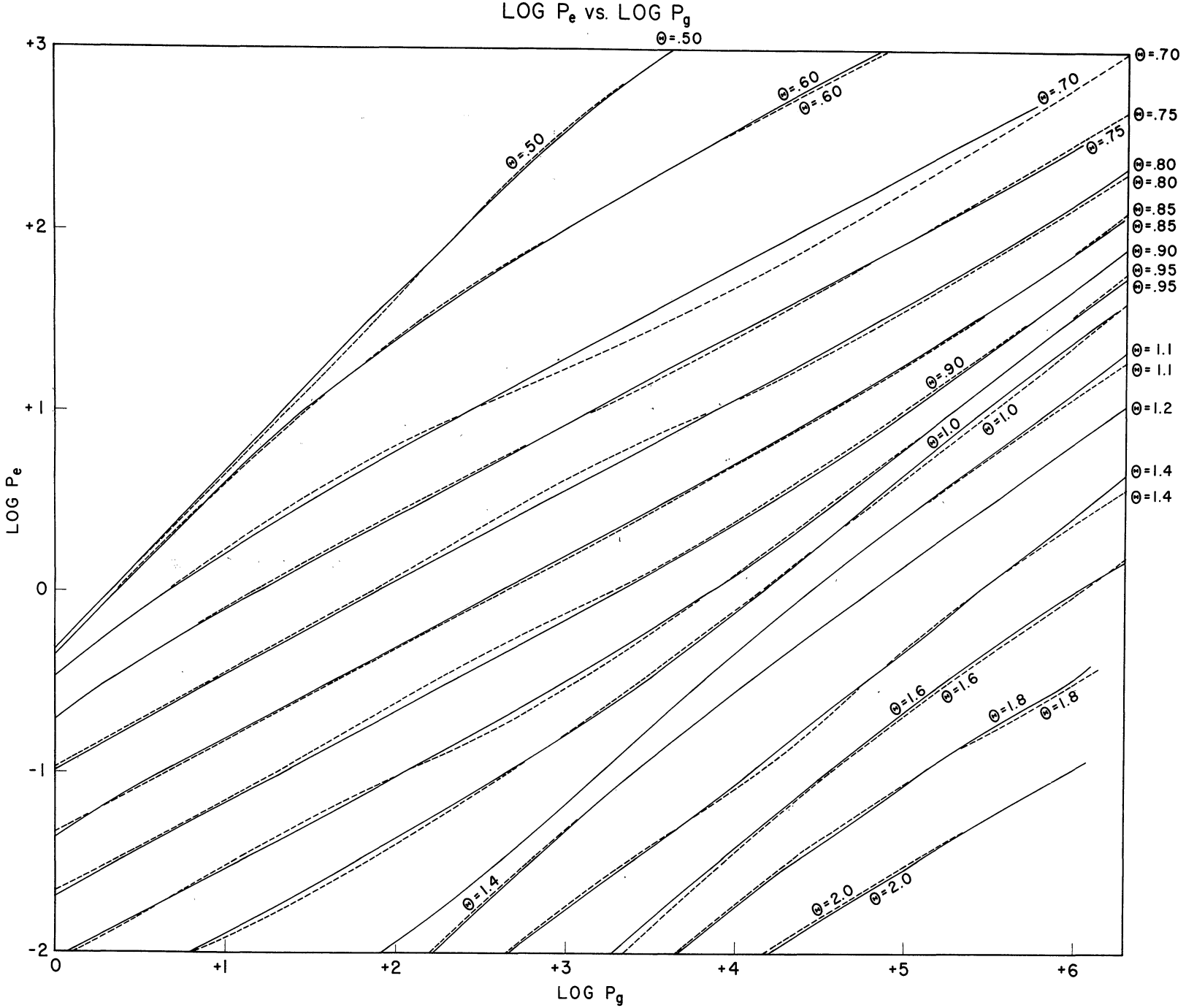

FIG. 1

RELATIVE ABUNDANCE

H=1,000,000.		Ne=	2,000.	Misc.=	2.
He=140,000.		Si=	40.	Ca=	2.4
C=	250.	Fe=	6.	Al=	1.6
N=	410.	Mg=	19.	Na=	2.0
O=	1,300.	Ni=	0.6	K=	0.09

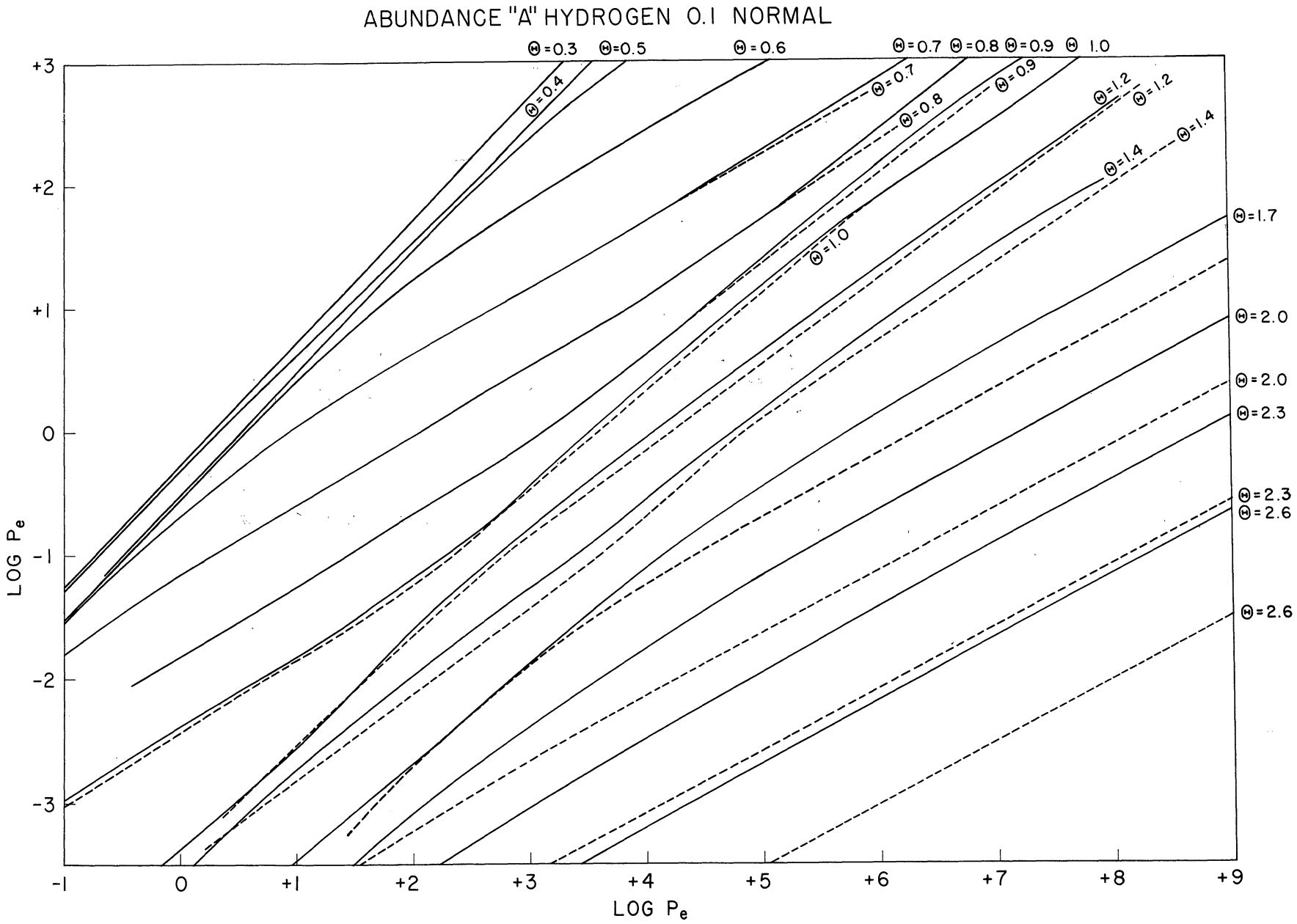

FIG. 2

ABUNDANCE "A"

He=	160,000.	C=	1,000.	(other metals)	2.
Ne=	500.	Si=	32.	Ca=	1.6
H=	100,000.	Fe=	4.	Al=	1.6
N=	125.	Mg=	25.	Na=	2.0
O=	800.	Ni=	0.9	K=	0.07

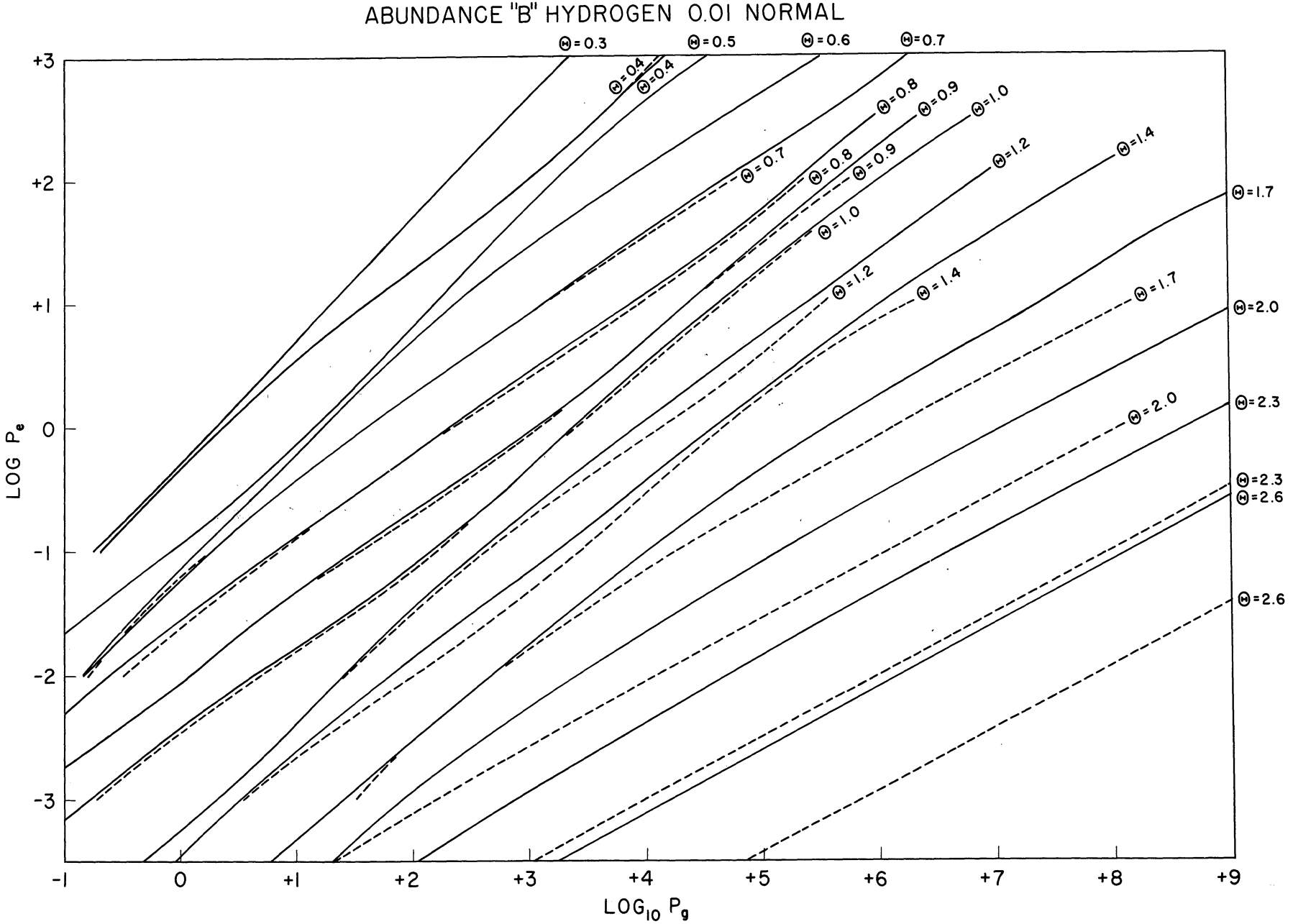

FIG. 3

ABUNDANCE "B"

He=	160,000.	C=	1,000.	(other metals)	2.
Ne=	500.	Si=	32.	Ca=	1.6
H=	10,000.	Fe=	4.	Al=	1.6
N=	125.	Mg=	25.	Na=	2.0
O=	800.	Ni=	00.9	K=	0.07

THE UNIVERSITY OF MICHIGAN
COLLEGE OF LITERATURE, SCIENCE, AND THE ARTS
Department of Astronomy

Technical Note No. 5

ABUNDANCES OF ELEMENTS IN STARS AND NEBULAE

(The Manganese Star 53 Tauri)

L. H. Aller
The University of Michigan Observatory

and

W. P. Bidelman
Lick Observatory, The University of California

ORA Project 03719

under contract with:

AIR FORCE OFFICE OF SCIENTIFIC RESEARCH
AIR RESEARCH AND DEVELOPMENT COMMAND
CONTRACT NO. AF 49(638)-807
WASHINGTON, D.C.

administered through:

OFFICE OF RESEARCH ADMINISTRATION ANN ARBOR

July 1962

PREFACE

In the study of stellar chemical compositions, our attention has been focussed mainly on hydrogen-deficient objects but hydrogen deficiency is often correlated with abundance anomalies of other kinds. Conversely, if a star showing abundance anomalies does not show a hydrogen deficiency this fact is likewise of interest, since it implies that the abnormal abundance must have been produced by processes that did not at the same time seriously affect the hydrogen concentration.

Granted that hydrogen is much more abundant than the metals, most nuclear processes invoked to explain abnormal abundances require mixing of surface layers with hydrogen-deficient cores—or processes in the atmospheric layers which themselves might be expected to affect seriously the concentration of hydrogen in these layers. Abundance anomalies of the type described here differ from one star to another.

We are indebted to Mrs. Anne Cowley for her care in making the microphotometer tracings and for her other assistance with the redictions. Thanks are due to Miss C. Parks, and Messrs. John Dickel, Jerry Ehman and Harold Graboske for their help in the reductions. We are grateful to Dr. J. Jugaku and Dr. W. Sargent for communicating to us their spectral energy results in advance of publication.

L. H. Aller
The University of Michigan Observatory
July 23, 1962

TABLE OF CONTENTS

LIST OF ILLUSTRATIONS

ABSTRACT

The chemical composition of the Manganese star 53 Tauri was studied with the aid of data secured with the coudé spectrograph of the 120-inch reflector at the Lick Observatory. Transition probabilities required for the problem are obtained from laboratory sources whenever possible, but some are obtained by the calibration of stellar data. The temperature of the star, deduced from ionization equilibrium, is near 11,000°K—a value in good agreement with that found from spectral energy scans by Jugaku and Sargent. The electron pressure in the atmosphere, deduced from the total intensities of hydrogen lines, appears to lie in the neighborhood of 500 dynes cm^{-2}. Several striking abundance anomalies are found; they cannot be explained by deviations from local thermodynamic equilibrium. Manganese seems to be the most abundant metal in the star, but gallium appears to show the greatest enhancement of abundance over the "normal" value. Strontium, yttrium, and zirconium are also enhanced in abundance, whilst magnesium, and calcium seems to be depleted.

I. INTRODUCTION: THE OBSERVATIONAL DATA

Spectral class A includes objects with a variety of peculiarities. Metallic line stars and magnetic stars have attracted the most attention. Of these objects perhaps the most exotic are the magnetic stars whose spectral peculiarities are linked with changes in magnetic fields. Less intensively studied have been the so-called "silicon," "strontium," and "manganese" stars.

As an example of a manganese star we have selected for studys 53 Tauri [$\alpha = 4^n\ 16^m\ 29^s$ (1950); $\delta = +21°\ 1'\ 23''$ (1950)]. This star is also designated as Boss PGC 997, GC 5210, BD + 20° 733, and HD 27295. Its magnitude is 5.39, Draper spectral class B8, and Mt. Wilson spectral class A1S; it is a sharp-lined star.

The most noticable characteristic of 53 Tauri is the great strength of the lines of manganese, particularly those of MnII. Excess manganese abundance is sometimes associated with other abundance anomalies as noted, for example, by Sargent and Jugaku in kappa Cancri.[1] Other stars of peculiar composition, e.g., 3 Centauri, which has been studied by Sargent, Jugaku, and Greenstein,[2] may be associated with these manganese stars. Some manganese stars also show strong chromium lines, but 53 Tauri shows the strongest manganese line spectrum.

Plates 1-7 reproduce the spectrum of 53 Tauri from about λ3650 to λ4670 as photographed with the 120-inch reflector coudé spectrograph at the Lick Laboratory. The strong, broad hydrogen lines are characteristic of spectral classes A or late B. Note the sharpness of the metallic lines. Only the "K" line of CaII shows a distinct fuzziness—due to collision broadening and radiation damping coupled with a large number of absorbing atoms. The richness of the MnII spectrum is particularly striking; many lines are not even listed in the Revised Multiplet Table.[3] There are large numbers of lines of other ions as well, e.g., CrII, ZrII, and TiII. The FeII lines which so often dominate the enhanced metallic spectrum of an A-type star are present but are generally weaker than the MnII lines. The CII pair at 4267 and 3919, 3920 are present but weak; λ3856,62; λ4128,4131 of SiII are strong. The GaI λ4172.06 line is unmistakably present and measurable—indicating, as we shall see, a remarkably high abundance for this metal (see Fig. 1).

Table I gives line intensities and other data relevant to an analysis of the spectrum of 53 Tauri. The first column gives the measured wavelength of the line. The second column gives the identification; the number in parentheses indicates the number of the multiplet in the Revised Multiplet Table.[3] For many of the MnII lines no classification is available. Other MnII lines identified and classified by Laura Iglesias[4] at Catalan's laboratory in Madrid are designated by (igl). The third column gives the equivalent width of the line in angstrons, tabulated to the nearest milliangstrom. The fourth column, denoted "Eff.

Cont.," gives the amount by which the background continuum at the position of the line is affected by wings of strong lines, particularly those of hydrogen; thus a "1.0" means that there is no blending and a number such as 0.87 means that the continuum is depressed by 13%, i.e., the intensity in the hydrogen line is 0.87 of the continuum intensity at the point where the line is formed. The fifth column gives the quantity log W/λ c/v which is used as the ordinate of the curve of growth. Here c is the velocity of light and v is the most probable speed of the atom, viz.,

$$v = \sqrt{\frac{2kT}{M} + \xi_t^2} \qquad (1)$$

where M is the mass of the atom, T is the gas kinetic temperature, k is the Boltzmann constant, and ξ_t is the most probable "turbulent" velocity. The sharpness of the lines and the character of the curve of growth both suggest that turbulent velocities are small. Accordingly, for the purpose of a first reconnaissance we have assumed that $\xi_t = 0$ and have taken the gas kinetic temperature as 12,000°K.

The sixth column gives log $gf\lambda$, where g is the statistical weight of the lower level of the transition involved and f is the Landenburg f or oscillator strength. The seventh column gives the excitation potential of the lower level, and the last column gives a quantity essential for the curve of growth analysis. The oscillator strengths have been taken from various sources as will be described in the following sections. For the metallic lines we have used mostly the data obtained by Corliss at the National Bureau of Standards,[5] supplemented for lines of several ions—particularly FeII—by data extracted from stellar curves of growth.

II. THE CURVE OF GROWTH

The chemical analysis of a star may be carried out to several different degrees of precision, depending on the character of the input data, the accuracy of the observed line intensity, the reliability of the f-values, and how much we know about the star's surface gravity and effective temperature. In a first reconnaissance it is wise to adopt the curve of growth procedure which permits one to obtain a quick survey of the problem—the atmospheric pressure and temperature and a rough idea of the compositions. Later, when adequate observational material of sufficient high accuracy has been accumulated and the temperature and surface gravity of the star has been reasonably well evaluated, a model atmosphere approach may be justified. We should note, however, that the time and effort involved in a model atmosphere type of analysis is several times greater than that entailed in a curve of growth study.

Several theoretical curves of growth have been calculated by various workers. Among these we may mention especially those of Unsöld,[6] Menzel,[7] and Wrubel,[8] which have used by many workers in this field. Unsöld's and Menzel's formulations were proposed originally for the Schuster-Schwarzschild model, in which it is supposed that the continuous spectrum is produced wholly in underlying strata, whilst the line spectrum is entirely produced in a thin overlying layer. The physical model is thus a highly simplified one. Wrubel has published curves both for this Schuster-Schwarzschild model and for the Milne-Eddington model, in which it is supposed that the ratio of line to continuous absorption coefficient is independent of optical depth. That is, the line and continuous spectra are both formed in <u>exactly</u> the same layers. A further assumption made in the equations used by Wrubel is that the source function depends linearly on the optical depth in the continuum:

$$B_\nu (\tau_\nu) = B_0 + B_1 \tau_\nu \tag{2}$$

where B_ν is the Planckian function

$$B_\nu(T) = \frac{2h\nu^3}{c^2} \frac{1}{e^{h\nu/kT} - 1} \tag{3}$$

and the temperature $T(\tau_\nu)$ is a known function of the optical depth τ_ν;

$$d\tau_\nu = \kappa_\nu \rho \, dh \tag{4}$$

where κ_ν is the coefficient of continuous absorption, ρ is the density, and dh is the element of geometrical height.

The Wrubel curve of growth depends not only on the ratio of the damping constant to the Doppler width but also on the value of B_o/B_1. Hence different curves will apply to different regions of the spectrum. If one wishes to use the same curve over an extended range, it is necessary to apply to the abscissa small corrections that depend not only on the wavelength but also on the intensity (equivalent width) of the line. In a first reconnaissance it is doubtful that the extra effort involved is really justified; at this stage of the analysis one may just as well use the Unsöld or Menzel formulation. The more sophisticated model atmosphere treatment yields different curves of growth for different stages of ionization,[9] a refinement which is hardly possible at this stage of the analysis.

All of these curves of growth are based on the assumption that the lines are formed by the mechanism of pure scattering (Milne's monochromatic radiative equilibrium). If we suppose that the lines are formed by the mechanism of pure absorption, the curves are modified[9] and the variation of B_o/B_1 has to be taken into account quite carefully. The "scattering" curves of growth seem adequate for the first treatment of the problem.

We have chosen for this analysis a curve of growth published by K. O. Wright[10] for lines of iron in the sun. It is essentially Menzel's curve of growth with small empirical corrections. The ordinate is log W/λ c/v, and the abscissa is log X_o given by:[9]

$$\log X_o = \log N_a - \theta_{ex}\chi + \log gf\lambda + c_3(\lambda) \tag{5}$$

Here

$$\theta_{ex} = \frac{5040}{T_{ex}} \tag{6}$$

where T_{ex} is the excitation temperature of the atmosphere. χ is the excitation potential of the lower level of the line (tabulated in the seventh column of Table I). N_a is the number of atoms "above the photosphere" at λ4200A; and

$$c_3(\lambda) = \log \frac{\sqrt{\pi e^2}}{mc} - \log v - \log u(T) + \log \kappa(\lambda_o)/\kappa(\lambda). \tag{7}$$

Here v is the most probable velocity, $\sqrt{2kT/M}$, $u(T)$ is the partition function, and the first term is a numerical constant. The last term allows for the changing

"depth of the photosphere" as one goes from one spectral region to another. In regions where the coefficient of continuous absorption $\kappa(\lambda)$ is large the atmosphere is more opaque; hence fewer atoms lie "above the photosphere." In more transparent regions $\kappa(\lambda)$ is smaller and the depth of the photosphere is greater. We have chosen $\lambda_o = 4200$ as the standard wavelength.

III. THE ATMOSPHERIC ELECTRON PRESSURE

Certain essential step in the curve of growth analysis must be carried out by successive approximation. We do not know the temperature of the star, nor the electron pressure in its atmosphere a priori. From the spectral type and level of excitation in the atmosphere we know that the effective temperature of the star must lie between about 10,000°K and about 13,000°K. As noted in Section IV, this range is further narrowed by spectrophotometric data secured by Sargent and Jugaku. We finally adopted T = 11,200°K.

The electron pressure may be assessed in a number of ways. If the temperature were known accurately, one could determine the electron pressure from the ionization equilibrium.* Another method is to use the hydrogen lines. The confluence of the Balmer series gives one estimate of log N_ϵ by the Inglis-Teller formula;[11] another guess may be made from the total intensities of the hydrogen lines.

The Inglis-Teller relation between the ion (or electron) density and the last resolvable member of the Balmer series is:

$$\log N = 23.26 - 7.5 \log N_m \tag{8}$$

From visual inspection of the plate, $N_m \geq 17$, whence log N = 14.04, and log P_ϵ = 2.23 if T = 11,000°K.

Still another method is to adapt a procedure suggested by Unsöld[12] to employ the total intensities of the hydrogen lines H_γ and Hδ. The depth in the line is presumed to be given by Minnaert's empirical formula

$$R = \frac{1}{\frac{1}{x_\nu} + \frac{1}{R_c}} \tag{9}$$

where R_c is the central depth of the line. In 53 Tauri, R_c = 0.84 for H_γ, 0.78 for Hδ, and 0.76 for Hε; x_ν is the absorption coefficient in the line, viz.,

---

*In theory, one could get both T and P_ϵ by comparing two elements with appreciably different ionization potentials in two successive stages of ionization. In practice, however, this procedure does not work out as the relative numbers of atoms are rarely determined with the accuracy required.

$$x_\nu = \alpha(\Delta\lambda)\, n_{02} \tag{10}$$

where n_{02} is the number of hydrogen atoms in the second level above the photosphere and $\alpha(\Delta\lambda)$ is the line absorption coefficient which can be written in the form[13]

$$\alpha(\Delta\lambda) = \frac{CE_o^{3/2}}{(\Delta\lambda)^{5/2}} \left[1 + \mathcal{R}(N_\epsilon, T)\sqrt{\Delta\lambda}\right] \tag{11}$$

where E_o is the average microscopic field produced by the surrounding ions at the radiating hydrogen atom. That is,

$$E_o = 2.60\, \epsilon\, N_i^{2/3} \tag{12}$$

N_i is the number of ions per cm^3, ϵ is the charge on the electron, and C is a constant that has been tabulated by Traving for the higher members of the Balmer series. Then, approximately,

$$W_\lambda = \int R d\lambda = \int \frac{d(\Delta\lambda)}{\frac{\Delta\lambda^{5/2}}{CE_o^{3/2}\, N_{02}\left[1 + \mathcal{R}\sqrt{\Delta\lambda}\right]} + \frac{1}{R_c}} \tag{13}$$

where $\mathcal{R}(N_\epsilon, T)$ is a correction factor to the Holtsmark equation that has been tabulated by Kolb, Griem, and Shen.[12]

For various estimates of $N_i = N_\epsilon = P_\epsilon/kT$ and an adopted value of n_{02}, we calculate W_λ and interpolate to obtain N_ϵ. Thus in order to apply the method one must have some estimate of n_{02}, which we obtain by a procedure proposed by Unsöld.[11] If the hydrogen lines were formed in an optically thin layer we would have that

$$W_\lambda \sim 0.886 \times 10^{-12}\, \lambda^2 f\, n_{02} \tag{14}$$

For the lower members of the Balmer series, this equation will certainly fail because the thin-layer approximation is far from valid, while for the higher members of the series, overlapping wings will cause the continuum to be estimated too low and W_λ will be too weak. Unsöld's procedure is to plot n_{02} against the quantum number n and extrapolate to obtain a limiting value. In this fashion a value of $\log n_{02} = 16.55$ is obtained (see Fig. 2).

line	observed equivalent width	log P_ϵ
Hγ	8.9Å	2.73
Hδ	11.4	2.77
Hϵ	11.9	2.80:

Adopted value log P_ϵ = 2.75

The value derived from H_ϵ is approximate and is not used in the final average.

Note that the value of log P_ϵ obtained in this way is only approximate. We assume that the hydrogen-line profiles can be represented as though they were formed in an atmosphere at constant pressure and temperature.

If we take the above—derived values of n_{02}, P_ϵ, and the assumed T = 11,000°K we find a total quantity of hydrogen above the photosphere that is about an order of magnitude smaller than the quantity reckoned from the continuous absorption coefficient on the assumption that the photosphere lies at an optical depth τ=0.5. If a larger value of n_{02} is adopted, the derived log P_ϵ is reduced and the required ionization temperature is slightly lowered, but the transparency of the atmosphere is increased. Hence the discrepancy remains. If 53 Tauri lies on the main sequence, the predicted log P_ϵ is about 2.56 for an optical depth τ=0.40 at λ4235. It appears that the difficulties can be resolved only by detailed line profile computations based on an appropriate model atmosphere. We have retained log P_ϵ = 2.75 in our subsequent calculations. Perhaps a smaller value, log P_ϵ = 2.50, would have been better, but then the ionization equilibrium would have required a lower ionization temperature. Furthermore the spectrophotometric data appear to favor the higher temperature, T $\cong$ 11,000°K.

IV. DETERMINATION OF THE IONIZATION TEMPERATURE

Basically, our procedure was to estimate a rough temperature from the spectral class. Then, from the broadening of the hydrogen lines according to the Kolb-Griem theory, the electron pressure could be assessed. The next step was to improve the temperature estimate by using the ionization equilibrium of elements that appear in two stages of ionization, e.g., FeI and FeII, SiI and SiII, and MnI and MnII. From the curve of growth analysis we derived log N(I) and log N(II) for each of these elements.

One may compare $N_{r,s}$ with $N_{r-1,s}$, to obtain a combined excitation and ionization temperature. Such a situation occurs when lines arising from low levels in a neutral atom are compared with lines arising from high levels in the corresponding ion.

The ionization or ionization-excitation temperatures derived in this way for Mn, Fe, and Si all agreed in giving a temperature near 11,200°K, $\theta = 0.45$. This value was used in subsequent calculations.

Later we learned that Sargent and Jugaku had measured the energy distribution in the spectrum of 53 Tauri. They found that the energy distribution is very close to that of α Leonis; hence our ionization temperature of 11,000 seems reasonable. A more elaborate procedure would entail representing this energy distribution by means of a model atmosphere, which could then be employed to predict spectral line intensities by the Pecker theory or some more elaborate procedure. The hydrogen line profiles could be represented by the model atmosphere and the Kolb-Griem theory to fix the proper value of the surface gravity, and to check the run of temperature and density in the adopted model.

V. RESULTS OF THE CURVE OF GROWTH ANALYSIS

We shall now present results for the individual elements whose abundances have been determined by the curve of growth method. Throughout, we have assumed $\theta_{ex} = \theta_{ion} = 0.45$.

A. CARBON

Multiplets (4) and (6) are represented in the spectrum of 53 Tauri. The f-values are calculated by the Bates-Damgaard[14] method, which seems to yield reliable results for light atoms of this type. We obtain for the number of atoms above the photosphere

$$\log N(CII) = 19.44$$

after allowing for the small contribution of neutral carbon we find

$$\log N(C) = 19.45$$

B. MAGNESIUM

MgI is represented by very weak lines λ3829, λ3838, whose intensities are uncertain; MgII is represented by the strong 4481 pair. With our adopted $\theta = 0.45$, we obtain

$$\log N(MgI) = 12.00$$

$$\log N(MgII) = 16.60$$

The corresponding ionization temperature would be implausibly high; therefore we have adopted the abundance from the MgII lines which yield

$$\log N(Mg) = 17.19$$

The corresponding value from MgI would be 16.40; evidently further study of this element is needed, possibly by means of a model atmosphere approach.

C. SILICON

SiI is represented by λ3905, from whose intensity we derive a concentration

$$\log N(SiI) = 13.91$$

Ionized silicon is represented by lines of multiplets (1) and (3). The f-values were taken from the Kiel work; we obtain

multiplet	log N-θχ	θχ	log N(SiII)
(1)	14.12	3.08	17.20
(3)	12.74	4.41	17.15

mean log N(SiII) = 17.19

The N(SiII)/N(SiI) ratio yields an ionization temperature near 11,000°K, which is in good agreement with that obtained from other ratios. The finally adopted abundance of silicon is

log N(Si) = 1722:

see however the note on p. 16.

D. CALCIUM

We observe only the lines of ionized calcium.

multiplet	log N-θχ	θχ	log N(CaII)
(1)	13.83	0.00	13.83
(3)	12.36	1.40	13.80

The K line gives a result which is in excellent accord with that found from other, weaker lines of ionized calcium. Most of the calcium is doubly ionized.

log N(Ca) = 15.08

E. TITANIUM

Numerous lines of TiII are observed in the spectrum of 53 Tauri. They arise from levels with excitation potentials between 0.59 ev and 3.11 ev. For each excitation potential χ, we plot log W/λ c/v against C_3 + log gfλ and fit each plot of points to the theoretical curve in order to obtain log N - θχ.

χ	number of lines	log N-θχ	χ	number of lines	log N-θχ
0.59	9	14.76	1.57	8	14.12
1.08	11	14.56	1.88	2	13.84
1.11	7	14.56	2.04	2	14.74
1.16	9	15.04	2.05	1	14.44
1.23	10	15.14	2.58	5	13.44
			2.11	2	13.0:

From a plot of log N-θχ against χ we obtain log N(TiII) by fitting a line with a slope θ = 0.45. The points derived from a small number of lines show a consiberable scatter. The adopted concentration of TiII is

$$\log N(\mathrm{TiII}) = 15.24$$

Most of the titanium atoms are doubly ionized. No lines of TiI are observed. After correction for ionization equilibrium the abundance of titanium is found to be

$$\log N(\mathrm{Ti}) = 15.95$$

The curve of growth for titanium is given in Fig. 3.

F. CHROMIUM

This metal is represented by lines of CrII. The f-values (taken from data given in Technical Report No. 3 of this series) are obtained from stellar line intensities calibrated with the aid of Croliss f-value measurements secured at the National Bureau of Standards. The scatter from some of the high-level lines may be at least partially attributed to inaccuracies in these empirical f-values.

χ	number of lines	$\log N-\theta\chi$	χ	number of lines	$\log N-\theta\chi$
2.69	3	12.82	4.04	7	13.59
3.09	3	14.09	5.30	2	11.85
3.81	1	12.82	5.64	1	11.42
3.84	5	13.87	6.46	4	11.32

From a plot of $\log N - \theta\chi$ against χ represented by a line of slope $\theta = 0.45$ there results:

$$\log N(\mathrm{CrII}) = 14.68$$

Allwoing for the effects of ionization, we find

$$\log N(\mathrm{Cr}) = 14.91$$

This value is somewhat uncertain because of the scatter of the $\log N - \theta\chi$ plot. The curve of growth for ionized calcium and ionized chromium is given in Fig. 4.

G. MANGANESE

This appears to be the most abundant metal in the star. Lines of both MnI and MnII are present. Laboratory transition probabilities are available for the lines of MnI but unfortunately very little f-value data are available for the lines of ionized manganese. For this ion we have had to use empirical solar f-values which suffer from two very grave defects: (1) since the lines are all very weak

and may be affected by blends, the so-determined line strengths are highly uncertain; and (2) there may be a zero-point error due to a wrong estimate of the ionized manganese concentration in the sun—or an error in the excitation temperature.

For MnI we obtain the following results:

χ	number of lines	log N-$\theta\chi$
0.00	3	13.57
2.13	11	12.04

$$\log N(\mathrm{MnI}) = 13.35$$

while we find that the concentration of the MnII ion may best be found from the lines arising from the levels at 1.82 ev, viz.,

$$\log N(\mathrm{MnII}) = 16.75$$

There are also a number of MnII lines arising from levels at 5.36 ev. These gave a ridiculously small abundance of MnII. Presumably the empirical gf-values were at fault; probably too small on excitation temperature had been assumed for the sun.

Adopting these concentrations of MnI and MnII we can solve for the ionization equilibrium. The resultant ionization temperature lies near that found from silicon and from iron. The finally adopted abundance of manganese is based mostly on the MnI data. It is

$$\log N = 1730$$

The curve of growth for manganese is given in Fig. 5.

H. IRON

There are three lines of FeI from multiplets (20) and (41) at χ = 0.86 eV, and (43) at χ = 1.48 eV. They yield an FeI concentration of log N(FeI) = 12.90. The FeII data are more extensive. Using the empirical log $gf\lambda$ values obtained from solar and stellar data we find

χ	number of lines	log N-$\theta\chi$
2.66	6	15.24
2.81	8	15.48
5.90	2	14.20:

whence we find

$$\log N(\mathrm{FeII}) = 16.62$$

From the ratio log N(FeII)/N(FeI) we obtain an ionization temperature of 11,200°K, which is in good agreement with that found from manganese and silicon:

$$\log N(Fe) = 16.75$$

The curve of growth for iron is given in Fig. 6.

I. GALLIUM

Perhaps the most remarkable feature of the spectrum of 53 Tauri is the presence of neutral gallium. only one line is suitable for measurement and since it is perturbed by a neighboring, stronger, line there is some uncertainity. We get

$$\log N(GaI) \leq 11.65$$

while after correction for ionization effects we find

$$\log N(Ga) \leq 15.3$$

The curves of growth for GaI, as well as for CII, MgII, SiII, SrII, and YII, are given in Fig. 7.

J. STRONTIUM

Strontium is represented by the λ4077,4215 lines of SrII, from which we obtain

$$\log N(SrII) = 12.98$$

most of the strontium is doubly ionized so we get

$$\log N(Si) = 14.62$$

K. YTTRIUM

From four lines of ionized YII for which gf-values have been measured by Corliss we find

$$\log N(YII) = 12.89$$

$$\log N(Y) = 14.16$$

L. ZIRCONIUM

Zirconium is represented by a fair number of lines of ZrII for all of which N.B.S. laboratory log gf-values are available.

χ	number of lines	log N-$\theta\chi$
0.52	4	13.91
0.72	11	13.82
1.22	3	13.68

The curve of growth for ZrII is given in Fig. 8; the extrapolation to log N(ZrII) is given in Fig. 9. We obtain log N(ZrII) = 14.16. Correction for the ionization of this metal leads to a final value

$$\log N(Zr) = 14.62$$

Table II summarizes the abundances in 53 Tauri, as compared with a so-called "normal" scale of abundances derived for the solar system.[15] The scale is normalized for hydrogen on the assumption that the proportion of this element is the same in the sun and in 53 Tauri. We could equally well have used iron; doing so would not have changed the essential conclusions.

Carbon appears to be more abundant in 53 Tauri than in the sun by a factor of slightly more than two, but this result could be modified by a slight change in the temperature. If the temperature is slightly higher, the abundance difference is eradicated.

Magnesium and silicon may be about four or five times less abundant than in the sun, and calcium is about thirty times less abundant. If the ionization temperature is higher, this difference could be reduced somewhat but probably it could not be eliminated, at least for calcium.

Titanium appears to be about four times more abundant in 53 Tauri than in the sun, but the scatter of the individual determinations is large. Chromium is about eight times less abundant in 53 Tauri. Here again the scatter of individual determinations is fairly large, but not large enough to account for the difference. An appreciable depletion of chromium must exist.

Manganese is nearly sixty times as abundant as in the sun; in fact it appears to be more abundant than any other metal. It is three times as abundant as iron, which may be slightly less abundant in 53 Tauri than in the sun.

Gallium presents a special problem. The presence of lines of GaI in a star as hot as 53 Tauri indicates that this element must be very abundant—probably at least a hundred times as abundant as in the sun. Strontium yttrium, and

zirconium are appreciably more abundant than in the sun, by factors of thirty, twenty, and fifty respectively.

It is difficult to explain these abundance anomalies in terms of nucleogenesis patterns. Elements of the iron group are presumably produced by equilibrium reactions. Then iron is always the most abundant, and it is hard to see how manganese can be so prominent. Before pursuing this matter further it will be well to obtain abundance data for additional elements. Sargent and Jugaku find oxygen to be normal but it would be valuable to obtain data on nitrogen and sodium also.

Since the preceding was written Wallace Sargent has informed us of his and Searle's conclusion that the abundance of silicon in 53 Tauri is probably not much depleted since the "equivalent width of 4130 of SiII is entirely normal." Magnesium may be deficient but a factor of five may be too much. With respect to iron, silicon and magnesium are depleted by factors between two and three according to the results presented here. The SiII lines have fairly high excitation potentials. A slight error in the excitation temperature of ionized silicon could remove the discordance with Sargent's conclusion; possibly application of model atmosphere methods will remove the discrepancy entirely.

REFERENCES

1. W. Sargent and J. Jugaku, Astrophysical Journal, (in press, 1962).

2. W. Sargent, J. Jugaku, and J. L. Greenstein, Astrophysical Journal, Vol. 134, 1961, p. 783.

3. C. E. Moore, Revised Multiplet Table, Princeton University Contribution Contribution No. 22, 1945.

4. L. Iglesias, Journal of the Optical Society of America, Vol. 46, 1956, p. 449; Vol. 47, 1957, p. 852.

5. C. Corliss, National Bureau of Standards Monograph (in press).

6. A. Unsöld, Physik der Sternatmosphären, Springer-Verlag, Berlin, 1955.

7. D. H. Menzel, Astrophysical Journal, Vol. 84, 1937, p. 462.

8. M. Wrubel, Astrophysical Journal, Vol. 109, 1949, p. 66; Vol. 111, 1950, p. 157.

9. See e.g., Chapter 4 of Stellar Atmospheres, Compendium on Stars and Stellar Systems, Vol. 6, ed. by J. L. Greenstein, University of Chicago Press, 1960.

10. K. O. Wright, Astrophysical Journal, Vol. 99, p. 249, 1944.

11. D. R. Inglis and E. Teller, Astrophysical Journal, Vol. 90, 1939, p. 439.

12. A. Unsöld, Zeitschrift für Astrophysik, Vol. 21, 1941, p. 37.

13. A. C. Kolb, H. Griem, and K. Y. Shen, Physical Review, Vol. 116, 1949, p.4.

14. D. R. Bates and A. Damgaard, Philosophical Transactions, Royal Society of London, Ser. A, No. 242, 1949, p. 101.

15. L. H. Aller, Abundances of the Elements, Interscience, New York, 1961, p. 192.

TABLE I

EQUIVALENT WIDTHS IN THE SPECTRUM OF 53 TAURI

λ	I.D.	W	Eff. Cont.	log W/λ c/v	log gfλ	χ	C_3+log gfλ
3677.69	CrII(12)	.026	1.0	+.037	-4.624	2.69	-12.97
3677.91	CrII(12)	.030	1.0	+.090	-4.444	2.69	-12.79
3679.71	TiII(75)	.016	1.0	-.206	-5.70	1.57	-14.67
3685.07	MnII(8)	.025	1.0		NA		
3685.22	TiII(14)	.074	1.0	+.468	-4.083	0.59	-13.06
3706.03	CaII(3)	.035	0.92	+.109	-4.651	3.11	-12.33
3706.24	TiII(73)	.027	0.95	+.034	-4.481	1.56	-13.47
3706.89	MnII(8)	.013	0.97	-.258	-3.96	5.37	-12.00
3708.05	MnII(8)	.012	1.0	-.311	-2.93	5.37	-10.97
3712.95	CrII(12)	.033	0.84	+.139	-4.330	2.69	-12.71
3715.40	CrII(145)	.016	0.97	-.175		4.91	
3729.50	MnII(8)	.066	0.987	+.447	-4.33	5.37	-12.38
3736.93	CaII(3)	.052	0.76	+.269	-4.537	3.14	-12.22
3738.38	CrII(20)	.022	0.87	-.038	-5.67	3.09	-14.05
3741.65	TiII(72)	.070	1.0	+.438	-4.117	1.57	-13.11
3743.38	MnII (no class)	.052	1.0		NA	3.09	
3745.93	ZrII(112)	.017	0.75	-.030	-3.616	1.75	-12.53
3748.02	TiII(107)	.061	0.93	+.381		2.59	
3754.59	CrII(20)	.026	0.82	+.018		3.09	
3755.21	MnII (no class)	.023	0.84		NA		
3757.68	TiII(72)	.063	1.0	+.392	-4.505	1.56	-13.50
3759.29	TiII(13)	.100	1.0	+.601	-4.085	0.60	-13.08
3761.32	TiII(13)	.095	1.0	+.570	-4.185	0.57	-13.18
3761.87	TiII(107)	.044	1.0	+.232	-3.975	2.58	-12.97
3763.74	MnII (no class)	.068	0.900		NA		
3765.61	CrII(20)	.009	0.78	-.432	-5.94	3.09	-13.53
3774.35	YII(7)	.013	0.64	-.147	-4.583	0.13	-12.92
3776.05	TiII(72)	.039	1.0	+.183	-5.183	1.57	-14.20
3778.32	MnII (no class)	.043	0.90		NA		
3783.89	MnII (igl)	.016	1.0		NA		
3786.35	TiII(12)	.016	0.99	-.212		0.60	
3788.71	YII(7)	.010	0.87	-.277	-4.762	0.10	-13.12
3806.71	MnI(6)	.022	0.86	-.038	-3.45	2.11	-11.74
3812.25	MnII (igl)	.040	1.0		NA		
3812.53	MnII (igl)	.012	1.0		NA		
3813.39	TiII(12)	.037	1.0	+.156	-5.25	0.60	-14.27
3814.59	TiII(12)	.051	1.0	-.706	-5.41	0.57	-14.43

TABLE I (Continued)

λ	I.D.	W	Eff. Cont.	log W/λ c/v	log $gf\lambda$	χ	C_3+log $gf\lambda$
3820.42	FeI(20)	.015	0.97	-.202	-3.99	0.86	-12.88
3823.51	MnI(6)	.017	0.94	-.160	-3.61	2.13	-11.91
3823.87	MnI(6)	.011	0.93	-.328	-4.32	2.15	-12.62
3825.02	MnII (igl)	.022	0.89		NA		
3829.37	MgI(3)	.013	0.69	-.446	-4.04	2.70	-11.49
3832.94	YII(7)	.020	0.51	+.009	-4.976	0.18	-13.35
3844.17	MnII (igl)	.053	0.82		NA		
3848.24	MgII(5)	.011	0.94		NA		
3848.62	MnII (igl)	.013	0.96		NA		
3849.57	NiII(11)	.018	0.98	-.115		4.01	
3850.38	MnII(5)	.013	1.0		NA		
3853.67	SiII(1)	.062	1.0	+.255	-6.11	6.83	-14.04
3856.01	SiII(1)	.110	1.0	+.506	-5.16	6.83	-13.10
3862.59	SiII(1)	.089	1.0	+.415	-5.38	6.83	-13.31
3863.44	MnII (igl)	.032	1.0		NA		
3865.60	CrII(167)	.029	0.029	+.066		5.30	
3879.00	MnII (igl)	.028	0.80		NA		
3882.30	TiII(34)	.029	0.67	+.036	-4.93	1.11	-13.98
3897.60	MnII (igl)	.036	0.76		NA		
3898.09	MnII (igl)	.041	0.78		NA		
3900.55	TiII(34)	.064	0.67	+.380	-4.429	1.13	-13.48
3902.40	MnII (igl)	.010	0.91		NA		
3905.48	SiI(3)	.023	0.96	-.174	-5.118	1.90	-13.37
3905.67	CrII(167)	.027	0.96	+.031		5.31	
3913.48	TiII(34)	.094	1.0	+.548	-4.467	1.11	-13.52
3915.97	ZrII(17)	.019	1.0	-.011	-5.297	.52	-14.27
3917.33	MnII (igl)	.039	1.0		NA		
3918.95	CII(4)	.010	1.0	-.722	-4.67	16.26	-12.80
3920.66	CII(4)	.022	1.0	-.686	-4.98	16.26	-13.11
3926.13	MnII (igl)	.015	1.0		NA		
3926.45	MnI(44)	.031	1.0	+.089	-3.91	3.83	-12.24
3930.99	MnII (igl)	.016	1.0		NA		
3932.01	TiII(34)	.047	1.0	+.244	-5.605	1.13	-14.67
3934.79	ZrII(43)	.0098	1.0	-.296	-5.315	0.71	-14.30
3938.98	FeII(190)	.0051	1.0	-.686	-5.87	5.89	-14.81
3941.23	MnII (igl)	.024	1.0		NA		
3943.60	MnII (igl)	.019	1.0		NA		
3950.37	YII(6)	.010	0.98	-.294	-5.113	0.10	-13.52
3952.43	MnII (igl)	.009	0.94		NA		
3958.22	ZrII(16)	.018	0.820	-.040	-4.832	0.52	-13.82
3967.95	MnII (igl)	.009	0.40		NA		
3968.46	CaII (none)	.12	0.370	+.613	-5.371	0.00	-13.13

TABLE I (Continued)

λ	I.D.	W	Eff. Cont.	log W/λ c/v	log gfλ	χ	C_3+log gfλ
3979.53	CrII(183)	.017	0.76	-.190		5.65	
3982.01	TiII(11)	.014	0.840	-.275	-6.28	0.57	-15.36
3986.60	MnII (igl)	.013	0.91		NA		
3987.60	TiII(11)	.013	0.92	-.330	-6.99	0.60	-16.07
3991.16	ZrII(30)	.027	0.96	+.132	-4.699	0.75	-13.69
3995.30	MnII (igl)	.013	1.0		NA		
3998.97	ZrII(16)	.020	1.0	+.014	-4.898	0.56	-13.89
4000.04	MnI (igl)	.026	1.0		NA		
4003.30	CrII (194)	.021	1.0	-.089	-3.80	6.46	-12.27
4012.40	TiII(11)	.052	1.0	+.282	-5.877	0.57	-14.96
4012.55	CrII(183)	.014	1.0	-.260	-3.38	5.64	-11.85
4018.07	MnI(5)	.011	1.0	-.370	-4.05	2.11	-12.40
3838.28	MgI(3)	.020	1.0	-.256	-3.49	2.18	-10.95
3933.67	CaII(1)		1.0	+1.073	-3.075	0.00	-10.80
4018.07	MnI(5)	.016	1.0	-.197	-4.046	2.105	-12.41
4025.15	TiII(11)	.035	1.0	+.102	-6.085	0.60	-15.18
4028.35	TiII(87)	.051	1.0	+.272	-4.815	1.88	-13.91
4029.70	ZrII(41)	.014	1.0	-.139	-5.045	0.71	-14.05
4030.77	MnI(2)	.042	1.0	+.215	-4.875	0.00	-13.24
4033.07	MnI(2)	.042	1.0	+.210	-5.035	0.00	-13.40
4034.52	MnI(3)	.026	1.0	+.001	-5.275	0.00	-13.64
4035.73	MnI(5)	.016	1.0	-.197	-4.025	2.13	-12.39
4038.00	CrII(194)	.022	1.0	-.071	-3.36	6.46	-11.83
4041.39	MnI(5)	.034	1.0	+.116	-3.466	2.11	-11.83
4045.60	ZrII(30)	.018	1.0	-.049	-5.053	0.71	-14.06
4045.83	FeI(43)	.013	1.0	-.306	-3.673	1.48	-12.62
4048.71	ZrII(43) MnI(5)	.035	1.0	+.138	-4.14	2.15	-12.50
4049.13	CrII(193)	.016	1.0	-.207	-2.59	6.46	-11.06
4050.32	ZrII(43)	.007	1.0	-.460	-5.353	0.71	-14.37
4051.97	CrII(19)	.018	1.0	-.173	-6.25	3.09	-14.73
4053.83	TiII(87)	.052	1.0	+.272	-4.28	1.88	-13.38
4054.09	CrII(19)	.011	1.0	-.390		3.09	
4055.56	MnI(5)	.023	1.0	-.059	-3.922	2.13	-12.29
4058.94	MnI(5)	.010	1.0	-.429	-4.132	2.17	-12.50
4064.36	TiII(106)	.013	1.0	-.331		2.59	
4067.06	NiII(11)	.009	1.0	-.419		4.01	
4070.86	CrII(193)	.010	1.0	-.429	-3.41	6.46	-11.89
4075.46	SiII (none)	.020	1.0	-.265			
4076.78	SiII (none)	.016	1.0	-.363			
4077.71	SiII(1)	.039	1.0	+.277	-5.170	0.00	-12.76
4079.24	MnI(5)	.014	1.0	-.256	-4.290	2.18	-12.66

TABLE I (Continued)

λ	I.D.	W	Eff. Cont.	log W/λ c/v	log $gf\lambda$	χ	C_3+log $gf\lambda$
4081.45	MnII (igl)	.039	1.0		NA		
4083.65	MnII(2)	.014	0.942	-.277	-4.149	2.15	-12.52
4085.41	MnII (igl)	.022	1.0		NA		
4110.62	MnII (igl)	.023	0.764		NA		
4111.00	CrII(1826)	.018	0.79	-.167	-5.87	3.09-3.74	-14.36
4128.08	SiII(3) MnII(2)	0.12	1.0	+.655	-4.16	1.77	-12.16
4129.12	SiII(1)	.012	1.0	-.479			
4130.87	SiII(3)	.095	1.0	+.413	-3.98	9.80	-11.98
4136.91	MnII (igl)	.060	1.0		NA		
4140.47	MnII (igl)	.016	1.0		NA		
4145.78	CrII(162)	.023	1.0	-.067	-3.31	5.30	-11.81
4149.22	ZrII(41)	.026	1.0	+.102	-4.512	0.80	-13.55
4150.98	ZrII(42) CrII(163)	.012	1.0	-.357	-5.402	5.31	-13.90
4156.24	ZrII(29)	.011	1.0	-.274	-5.231	0.71	-14.27
4158.27	MnII (igl)	.012	1.0		NA		
4161.19	ZrII(42)	.018	1.0	-.051	-5.091	0.71	-14.13
4161.53	TiII(21)	.028	1.0	-.011	-5.58	1.08	-14.70
4163.65	TiII(105)	.078	1.0	+.441	-3.931	2.58	-13.05
4171.05	MnII (igl)	.016	1.0		NA		
4171.53	MnII (igl)	.014	1.0		NA		
4171.92	TiII(105)	.064	1.0	+.355	-4.160	2.59	-13.28
4172.06	GaI(1)	.016	1.0	-.156	-4.650	0.10	-12.51
4173.45	FeII(27)	.010	1.0	-.442		2.57	
4173.52	TiII(21)	.033	1.0	+.066		1.08	
4174.10	TiII(105)	.019	1.0	-.182	-6.76	2.59	-15.88
4174.34	MnII(2)	.037	1.0		NA		
4177.52	MnII (igl) YII(14)	.027	1.0		NA		
4178.89	FeII(28)	.025	1.0	-.022	-6.45	2.57	-15.45
4179.45	CrII(26)	.022	1.0	-.098	-4.35	3.81	-12.86
4184.29	TiII(21)	.011	1.0	-.430	-6.02	1.08	-15.15
4184.47	MnII (igl)	.020	1.0		NA		
4200.28	MnII (igl)	.027	1.0		NA		
4205.39	MnII(2)	.051	1.0	+.278	-7.40	1.80	-15.58
4206.39	MnII(7)	.078	1.0	+.464	-3.26	5.37	-11.44
4207.22	MnII(2)	.007	1.0	-.553	-8.74	1.82	-16.92
4209.01	ZrII(41)	.009	1.0	-.348	-4.916	0.71	-13.97
4211.89	ZrII(15)	.0096	1.0	-.336	-5.586	0.52	-14.64
4215.54	SrII(1)	.024	1.0	+.048	-5.365	0.00	-12.98

TABLE I (Continued)

λ	I.D.	W	Eff. Cont.	log W/λ c/v	log gfλ	χ	C_3+log gfλ
4233.19	FeII(27)	.046	1.0	+.232	-6.11	2.57	-15.13
4235.33	MnI(23)	.015	1.0	-.260	-3.794	2.88	-12.21
4237.85	MnII(7)	.014	1.0		NA		
4238.81	MnII(2)	.029	1.0	+.032	-7.74	1.82	-15.93
4239.21	MnII(7)	.034	1.0		NA		
4240.39	MnII (igl)	.019	1.0		NA		
4242.96	MnII(7)	.016	1.0		NA		
4244.27	MnII(7)	.031	1.0	+.060	-4.41	5.35	-12.60
4247.97	MnII (igl)	.032	1.0		NA		
4251.74	MnII (igl)	.035	1.0		NA		
4252.62	CrII(31)	.016	1.0	-.234	-5.60	3.84	-14.12
4252.99	MnII(7)	.052	1.0		NA		
4253.16	MnII (igl)	.019	1.0	-.158	-3.65	5.36	-11.84
4259.20	MnII(7)	.065	1.0		NA		
4260.49	MnII(2)	.012	1.0		NA		
4261.92	CrII(31)	.040	1.0	+.153	-5.06	3.85	-13.59
4266.98	CII(6)	.014	1.0	-.620	-4.09	17.97	-12.29
4267.26	CII(6)	.016	1.0	-.564	-3.63	17.97	-11.83
4269.27	CrII(31)	.014	1.0	-.290	-5.88	3.84	-14.41
4275.58	CrII(31)	.030	1.0	+.030	-5.40	3.84	-13.93
4275.89	MnII (igl)	.010	1.0		NA		
4278.61	MnI(6)	.024	1.0		NA		
4284.18	CrII(31)	.030	1.0	.032	-5.48	3.84	-14.01
4284.44	MnII(6)	.031	1.0	+.062	-3.88	5.35	-12.09
4287.89	TiII(20)	.041	1.0	+.143	-5.72	1.08	-14.88
4288.07	MnII (igl)	.024	1.0		NA		
4289.60	MnII(6)	.003	1.0		NA		
4290.23	TiII(41)	.083	1.0	+.456	-5.158	1.16	-14.31
4292.23	MnII(6)	.065	1.0		NA		
4294.11	TiII(20)	.072	1.0	+.390	-5.157	1.08	-14.31
4300.06	TiII(91)	.075	1.0	+.410	-4.917	1.18	-14.07
4300.27	MnII(6)	.024	1.0	-.058	-3.44	5.36	-11.65
4301.95	TiII(41)	.061	1.0	+.321	-5.316	1.16	-14.47
4303.18	FeII(27)	.020	1.0	-.128	-6.70	2.69	-15.73
4307.89	TiII(41)	.056	1.0	+.284	-4.986	1.16	-14.14
4308.18	MnII (igl)	.027	1.0		NA		
4312.88	TiII(41)	.063	1.0	+.333	-5.305	1.18	-14.46
4414.99	TiII(41)	.064	1.0	+.336	-5.02	1.16	-14.18
4316.82	MnII (igl) TiII(44)	.018	1.0	-.223	NA		
4317.77	MnII (igl)	.009	1.0		NA		
4320.99	TiII(41)	.032	1.0	+.032	-6.17	1.16	-15.33

TABLE I (Continued)

λ	I.D.	W	Eff. Cont.	log W/λ c/v	log gfλ	χ	C_3+log gfλ
4325.07	MnII(6)	.018	0.97		NA		
4330.24	TiII(94)	.021	0.864	-.173	-5.94	2.04	-15.10
4330.70	TiII(41)	.020	0.86	-.173		1.18	
4337.93	TiII(20)	.032	0.48	+.041	-5.143	1.08	-14.30
4344.01	MnII(6)	.050	0.53	+.059	-3.47	5.37	-11.68
4344.27	TiII(20)	.011	0.55	-.422	-5.952	1.08	-15.11
4345.64	MnII(6)	.014	0.64	-.286	-4.35	5.37	-12.56
4346.40	MnII (igl)	.016	0.71	-.248	NA		
4348.42	MnII (igl)	.035	0.78	+.097	NA		
4350.81	TiII(94)	.013	0.86	-.355	-5.46	2.05	-14.63
4351.77	FeII(27)	.017	0.88	-.220	-6.17	2.69	-15.21
4356.63	MnII (igl)	.039	1.0	+.148	NA		
4359.75	ZrII(79)	.011	1.0	-.302	-4.761	1.23	-13.85
4363.27	MnII (igl)	.025	1.0	-.042	NA		
4365.24	MnII (igl)	.029	1.0	+.025	NA		
4367.66	TiII(104)	.041	1.0	+.135	-4.00	2.58	-13.17
4370.99	ZrII(79)	.018	1.0	-.084	-5.130	1.20	-14.22
4377.77	MnII (igl)	.021	1.0	-.116	NA		
4383.60	FeI(41)	.006	1.0	-.649	-4.01	1.48	-13.04
4384.64	MnII(10)	.017	1.0	-.217	NA		
4385.41	FeII(27)	.012	1.0	-.380	-6.67	2.59	-15.72
4386.88	TiII(104)	.034	1.0	+.055	-5.08	2.59	-14.25
4390.59	MnII(10)	.031	1.0	+.048	NA		
4391.03	TiII(41)	.020	1.0	-.166			
4393.39	MnII (igl)	.024	1.0	-.075	NA		
4394.07	TiII(51)	.035	1.0	+.062	-5.87	1.22	-15.04
4395.04	TiII(19)	.092	1.0	+.487	-4.817	1.08	-13.99
4395.85	TiII(61)	.036	1.0	+.082	-5.34	1.24	-14.51
4399.78	TiII(51)	.058	1.0	+.290	-5.417	1.23	-14.59
4403.52	MnII (igl)	.081	1.0	+.461	NA		
4409.51	TiII(61)	.016	1.0	-.281	-6.93	1.23	-16.11
4411.08	TiII(115)	.039	1.0	+.111		3.08	
4411.90	TiII(61)	.008	1.0	-.586	-6.65	1.24	-15.83
4416.80	FeII(27)	.011	1.0	-.412	-6.75	2.77	-15.80
4417.72	TiII(40)	.057	1.0	+.279	-5.485	1.16	-14.66
4418.34	TiII(51)	.029	1.0	-.022	-6.19	1.23	-15.37
4421.94	TiII(93)	.021	1.0	-.163	-5.88	2.05	-15.06
4434.06	MnII (igl)	.035	1.0		NA		
4441.73	TiII(40)	.016	1.0	-.277		1.18	
4441.99	MnII (igl)	.009	1.0		NA		
4443.02	ZrII(88)	.067	1.0	+.486	-4.842	1.48	-13.95
4443.80	TiII(19)	.088	1.0	+.464	-5.002	1.08	-14.19

TABLE I (Continued)

λ	I.D.	W	Eff. Cont.	log W/λ c/v	log gfλ	χ	C_3+log gfλ
4444.54	TiII(31)	.021	1.0	-.155	-6.69	1.11	-15.87
4450.48	TiII(19)	.047	1.0	+.194	-5.882	1.08	-15.07
4456.62	TiII(115)	.009	1.0	-.541	-4.10	3.11	-13.29
4462.03	MnI(28)	.016	1.0	-.238	-3.67	3.06	-12.13
4464.45	TiII(40)	.042	1.0	+.137	-6.33	1.16	-15.52
4468.51	TiII(31)	.095	1.0	+.494	-4.93	1.13	-14.12
4469.13	TiII(18)	.009	1.0	+.485	-6.74	1.08	-15.93
4470.85	TiII(40)	.019	1.0	-.200		1.16	
4478.63	MnII (igl)	.056	1.0	+.293	NA		
4481.14	MgII(4)	.15	1.0	+.556	-3.87	8.83	-11.51
4481.35	MgII(4)	.14	1.0	+.514	-3.64	8.83	-11.28
4488.33	TiII(115)	.059	1.0	+.284	-4.068	3.11	-13.26
4489.19	FeII(37)	.013	1.0	-.347	-7.04	2.82	-16.11
4491.40	FeII(37)	.017	1.0	-.215	-6.93	2.84	-16.00
4496.98	ZrII(40)	.007	1.0	-.488	-5.477	0.71	-14.59
4501.28	TiII(31)	.092	1.0	+.477	-5.027	1.11	-14.23
4503.18	MnII (igl)	.018	1.0		NA		
4508.28	FeII(37)	.027	1.0	-.022	-6.52	2.84	-15.60
4515.33	FeII(37)	.012	1.0	-.390		2.83	
4518.34	TiII(18)	.012	1.0	-.409	-6.84	1.08	-16.04
4518.94	MnII (igl)	.037	1.0		NA		
4519.23	MnII (igl)	.014	1.0		NA		
4520.22	FeII(37)	.023	1.0	-.102	-6.69	2.79	-15.77
4522.62	FeII(38)	.040	1.0	+.149	-6.30	2.83	-15.38
4525.32	MnII (igl)	.021	1.0		NA		
4529.48	TiII(82)	.039	1.0	+.100	-6.11	1.56	-15.31
4533.95	TiII(50)	.093	1.0	+.480	-4.844	1.23	-14.04
4544.01	TiII(60)	.009	1.0	-.556	-6.86	1.24	-16.07
4549.49	FeII(38)	.028	1.0	-.008		2.82	
4549.62	TiII(82)	.090	1.0	+.465	-4.502	1.58	-13.71
4554.99	CrII(44)	.035	1.0	+.072	-5.15	4.05	-13.74
4555.89	FeII(37)	.015	1.0	-.294	-6.45	2.82	-15.53
4558.64	CrII(44)	.061	1.0	+.314	-4.221	4.06	-12.81
4563.77	TiII(50)	.084	1.0	+.430	-5.211	1.22	-14.42
4565.74	CrII(39)	.018	1.0	-.213	-5.63	4.02	-14.22
4568.33	TiII(60)	.007	1.0	-.661	-7.17	1.22	-16.38
4571.96	TiII(82)	.084	1.0	+.433	-4.520	1.56	-13.73
4583.82	FeII(38)	.035	1.0	+.089	-6.05	2.79	-15.14
4588.20	CrII(44)	.062	1.0	+.315	-4.47	4.05	-13.07
4589.95	TiII(50)	.028	1.0	-.054	-5.848	1.23	-15.06
4591.08	CrII(44)	.030	1.0				
4616.65	CrII(44)	.038	1.0	+.096	-3.11	4.05	-11.71

TABLE I (Concluded)

λ	I.D.	W	Eff. Cont.	log W/λ c/v	log gfλ	χ	C_3+log gfλ
4618.81	CrII(44)	.053	1.0	+.242	-4.90	4.06	-13.50
4629.32	FeII(37)	.024	1.0	-.090	-6.54	2.79	-15.63
4634.07	CrII(44)	.043	1.0	+.151	-4.82	4.05	-13.42
4635.34	FeII(186)	.019	1.0	-.186	-5.64	5.93	-14.74
4657.22	TiII(59)	.022	1.0	-.159		1.24	
4727.85	MnII(5)	.050	1.0		NA	5.35	
4730.39	MnII(5)	.044	1.0		NA	5.35	
4738.31	MnII(5)	.049	1.0		NA	5.36	
4755.71	MnII(5)	.084	1.0		NA	5.37	
4283.78	MnII(6)	.028	1.0		NA	5.35	

TABLE II

SUMMARY OF ABUNDANCES IN 53 TAURI

Element	log N 53 Tau	log N "normal"	Δ log N
H	22.42	22.42	
C	19.45	19.02	+0.43
Mg*	17.19(?)	17.82	-0.63
Si*	17.22(?)	17.92	-0.80
Ca	15.08	16.61	-1.53
Ti	15.95	15.31	+0.64
Cr	14.91	15.80	-0.89
Mn	17.30	15.54	+1.76
Fe	16.75	17.00	-0.25
Ga	<15.3	12.87	<2.4
Sr	14.62	13.12	1.50
Y	14.16	12.87	1.29
Zr	14.62	12.92	1.70

*see note on p. 16.

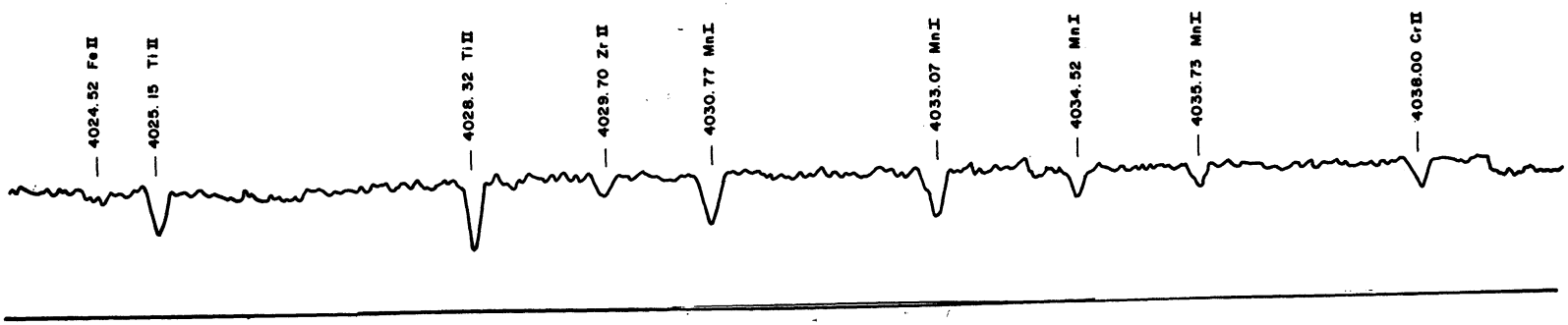

Fig. 1. Tracings of a portion of the spectrum of 53 Tauri.

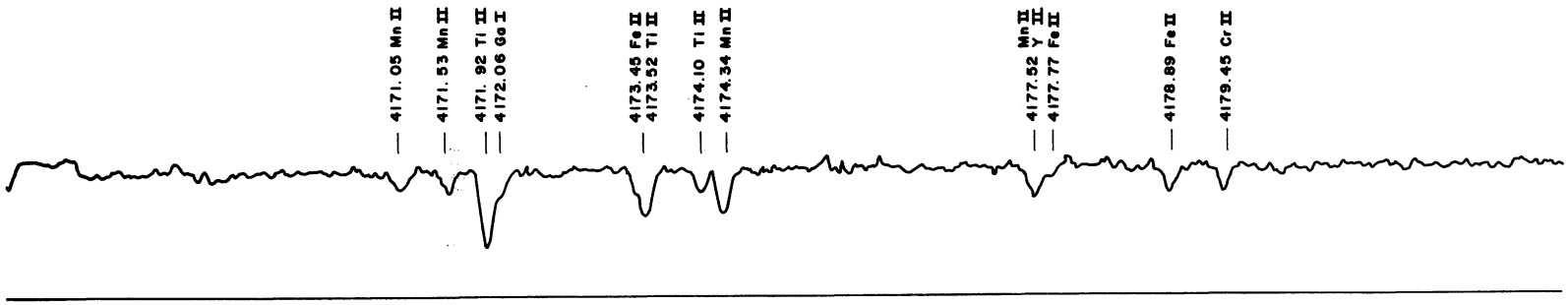

Fig. 1 (Concluded)

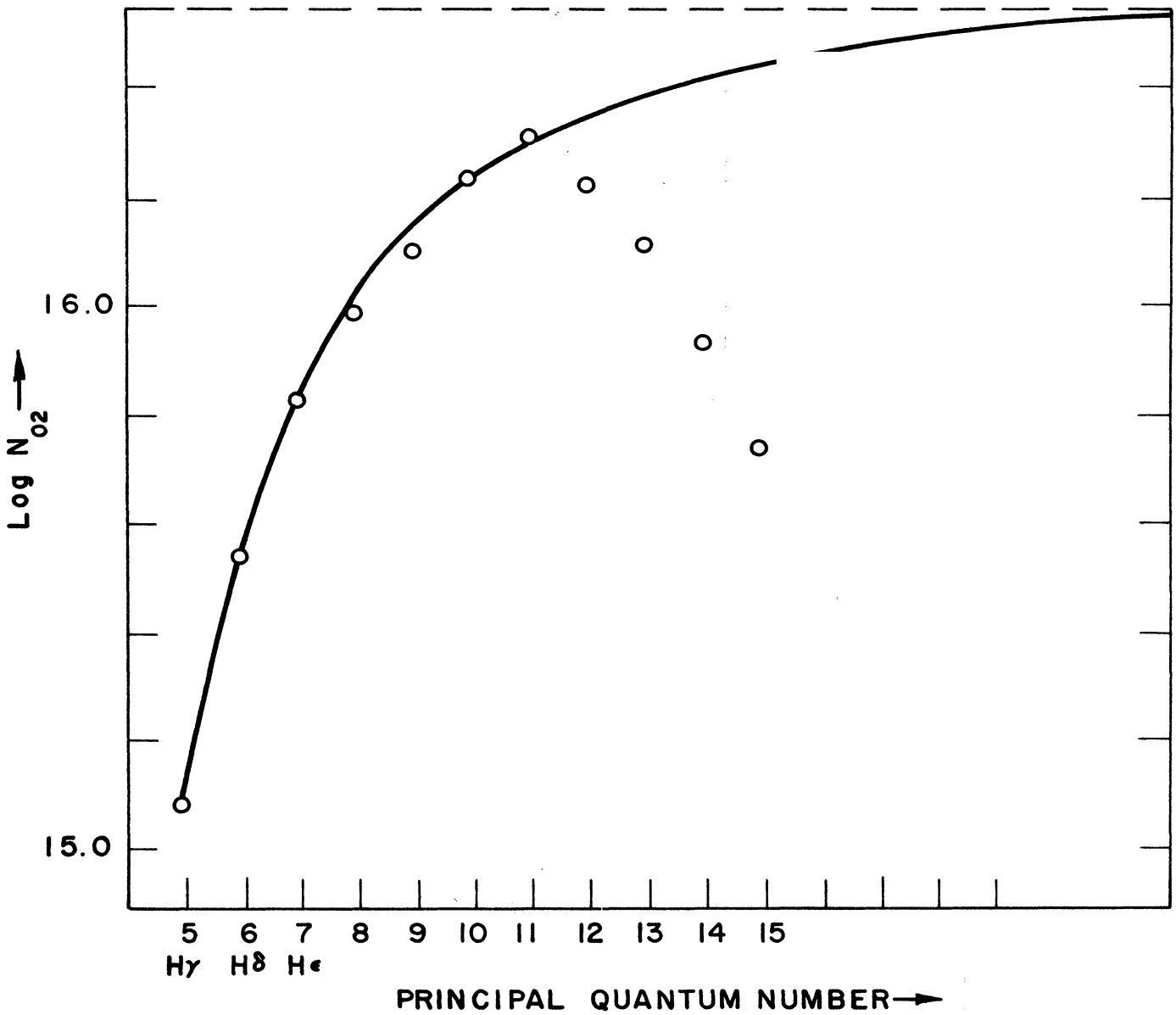

Fig. 2. Determination of the number of neutral hydrogen atoms in the second level. Following Unsöld's procedure, we plot N_{02}, calculated from Eq. 14 against the principal quantum number, n, and extrapolate to obtain an asymptotic calue of N_{02}.

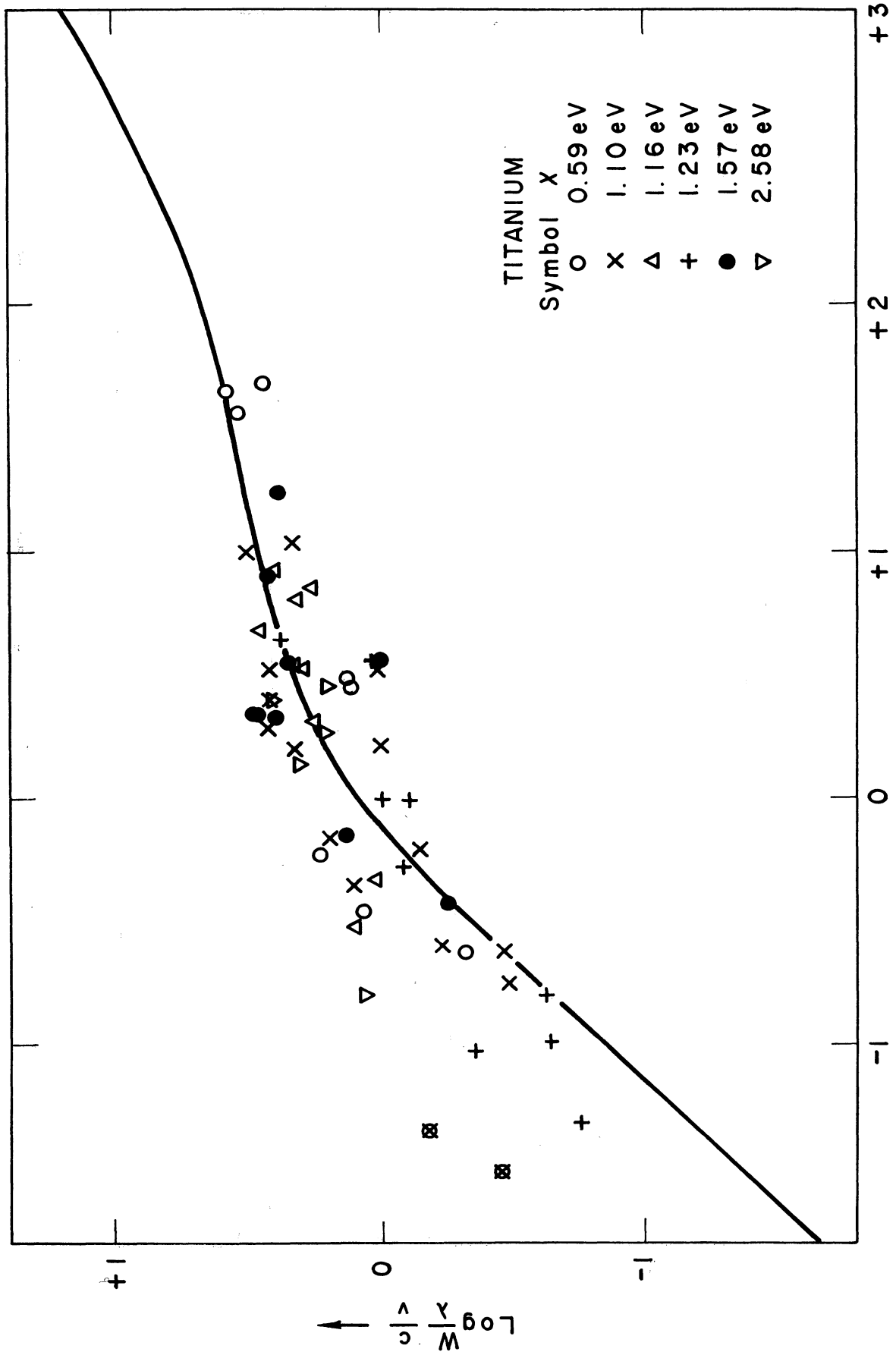

Fig. 3. Curve of growth for titanium. Lines arising from levels of very nearly the same excitation potential are plotted against C_3 + log gfλ and each group is fitted separately to the theoretical curve of growth. The ordinate is log W/λ c/v, the abscissa is log X_o.

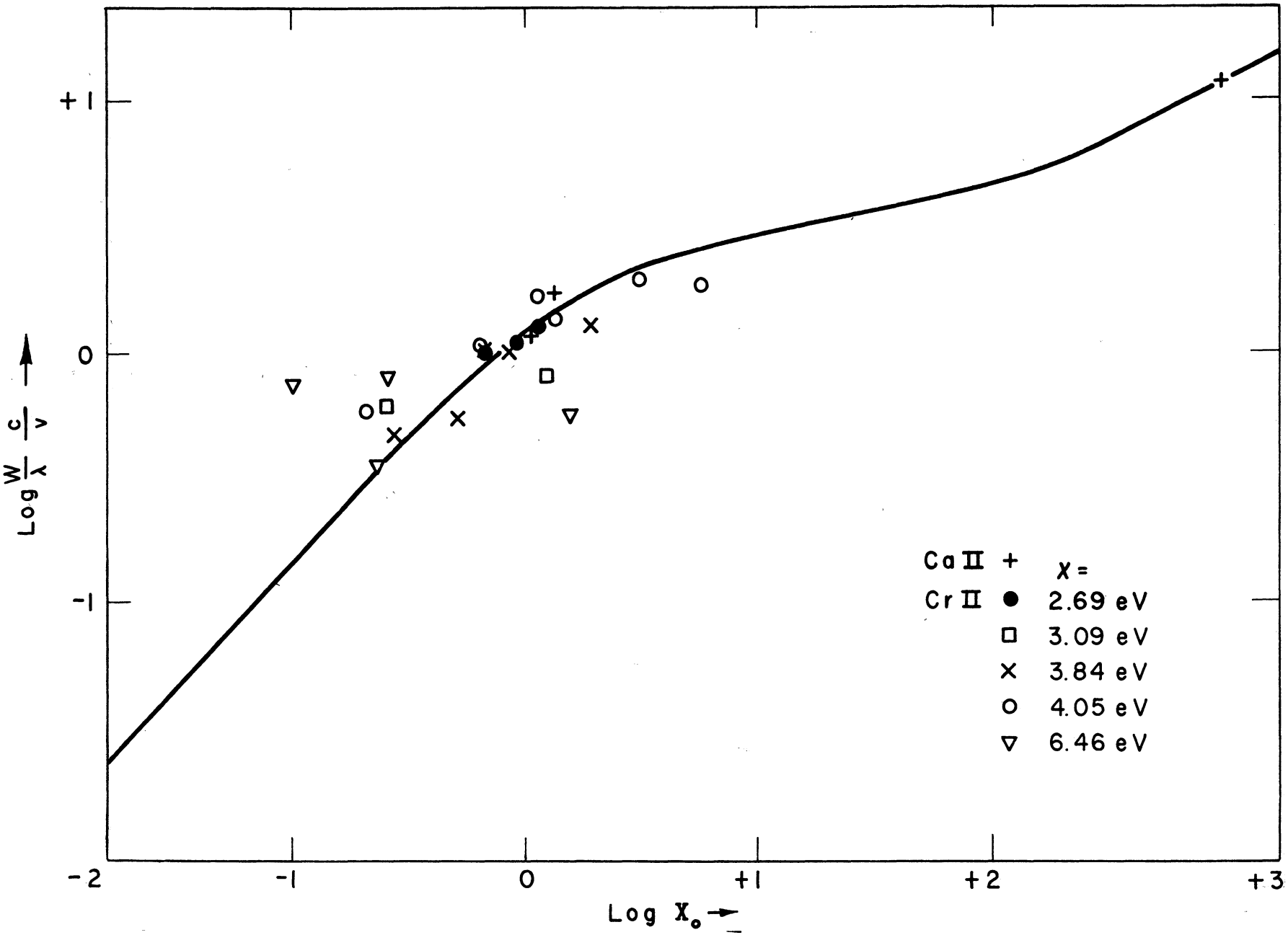

Fig. 4. Curve of growth for ionized calcium and ionized chromium. We plot log W/λ c/v against log X_o.

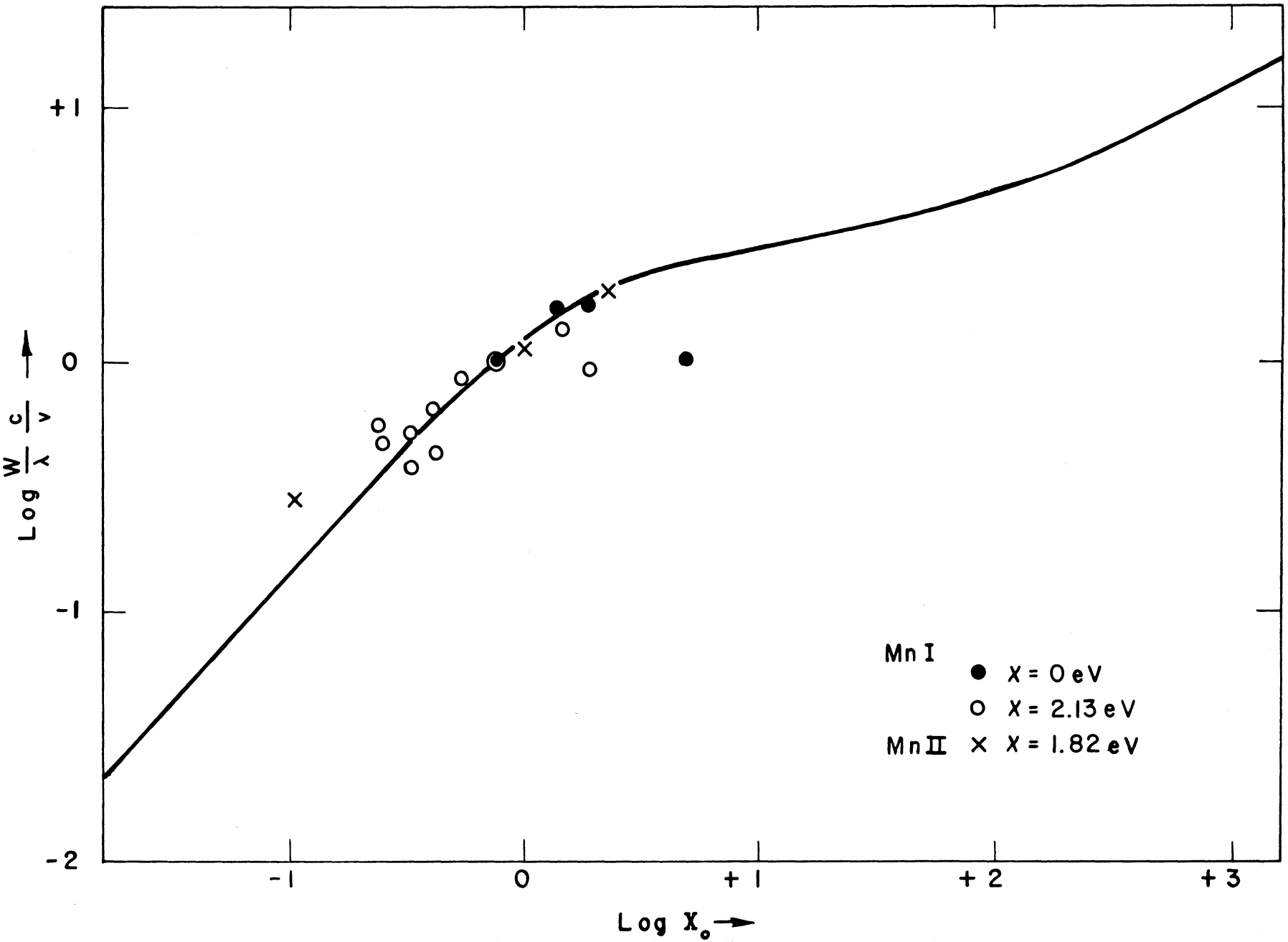

Fig. 5. Curve of growth for neutral and ionized manganese. Data for the 5.8 eV lines are not included.

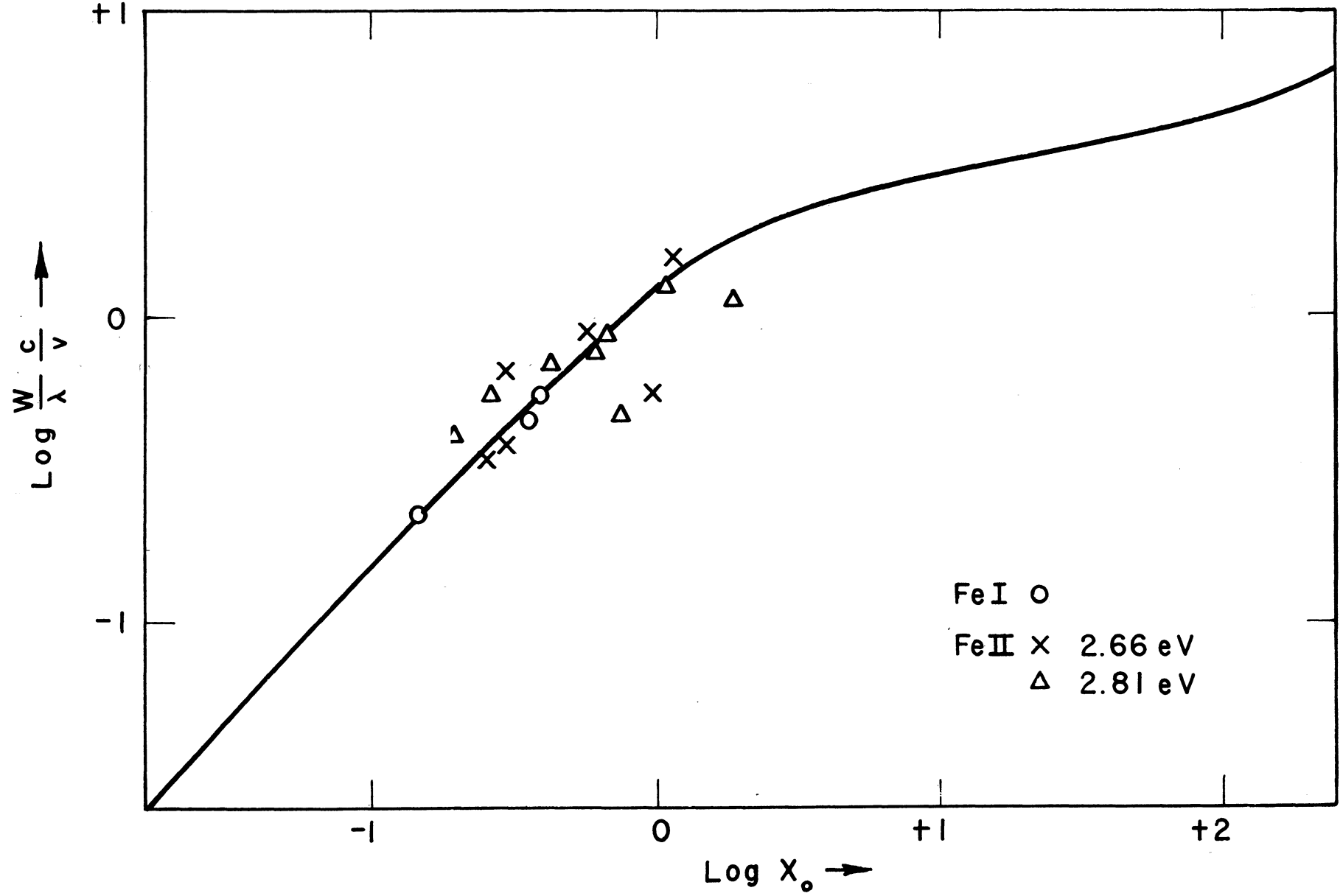

Fig. 6. Curve of growth for neutral and ionized iron.

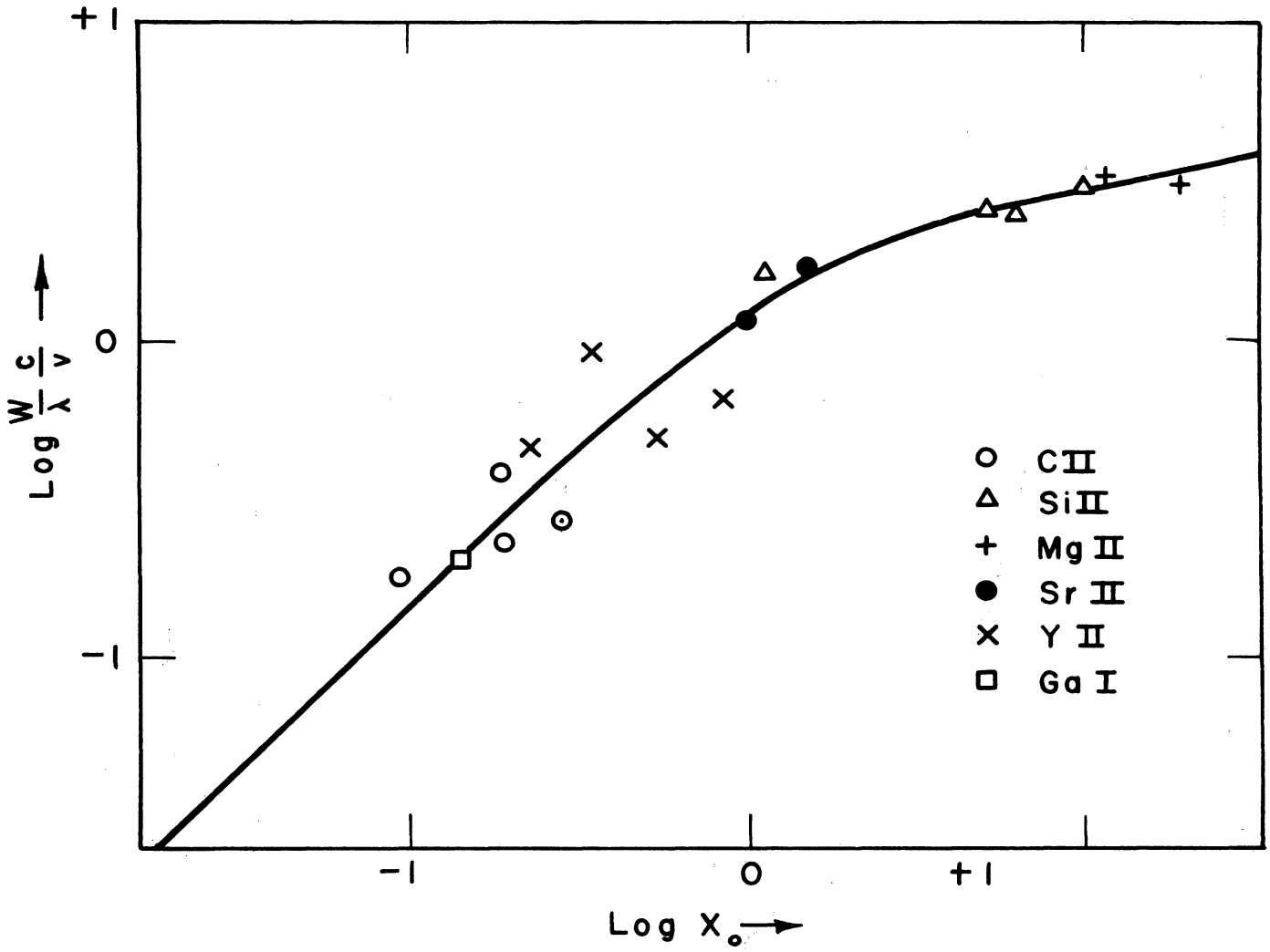

Fig. 7. Curve of growth for CII, MgII, SiII, GaI, SrII, and YII.

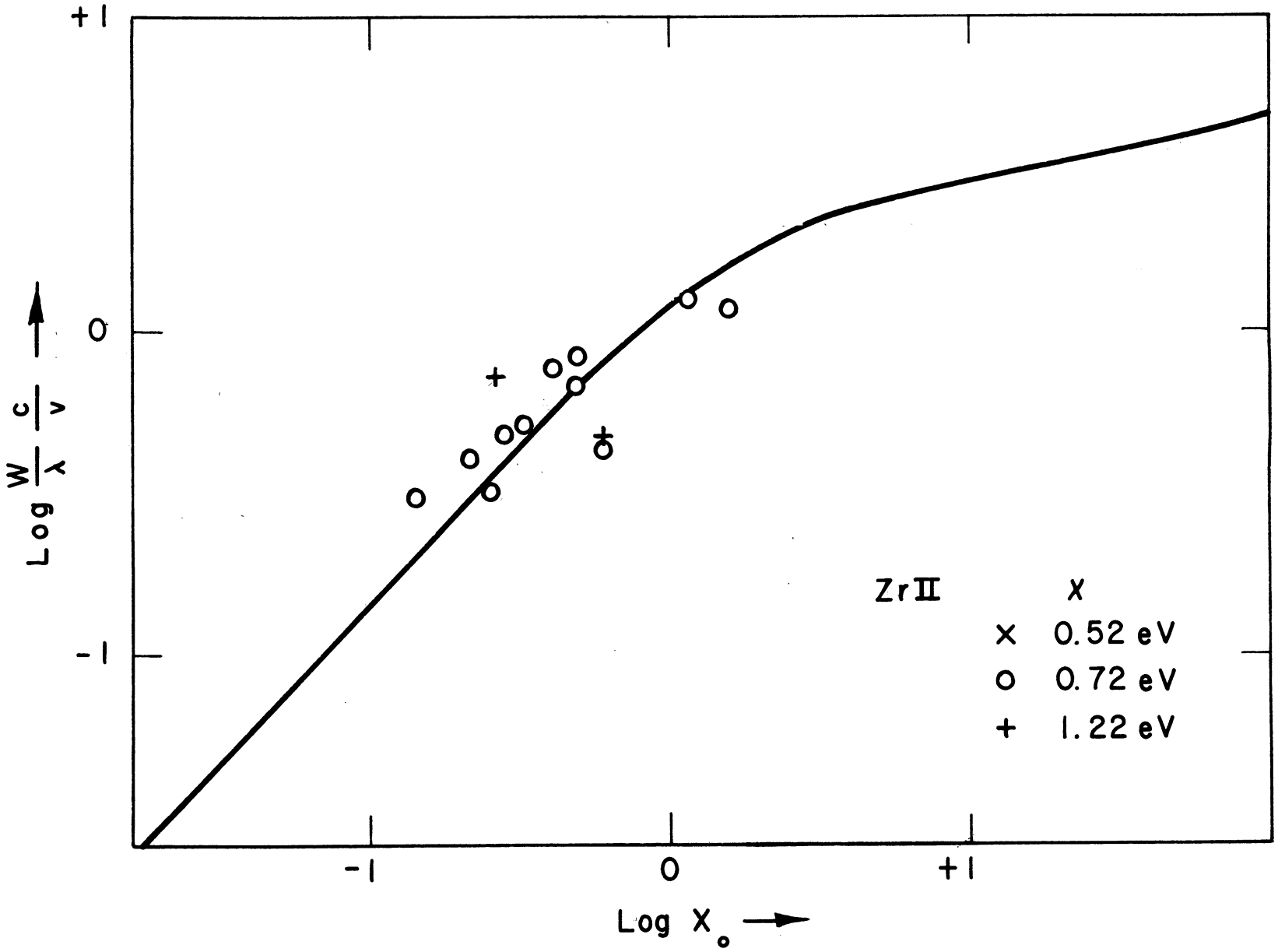

Fig. 8. Curve of growth for ZrII.

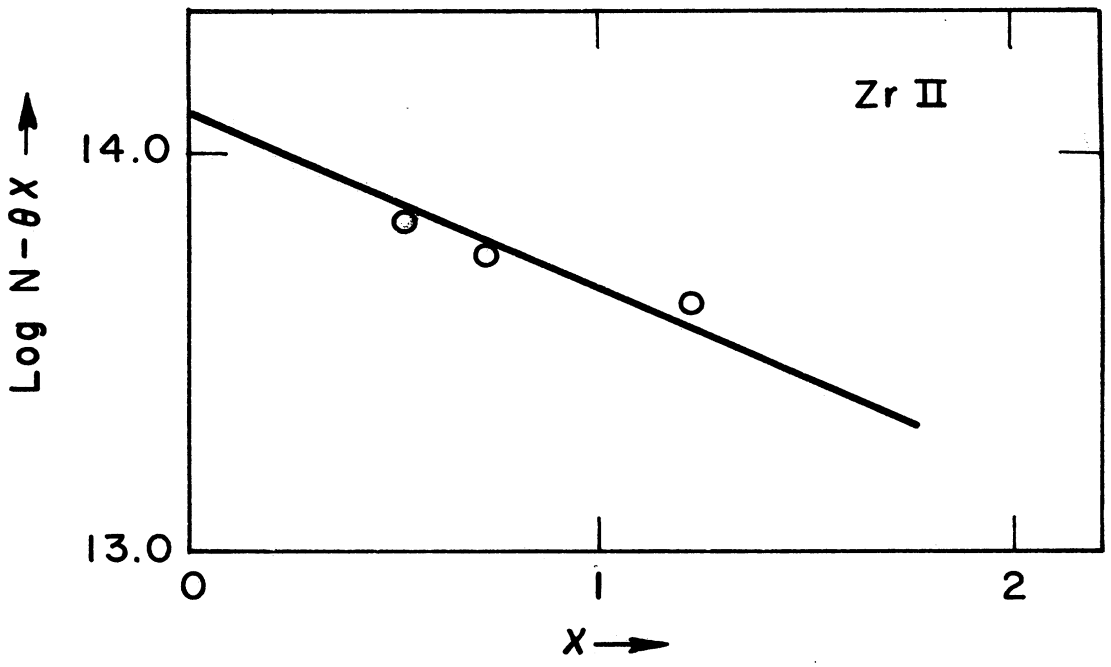

Fig. 9. Determination of the concentration of ionized zirconium atoms. We plot log N - $\theta\chi$ = log C_3 + log $gf\lambda$ against χ. The slope of the straight line corresponds to θ = 0.45. Its intercept with the χ = 0 axis gives log N(ZrII).

Plate I

53 Tauri

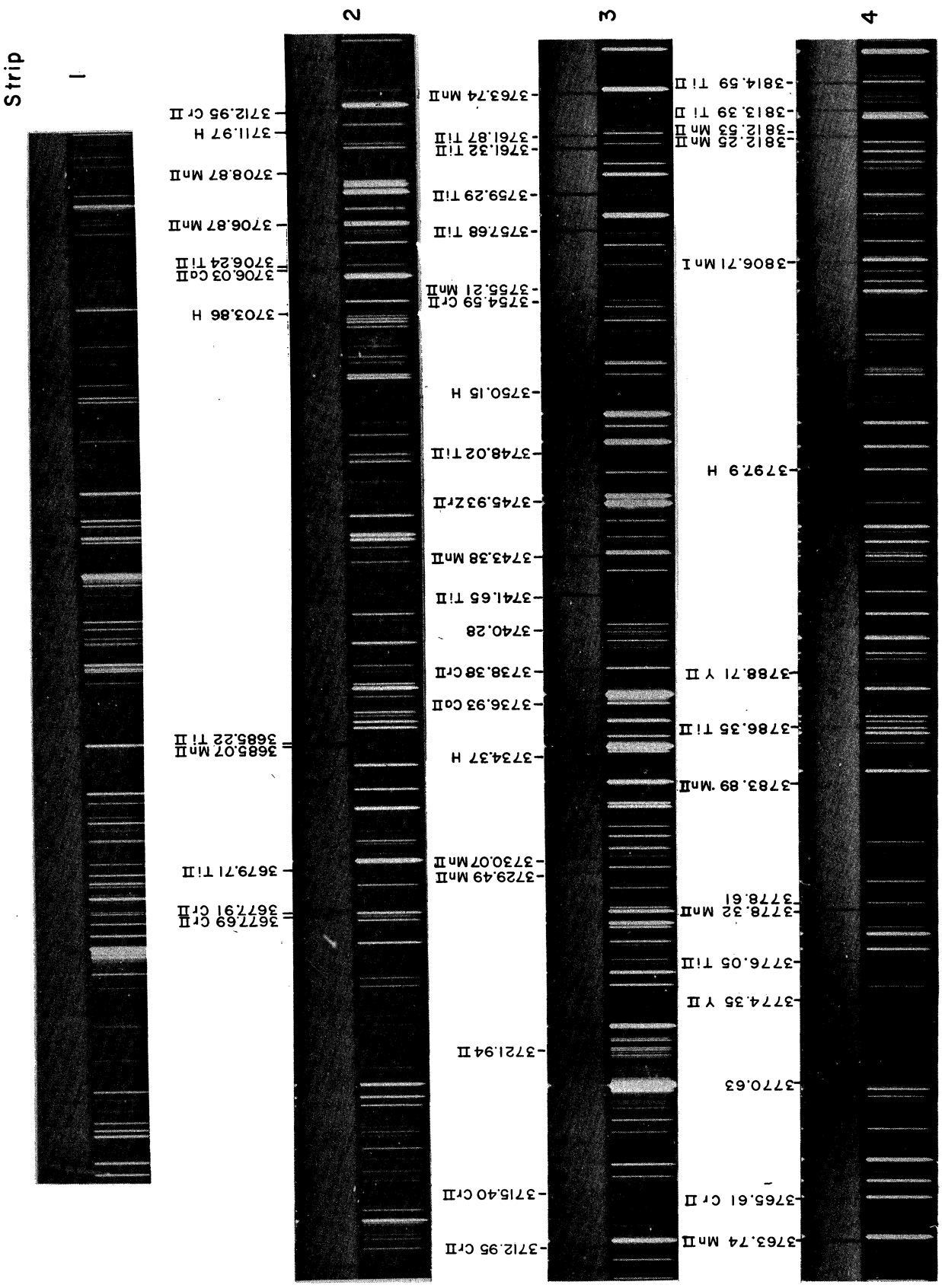

Plate 2

53 Tauri

Plate 3

53 Tauri

Plate 4

53 Tauri

Plate 5

53 Tauri

Plate 6

53 Tauri

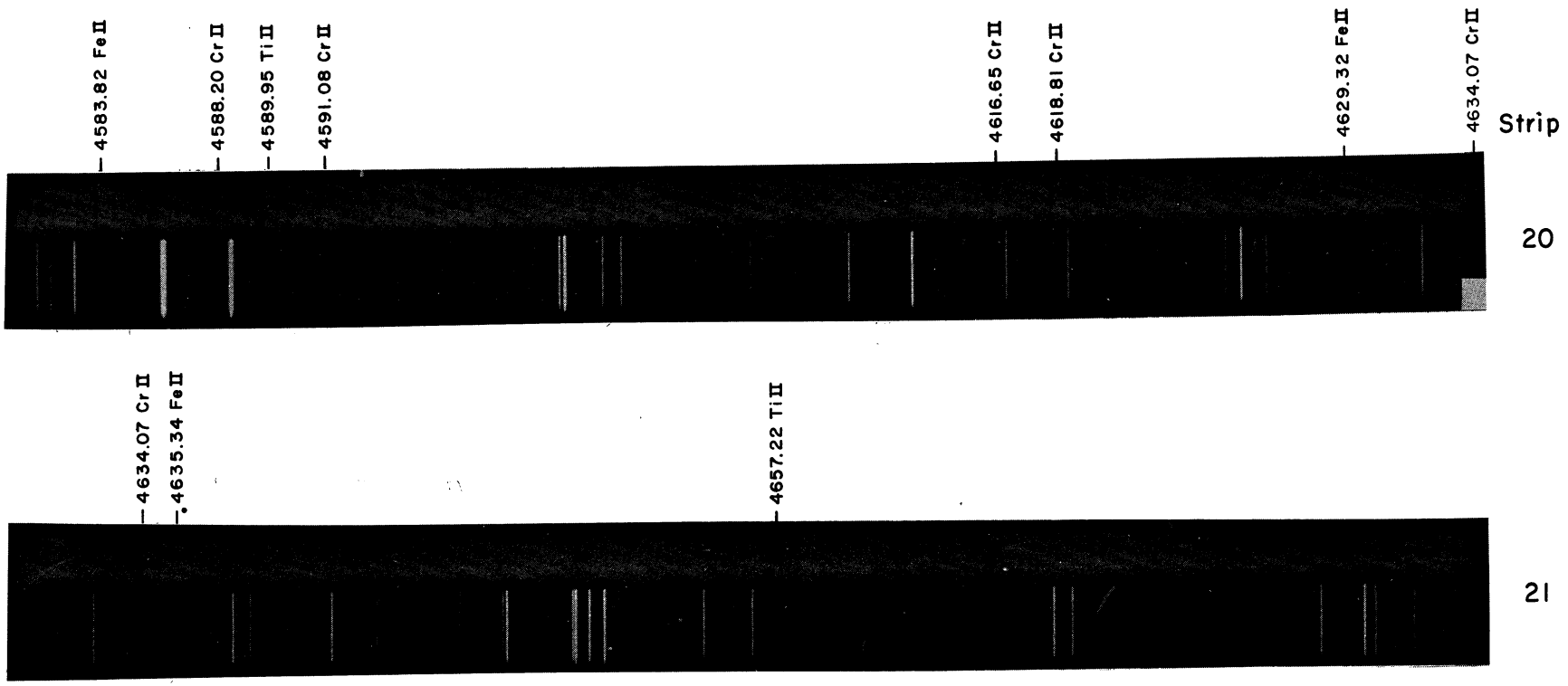
4583.82 Fe II
4588.20 Cr II
4589.95 Ti II
4591.08 Cr II
4616.65 Cr II
4618.81 Cr II
4629.32 Fe II
4634.07 Cr II
Strip
20
4634.07 Cr II
4635.34 Fe II
4657.22 Ti II
21

THE UNIVERSITY OF MICHIGAN
COLLEGE OF LITERATURE, SCIENCE, AND THE ARTS
Department of Astronomy

Final Report

ABUNDANCES OF ELEMENTS IN STARS AND NEBULAE

L. H. Aller

ORA Project 03719

under contract with:

AIR FORCE OFFICE OF SCIENTIFIC RESEARCH
AIR RESEARCH AND DEVELOPMENT COMMAND
CONTRACT NO. AF 49(638)-807
WASHINGTON, D.C.

administered through:

OFFICE OF RESEARCH ADMINISTRATION ANN ARBOR

September 1962

ACKNOWLEDGMENTS

The investigations described in this summary and in the preceding technical reports could not have been undertaken without the generous help of many individuals and institutions.

The study of the spectrum of NGC 7009 and two other planetary nebulae was made possible by a cooperative arrangement with the Mt. Wilson and Palomar Observatories. I am indebted to Director I. S. Bowen for many helpful discussions in connection with this work.

All of the work carried on in the southern hemisphere, viz., (1) spectrophotometry of gaseous nebulae in the Magellanic Clouds, (2) spectrophotometry of clusters, and (3) studies of γ Velorum and HD 96446, were made possibly by the award of a Senior Postdoctoral Fellowship at the Austrialian National University for 1960-61, and by generous cooperation and assistance from the Australian National University. In particular I would like to cite help received from Director Bart J. Bok, Prof. T. Dunham, Jr., Dr. S.C.B. Gascoigne, Dr. A. Hogg, Dr. H. Gollnow, Dr. A. Przybylski, and members of the technical staffs of the Mt. Stromlo Observatory and Mt. Bingar Field station. These astronomers generously gave up time from their own investigations and programs to permit us to carry out our spectrophotometric and spectroscopic programs. D. J. Faulkner supplied valuable data after my return to the U.S.A.

Thanks are due to Mrs. Anne Cowley, who supervised much of the routine work and carried out a number of the investigations, to Mrs. H. Dickel for her thorough discussion of the spectrophotometric data for the Large Magellanic Cloud, to Mrs. Katherine Grey, who reduced the data for NGC 7009, to Mr. Herbert Rood, who verified the reductions of the star clusters and γ Velorum, and to Tom Toon, Eric Leighton, and Tom Jones, who did much of the routine work. Individual acknowledgments are also included in the technical reports.

TABLE OF CONTENTS

LIST OF TABLES

LIST OF TABLES (Concluded)

LIST OF FIGURES

LIST OF FIGURES (Concluded)

SECTION 1

SUMMARY OF THE YEAR'S ACTIVITIES

The program on the "Abundances of the Elements in Stars and Nebulae" carried out from August 1961 through August 1962 in the Astronomy Department of The University of Michigan has involved both theoretical and observational studies. Some of these are reported in previous technical reports and others are described here in Sections II-VIII.

Our investigations of the gaseous nebulae are described in Sections V and VI, written by Helene R. Dickel, D. J. Faulkner, and L. H. Aller, and in Section VII. Our work this year has been entirely concerned with observational problems. A series of photoelectric spectrophotometric measurements of emission nebulosities in both the Small Magellanic Cloud and the Large Magellanic Cloud were made in Australia by Faulkner and Aller. They have been analyzed and discussed by Mrs. Dickel; the principal results may be summarized briefly as follows. The nebulosities appear to be similar to those found in our own galaxy although a number are larger and more massive than the best known galactic diffuse nebulae in our own neighborhood. Since the distance of the clouds is known, we can convert the measured surface brightnesses (expressed in conventional c.g.s. units) into emissions per unit volume and derive electron densities, provided the electron temperature is known or can be inferred. These mean densities turn out to be rather low compared with those found in objects like the Orion nebula, but when effects of filamentary structure are taken into account, the actual densities are probably more nearly comparable. The intensities of the strongest forbidden lines of [OII], [OIII], and [NeIII] have been measured and from these the ionic concentrations are found. The ratios of O^{+}/H, O^{++}/H, and Ne^{++}/H are comparable with those found in emission nebulosities in our own galaxy. In all gaseous nebulae it is difficult to find the actual abundance of an element such as O or Ne from the abundance of only a few of its ions, and these difficulties are particularly severe for diffuse nebulae in which only a few lines can be observed. From results obtained for a large number of nebulosities, it is concluded that the ratio of oxygen to hydrogen and of neon to hydrogen is about the same in the Large Magellanic Cloud and in the galaxy. A similar situation probably holds for the Small Magellanic Cloud but the diffuse nebulae are fewer and generally fainter, so that a definitive study is more difficult. Spectroscopic observations of the brighter diffuse nebulae in both clouds are urgently needed.

In Section VII we describe in detail the spectrum of the planetary nebula NGC 7009 and present lists of lines, their identifications, and rough intensities. The purpose of this investigation is to provide material for theoretical studies, which are being carried out in collaboration with Stanley Czyzak of the Fundamental Physics Laboratory at Wright-Patterson Air Force Base.

Stellar investigations have involved both theoretical and observational studies. During the fall of 1961 Dr. Donald Mugglestone spent several months with us studying basic problems in the determination of abundances in stellar spectra; his own summary of his work is presented in Section VIII.

An urgent necessity for improving stellar and solar abundances is improved f-values. We have employed gf-values determined by Corliss at the National Bureau of Standards to obtain improved abundances for a number of metals in the sun. The results were described in Technical Report No. 2. In addition we have attempted to obtain gf-values for a number of ions by combining laboratory and stellar data (Technical Report No. 3). These gf-values were then employed in a curve-of-growth analysis for a remarkable star rich in manganese observed by William P. Bidelman at Lick Observatory (Technical Report No. 5).

Among purely theoretical investigations, mention must be made of the work of Anne and Charles Cowley, who developed a machine routine for computing the relation between gas and electron pressure for stellar atmospheres of arbitrary composition (Technical Report No. 4). The advantage of this technique is that one may allow for the effect produced by individual atoms that are easily ionized.

One of the objectives of our work was an investigation of properties of hydrogen deficient stars. In detailed theoretical study made of a pure helium atmosphere (Technical Report No. 1) it was demonstrated that conventional mathematical methods capable of yielding good results for a pure hydrogen atmosphere failed when applied to one of pure helium. The reason for this discordance is not known, and a separate study will have to be devoted to it.

Prominent among hydrogen deficient stars are those of the Wolf-Rayet type. In Section III we describe some results obtained for the brightest of these objects, γ_2 Velorum, a star of the "carbon" type. Accurate spectrophotometry must provide one of the bases for assessment of these objects. This star appears to be remarkably blue; its energy distribution corresponds to a temperature of 32,000°K, indicating that there exists little if any space reddening. The remarkable hydrogen deficient star HD 96446 appears to be one of the brightest absorption-line objects, but with the data we were able to secure it has been possible to determine only the hydrogen/helium ratio. The ratios of other elements cannot be determined until better spectrograms are obtained.

In extending composition studies to remote stellar systems, one can no longer work with individual stars and must investigate the composite spectra of many of them. By observing the spectra of clusters and galaxies, one may observe certain lines and molecular bands that are sensitive to luminosity, temperature, and the metal/hydrogen ratio. If one can also measure the energy distribution in the spectra of such clusters or galaxies, it may be possible to determine the metal/hydrogen ratios. With this hope in mind we present in Section II the results of an extended study of the energy distributions in globular clusters, both in our own galaxy and in the Magellanic Clouds. Comparison of the energy distributions which are expressed in terms

of spectral types of standard stars with estimated spectral classes for the clusters provides some clue to metal deficiencies, but it should be emphasized that quantitative results are possible only when color-magnitude diagrams and luminosity functions are available for the stars under consideration and when energy distributions in stars of various degrees of metal deficiency are known.

SECTION II

ENERGY DISTRIBUTION IN GLOBULAR STAR CLUSTERS

by L. H. Aller and D. J. Faulkner

A. INTRODUCTION

Some of the most engaging opportunities for the study of stellar evolution and differences in stellar composition are provided by star clusters. Differences in apparent brightness correspond to differences in intrinsic brightness, whereas observed differences in color correspond to true differences in color. Furthermore the stars of a cluster (with the possible exception of the very faintest ones) all have the same age.

Some clusters of the "open" or "galactic" type are sufficiently close to the sun to permit detailed studies of individual stars. In more remote clusters such as those of the globular type, spectra of individual stars cannot be investigated except with the very largest telescopes. Even then, it is possible to study only the very brightest stars in the very nearest clusters. For most clusters we are limited to the following observational data:

(1) Magnitudes and colors of individual stars;

(2) Integrated magnitude and colors of the cluster;

(3) Integrated spectrum of the cluster;

(4) Radial velocity of the cluster; and

(5) Energy distribution in the integrated light of the cluster.

Most attention has been paid to the construction of color-magnitude arrays for individual clusters, as these have given much useful information that can be interpreted in terms of theories of stellar evolution. Theoretical color-magnitude arrays can be calculated; from a comparison of observed and computed arrays it is then possible to estimate the age of the cluster and the metal/hydrogen ratio.

The chemical composition of a star or at least the metal/hydrogen ratio determines not only the relation between its color and effective temperature but also its evolutionary track in the color-magnitude [Russell-Hertzsprung] diagram. For example, a metal deficient star of about 1.2 or 1.5 solar masses becomes brighter in the late stages of its evolution than does one of normal stellar composition. By comparing theoretical evolutionary tracks computed for different metal/hydrogen ratios with the observed color-magnitude arrays it is possible to estimate abnormalities in the metal/hydrogen ratios.

The integrated magnitude of a cluster can be measured with a relatively small telescope, and it is also possible to measure colors with a relatively long baseline in wavelength. Such studies are very valuable in that they

provide convenient checks on the assumed stellar content and chemical composition of a cluster.

Spectrograms secured with a slit spectrograph yield not only spectral classifications but also radial velocities, which are necessary for assessing the kinematics of these objects.

The present investigation is concerned with the energy distributions in globular clusters. In a sense energy-distribution measurements are comparable with multi-color photometry. The chief advantage is that narrower band passes may be used and the entire spectrum traced, whereas in multi-color photometry one is limited to effective wavelengths determined by the filter and a rather broad band-pass. On the other band, broad band-pass photometry often permits one to cover a broader spectral range, and to work much faster. Since the time required for a single observation is much shorter, the observer is less at the mercy of the sky transparency. Hence a greater accuracy can be obtained.

We want to emphasize that energy distribution measurements such as those we have secured with purities of 20A, 40A, or sometimes worse should be supplemented by slit spectrograms. A judicious combination of spectrograms of moderate dispersion and energy scans should provide valuable boundary conditions for testing hypotheses of the compositions of stars contained in star clusters.

Ideally, one could proceed as follows. From color-magnitude arrays we synthesize the spectrum and energy distribution in a star cluster. For each interval of magnitude we know the number of stars and the distribution of these stars with respect to color. The only adjustable parameter is the chemical composition. In our own galaxy we can find stars of different chemical composition and can determine their energy distributions, colors, and spectral characteristics. For each assumed ratio of metals to hydrogen, one can construct what the integrated spectrum and energy distribution of a star cluster would look like—given its color-magnitude array and luminosity function.

Thus, the problem is a well determined one. The metal/hydrogen ratio in a cluster can be found provided we know:

(1) The color-magnitude array for a star's contributing to the integrated light of the cluster;

(2) The luminosity function for all stars contributing appreciably to the integrated light of the cluster;

(3) The spectral class and the intensities of strategic luminosity-dependent and composition-dependent lines;

(4) The energy distribution in the integrated spectrum or the energy flux from the cluster at certain pre-selected wavelengths, with a band-pass $\Delta\lambda$;

(5) The energy distributions in stars of different temperatures, intrinsic luminosities, and chemical compositions.

Unfortunately, this program cannot yet be carried out for a single cluster. For only a few clusters (see Part B of this Section) do we have detailed color-magnitude arrays and luminosity functions. The spectroscopic observations have almost all been carried out with low dispersions and give only fragmentary data on line ratios needed for luminosity classifications and chemical compositions.

On the other hand, energy distributions have been measured for only a limited number of stars, most of which are of normal chemical composition. Energy distributions have been measured for only a few stars of abnormal chemical composition!

In the present study we have attempted to supply data on the energy distributions in several southern globular clusters. We have included several objects in the Large Magellanic Cloud, LMC, and one object, IC 419, in the Small Magellanic Cloud, SMC. Part B is based on a compilation by Herbert Rood and gives a brief summary of some of the salient features of the clusters observed, while Part C describes our observational techniques, the results obtained therewith, and some conclusions that may be drawn from our study.

B. DATA FOR SOUTHERN GLOBULAR CLUSTERS*

1. PROPERTIES OF SOME SOUTHERN GLOBULAR CLUSTERS (TABLE 2-1)

Table 2-1 gives data for the southern globular clusters contained in our program. The number in brackets [ ] denotes the reference from which the data were obtained. The superscript after brackets denotes the number of the relevant footnote.

Column

1 NGC Number.

2 Right ascension and declination for 1950.

3 Galactic latitude and longitude for 1900 (based on the old coordinates of the pole).

*Prepared by H. Rood.

Column

4 Reference to place where color-magnitude diagram is found.

5 Reference to place where luminosity function is found.

6 Spectral type as estimated by CH/Hγ intensity ratio, Hγ strength, strength of FeI from λ4250 to λ4400. Spectral types of [30] are Harvard types.

7 Photographic magnitude P or m_{pg}.

8 Color index P-V or $m_{pg}-m_{pv}$.

9 Distance modulus corrected for interstellar absorption and reduced to a value of the absolute magnitude of the RR Lyrae stars of $M_{RR} = +0.5$. Number in parenthesis is probable error.

10 Distance in KPC calculated from the eq. log(dist) = 0.2(cor. mod.+5)-3
= 0.2(cor. mod.-10).

11 Measured radial velocity in km/sec. Number in parenthesis is probable error.

12 Mass of cluster in solar masses.

13 Concentration class on the system of Shapley and Sawyer, Harvard Bull. No. 849(1927).

14 Apparent angular diameter. Refs. [18] and [29] give estimates from images on plates. Ref. [15] gives estimate from star counts. Ref. [28] gives photoelectric diameter, the diameter within which is found 1/2 the light = effective diameter. Ref. [31] gives 2 x mean distance of RR Lyrae stars from cluster center = mean diameter.

2. DISTANCE TO THE GLOBULAR CLUSTERS OF THE MAGELLANIC CLOUDS

a. The Distance Modulus

Thackeray (IAU Symp. 7, Co-ordination of Galactic Research p. 81, 1959) states that the "uncertainty regarding location in depth within the clouds adds a random error of about ±0.13 magnitudes.") As we shall see later, this is much smaller than the uncertainties in distances to the clouds. Furthermore, if we assume that the clouds' globular clusters are of the order of or less than a typical dimension of each cloud away from the cloud center, then the true distance modulus to each cloud equals the true distance modulus of its clusters to well within the total uncertainty of the distance modulus.

Color-magnitude diagrams have been obtained for NGC 1783, NGC 1978, NGC 330, and NGC 419. To construct a color-absolute magnitude diagram, the true distance modulus and absorption must be known. Their values as used in connection with observed color-magnitude diagrams are given below.

NGC 1783: Sandage and Eggen [17] take the true modulus to the LMC = true modulus of NGC 1783 as 18.7. They assume no reddening even though the redness of some stars may be explained if $E_{B-V} = +0^m.6$, because some stars are observed near the theoretical blue limit of B-V = -0.4 inside and nearby the cluster.

NGC 1978: Hodge [23] takes the distance modulus of LMC = distance modulus of NGC 1978 as 18.7. He does not consider reddening.

NGC 330 and NGC 419: Arp [24] and [26] uses as distance modulus of SMC = distance modulus of NGC 330 = distance modulus of NGC 419 = 19.2. He does not consider reddening.

IAU Transactions for 1961, p. 296, gives 19.0±0.5 magnitudes as probably the best present value of the distance modulus of the clouds.

Since absorption is probably close to zero (as far as can be concluded from present data), and the LMC and SMC have the same modulus (within the accuracy of present data), we will use as the distance modulus to every cloud cluster:

$$m - M = 19.0 \pm 0.5$$

or a distance of 63(+19, -13)KPC.

b. The Individual Clusters

We now consider data for the individual clusters that have been observed.

(1) 47 Tucanae.—The distance of 47 Tucanae has been studied in recent years by Feast and Thackeray [8], by Wildey [3], and by Kinman [12]. From studies of foreign stars Feast and Thackeray estimated the absorption to be 0.2 magnitudes; they adopted the absolute magnitudes of the RR Lyrae stars as +0.5 and obtained a corrected distance modulus of 13.2, corresponding to a distance of 4.4 kiloparsecs. Wildey concluded that if the absolute visual magnitude of the stars in the horizontal branch of the color-magnitude array is 0.0, then m-M, the distance modulus, = 14.1. If the blue end of the horizontal branch is as faint or fainter than the horizontal branch of NGC 6356, taken as M = 0.9, then $m-M \leq 13.2$.

From a discussion of all available data and methods of distance determination, Kinman found m-M = 13.8±0.4 for $M_{RR} = 0$. Wildey constructed a color-magnitude diagram from 300 stars to a limiting magnitude B = 15.4, V = 14.6

(Johnson-Morgan magnitudes being denoted here by U = ultraviolet, B = blue, and V = visual). He finds this giant branch to be fainter than the giant branch in most globular clusters (which are hydrogen deficient) and concludes that 47 Tucanae has a metal/hydrogen ratio more nearly comparable with that of the sun than with that of extreme population type II.

Gascoigne and Burr [7] measured photoelectrically the surface brightness, integrated magnitudes, and color of 47 Tucanae. They determined an integrated magnitude P = 4.7±0.05 and a color P-V = 0.67. They found 47 Tucanae to be redder at the center than at the edge.

Kinman [5] finds an integrated spectral type of G3, and Feast and Thackeray [8] have determined the spectral types of 32 bright stars by comparing them with standards on the MK system. They find that the red giant stars in 47 Tucanae are much closer to "normal" population type I giants than to the extreme population II globular cluster stars, and conclude that the metal/hydrogen ratio is not less than about 0.25 normal. The brightest star in the cluster, $M_V = -3.0$, has a normal B8III spectrum. Thackeray [9] and Thackeray and Wesselink [13] note that 47 Tucanae is unique in that it is the only globular cluster in the galaxy known to contain M stars. Kinman [5] studied the spectra of some bright giant K stars in 47 Tucanae and found them to be "normal."

Feast and Thackeray [8] found no rotation in 47 Tucanae from the radial velocities of red giant stars, although they did find some indication that late-type giants may be losing mass since their radial velocities became more negative with advancing spectral class from G8 to M2. If this correlation is taken into account, the virial theorem gives an upper limit to the mass for the cluster as 250,000 M_{sun}. Then $M/L \leq 0.3$ solar units, which is much less than for elliptical galaxies.

Data on variable stars are given by Mrs. Hogg [16]. See also Feast, Thackeray, and Wesselink [13].

(2) ω Centauri = NGC 5139.—From a discussion of all available data, Kinman [12] gets a distance modulus m-M = 13.5±0.7. The apparent diameter of this very large cluster is given by Mrs. Hogg [1] as 65.4' whereas Lindsay [15] from star counts finds a diameter of 101'. The cluster is noticeably elliptical.

Belserene [4] has obtained a color-magnitude diagram in B and V to a limiting magnitude of B = 19.5 and has also obtained the luminosity function from star counts. A stellar density 25,000 times that near the sun is estimated for the center of the cluster!

From the CH/Hγ ratio, Kinman [5] obtained an integrated spectral type F7. Morgan classified the spectrum by comparing intensity ratios and intensities with a sequence of standard dwarfs on the MK system, viz.,

CH/Hγ gives F7 (in agreement with Kinman);
Hγ intensity gives a "hydrogen" type F8; and
FeI intensity gives a "metallic line type" F0.

Since the metallic lines are weak, the metals appear to be deficient. In Morgan's system of eight groups I-VIII in order of increasing metallic abundance, ω Centauri falls in group II.

Since the pioneer work of Popper, the weakness of metallic lines in individual stars has been confirmed (Kinman [5]).

Gascoigne and Burr [7] obtained the integrated mangitude, brightness distribution, and color for ω Centauri. They find P = 4.25; and P-V = 0.68.

The extensive literature on the variable stars up to 1959 has been summarized by Mrs. Hogg [16]. See also Belserene [14].

(3) NGC 6572.—Kinman studied the spectra of some giant stars in this cluster and found that if they were red giants, their metallic lines were weakened but not very much weakened.

c. Clusters of the Large Magellanic Cloud

In discussing the four clusters of the Large Magellanic Cloud we refer to Section 2a, "The Distance Modulus."

(1) NGC 1783.—Sandage and Eggen [17] obtained a color-magnitude diagram to V = 17. Three features indicate that NGC 1783 is different from "normal" clusters in the galaxy:

(a) The giant branch is well populated up to B-V = 2.4, whereas all clusters in our galaxy terminate at B-V about 1.6. No giant stars in clusters in the galaxy are as red as B-V = +2.4.

(b) The slope $\delta V/\delta(B-V) = 1.25$ is gentler than that of the giant branches in normal clusters.

(c) There is no drop towards a vertical subgiant sequence beginning at $(B-V)_0 = +0.9$. The giant sequence remains linear to the limit of the observations.

The diagrams for NGC 419 and for NGC 1978 as obtained by Arp and Hodge are very similar to that of NGC 1783, the giant-branch slopes being almost the same. The spectra of the stars in NGC 6356 imply a high metal abundance. The color indices of some stars in NGC 1783 are as red as B-V = 2.4 and are not limited by TiO bands at B-V = 1.7 as are stars with high metal abundance.

Why then are the NGC 6356 and NGC 1783 giant-branch slopes the same?

Gascoigne [28] gives the photoelectric effective diameter of the cluster as 1.2'. This is the diameter within which is concentrated half the light of the cluster.

(2) NGC 1831.—Hodge [20] describes the color-magnitude diagram as similar to that for M11. NGC 1831 is similar in appearnce to globular clusters but is much younger. It differs from galactic clusters by the enormous quantity of stars and the location of the giants in the color-magnitude diagram. They are bluer and brighter than in the open clusters. Hodge [21] describes the cluster as "large and concentrated." Gascoigne derives a photoelectric effective diameter of 1.0'. The magnitudes of the half-dozen brightest measurable stars are roughly $m_{pg} = 18.0 \pm 0.5$.

(3) NGC 1866.—Preliminary results (cf. Arp, Sandage, and Thackeray [22]) indicate that the color-magnitude diagram for this cluster resembles that of M11. Thackeray [9] regards it as the prototype of early-type globulars. It contains many 3-day Cepheids, is rich in bright blue stars, and has many red ones.

Hodge [21] found more than 2000 stars from $m_B = 16.6$ to $m_B = 19.0$ in the brightest part of the luminosity function.

(4) NGC 1978.—This cluster is described by Hodge [23] as an unusual eccentric ellipse. He has determined a color-magnitude diagram which has a heavily populated giant branch, whose gentle slope implies a relatively high metal abundance. It is a rich cluster with some remarkable variable stars. See also Hodge [23], Hogg [16], and Thackeray and Wesselink [27].

d. Clusters of the Small Magellanic Cloud

In the Small Magellanic Cloud we studied two clusters, NGC 330 (which is not a globular cluster) and NGC 419.

(1) NGC 330.—For this cluster the right ascension and declination for 1950 is: $\alpha = 0^h\ 54^m.9$, $\delta = -72°4$]

Arp [24] obtained a color-magnitude diagram to V = 19. It differed considerably from that of h and χ Persei, the red supergiants being bluer and more abundant, and the Hertzsprung gap narrower. The brightest stars are comparable in luminosity with their counterparts in h and χ Persei. Arp suggests that the differences in the color-magnitude diagrams are due to composition differences; but since the spectra of the bright SMC stars indicate no significant metal deficiency (Feast and Thackeray, 1958-Observatory 28, 156), the composition differences may suffice to affect the internal structure but not the spectrum of the star. Arp found that the main sequence was narrow

and well populated up to M_V = -4.5, above which occurred A and F supergiants between -4.5 and -5.5 and some red supergiants at -5. The integrated magnitude is P = 9.0 (de Vaucouleurs [25]).

(2) NGC 419.—Arp [26] found the color-magnitude diagram for this globular cluster to resemble that of the clusters in our galaxy. The reddest stars in NGC 419, however, have B-V = +2.0 as compared with B-V = 1.6 in similar clusters in our galaxy. The color-magnitude diagram which Arp measured to V = 19.4 and B = 20.1 has no horizontal branch.

Kron [6] observed the luminosity distribution in NGC 419 by measuring it with apertures of different size. The distribution of luminosity with distance from the center strikingly resembles that of M3 in our galaxy. In other words, globular star clusters tend to be built on the same models in our own galaxy and in the Magellanic Clouds.

3. SUMMARY

In summary, then, the published data suggest that the color-magnitude arrays for clusters in the Magellanic Clouds imply that there are composition differences between the galaxy and these stellar systems. On the other hand, the appearance of the spectra of individual stars as observed particularly by Thackeray and his associates suggest that these differences are not large. Here, then is the paradox; can colors or energy distributions in the integrated light of Magellanic Cloud star clusters throw any light on it? Unfortunately, we cannot yet get a clear-cut answer, but we are convinced that energy distribution measurements can help to solve this problem, although such measurements alone certainly do not suffice.

C. MEASUREMENTS OF THE ENERGY DISTRIBUTIONS IN SOUTHERN GLOBULAR CLUSTERS

In order to observe the spectral energy distributions in globular clusters we employed the photoelectric spectrophotometer built at The University of Michigan by W. Liller with aid of a grant from the Rackham Foundation. The device was built originally to study particularly gaseous nebulae (see Section V), but has also been used for many other problems—stellar energy distributions, comets, etc. Since the instrument has been described in detail by Liller [33] we restrict ourselves here to a brief description of its principles and operation.

Figure 2-1 is a schematic diagram of the spectrophotometer. Since the instrument was originally designed for an f/5 system and has to be used in Australia on telescopes of such aperture ratios as f/15 or f/18, it was necessary to install an auxiliary optical system in front of the entrance slit—

more properly called an entrance slot. We also provided a guiding diagonal consisting of an unsilvered, thick glass plate which was placed in the beam.

The entrance slot can be varied depending on the purity of the spectrum one wishes to obtain for an extended object. Slot A gives a purity of 6A, B one of 15A, C one of 25A, and D one of 59A. The length of the slot can be limited by a circular aperture which can be varied from 0.5 to 4.0 mm (corresponding to 11" to 88" at the focus of a 74-inch reflector). The light then falls on the Newtonian flat and passes to the collimator mirror and thence to the grating, which is rotated by a motor. With a 60 cycle current the rate of scan is 30A/min at slow speed, 90A/min at medium speed, and 270A/min at high speed.

The spectrum formed by the grating is reflected by a second Newtonian flat through the exit slots and a Fabry lens, and thence to the photocell. The exit slots have purities of 2A, 9A, 19A, and 47A. Thus a combination of two B-slots (B-B) gives a purity of 24A, C-C gives a purity 44A, and D-D gives a purity of 106A—provided the cluster under observation fills the entrance slot.

Figure 2-2 shows the instrument mounted on the 50-inch telescope at Mt. Stromlo. At the extreme right is the control panel. The guiding eyepiece is fitted with illuminated cross-wires and provision for removing the glass plate. An eyepiece can be inserted in the beam directly behind the entrance aperture and slot so that the observer can verify what the cell "sees." The four knobs controlling the sizes of the aperture and widths of the slots are plainly visible. Above and to the left is seen the wavelength recorder. The grating can be unlocked from the motor and turned by hand when necessary. The cold box which contains the photocell hangs at the bottom of the instrument; from its base dangles the signal lead. The photocell current is further amplified with a GR amplifier and the resultant potentiometer deflections are displayed on a Brown recorder.

Let h_λ denote the deflection on the recording paper as normalized to some selected amplification. Let the true flux from a star or cluster in the wavelength range λ to $\lambda+d\lambda$ at the top of the earth's atmosphere be denoted by F_λ. Let S_λ denote the combined effects of the sensitivity of the photocell and the transmission of the optics of the scanner plus that of the telescope. Then

$$h_\lambda = S_\lambda F_\lambda e^{-k_\lambda \sec z}$$

where k_λ is the coefficient of atmospheric extinction, and z is the zenith distance.

A priori, the atmospheric extinction is not known; neither is the sensitivity function, S_λ. We determine these quantities in a straightforward way

by observing a star whose energy distribution is known, and if necessary by taking another star which can be observed in the course of the night at widely different altitudes. In the northern hemisphere, where fundamental energy distributions have been carried out for a number of stars, one could often choose a single star to serve both purposes. In the southern hemisphere, however, it was necessary to pick a star near the celestial equator whose energy distribution had been measured; we used these stars to determine secondary standards of energy distribution for use in the southern hemisphere. This problem is being treated in a separate investigation. In praxis, it turned out that we determined the atmospheric extinction each night by observing one of a relatively small number of southern stars that were to serve eventually as southern standards. These stars were in turn compared with northern standard stars. Hence it was possible to determine both S_λ and the atmospheric extinction.

Of course, one need not determine S_λ explicitly. He can compare the cluster or nebula directly with a standard star—taking into account the effects of differential atmospheric extinction.

We observed the clusters as close to the meridian as possible so as to minimize effects of atmospheric extinction. Table 2-2 summarizes the individual observations. The first column gives the designation of the cluster and its position. The second gives the date of observation; all observations were secured between August 23, 1960, and March 18, 1961, so the year is not entered. The third column gives the instrument employed. Bin denotes the 26-inch reflector at the Mt. Stromlo field station on Mt. Bingar, near Yenda, N.S.W. The 50-inch reflector at Mt. Stromlo was originally the "Great Melbourne Telescope" installed at the now-defunct Melbourne Observatory a century ago. It was purchased by R.v.d.r. Woolley and mounted on Mt. Stromlo. The 74-inch reflector on Mt. Stromlo was made by Grubb-Parsons. Column 4 gives the scan speed—fast, medium, or slow. With the 50-cycle current, the slow speed was 25A/mm, the medium was 75A/mm, and the fast was 225A/mm. The slots and apertures are denoted in the fifth column. For example, C4-C4 means entrance slot C, aperture 4 (3.0-mm diameter) and exit slot C, aperture 4 (5.0-mm diameter). Entrance aperture 5 has a diameter of 4.0 mm; exit aperture 5 has a 5-mm diameter with a yellow filter. The spectral range covered is listed in the last column.

Figure 2-3 shows a scan of the spectrum of 47 Tucanae, as obtained with a medium speed on August 25 with the 50-inch reflector. The spectral resolution is 24A. The yellow filter is introduced to cut out overlapping orders. Tracings were made both in the direction of increasing wavelength and in the reverse direction in order to secure a check on the guiding and the atmospheric transparency. These tracings were then superposed to obtain a final "mean" trace. The discrepancies are larger than we would like—probably they are at least partly due to the drifting of individual stars off from and into the slot. For this reason it is advantageous to use a small telescope in working on a large extended cluster such as ω Centauri.

Figure 2-4 shows a scan of NGC 1866, as observed with the 74-inch reflector on Mt. Stromlo. Notice the prominent hydrogen lines, characteristic of a spectrum near A5, and the atmospheric line at 5577, which serves as a valuable fiducial mark. Here the spectral resolution is 44A.

The final results are summarized in Table 2-3 and in Figs. 2-5, 2-6, and 2-7. We measured the scans at the wavelenths chosen by Code [34] and also at many other positions of the spectrum, particularly in the neighborhood of the G band ($\lambda \sim 4308$), λ4227, the "H" and "K" lines λ3968 and 3933, and also numerous points in the ultraviolet. We compared the clusters individually with stars observed by Code.

The primary entries in Table 2-3 give the brightness $F(1/\lambda)$ of the globular cluster in magnitudes relative to the brightness at $1/\lambda_o = 1.80$. One magnitude corresponds to 4 db. The secondary entries for each cluster give an estimate of the error involved. The size of the error increases at the limits of the scan because of the decreased sensitivity of the photocell, and decreased in the ultraviolet because of the increased uncertainty in the atmospheric transmission.

In Figs. 2-5, 2-6, and 2-7 the brightness is plotted in magnitudes against $1/\lambda$ (in reciprocal microns as abscissa). Vertical dotted lines indicate the order of magnitude of the errors involved. They are estimated uncertainties, not errors calculated by statistical theory.

We deemed it best to retain the "wiggles" in the individual curves. Some of them are almost certainly spurious, but others, such as those corresponding to the "G-Band" and particularly to the H and K lines, seem to be unambiguously established. We must emphasize, however, that these fine features of the spectra can be observed only with slit spectrograms; the resolution of the scanner is too low and the noise level too high to permit delineation of many spectral characteristics that are useful for assessing absolute magnitude effects, metal deficiencies, etc.

In Fig. 2-5 we compare NGC 362, ω Centauri, NGC 2808, and 47 Tucanae. Of these clusters, 47 Tucanae is probably the most "metal rich." There is a sharp drop in the continuum in the neighborhood of the H and K lines because of the many overlapping metallic lines in this spectral region. The spectral distribution fits η Hercules G4III for $1/\lambda < 2.6$, but is brighter than this star in the ultraviolet ($1/\lambda > 2.6$) by about 0.3 magnitudes. If we fit the energy distribution of 47 Tucanae to that of 31 Comae GOIII, we find that a good fit can be obtained for $1/\lambda > 2.3$. That is, 47 Tucanae is redder than GOIII. It probably corresponds to about G2III.

The cluster NGC 2808 appears to have about the same energy distribution as 47 Tucanae; i.e., it corresponds to about G2III, being redder than a G4-dwarf. It appears to be more metal deficient than 47 Tucanae but is certainly not an extreme type II population object such as a subdwarf.

The energy distribution in ω Centauri falls between that of a G4V star such as 51 Pegasi, and that of a G2V star such as 16 Cyg A. It appears to be metal deficient in comparison with 47 Tucanae.

We experienced some difficulty in measuring the ultraviolet energy distribution in NGC 362 ($1/\lambda > 2.7$) when the highest resolution 24A was sought, so we have disregarded these measurements in drawing the final curve. The cluster appears to be definitely metal deficient; its energy distribution fits that of a G4V star to within the estimated error of the measurements, although it may be slightly redder. It is much bluer than a G4III star. We estimate its energy distribution as corresponding to that of a G5V star.

In Fig. 2-6 we compare 47 Tucanae with NGC 6752 and NGC 419, a globular cluster in the Small Magellanic Cloud. NGC 6752 fits 51 Pegasi G4V over nearly the entire range covered. Because of its faintness, NGC 419 was observed only in the blue. In the interval $2.0 < 1/\lambda < 2.6$ its energy distribution fits that of 51 Pegasi G4V but it has strong H and K lines and a strong G band. The weakness of the cluster in the ultraviolet may partly arise from observational error, but part of it may arise from the influence of the extremely red stars noted by Arp [26]. Further observations of this cluster are essential, since the present fragmentary data would suggest that the cluster is abnormally rich in metals.

Figure 2-7 shows the data for the clusters in the Large Magellanic Cloud. NGC 1866 and NGC 1831 were observed with higher resolution, i.e., 44A, than the other two clusters, NGC 1783 and NGC 1978, which could be measured only with a resolution of 106A. The energy distribution in NGC 1866 resembles that of a late A-type star. In the interval $1.8 < 1/\lambda < 2.6$ the slopes of the energy curve corresponds to a spectral class a little later than A5III, although the curve shows a drop in the extreme red. The Balmer jump corresponds to that of B Tri spectral class A5III. The strong Balmer lines are easily visible upon the tracing and show clearly that the spectral class is definitely A, in agreement with Thackeray's result (cf. remarks to Table 2-1).

The energy distribution in the cluster NGC 1831, which was also observed with the 74-inch reflector, shows a good fit to 110 Hercule's F6V in the interval $1.7 < 1/\lambda < 2.5$, but the Balmer jump seems to be too large and the ultraviolet portion of the spectrum appears to be relatively too faint by about 0.5 magnitude in the region $2.65 < 1/\lambda < 2.9$. Here again we must emphasize that the ultraviolet data are uncertain and that further observations should be obtained. The Balmer lines still seem to be relatively strong.

The clusters NGC 1783 and NGC 1978 are fainter than NGC 1866 and NGC 1831. Unfortunately we were unable to observe them with the large telescope. Not only is the spectral purity lower but the influence of sky background is greater, particularly in the ultraviolet. The energy distribution in NGC 1783 appears to resemble that of 51 Pegasi G4V for $1/\lambda < 2.65$. In the ultraviolet the errors appear to be large because of effects of the sky. The star

is bluer than η Hercules G4III except in the ultraviolet. The energy distribution in NGC 1978 seems to fit that of a G2V star to within the observational error.

Note that what we have derived are energy distribution equivalents, not spectral classes. The results are summarized in Table 2-4. Among globular clusters associated with our galactic system, the spectral classes tend to be earlier than the energy distribution equivalents—which is exactly the effect we would anticipate for stars that were deficient in metals! The exception is 47 Tucanae, which everyone agrees has a normal or nearly normal metal/hydrogen ratio. Because accurate spectral classes are not now available for the clusters in the Magellanic Clouds, similar comparisons cannot be made. The fragmentary data do suggest that perhaps the metal/hydrogen ratio tends to be more nearly "normal" in the globular clusters in the clouds than in those of our own galaxy.

Note that the energy distribution equivalent of NGC 1783 is later than the assigned spectral class, whereas the opposite is true for NGC 1831. Possibly the spectral classes are themselves in error; the energy distributions in NGC 419, NGC 1978, and NGC 1783 are very similar, as are their color-magnitude arrays.

No emphasis can be laid on the amount of the quantitative difference between the energy distribution equivalents and the spectral classes. In each instance one deals with the composite spectra of a host of stars. A stellar distribution ranging from F0 to K5 may give a spectral class resembling G2, but the energy distribution may differ from that of a G2 star.

The present investigation suggests that spectral scans of star clusters may be helpful in getting an estimate of the metal/hydrogen ratio. Before the data can be interpreted quantitatively, it will be necessary to supplement it with spectroscopic observations (for line intensities), color-magnitude arrays, and luminosity functions.

There is some question whether spectral scans of the type we have obtained are the most useful kind of observations to be secured with a spectral scanner. When quantitative studies of the composite spectra of clusters are carried out, it will be possible to select certain spectral features for special attention. An extension of the Strömgren photometric technique to globular clusters is clearly suggested, but the actual spectral intervals must be chosen with care. Furthermore, attention must be paid to getting spectral energy distributions for a variety of stars of different hydrogen/metal ratios and surface temperatures.

We secured spectral scans of NGC 330 in the SMC. This object is an open cluster containing many stars of early spectral type; Fig. 2-8 shows its energy distribution. Although the Balmer jump corresponds to that of a B3 star, the energy distribution and the strength of the hydrogen lines correspond to a later spectral class.

SECTION II:

TABLES, FIGURES, AND REFERENCES

TABLE 2-1

PROPERTIES OF SOME SOUTHERN GLOBULAR CLUSTERS
(Compiled by Herbert Rood)

(1) NGC	(2) α(1950) h m	(2) δ ° '	(3) l(1900)	(3) b	(4) C-m	(5) l-f	(6) Spectral CH/Hγ	(6) Hγ	(6) FeI	(7) P-m	(8) P-V	(9) Mod.	(10) Dist.	(11) V_r	(12) Mass	(13) Conc.	(14) Diam.
(47 Tuc) 104	00 21.9 [1]	-72 21 [1]	272 [1]	-45 [1]	[3]		G3 [5]	G3 [5]	G3 [5]	4.7 [7][1]	0.67 [7]	13.3(.4) [12][2]	4.6	- 24(3) [5]	$\leq 6\times10^5$ [8]	III [1]	44 [1]
ωCent 5139	13 23.8 [1]	-47 03 [1]	277 [1]	+15 [1]	[4]	[4]	F7 [10]	F8 [10]	F0 [10]	4.25 [7]	0.68 [7]	13.0(.7) [12]	4.0	+230(7) [5]		VIII [1]	101 [15] 65.4 [1] 10.4 [31]
362	01 00.6 [1]	-71 07 [1]	268 [1]	-47 [1]			F8 [5]	G0 [5]	F7 [5]	8.0 [1]		15.0(.7) [12]	10	+221(7) [5]		III [1]	17.7 [1] 4.0 [31]
2808	09 10.9 [1]	-64 39 [1]	250 [1]	-11 [1]			F8 [5]	F7 [5]	F7 [5]	7.8 [1]		14.0(.8) [12]	6.3	+101(7) [5]		I [1]	18.8 [1]
6752	19 06.4 [1]	-60 04 [1]	304 [1]	-27 [1]			F6 [5]	F7 [5]	F5 [5]	7.2 [1]		13.5(.8) [12]	5.0	- 39(5) [5]		VI [1]	41.9 [1]
LMC 1783	4 59.0	-66 03			[17]			F5 [28]		10.55 [19]	+0.48 [19]	[-][7]	[-][7]			VI [18] VI [29]	2.1 [18] 1.2 [28] 1.4 [29]
LMC 1831	5 6.1	-64 59			[20]			G5 [28]		10.65 [19]	+0.18 [19]					V [29] "Large Concentrated" [21]	1.0 [28] 1.3 [29]
LMC 1866	5 13.5	-65 31						F8 [30][4]		9.38 [19]	+0.07 [19][5]					IV [29] "Large Concentrated" [21]	0.9 [28] 2.2 [29]
LMC 1978	5 28.0	-66 16			[23]			G [28]		10.59 [19]	+0.64 [19]	[-][7]	[-][7]			VI [29] V [18]	1.9 [18] 1.0 [28] 1.0 [29]
SMC 419	1 7.1	-73 6			[26]			G [28]		10.62 [19][3]	0.54 [19][5]	[-][7]	[-][7]				0.8 [28] 1.4 [28][6]

1. Kron [6] gives a plot of relative magnitude vs. the 6 colors of Stebbin and Whitford.
2. Feast and Thackeray [8] obtain corrected modulus = 13.2. Wildey [3] obtains corrected modulus = 14.1 if $M_V = 0.0$ for the horizontal branch. He gets corrected modulus $\leq$ 13.2 if the blue end of horizontal branch is as faint or fainter than the horizontal branch of NGC 6356.
3. Kron [6] gives a plot of relative magnitude vs. the 6 colors of Stebbin and Whitford.
4. In [28] it is stated that Thackeray gets Type A3 from a slit spectrum.
5. In [28] it is stated in Note (3) under Table XV that Irwin (private communication) has measured photoelectric colors: For NGC 1866 P-V = 0.01; for NGC 419, P-V = 0.55.
6. In [28] Gascoigne lists the diam. 1!4 from Harvard plates, given "somewhere" in the literature.
7. See Section 2a, "The Distance Modulus."

TABLE 2-2

SOUTHERN HEMISPHERE GLOBULAR CLUSTER SCANS

Name	Scan Date	Instrument	Scan Speed	Slots	Spectral Range
ω Centauri					
$\alpha = 13^h23^m.8$ (1950)	March 14-15	Bin	Slow	B	3570A-4800A
$\delta = 47°03'$	March 15-16	Bin	Medium	C4-C4	3400A-5900A
	March 11(?)	Bin	Medium	C4-C4	3400A-5900A
	March 11-12	Bin	Fast	D4-D4	3300A-6100A
47 TUC					
	Oct. 12-13	Bin	Medium	B5-B4	3400A-6000A
	Aug. 25-26	50"	Medium	C5-C4	3400A-5000A
$\alpha = 00^h21^m.9$ (1950)	Aug. 25-26	50"	Medium	B5-B5	3600A-5900A
$\delta = 72°21'$	Aug. 24-25	50"	Fast	C5-C4	3400A-5900A
	Aug. 25-26	50"	Fast	B	5000A-5868A
	Aug. 26-27	50"	Fast	C5-C4	3400A-5900A
NGC 362					
	Aug. 26-27	50"	Medium	B5-B4	3600A-5700A
$\alpha = 01^h00^m.6$ (1950)	Aug. 24-25	50"	Fast	C5-C4	3500A-6100A
$\delta = 71°07'$	Aug. 25-26	50"	Fast	B5-B4	3500A-6000A
	Nov. 9-10	Bin	Medium	C4-C4	3500A-6000A
NGC 2808					
$\alpha = 09^h10^m.9$ (1950)	March 16-17	Bin	Medium	C4-C4	3800A-6000A
$\delta = 64°39'$	March 16-17	Bin	Fast	D4-D4 D4-D5	3400A-6000A
NGC 6752					
$\alpha = 19^h06^m.4$ (1950)	Oct. 16-17	Bin	Fast	D5-D4	3400A-6000A
$\delta = -60°04'$	Oct. 16-17	Bin	Fast	C5-C4	3400A-4900A
LMC-NGC 1831					
	Nov. 14-15	74'	Medium	C5-C4	3800A-4950A
$\alpha = 5^h6^m.1$ (1950)	Nov. 14-15	74'	Fast	D5-D4	3400A-5900A
$\delta = -64°59'$	Jan. 14-15	Bin	Fast	D4-D4	3400A-4900A
LMC-NGC 1783					
$\alpha = 4^h59^m.0$ (1950)	Sept. 20-21	50"	Fast	D5-D4	3500A-5900A
$\delta = -66°3'$	Jan. 13-14—14-15 (Composite)	Bin	Fast	D4-D4	3500A-4900A
LMC-NGC 1866					
	Oct. 27-28	74"	Medium	C4-C5	3500A-5800A
$\alpha = 5^h13^m.5$ (1950)	Jan. 13-14	Bin	Fast	D4-D4	3400A-5900A
$\delta = -65°31'$	Oct. 27-28	74"	Fast	D4-D5	3400A-5900A
LMC-NGC 1978					
	Jan. 17-18	50"	Fast	D5-D4	3400A-6000A
$\alpha = 5^h28^m.0$ (1950)	Nov. 23-24	50"	Fast	D5-D4	3400A-5900A
$\delta = -66°16'$	Jan. 9,13-14,14-15 (Composite)	Bin	Fast	D4-D4	3400A-4900A
SMC-NGC 419					
	Sept. 19	50"	Medium	C4-C4	3600A-4900A
$\alpha = 1^h7^m.1$ (1950)	Sept. 19	50"	Fast	D4-D4	3400A-5000A
$\delta = -73°6'$	Aug. 28-29,30-31 (Composite)	50"	Fast	D4-D4	3400A-4900A
SMC-NGC 330					
	Nov. 22-23	50"	Medium	C5-C4	3400A-5000A
$\alpha = 0^h54^m.9$ (1950)	Nov. 22-23	50"	Fast	D5-D4	3400A-5900A
$\delta = -72°41'$	Aug. 31*	50"	Fast	C3-C4	3900A-5000A
S26= SMC-"Kron's Blue Cluster"					
				D4-D4	
$\alpha = 0^h55^m.8$ (1950)	Nov. 23-24	50"	Fast	D4-D5	3400A-6000A
$\delta = -72°32'$	Nov. 23-24	50"	Fast	D3-D4	3400A-4900A

*Very low weight; scale uncertain; sky uncertain.

TABLE 2-3

GLOBULAR CLUSTER MAGNITUDES RELATIVE TO $1/\lambda_o = 1.80$

$1/\lambda^*$ =	2.94	2.74	2.59	2.48	2.39	2.18	1.975	1.80	1.72
ω Centauri	2.12	1.56	1.19	.83	.79	.43	.21	0.0	-.25
Est. Error	.40	.10	.10	.05	.05	.10	.10	.10	.40
47 TUC	2.25	1.90	1.75	1.15	1.09	.53	.22	0.0	-.10
Est. Error	.25	.15	.08	.05	.05	.04	.05	.12	.15
NGC 362	1.88	1.65	1.34	1.03	.86	.48	.28	0.0	-.15
Est. Error	.50	.50	.20	.10	.05	.04	.10	.15	.25
NGC 2808	2.18	1.96	1.63	1.33	1.11	.71	.38	0.0	-.10
Est. Error		.07	.10	.15	.05	.08	.15	.20	.30
LMC-NGC 1831	2.17	1.78	.97	.49	.46	.26	.14	0.0	-.06
Est. Error		.15	.07	.05	.10	.05	.07		
LMC-NGC 1866	1.75	1.21	.40	.15	.13	.07	-.12	0.0	.18
Est. Error	.40	.20	.05	.07	.05	.10	.20	.15	.25
LMC-NGC 1783	2.41	1.80	1.26	.76	.54	.46	.26	0.0	-.07
Est. Error	.80	.20	.15	.10	.10	.10	.10		
NGC 6752	1.92	1.46	1.21	.88	.78	.46	.22	0.0	-.06
Est. Error	.40	.15	.10	.10	.05	.05	.10	.05	.10
LMC-NGC 1978	2.04	1.63	1.33	.99	.78	.47	.25	0.0	-.10
Est. Error	.20	.20	.10	.20	.10	.10	.15	.10	.13
SMC-NGC 330	.34	.28	-.13	-.11	-.10	-.07	-.03	0.0	.16
Est. Error	.20	.05	.10	.07	.05	.05	.10	.15	.20

*$1/\lambda$ is given in reciprocal microns.

TABLE 2-4

ENERGY DISTRIBUTION EQUIVALENTS FOR GLOBULAR CLUSTERS

Name	NGC	Energy Distribution Equivalent	Spectral Class (See Table 2-1)
47 Tucanae	104	G2III	G3
	362	G4V	F8
	2808	G2III	F7
ω Centauri	5139	G4V	F8
	6752	G4V	F6
SMC Cluster	419	G4V	G
LMC Clusters	1783	G4V	F5
	1831	F6V	G5
	1866	A8III	A
	1978	G2V	G

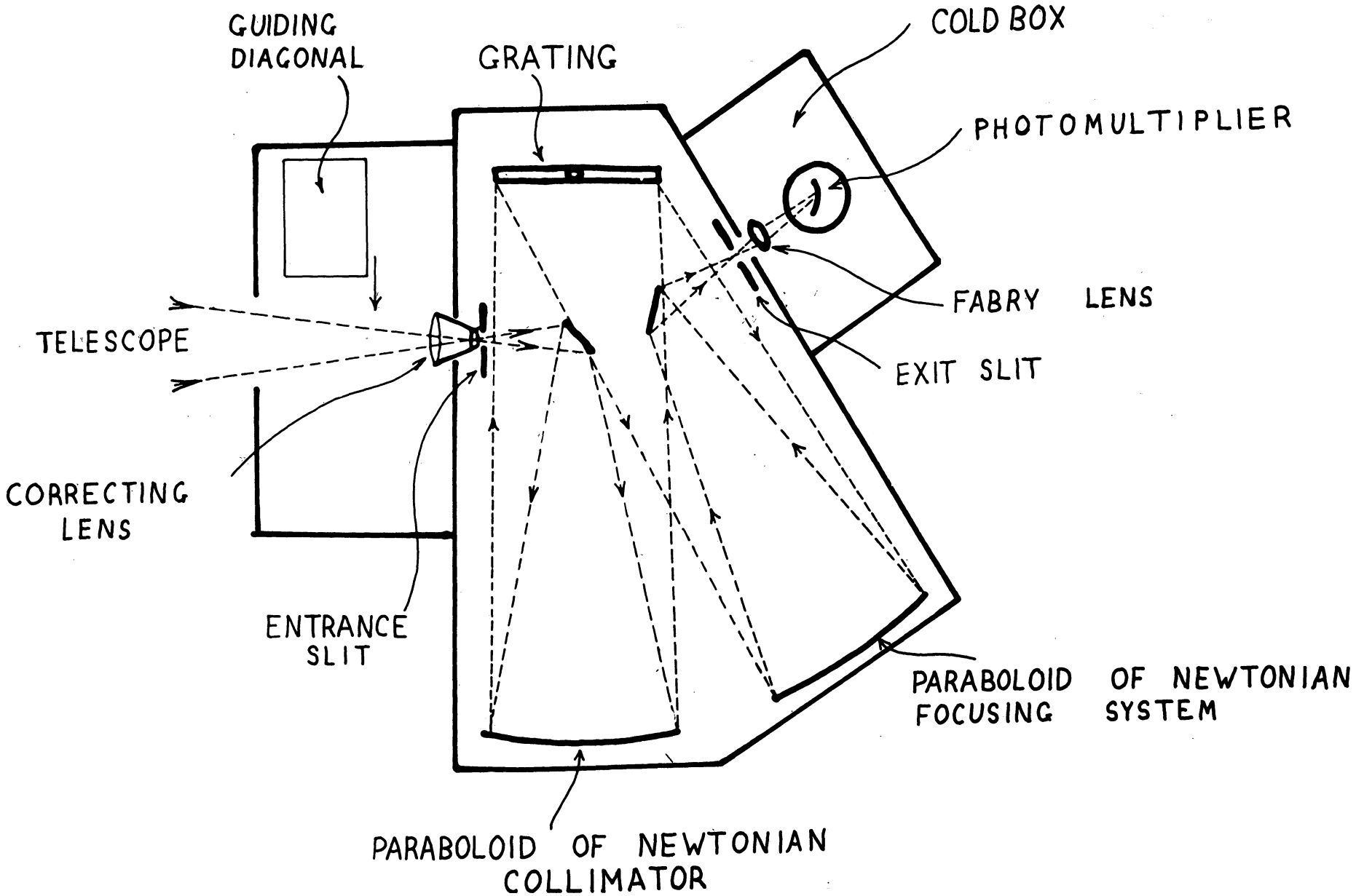

Fig. 2-1. Schematic diagram of the Michigan spectrophotometer.

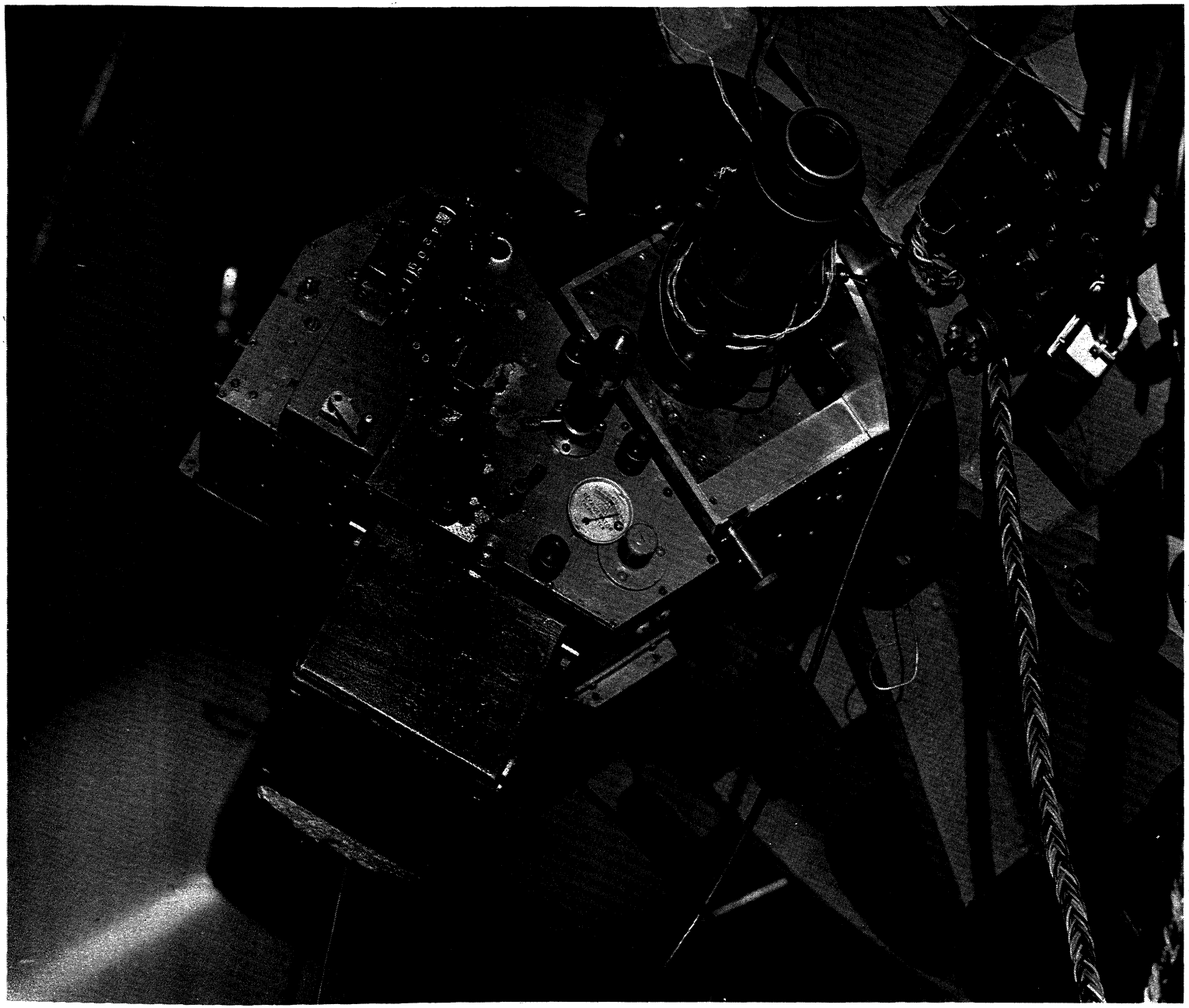

Fig. 2-2. The Michigan spectrophotometer mounted on the 50-inch telescope at Mt. Stromlo.

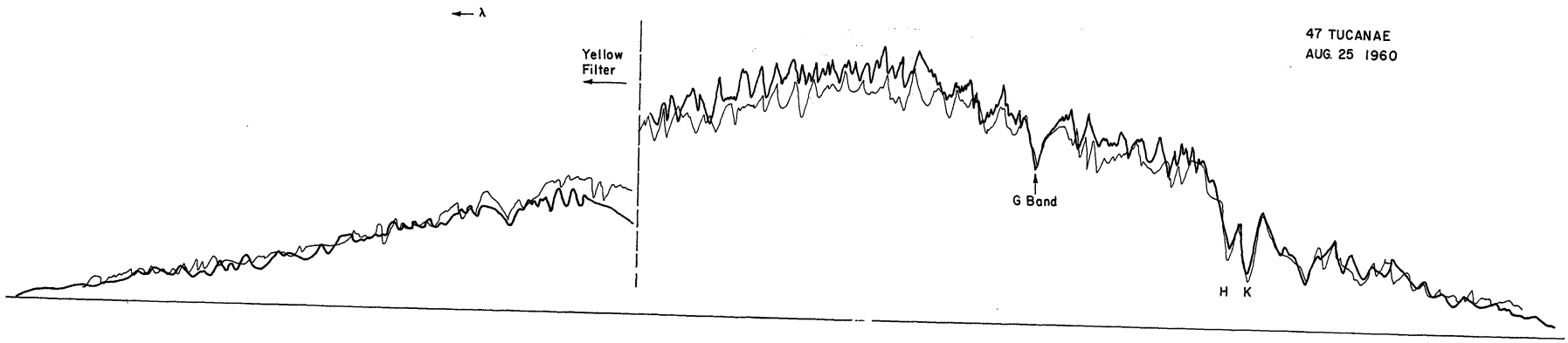

Fig. 2-3. Scan of 47 Tucanae (Aug. 25, 1960).

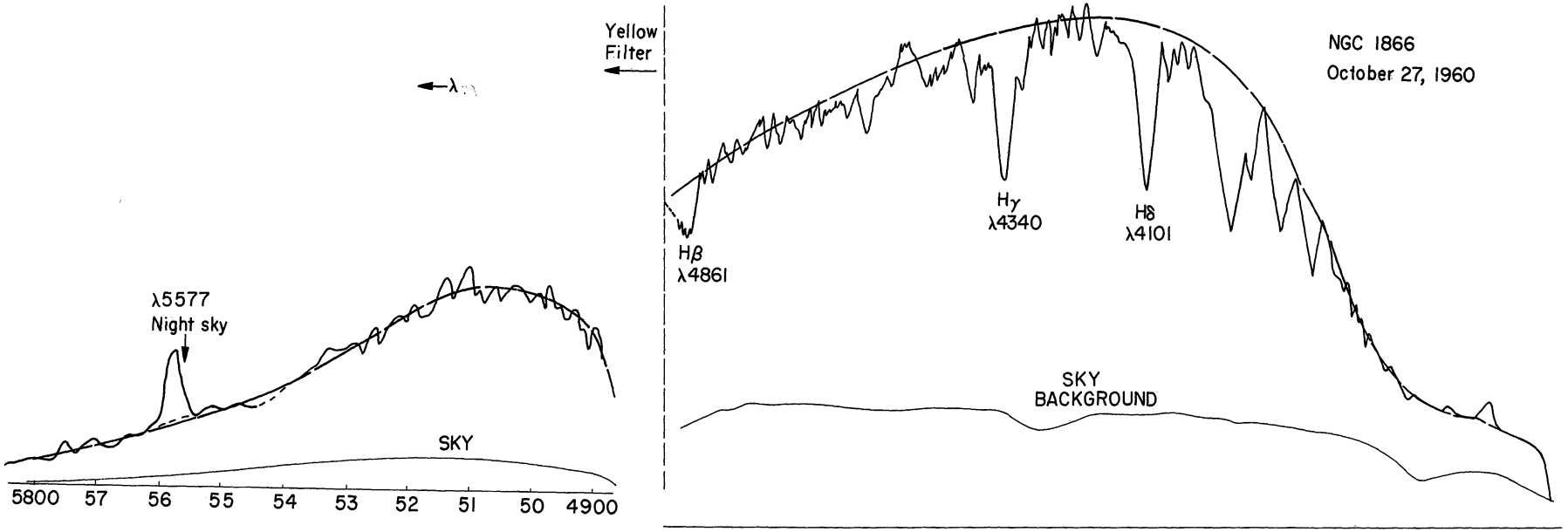

Fig. 2-4. Scan of NGC 1866 (Oct. 27, 1960).

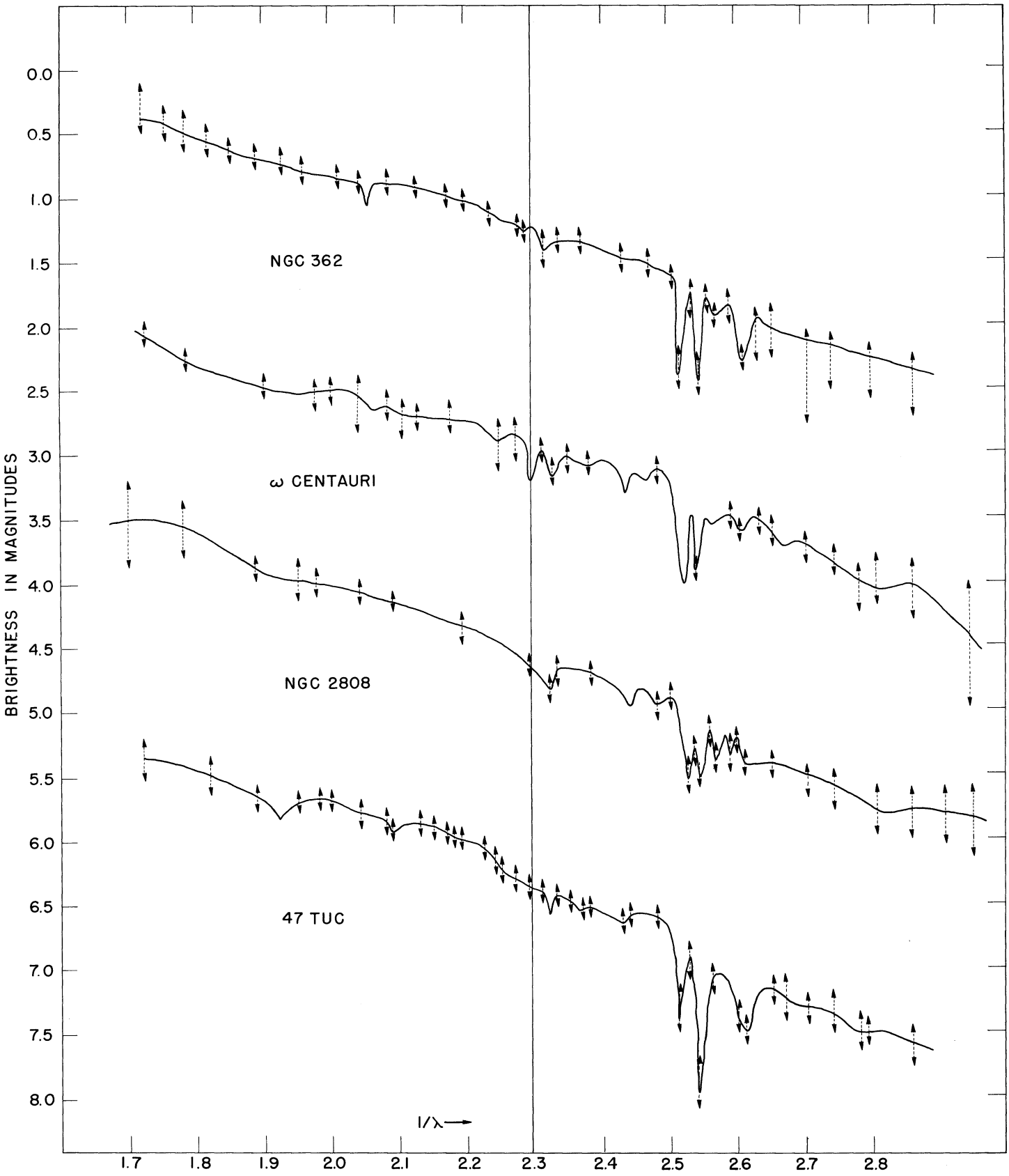

Fig. 2-5. Energy distributions for NGC 362 ω Centauri, NGC 2808, and 47 Tucanae.

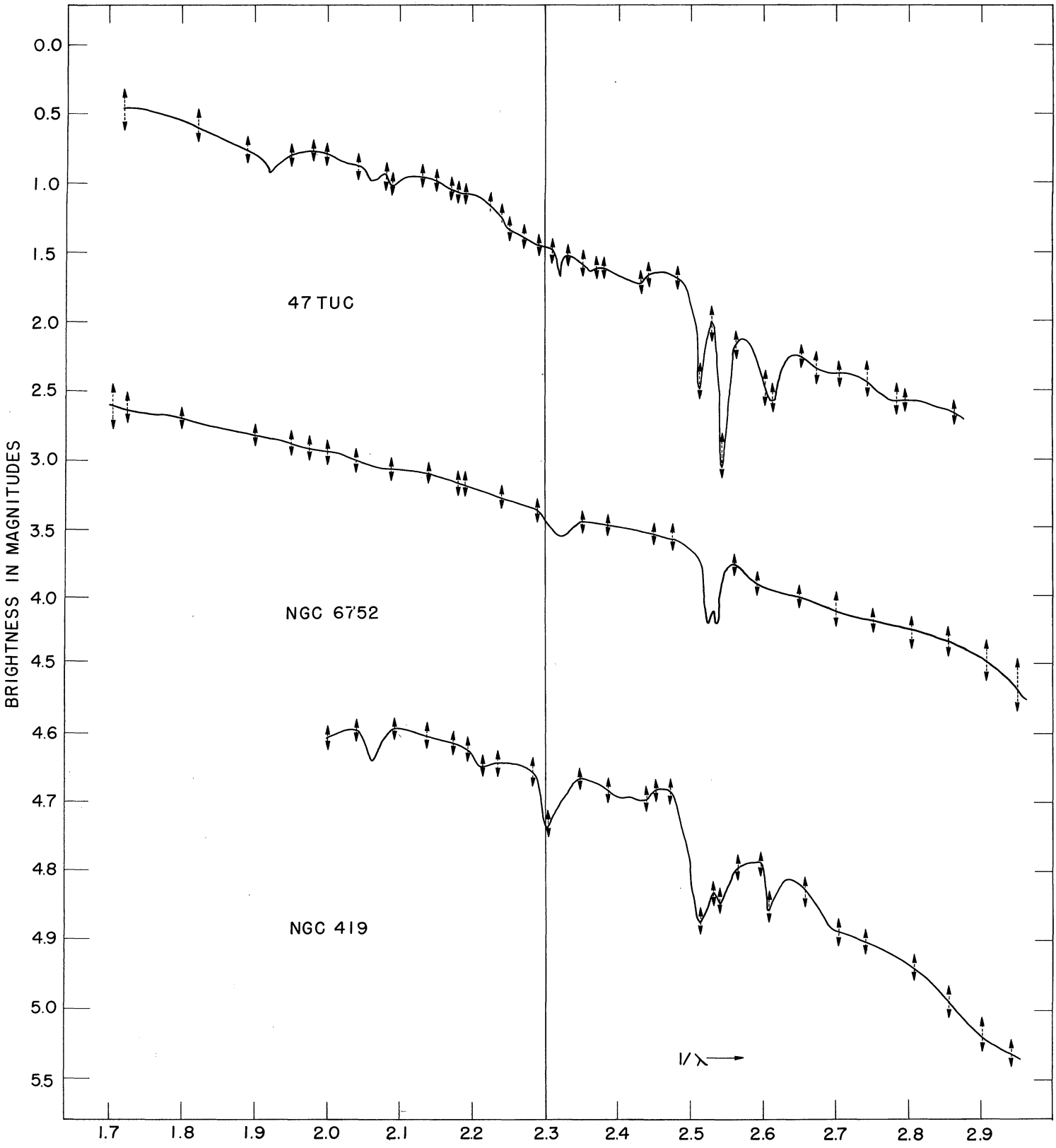

Fig. 2-6. Energy distributions for 47 Tucanae, NGC 6752, and NGC 419.

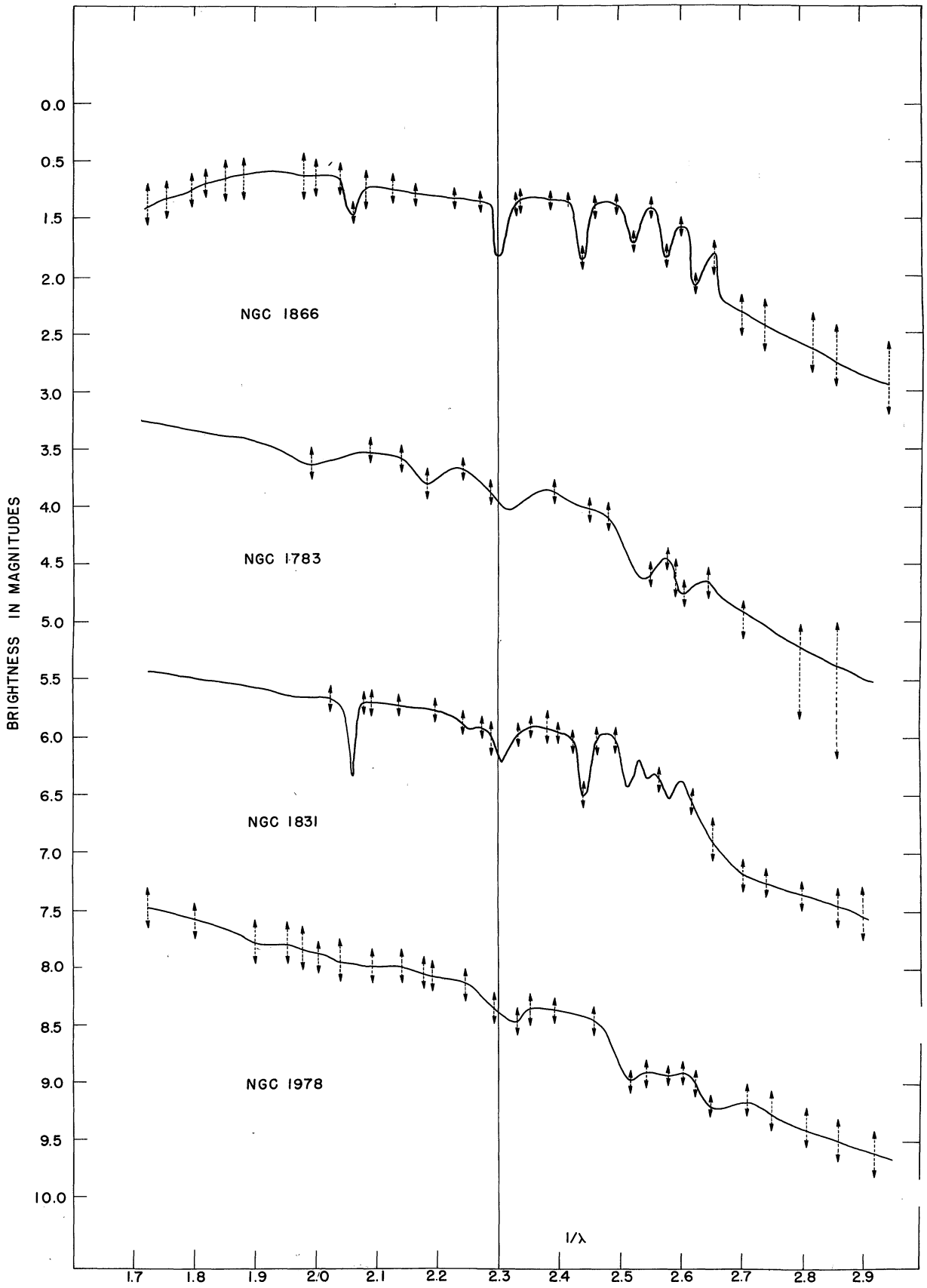

Fig. 2-7. Energy distributions for NGC 1866, NGC 1783, NGC 1831, and NGC 1978.

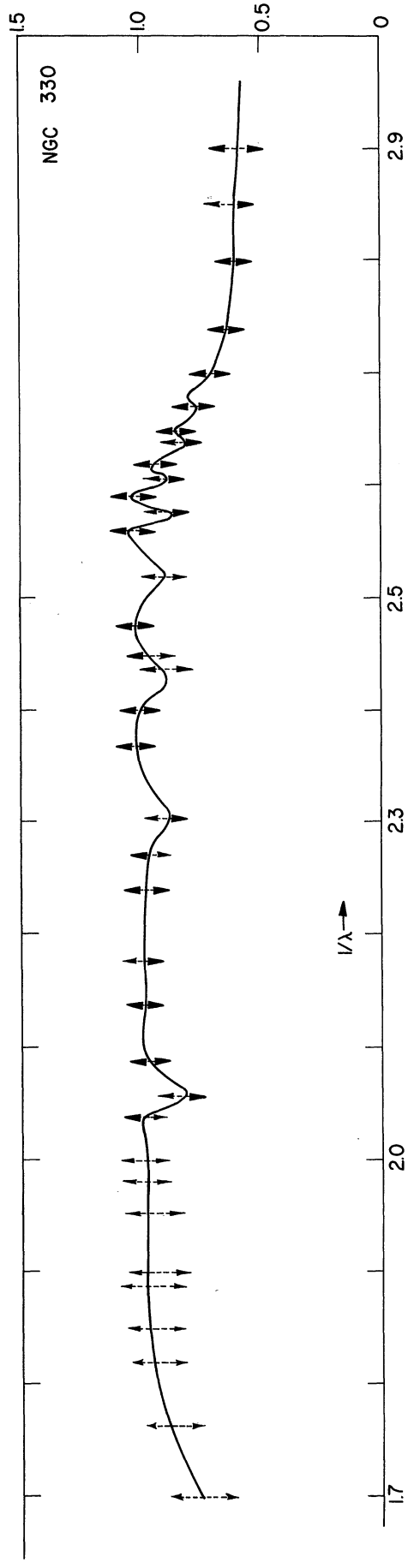

Fig. 2-8. Energy distribution for NGC 330.

REFERENCES

1. Helen Sawyer Hogg, Handbuch der Physik LIII, 204-206 (1959).

2. J.L.E. Dreyer, New General Catalogue of Nebulae and Clusters of Stars (1888).

3. R. L. Wildey, Ap. J. 133, 430 (1961).

4. E. P. Belserene, A. J. 64, 58 (1959).

5. T. D. Kinman, M. N. 119, 538 (1959).

6. G. E. Kron, P.A.S.P. 73, 202 (1961).

7. S.C.B. Gascoigne and E. J. Burr, M.N.R.A.S. 116, 570 (1956).

8. M. W. Feast and A. D. Thackeray, M.N 120, 463 (1960).

9. A. D. Thackeray, A.J. 64, 437 (1959).

10. W. W. Morgan, P.A.S.P. 68, 509 (1956).

11. W. W. Morgan, A.J. 64, 432 (1959).

12. T. D. Kinman, M.N.A.S.S.A. XVII, No. 3 (1958) = Radcliffe Observatory Reprint No. 9.

13. M. W. Feast, A. D. Thackeray, and Wesselink, M.N. 120, 64 (1960).

14. E. P. Belserene, A.J. 66, 38 (1961)A.

15. E. M. Linsay, Irish Astronomical Journal 2, pp. 145-146 (1953).

16. Helen Sawyer Hogg, Handbuch der Physik LIII, 182 (1959), David Dunlap Publ. 1, No. 20 (1939) and 2, No. 2 (1955).

17. A. Sandage and O. Eggen, M.N. 121, 232 (1960).

18. P. W. Hodge, Ap. J. 131, 351 (1960).

19. S.C.B. Gascoigne and G. E. Kron, P.A.S.P. 64, 196 (1952).

20. P. W. Hodge, Nature 186, 622 (1960).

21. P. W. Hodge, Ap. J. 133, 413 (1961).

22. H. C. Arp, A. Sandage, A. D. Thackeray, Mt. Wilson and Palomar Report 1956-57, p. 51.

23. P. W. Hodge, Ap. J. 132, 346 (1960).

24. H. C. Arp, A.J. 64, 254 (1959).

25. G. de Vaucouleurs, P.A.S.P. 71, 202 (1959).

26. H. C. Arp, A.J. 63, 273 (1958).

27. A. D. Thackeray and A. J. Wesselink, Nature 171, 693 (1953), M.N.A.S.S.A. 13, 99 (1954).

28. S.C.B. Gascoigne, Suppl. to the Australian Journal of Science, Vol. 17, No. 3, Dec. 1954, pp. 27-28.

29. H. Shapley and H. B. Sawyer, Harvard Bull. 852, 22 (1927).

30. Annie J. Cannon, Harvard Bull. 868, 1 (1929).

31. S. van Den Bergh, Z. Ap. 41, 61 (1956).

32. P. N. Kholopov, Var. Stars 11, No. 3, 202 (1958), H. Wilkens, Circ. La Plata Obs. No. 16 (1960).

33. W. Liller, Publ. Astron. Soc. Pac. 69, 511 (1957).

34. A. Code, Stellar Atmospheres, ed. V. L. Greenstein, Univ. of Chiago Press (1960).

SECTION III

SPECTROPHOTOMETRY OF THE WOLF-RAYET STAR OF γ_2 VELORUM

by L. H. Aller, D. J. Faulkner, and Herbert Rood

Wolf-Rayet stars are among the most perplexing of the hydrogen deficient stars in the sky. They are high temperature objects with broad emission lines of helium, carbon, nitrogen, and oxygen, and often with sharp absorption lines on the violet edge of the emission structure. A number of these objects occur in the constellation of Cygnus, where they have been intensively studied by numerous investigators.

The brightest Wolf-Rayet star in the sky is the more luminous component of the binary γ Velorum (visual magnitude = 2.22). The fainter component some 40" away, γ Velorum = HD 68243, spectrum B2IV (visual magnitude = 4.57), appears to be a normal star, whose absolute magnitude is about -3.1. Hence γ_2 Velorum must have an absolute magnitude $M_V \simeq -5.6$. Henry V. Smith [1] suggusts that γ_2 Velorum and Zeta Puppis, a star of somewhat similar temperature and absolute magnitude, are not only apparently close together in the sky but actually close together in space. They may be associated with an association of bright B stars, and the two of them together probably excite the gaseous nebula discovered by Gum [2]. The true dimensions of this nebula are greater than 650 light years, making it the largest such object known in our galactic system.

The spectrum of γ_2 Velorum is unusual in that its spectrum is composite and variable. Superposed on the wide lines of a carbon Wolf-Rayet star spectral class WC7 are broad hydrogen and helium absorption lines characteristic of an early O star, which Smith classifies as O7. Many of the strong emission lines have strong central absorptions.

Remarkable spectral variations involving both emission and absorption features were noted by Perrine [3] and studied intensively by Smith in March 1953, who notes that periods of activity are ephemeral and infrequent. Shells of material appear to be ejected from the star from time to time. Other examples of Wolf-Rayet stars with variable spectra are known, e.g., HD 45166.

A spectrophotometric study of both components of this system was undertaken by us at Bingar and at Stromlo. Spectral scans of the fainter component were difficult to secure and most of our effort was concentrated on measuring the energy distribution in the brighter component.

Scans were obtained on the nights of Oct. 12-13 and Nov. 5-6, 1960 at Bingar and Jan. 28-29, Jan. 30-31, and Jan. 31, 1961 at Stromlo. Figure 3-1 shows a scan obtained with medium speed. Different gain settings of the amplifier were required. If after reducing each scan to a common amplifier gain, the wavelength (abscissa) is measured in Angstroms and the height of the continuum (ordinate) is measured in arbitrary units, then the quantity A_λ (called "Equivalent Angstroms") may be defined for each observed spectral line on the tracing by

$$A_\lambda = \frac{\text{area of the line at } \lambda}{\text{height of the continuum at } \lambda} .$$

A_λ is thus the width (in Angstroms) of a rectangle, the height of which is equal to the height of the continuum at λ and the area of which is equal to the area of the line at λ. We may use A_λ values to derive relative line intensities as soon as the energy distribution in the star is known.

Table 3-1 gives A_λ values for the observed lines. Column 1 gives the wavelength of each line. Column 2 gives its identification (when known). The next 10 column give, for each night, the average A_λ value obtained from the scans of that night and the uncertainty estimate, which is taken as the mean difference between the average A_λ value and the A_λ value for each tracing of the night. Where no uncertainty estimate is listed, there was only scan. The last column gives $\bar{A}_\lambda$, the average A_λ value for all the nights.

The color temperature is obtained by the following procedure. For a given wavelength, the apparent magnitude of the continuum $m_{1/\lambda}$ (corresponding to intensity per unit wave-number) is obtained from the formula

$$m_{1/\lambda} = -(2.5\log h_\lambda + k_\lambda \sec z + S_\lambda) + \text{constant}$$

where h_λ is the continuum height at λ measured in arbitrary units, k_λ is the atmospheric absorption at the zenith (in magnitudes) at the place of observation, z is the zenith distance at the time of observation, and S_λ is the relative sensitivity of the telescope-photocell combination in magnitudes (per unit wave number) obtained by comparing the tracings of standard stars with the known intensity distributions given by Code (see [34] of Section II). The constant depends on the units in which h_λ is measured. Since only differences in magnitudes at various wavelengths are used to obtain the color temperature, we need not know the value of the constant and the magnitudes given in Table 3-2 are obtained by arbitrarily setting the constant equal to zero. Table 3-2 gives $-m_{1/\lambda}$ at spectral line wavelengths for the five nights of observation, the estimated uncertainty, and the average value of $-m_{1/\lambda}$ for the five nights. Plots of $-m_{1/\lambda}$ vs. $1/\lambda$ were constructed for each of the five nights and superimposed to obtain the final linear $-m_{1/\lambda}$ vs. $1/\lambda$ plot given in Fig. 3-2. With use of this graph, the color temperature may be easily obtained, from the Planckian formula

$$\log B(1/\lambda_1) - \log B(1/\lambda_2) = \log\lambda_2^3 (1^{hc/kT\lambda_2} - 1) - \log\lambda_1^3 (1^{hc/kT\lambda_1} - 1)$$

where $B(1/\lambda_1)/B(1/\lambda_2)$ is the intensity ratio for wave numbers $1/\lambda_1$ and $1/\lambda_2$, h = Plank's constant, k = Boltzmann's constant, c = speed of light, and T is the color temperature. Thus the color temperature is found to be 32,000°K.

Although the intensities of absorption lines may be expressed conveniently in equivalent angstroms, λ emission line intensities so described can be compared with one another only if the energy distribution in the continuous spectrum is known. That is, to compare $A(\lambda_1)$ with another line $A(\lambda_2)$

we must know $F(\lambda_1)/F(\lambda_2)$. We may express the relative intensities of all emission lines in terms of a hypothetical emission line of equivalent width $A(\lambda) = 1$ at $\lambda 5000$. Thus the intensity I_λ of any emission line of equivalent width A_λ is given by

$$\frac{I_\lambda}{I_o} = \frac{5000}{\lambda}^5 \frac{(1^{hc/5kTx10^{-5}} - 1)}{(1^{hc/\lambda kT} - 1)} A_\lambda$$

Table 3-3 gives I_λ/I_o at the spectral line wavelengths for the five nights of observation, the estimated uncertainties, and the average value of I_λ/I_o for each night.

"Apparent" excitation temperatures may be obtained by comparing intensities of emission lines arising from two suitable levels of a given ion. That is, using the above values of I_λ/I_o, the excitation temperatures for various combinations of lines are computed from Boltzmann's formula

$$\frac{I_{\lambda_1}/I_o}{I_{\lambda_2}/I_o} = e^{-(\chi_1 - \chi_2)/kT} \frac{\sum \tilde{\omega}_1 A_1 \nu_1}{\sum \tilde{\omega}_2 A_2 \nu_2}$$

where χ_1 and χ_2 are the excitation potentials for the lines of wave numbers $1/\lambda_1$ and $1/\lambda_2$, A_1 and A_2 are Einstein probability coefficients and $\tilde{\omega}_1$ and $\tilde{\omega}_2$ are statistical weights. For the lines used to obtain excitation temperatures, excitation potentials were obtained from Ref. [4], Table 7 and $\sum \tilde{\omega}_1 A_1 \nu_1$ were obtained from Ref. [4], Table 6. Excitation temperatures derived from various line combinations are given below:

CIII	4069/4650	23,000°K
CIII	3609/4650	22,000°K
CIV	3934/5805	85,000°K
CIV	4441/5805	110,000°K
CIV	3411/3562	36,000°K
CV	4124/5590	1,900,000°K

Abundances of various elements cannot be determined for this star until a more complete study of its spectrum is made.

SECTION III:

TABLES, FIGURES, AND REFERENCES

TABLE 3-1

A_λ VALUES OF γ_2 VELORUM

(A_λ = Area of Line at λ/Intensity of Continuum at λ)

λ (Å)	Ident.	Oct. 12-13, 1960		Nov. 5-6, 1960		Jan. 28-29, 1961		Jan. 30-31, 1961		Jan. 31, 1961		$\bar{A}_\lambda$ (Å)
		A_λ (Å)	E.U.* (Å)	A_λ (Å)	E.U.* (Å)	A_λ (Å)	E.U.* (Å)	A_λ (Å)	E.U.* (Å)	A_λ (Å)	E.U.* (Å)	
3411	OIV	2.98	(0.30)	2.88		3.54	(0.51)	2.96	(0.42)	3.94		3.26
3500				0.67								0.67
3560	OIII,OIV,HeI	1.20	(0.06)	1.49		1.20	(0.10)	1.64	(0.04)	1.33		1.37
3607	CIII	1.65	(0.14)	2.18		1.93	(0.48)	1.54	(0.20)	1.59		1.78
3687		2.55	(0.21)	3.10		2.72		4.41		3.89		3.33
3722	CIV	3.50	(0.34)	4.43		3.88	(0.70)	5.53	(0.31)	4.20		3.91
3758-3769	OIII	1.61	(0.05)	2.53		2.81	(0.45)	3.30	(0.07)	2.32		2.51
3811	OVI	0.98	(0.16)	0.69		1.70	(0.02)	1.40		1.01		1.16
3835	OVI	1.00	(0.35)					1.36	(0.27)	1.05		1.14
3889	HeI, CIII	3.96	(0.06)	2.50		5.22	(0.42)	5.34	(0.76)	5.45		4.49
3934	CIV	5.82	(0.63)	2.60		5.78	(0.37)	5.78	(0.13)	6.46		5.29
3965	HeII,OIII							0.81		0.81		0.81
4025	HeI,HeII							1.37		1.92		1.65
4069	CIII	6.32	(0.68)	5.95		6.84	(0.81)	7.48	(0.94)	7.45		6.81
41007	CIII	2.91	(0.67)	2.84		3.01	(0.59)	2.80	(0.44)	2.50		2.81
41231	OV											
4157	CIII	1.44	(0.13)	1.17		1.56	(0.32)	1.23	(0.33)	1.11		1.30
4189	CIV	1.54	(0.08)	1.61		1.48	(0.25)	2.12	(0.61)	2.32		1.81
4229	CIII	0.88	(0.11)	1.26		1.08	(0.20)	1.28	(0.43)	1.13		1.13
4235	HeII											
4267	CII	2.74	(0.26)	3.22		3.43	(0.35)	4.25	(0.70)	3.04		3.34
4330	CIII,HeII	3.64	(0.24)	3.22		4.48	(0.29)	4.11		3.62		3.81
4375	CIII,HeII	3.10	(0.23)	1.66		2.68	(0.36)	2.01	(0.01)	1.75		2.24
4441	CIV	4.38	(0.23)	4.00		4.60	(0.45)	4.48	(0.20)	3.57		4.21
4471	HeI	1.04	(0.18)	1.24		2.68	(0.52)	0.99	(0.61)			1.49
4513	CIII	1.02	(0.02)	0.72		1.95		0.84	(0.03)			1.13
4544	HeII	1.52	(0.03)	0.78		1.60		1.32	(0.36)			1.31
4650	CIV,CIII	61.8	(5.8)	57.8		79.4	(5.4)	67.2		76.0		68.4
4686	HeII	16.4	(2.4)	15.8		19.8	(0.3)	19.4		23.9		19.1
4786	CIV	1.47	(0.06)	1.94		2.50	(0.52)	2.71				2.16
4861	HeII	1.88	(0.18)	4.34		3.35		2.80		4.53		3.38
4923	HeI	1.37	(0.04)	1.59				1.57				1.51
5019	CIV,HeI	2.50	(0.41)	2.28		4.85		4.00		4.88		3.70
5060		0.85				0.87						0.86
5132	CIII	6.61	(0.82)	3.16		4.80		3.46		6.40		4.89
5248-5257	CIII	1.74	(0.53)	0.73		0.76		0.56		1.53		1.06
5411	HeII	2.79	(0.37)	1.76		4.36		3.08	(0.31)	3.51		3.10
5470	CIV	4.14	(0.21)	3.09		3.90		3.45	(0.25)	2.92		3.50
5592	OV,OIII					2.20		1.70		2.25		2.05
5695	CIII	51.2	(3.3)	60.2		53.4		54.4		55.0		54.8
5805	CIV	40.0	(0.5)	35.4		36.7		39.9		44.6		39.3
5876	HeI	8.56	(0.87)	7.51		10.1		13.9		14.4		10.9

*Estimated Uncertainty

Average % Error = Σ Estimated Error/ΣA_λ (with errors estimated) = 41.48/476.62 = 8.7%.

TABLE 3-2

$-m_{1/\lambda}$ VALUES OF γ_2 VELORUM
($-m_{1/\lambda}$ = Apparent Magnitude of the Continuum at λ)

λ (Å)	Oct. 12-13, 1960		Nov. 5-6, 1960		Jan. 28-29, 1961		Jan. 30-31, 1961		Jan. 31, 1961		$-\bar{m}_{1/\lambda}$
	$-m_{1/\lambda}$	E.U.*	$-m_{1/\lambda}$	E.U.*	$-m_{1/\lambda}$	E.U.*	$-m_{1/\lambda}$	E.U.*	$-m_{1/\lambda}$	E.U.*	
3411	5.99	(0.07)	6.48		5.77	(0.02)	5.89	(0.06)	5.70		5.97
3500			6.59								6.59
3560	5.95	(0.06)	6.60		5.67	(0.02)	5.79	(0.04)	5.61		5.92
3607	5.96	(0.07)	6.42		5.66	(0.03)	5.76	(0.03)	5.59		5.88
3687	5.92	(0.02)	6.53		5.56		5.73		5.53		5.85
3722	5.90	(0.04)	6.49		5.59	(0.04)	5.68	(0.02)	5.52		5.84
3758-3769	5.86	(0.03)	6.48		5.52	(0.06)	5.63	(0.03)	5.47		5.79
3811	5.85	(0.02)	6.52		5.52	(0.05)	5.65		5.47		5.80
3835	5.85	(0.02)					5.59	(0.05)	5.45		5.62
3889	5.86	(0.07)	6.42		5.48	(0.05)	5.58	(0.04)	5.41		5.75
3934	5.79	(0.01)	6.43		5.49	(0.05)	5.58	(0.04)	5.41		5.74
3965							5.54		5.42		5.48
4025							5.54		5.39		5.46
4069	5.75	(0.01)	6.37		5.50	(0.07)	5.56	(0.05)	5.40		5.72
41007-41231	5.75	(0.01)	6.31		5.49	(0.06)	5.56	(0.04)	5.40		5.70
4157	5.73	(0.01)	6.28		5.43	(0.05)	5.54	(0.04)	5.37		5.67
4189	5.73	(0.02)	6.26		5.44	(0.06)	5.53	(0.04)	5.37		5.67
4229-4235	5.70	(0.02)	6.23		5.42	(0.05)	5.50	(0.05)	5.34		5.64
4267	5.69	(0.02)	6.24		5.41	(0.06)	5.51	(0.04)	5.32		5.63
4330	5.65	(0.03)	6.22		5.39	(0.05)	5.52		5.32		5.62
4375	5.63	(0.00)	6.20		5.36	(0.05)	5.49	(0.03)	5.30		5.60
4441	5.65	(0.02)	6.19		5.35	(0.05)	5.48	(0.04)	5.31		5.60
4471	5.63	(0.02)	6.20		5.35	(0.06)	5.47	(0.03)	5.31		5.59
4513	5.64	(0.02)	6.21		5.41		5.47	(0.04)			5.68
4544	5.62	(0.02)	6.20		5.39		5.44	(0.04)			5.66
4650	5.66	(0.05)	6.27		5.35	(0.07)	5.46		5.22		5.59
4686	5.65	(0.04)	6.22		5.32	(0.08)	5.41		5.23		5.57
4786	5.62	(0.01)	6.17		5.26	(0.03)	5.34				5.60
4861	5.66	(0.01)	6.22		5.11		5.28		4.89		5.43
4923	5.69	(0.01)	6.26				5.36				5.76
5019	5.61	(0.02)	6.13		5.14		5.28		4.80		5.39
5060	5.48				5.15						5.31
5132	5.46	(0.00)	6.04		5.12		5.23		4.98		5.37
5248-5257	5.44	(0.00)	5.97		4.85		5.15		4.76		5.23
5411	5.35	(0.00)	5.91		4.93		5.10	(0.02)	4.82		5.22
5470	5.38	(0.01)	5.92		4.92		5.11	(0.02)	4.83		5.23
5592					4.91		5.11		4.82		4.94
5695	5.44	(0.02)	5.99		5.00		5.18		4.88		5.30
5805	5.32	(0.03)	6.01		4.82		4.98		4.66		5.16
5871	5.25	(0.16)	5.78		4.59		4.68		4.47		4.95

*Estimated Uncertainty

TABLE 3-3

I_λ/I_o VALUES OF γ_2 VELORUM
(I_λ/I_o = Intensity of Emission Line of Equivalent Width A_λ)

λ (Å)	Oct. 12-13, 1960		Nov. 5-6, 1960		Jan. 28-29, 1961		Jan. 30-31, 1961		Jan. 31, 1961		$\overline{I_\lambda/I_o}$
	I_λ/I_o	E.U.*	I_λ/I_o	E.U.*	I_λ/I_o	E.U.*	I_λ/I_o	E.U.*	I_λ/I_o	E.U.*	
3411	10.87	(1.10)	10.49		12.89	(1.86)	10.78	(1.53)	14.33		11.87
3500			2.12								2.12
3560	3.77	(0.19)	4.67		3.77	(0.31)	5.15	(0.13)	4.17		4.31
3607	5.00	(0.42)	6.61		5.85	(1.46)	4.66	(0.61)	4.82		5.39
3687	7.27	(0.60)	8.84		7.75		12.6		11.1		9.51
3722	9.65	(0.94)	12.2		10.7	(1.93)	9.74	(0.86)	11.6		10.78
3758-3769	4.30	(0.13)	6.76		8.71	(1.40)	9.04	(0.19)	6.20		7.00
3811	2.53	(0.41)	1.78		4.38	(0.05)	3.61		2.61		2.98
3835	2.51						3.41	(0.68)	2.64		2.85
3889	9.46	(0.14)	5.98		12.5	(1.01)	12.7	(2.52)	13.0		10.73
3934	13.4	(1.45)	5.98		13.3	(0.85)	13.3	(0.30)	14.9		12.18
3965							1.81		1.81		1.81
4025							2.88		4.04		3.46
4069	12.7	(1.37)	12.0		13.7	(2.00)	15.0	(1.88)	15.0		13.68
41007-41231	5.65	(1.30)	5.50		5.84	(1.15)	5.43	(0.85)	4.85		5.45
4157	2.69	(0.24)	2.18		2.92	(0.60)	2.30	(0.62)	2.08		2.43
4189	2.80	(0.15)	2.93		2.6)	(0.45)	2.86	(0.82)	4.22		3.10
4229-4235	1.54	(0.19)	2.20		1.89	(0.35)	2.24	(0.75)	1.98		1.97
4267	4.68	(0.44)	5.50		5.86	(0.60)	7.26	(1.19)	5.20		5.70
4330	5.97	(0.39)	5.29		7.36	(0.48)	6.75		5.94		6.26
4375	4.90	(o.36)	2.62		4.24	(0.57)	3.18	(0.02)	2.76		3.54
4441	6.57	(0.34)	6.00		6.90	(0.68)	6.73	(0.03)	5.35		6.31
4471	1.54	(o.27)	1.84		3.96	(0.77)	1.46	(0.90)			2.20
4513	1.46	(0.03)	1.03		2.79		1.20	(0.04)			1.62
4544	2.13	(0.04)	1.09		2.24		1.85	(0.51)			1.83
4650	80.4	(13.00)	75.2		103.0	(7.00)	87.4		98.8		89.0
4686	20.6	(3.0)	19.9		24.9	(0.38)	24.4		30.1		24.0
4786	1.85	(0.08)	2.27		2.93	(0.61)	3.17				2.56
4861	2.07	(0.20)	4.78		3.68		3.14		4.97		3.73
4923	1.45	(0.04)	1.69				1.66				1.60
5019	2.45	(0.40)	2.24		4.75		3.92		4.78		3.63
5060	0.80				0.82						0.81
5132	5.95	(0.74)	2.84		4.32		3.12		5.76		4.40
5248-5257	1.44	(0.44)	0.61		0.63		0.46		1.27		0.88
5411	2.12	(0.28)	1.34		3.32		2.34	(o.24)	2.66		2.36
5470	3.02	(0.15)	2.26		2.85		2.52	(0.18)	2.86		2.70
5592					1.50		1.16		1.53		1.40
5695	32.6	(2.10)	38.5		34.1		34.8		35.2		35.0
5805	24.0	(0.3)	21.2		22.0		24.0		26.8		23.6
5871	4.80	(0.49)	4.21		5.67		7.77		8.06		6.10

*Estimated Uncertainty

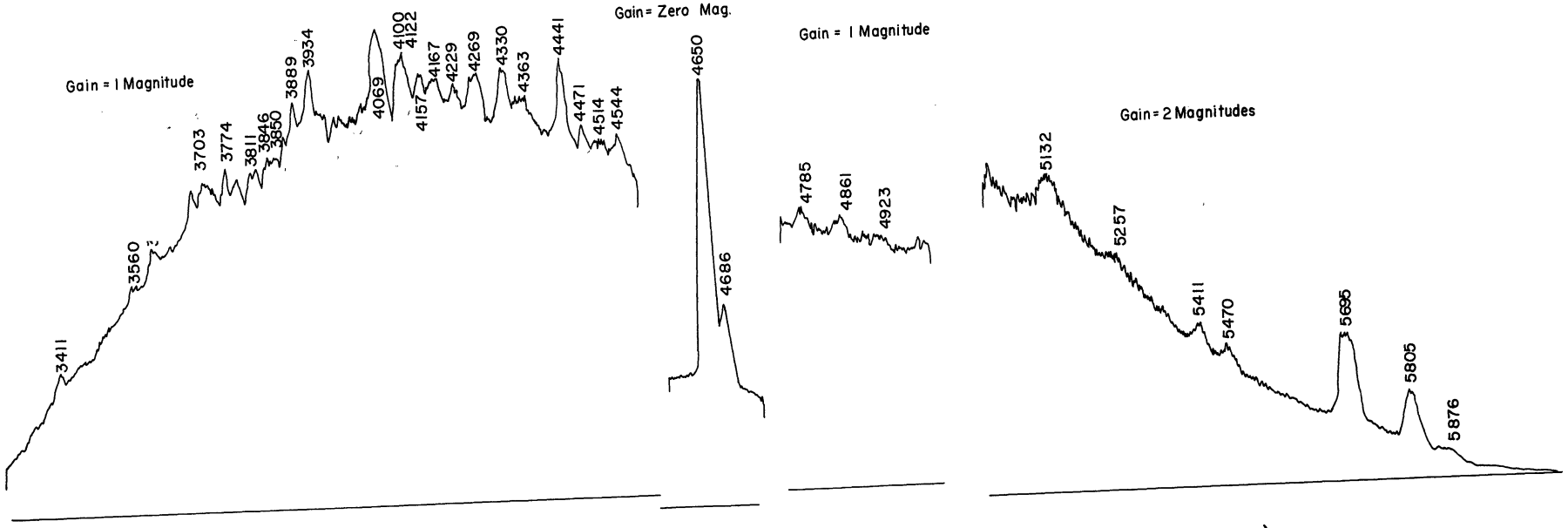

Fig. 3-1. Spectral scan of γ_2 Velorum (Oct. 12-13, 1960, Mt. Bingar).

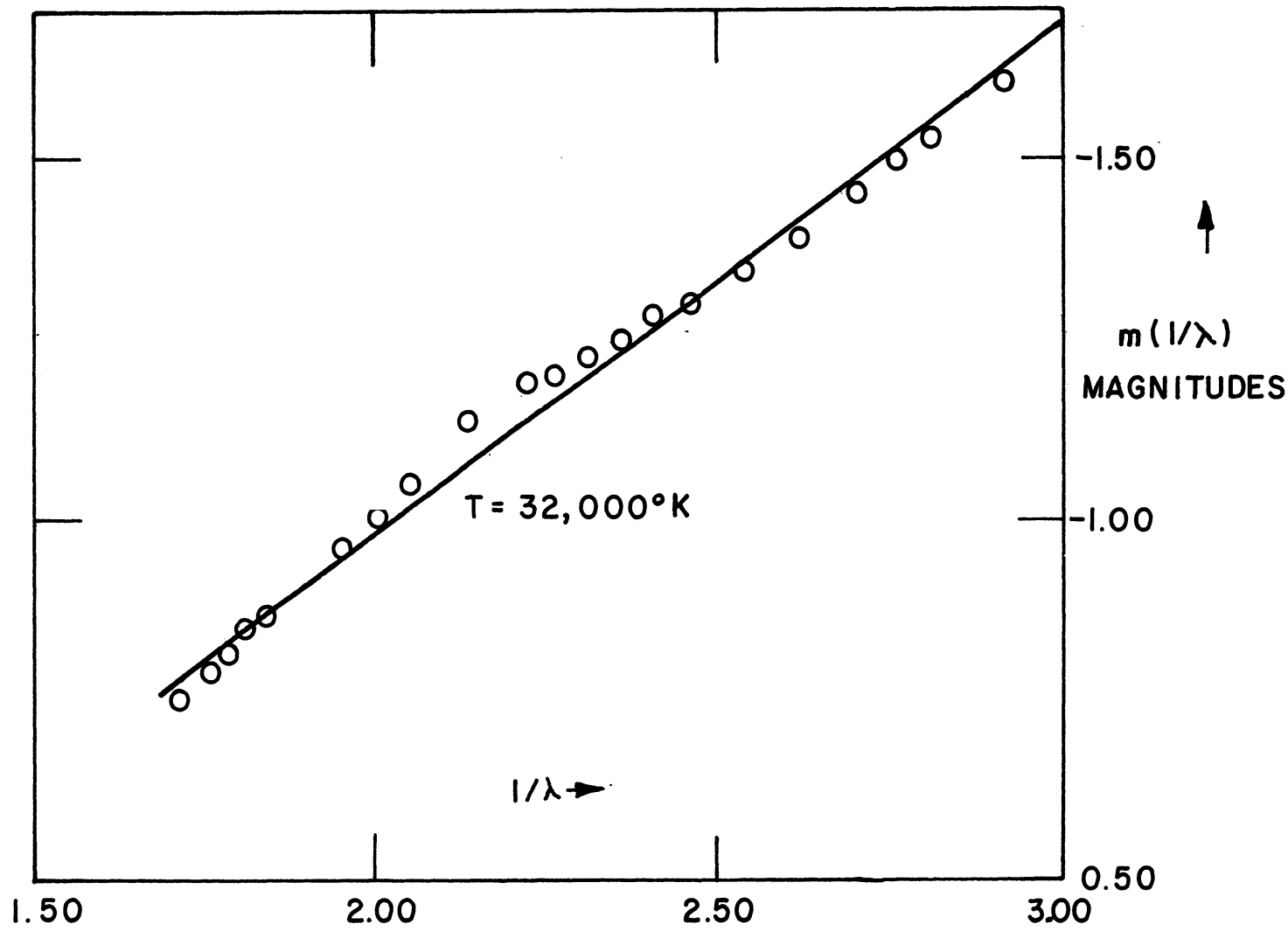

Fig. 3-2. Energy distribution for γ_2 Velorum.

REFERENCES

1. Smith, Henry, J. Thesis, Harvard, 1955.

2. Gum, C. S. Observatory 72, 151, 1952.

3. Perrine, C. D. Ap. J. 47, 52, 1918.

4. Aller, L. H. Ap. J. 97, 135, 1943.

SECTION IV

THE HYDROGEN/HELIUM RATIO IN HD 96446

by Anne Cowley and L. H. Aller

One of the brightest of the hydrogen deficient stars is HD 96446 (α = $11^h1.8^m$ δ = -59°24'; 1900), whose spectrum has been described by the Jascheks [1]. Its broad lines of hydrogen and helium suggest that the star is on or below the main sequence [2]. About 400 lines have been measured in the spectral range $\lambda\lambda$3350-4850 arising from H, He, CII, CIII, NII, NIII, OII, OIII, NeII, SiIII, SiIV, PII, SII, ClII, ArII, KII, CaII, FeIII, FeIV, NiIII, and possibly KrII. (The identification of the latter is uncertain becuase the strongest lines of this ion are not present.

Spectral scans of this star were secured by D. J. Faulkner and L. H. Aller at Mt. Bingar on the nights of Nov. 9-10 and Nov. 10-11, 1960, Jan. 14-15, 1961, and Feb. 24-25, 1962, by Faulkner. In Fig. 4-1 we reproduce a typical, medium-speed spectral scan. In addition to the strong lines of hydrogen Hβ, Hγ, Hδ, etc., there also appear prominent helium lines: 4471, 4388, 4143, 4121, 4026, 4009. The Balmer jump is not prominent. Figure 4-2 shows the reduced energy distribution; the monochromatic magnitude of the star is plotted against $1/\lambda$.

In order to make a detailed study of the spectrum T. Dunham and L. Aller secured a number of spectrograms with the Coudé spectrograph on the 74-inch reflector at Mt. Stomlo. Observing conditions were extremely unfavorable at the time, so that although a number of lines could be measured on the plates it was not possible to carry out a complete abundance analysis for this star. We selected the five plates which were most suitable for measurements of equivalent widths and traced them with the microdensitometer at The University of Michigan Observatory.

Photometric calibration had been provided by two spectra of a wedge slit illuminated by a lamp and photographed above and below the stellar spectrum simultaneously with it. Unfortunately the two wedges did not always give the same deflection-log I curve, indicating that one of the wedges had been poorly illuminated; in some instances the second wedge image was partially missing. For this reason we used only one of the wedges to determine the deflection-log I curves. We also measured equivalent widths of the stronger lines on the photoelectric scans. Table 4-1 gives the list of Coudé observations of HD 96446.

Table 4-2 gives the equivalent widths (Aλ) determined from Coudé plates and from photoelectric spectral scans. Column 1 gives the measured wavelength; Column 2 gives the identification; Column 3 gives the average equivalent width determined from plates Cd 19, Cd 119, Cd 124, Cd 134, and Cd 144; and Column 4 gives the equivalent widths of the stronger lines as obtained from the spectrum scans.

In this preliminary reconnaissance we follow the method proposed by Unsöld [3] to get the helium/hydrogen ratio. If one assumes that a Balmer line formed in an optically thin layer, its equivalent width will be related

to the number of atoms "above the photosphere" in the second level, $N_{0,2}H$, by

$$A_\lambda = 0.886 \times 10^{-12} \lambda^2 f N_{0,2}H .$$

This approximation fails for the earlier members of the series but it becomes more nearly valid the greater the principal quantum number, until the lines begin to overlap. Hence for each Balmer line of principal quantum number, n, one may plot $A_\lambda(n)$ against $N_{0,2}H$ and extrapolate to an asymptotic value of $N_{0,2}H$. Table 4-3 summarizes the relevant data. The principal quantum number, n, and the wavelength λ are given in the first two columns. The third column gives the equivalent width A_λ in cm; the fourth column gives the f-value; and the last column gives log $N_{0,2}H$. The asymptotic value is log $N_{0,2}H$ = 15.95.

A similar procedure may be carried out for helium, considering each of the various series, 2^3P-n^3D, 2^1P-n^1D, 2^3P-n^3S, and 2^1D-n^1S, separately (see Table 4-4). In this way we obtain the number of atoms $N_{r,s}$ above each cm^2 of the photosphere in the rth excitation level of the neutral (s = 0) stage of ionization. We may refer all helium atoms to the 2^3P level, for which we find

$$\log N(2^3P)H = 16.16.$$

The number of ionized helium atoms is related to the number of helium atoms in the 2^3P level by

$$\log \frac{N_{He^+}}{N(2^3P)} = -\frac{5040}{T}\left[I_{He}-\chi_{(2^3P)}\right] + \frac{5}{2}\log T - 0.48 + \log \frac{2u(He^+)}{g(2^3P)} - \log P_\epsilon .$$

A similar expression holds for hydrogen. Then since at the temperature T ~ 18,000°K and electron pressure ~ 10^3 dynes cm^{-2} for the atomsphere of HD 96446, both hydrogen and helium are essentially all ionized, and we can write

$$\log N_{He}(\text{total}) \sim \log N_{He^+}$$

$$\log N_H(\text{total}) = \log N_{H^+}$$

$$\log \frac{N_H}{N_{He}} = \log \frac{N_{0,2}}{N(2^3P)} - \frac{5040}{T}\left[(I_H-\chi_2) - (I_{He}-\chi_{2^3P})\right] + \log \frac{2u_1}{g_2} - \log \frac{2u(He^+)}{g(2^3P)}$$

or

$$\log \frac{N_H}{N_{He}} = \log \frac{N_{0,2}}{N(2^3P)} + \frac{5040}{T} \times 0.12 - \log 4 - \log \frac{4}{9}$$

since

$$I_H - \chi_2 = 3.39 \text{ ev}, \qquad I_{He} - \chi_{2^3P} = 3.51 \text{ ev},$$

$u_1 = 1$, $u(He^+) = 2$, $g_2 = 8$, $g(2^3P) = 9$. Hence if we assume $T \sim 17{,}000°K$ we find

$$\log \frac{N_H}{N_{He}} = -0.42 \text{ or } \frac{H}{He} \cong 0.38 .$$

The uncertainty in the temperature introduces a much smaller uncertainty in the final result than does that in the extrapolation procedure. Although HD 96446 is a hydrogen deficient star, it is not by any means an extreme example of this class. Further studies of this interesting star will require improved observational data.

SECTION IV:

TABLES, FIGURES, AND REFERENCES

TABLE 4-1

COUDÉ OBSERVATIONS OF HD 96446

Plate Number	Date	Emulsion
19	Feb. 25, 1961	103a-O
119	May 26, 1961	IIa-O
124	May 28, 1961	IIa-O baked
134	Feb. 6, 1961	IIa-O baked
144	June 6, 1961	IIa-O

TABLE 4-2

A_λ VALUES OF HD 96446

λ	Element	Coudé Average	Average From Scans
3634.37	HeI		2.50
3705.14	HeI		3.34
3770.65	H		
3797.92	H		2.71
3819.61	HeI	2.98	2.73
3835.39	H	4.20	3.26
3867.48	HeI	.64	
3871.82	HeI	1.78	1.62
3888.65	HeI	3.85	3.50
3889.05	H		
3918.98	CII	.09	
3920.68	CII	.10	
3926.53	HeI	2.20	1.37
3933.66	CaII	.30	
3935.91	HeI	.24	
3964.73	HeI	.53	
3968.47	CaII	.15	
3970.07	H	4.88	4.23
3995.00	NII	.07	
4009.27	HeI	2.60	1.96
4026.19	HeI	3.71	3.03
4069.77	OII	.09	
4072.16	OII	.06	
4075.87	OII	.08	
4101.74	H	4.65	5.01
4120.84	HeI	.82	1.16
4143.76	HeI	2.63	2.18
4169.23	OII	.39	
4267.17	CII	.16	
4340.47	H	4.69	4.61
4387.93	HeI	2.53	2.35
4437.55	HeI	.34	
4469.92	HeI	3.90	3.67
4471.48	HeI		
4481.23	MgII	.16	
4713.14	HeI	.57	.62
4861.33	H		3.17
4921.93	HeI		1.62

TABLE 4-3

DETERMINATION OF $N_{0,2}H$ FOR HYDROGEN

n	λ	A_λ (cm)	f	log $N_{0,2}H$
4	4861.33	3.17×10^{-8}	1.19×10^{-1}	14.104
5	4340.47	4.65×10^{-8}	4.47×10^{-2}	14.795
6	4101.74	4.83×10^{-8}	2.21×10^{-2}	15.166
7	3970.06	4.66×10^{-8}	1.27×10^{-2}	15.420
8	3889.00	Combined with He	8.04×10^{-3}	
9	3835.38	3.73×10^{-8}	5.43×10^{-3}	15.722
10	3797.92	2.71×10^{-8}	3.85×10^{-3}	15.740
	Extrapolated Value			15.95

TABLE 4-4

DETERMINATION OF $N_{r,s}$ FOR HELIUM

n	λ	A_λ (cm)	f	log NH	n	λ	A_λ (cm)	f	log NH
		$2^3P\text{-}n^3D$					$2^1P\text{-}n^1D$		
4	4471.48	3.67×10^{-8}	.1231*	14.226	4	4921.93	1.62×10^{-8}	.1205*	13.797
5	4026.19	3.37×10^{-8}	.04686*	14.700	5	4387.93	2.35×10^{-8}	.04293*	14.506
6	3819.61	2.86×10^{-8}	.0260	14.930	6	4143.76	2.40×10^{-8}	.0199	14.899
7	3705.14	3.34×10^{-8}	.0152	15.257	7	4009.27	2.28×10^{-8}	.0112	15.155
8	3634.37	2.50×10^{-8}	.00853*	15.344	8	3926.53	1.78×10^{-8}	.00737*	15.242
					9	3871.82	1.70×10^{-8}	.00471	15.434
		$2^3P\text{-}n^3S$					$2^1D\text{-}n^1S$		
4	4713.14	$.62 \times 10^{-8}$	.01075*	14.467					
5	4120.84	$.99 \times 10^{-8}$	.003**	15.341	5	4437.55	$.34 \times 10^{-8}$	.00320	14.785
6	3867.48	$.64 \times 10^{-8}$	.00183	15.421	6	4169.23	$.39 \times 10^{-8}$	.00156*	15.210

*Given by Trefftz, et al. [4].

**Given by Allen [5].

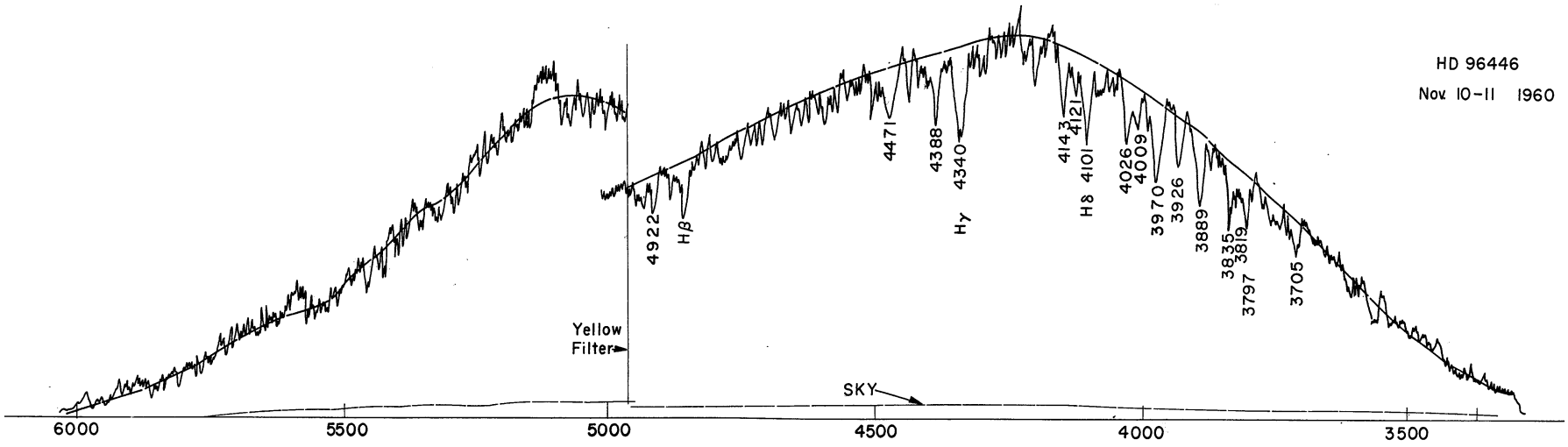

Fig. 4-1. Energy scan of HD 96446 (Nov. 10-11, 1960, Mt. Bingar).

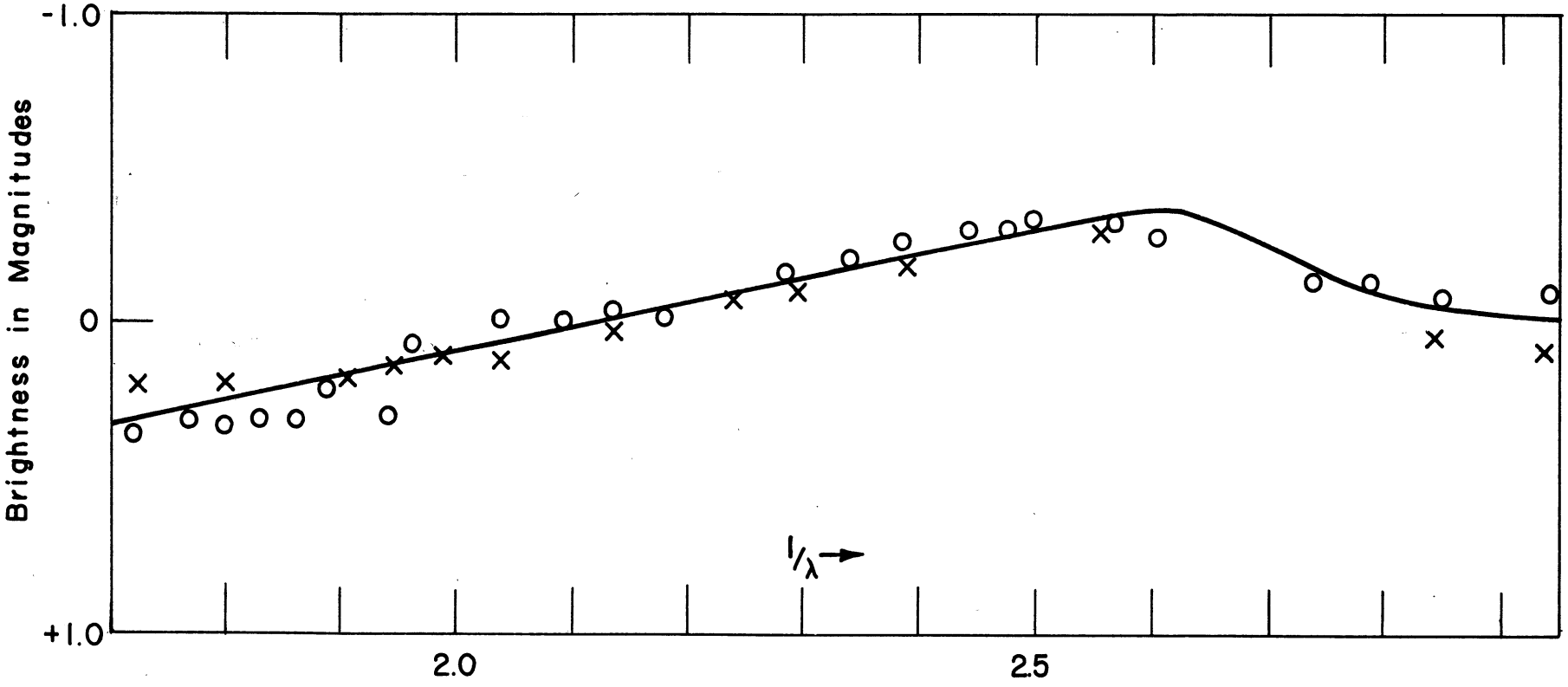

Fig. 4-2. Energy distribution for HD 96446.

REFERENCES

1. Jaschek, M. and Jaschek, C. Publ. Astron. Soc. Pac. 71, 465, 1959.

2. Aller, L. H., Buscombe, W. and Dunham, T. Astron. Journ. 67, 110, 1962.

3. Unsöld, A. Zeits für Astrophysik, 21, 22, 1941.

4. Trefftz, E., Schlüter, Detmar, and Jörgens. Zeits f. Ap. 44, 1, 1957.

5. Allen, C. W. Astrophysical Quantities, Athlone, London, 1960.

SECTION V

THE EMISSION NEBULOSITIES IN THE LARGE MAGELLANIC CLOUD

by H. R. Dickel, L. H. Aller, and D. J. Faulkner

The Magellanic Clouds are the nearest of all external galaxies. They contain many luminous stars, star clusters, emission nebulae, and large quantities of neutral hydrogen, as revealed by the 21-cm surveys. Some years ago Henize [1] published a catalogue of Hα emission stars and nebulae in the Magellanic Clouds. He employed a red-corrected 10-inch camera with a 15° objective prism, together with red-sensitive (Kodak 103aE) photographic emulsion and a red plexiglass filter so as to observe the emission nebulosities in the light of the red hydrogen line Hα (see Fig. 5-1). This catalogue gives the right ascension and declination of each nebulous patch for the Epoch 1950, the rectangular coordinates X and Y, the diameters x and y in seconds of arc, and other data including identifications with NGC objects. Other, less extensive discussions of emission nebulosities in the Large Cloud have been given by various observers. For example, Shopley and Miss Wilson [2] discussed 22 bright NGC objects in the Large Cloud, all of which are brighter than the Orion Nebula. The most spectacular object is 30 Doradus, the Tarantula Nebula for which Johnson [3] finds a mass 5,000,000 that of the sun (exclusive of its stellar content!) thus making it by far the most massive gaseous nebula known in our group of galaxies. With a diameter of the order of 500 parsecs, it mostly exceeds in size any other gaseous nebula. A detailed study of this object is being undertaken by D. J. Faulkner.

Photometric measurements of the emission nebulosities in the Large Magellanic Cloud are not numerous. Doherty, Henize, and Aller [4] microphotometered both widened and unwidened objective prism photographs covering a narrow wavelength range near Hα to obtain cross-sectional "intensity profiles" for certain nebulosities in the Large Cloud. These intensities were converted to surface brightnesses by tracing the widened spectra of stars of known magnitude and color and using the method of Ambarzumian [5]. Peak intensities for each scan across a nebulosity are given in ergs cm^{-2} sec^{-1} $steradian^{-1}$.

Many of the emission nebulosities in the LMC are filamentary in structure. The classic example is 30 Doradus but other objects such as Henize 144, 159, and 160 show a pronounced fine structure. (See Figs. 5-2, 5-3, 5-4, and 5-5.) This inhomogeneity must be taken into account when we convert surface brightness into electron densities. Densities in the filaments may appreciably exceed those found from averages taken over the volume occupied by the nebula.

Spectrophotometry of the emission nebulosities in the LMC was undertaken mostly at Mt. Bingar with the Michigan Photoelectric Scanner. Thanks to a generous allotment of time for this program, we were able to observe nearly all of the brighter nebulosities. Extension of the program to fainter nebulosities would have required a much larger telescope then was available to us.

Throughout, we used the D slots which sufficed to admit enough light to the photocell to resolve most of the lines of interest. Table 5-1 gives the data on the slot sizes including the dimensions in seconds of arc at the

focus on the slot and the area in steradians.

The observational procedure was to center the nebulosity in the slot, using the periscope immediately behind the entrance aperture. Then the spectrum was scanned from about 5200A to 3400A, the direction of the grating drive reversed, and the scan repeated. By superposing direct and reverse scans, the reliability of the tracing and spectral features displayed could be assessed. In Fig. 5-6 we compare direct and reverse scans for two nebulosities of somewhat different levels of excitation. The [OIII] λ4949 and λ5007 lines are much stronger in NGC 2040, indicating that it has a higher level of excitation.

The problem of nebulae spectrophotometry can be resolved into two aspects: (1) the surface brightness in one of the monochromatic emissions, e. g., Hβ; and (2) the relative intensities of the principal nebular lines. The second problem is relatively simple; one need know only the atmospheric extinction and sensitivity function of the photocell and the transmissivity of the optics. Both of these quantities can be obtained by observing proper "comparison" stars, as noted previously in Sections II and III.

The determination of the surface brightness is more troublesome in that one must compare the monochromatic radiation of, say, Hβ with the flux from a star in a unit wavelength interval at λ4861 and then determine the monochromatic magnitude of the star. Since we observed mostly stars of early spectral class whose colors differed from that of the sun, it was necessary to modify Ambarzumian's method to take this into account. If the B and V magnitudes of the comparison stars are known, we can determine their monochromatic magnitudes at λ4861 since their energy distributions have been measured. Since different spectral purities are involved (the stars being always observed with the B slots, i.e., a 9A resolution) this effect must also be taken into account. The method of reduction is straightforward although it is a little involved.

The principal results are summarized in Table 5-2. The first column gives the number in Henize's catalogue. The second column gives the quality of the scan of Hβ. For most of these nebulae, the quality was A or B, although occasionally poor deflections were obtained. Column 3 gives the slot sizes for both the entrance and exit slots. In most instances the D slots had to be used, yielding a spectral purity of 106A.

In many instances the nebulosities did not fill the slot. In yet others the slot was smaller than the nebula. Column 4 gives the estimated fraction of the slot area filled by nebulosity. An entry of "1" means that the nebula filled the slot. Stencils corresponding to slot sizes as reduced to the scales of appropriate photographs of the nebulosities were used to estimate the areas actually filled by the nebulosities. Extensive notes and sketches of the nebulosities as they appeared in the slot at the time of observation also aided the making of such estimates as are entered in Column 4. Column

5 gives the surface brightness in Hβ in units of 10^{-4} ergs cm^{-2} sec^{-1} $ster^{-1}$ (averaged over the amount of the nebula in the spot). In some instances the nebulosity consisted of a bright blob on a diffuse background. For example, in Henize 69, an intense blob filling only one-tenth of the slot gives S(Hβ)= 8 in our units; however, the average over the slot would be 0.8. In Column 6 we give the ratio of the sum of the intensities of the green nebular [OIII] lines to Hβ. From this ratio one may estimate the "excitation class" of the nebula [6]. For Henize 77 the excitation class is estimated from $I(N_1+N_2)/I(3727)$ to be 4.5. The larger the number in the last column the higher the level of excitation of the nebula.

Table 5-3 gives the relative intensities of the lines observed in the various nebulosities on the scale Hβ = 10. To each line measured on the tracing one may assign a quality raging from A (for good data) to E (for a line which is very poor). The lines listed are the green nebular lines 5007+4959 = N_1+ N_2 [OIII], Hβ = 10, HeI λ4472, Hγ λ4340, Hδ λ4101, λ3969 (Hε+[NeIII]), λ3865+ λ3889 ([NeIII]+H), λ3835 (rarely), and λ3727 [OII]. In all of these nebulosities the intensities of the helium lines are low and the quality of the measurements is poor. If we included all the nebulosities and take a straight average we get a He/H abundance ratio of 1/7, but the uncertainty is so large that this number must be regarded as meaningless. It is best to adopt the He/H ratio from the work of Hugh Johnson [3].

We now describe briefly the utilization of these data to derive ionic abundances for hydrogen oxygen (O^+ and O^{++}) and Ne^{++}. The methods have been adequately described in the literature (see e.g. [6] or [7]). The density of hydrogen can be obtained from the surface brightness if one postulates a uniformly radiating sphere and chooses an electron temperature. For most estimates we chose T_ϵ = 10,000°K.

For each nebulosity one estimates the radius in seconds of arc from Henize's catalogue. Assuming a distance to the LMC one can then convert this angular radius to radius in cms. For this purpose we assumed a distance of 46 kpc. Then

$$r_{neb} = 6.87 \times 10^{17} \theta_n''$$

where θ_n'' is the radius in seconds of arc. Then from the measured surface brightness one can calculate the electron density (assuming hydrogen is much more abundant than helium) of e.g. [8], p. 204. We use, however, the correction to the Boltzmann formula B_4 (10,000°K) obtained by Burgess [9]. Similar calculations may be carried out for T_ϵ = 15,000°K.

Turning to the forbidden lines of [OII] and [OIII], we may calculate

$$\frac{N(O^+)}{N(O^{++})} = \frac{I(3727)}{I(N_1+N_2)} P_\epsilon(N_\epsilon, T_\epsilon)$$

where I(3727) is the intensity of 3727 of [OII] and $I(N_1+N_2)$ is the sum of the intensities of the two green nebular lines. Here $P_\epsilon(N_\epsilon, T_\epsilon)$ is a known function of the electron temperature, electron density, and atomic parameters involved in the ground configurations of O^+ and O^{++}. For details see Aller [10] and Seaton and Osterbrock [11]. Similarly [10] we can write

$$N(O^{++}) = B(N_\epsilon, T_\epsilon) \frac{I(N_1+N_2)}{I(H\beta)}$$

where B can be tabulated as a function of N_ϵ and T_ϵ.

Table 5-4 gives the results for an electron temperature of 10,000°K. Successive columns give the number of the nebula in Henize's catalogue, the electron density (number of electrons per cm^3), the number of O^{++} ions calculated from the ration $I(N_1+N_2)/I(H\beta)$, and the ratio $N(O^+)/N(O^{++})$ calculated from $I(3727)/I(N_1+N_2)$.

In order to see what the effects of uncertainty in the electron temperature would be, we also carried out calculations for T_ϵ = 15,000°K (see Table 5-5). The electron density is increased by about 20%. The number of doubly ionized oxygen atoms is cut in half and $N(O^+)/N(O^{++})$ is reduced to about three quarters of its value for 10,000°K.

Similarly one may estimate the concentration of ions of Ne^{++} from the 3868 line. The [NeIII] lines are always relatively weak and are blended with Balmer lines. Hence only rough estimates of their intensities can be extracted from the data. To do this we plot the Balmer decrement from Hβ to Hδ and extrapolate with the aid of the well known theory [6], [7] to get the expected intensity of λ3868. The difference between the observed and calculated value is then attributed to [NeIII]. We can write [10]

$$\frac{N(Ne^{++})}{N(O^{++})} = \frac{I(3868)}{I(N_1+N_2)} P_{Ne}(N_\epsilon, T_\epsilon)$$

Numerically P_{Ne} = 4.04 for T_ϵ = 10,000 and 3.07 for T_ϵ = 15,000°K.

To obtain the ratios of oxygen and neon to hydrogen we now proceed as follows. Consider first the oxygen problem. Oxygen can exist as O, O^+, and O^{++}; little is triply ionized. If one plots a histogram of $N(O^+)+N(O^{++})/N(H)$, he can get an idea of the absolute abundance of oxygen by assuming that the nebula with the largest value of this ratio would contain oxygen in only these two stages of ionization. In this way one finds the limiting value to be

$$N(O) = 2.6 \times 10^{-4} N(H)$$

as compared with $4 \times 10^{-4} N(H)$ for the Orion Nebula [12].

For neon the problem is very much more difficult since we observe neon only in one stage of ionization, viz. Ne^{++}. Hence we must estimate $N(Ne^{++})/N(Ne)$. If we choose nebulae with about the same level of excitation as the Orion Nebula and assume that the distribution of atoms among various stages of ionization is the same for Orion and the nebulosities under consideration we can estimate the abundance of neon. The scatter in the resultant neon abundance is considerable. Most of this must arise from the distribution of atoms among various ionization stages and some of it comes from the uncertainties in the intensities which are guessed in only a very rough way.

We may summarize our results as follows. Let us assume an electron temperature of 10,000°K. The electron density ranges from 3 electrons cm^{-3} to 50 electrons cm^{-3} in the objects studied, with an average of 15. This value is considerably lower than that found for the Orion Nebula or the denser regions in 30 Doradus. The upper limit must be much too low as we have made no allowance for the effects of filamentary structure.

Most nebulae fall in excitation classes 3 or 4. That is, they are comparable with planetary nebulae such as IC 418 or IC 2149 in our own galaxy [6].

For every 10,000 hydrogen atoms we would find the following figures for atoms of other types:

Helium.—No reliable estimate can be obtained from the data herein presented since the helium line intensities are in all instances too uncertain. It is best to adopt Johnson's value for this ratio or that obtained by D. J. Faulkner from a photoelectric spectrophotometric study of the 30 Doradus nebula.

Oxygen.—The range for $N(O^{+}+O^{++})$ is from 0.9 to 2.6. We have adopted the upper limit on the assumption that all the oxygen would then be concentrated in these two ionization stages. If the electron temperature is lower than 10,000°K, the ratio may be higher.

Neon.—The range is from 0.10 to 1.7. For 17 of the 55 nebulosities studied, no measureable line was observed. The range and average values are adopted from the data for the 38 nebulae which were believed to show [NeIII] lines, albeit weak. The average is N(Neon) = 0.5. Probably this is much too low as we can imagine that the allowance for the atoms in the lower ionization stages is inadequate. Literally interpreted, the results would suggest that neon is less abundant in the Large Magellanic Cloud than in our galaxy, but we do not believe that this is correct.

The conclusion drawn from this investigation is that the abundance ratio of oxygen (and probably neon as well) is about the same in the LMC as in our galaxy. We must stress the uncertainty in this result, however, and urge that more detailed attention be paid to the brighter nebulosities, particularly 30 Doradus. Scanner observations should be supplemented by photographic spectroscopy of the fainter lines. In any event the biggest stumbling block is going to be the same as that found in the study of other gaseous nebulae, namely (1) allowing for the distribution of atoms among various stages of ionization and (2) allowing for the effects of filamentary structure.

Although the first difficulty will require both difficult observations and erudite theoretical studies, we can make some progress on the second. A study of the filamentary structure of 30 Doradus has been undertaken by D. J. Faulkner, and some of the brighter nebulosities are being studied by H. R. Dickel with the aid of the isophotometer. The objective is to find to what extent our average electron densities have to be increased in the filaments and lowered throughout the bulk of the volume occupied.

The data obtained in this program should be useful for another problem, namely the total amount of ionized hydrogen in the LMC. The amount of neutral hydrogen and its spatial distribution is being studied by the CSIRO radiophysics group with the large dish at Parkes. Regions of high gas density can readily be found and it will be interesting to see if most of the ionized hydrogen regions are simply Strömgren spheres. Results obtained with more modest equipment showed that the 30 Doradus region was the focal point of a concentration of gas unequalled by any other known nebula in the local system of galaxies.

SECTION V:

TABLES, FIGURES, AND REFERENCES

TABLE 5-1

SCANNER SLOTS AND APERTURE USED ON EMISSION NEBULOSITIES IN THE LARGE MAGELLANIC CLOUD

Bingar Slots	E-W Dimension Sec. of Arc	N-S Dimension Sec. of Arc	Slot Area in Steradians
D5	200	88	4.14×10^{-7}
D4	157	88	3.26×10^{-7}
D3	~ circular	r = 57	1.83×10^{-7}
DO	214	88	4.44×10^{-7}
C5	228	38	2.02×10^{-7}
C4	168	38	1.4×10^{-7}

TABLE 5-2

DATA FOR THE EMISSION NEBULOSITIES IN THE LARGE MAGELLANIC CLOUD

Henize Catalogue Number	Quality of Hβ	Slots (Entrance, Exit)	Estimated Fraction of the Slot Area Filled by Nebulosity	$S_{H\beta}$ Surface Brightness	$\frac{I(N_1+N_2)}{I(H\beta)}$	Excitation Class
5	B	D5-D4	1	.6	1.5	3
8	B	D5-D4	~ 3/8	1.7	4.1	4
9	C	D5-D4	1	.30	2.1	3
11AB	A	D5-D4	1	3.9	4.0	4
11B					4.4	4
11C					4.1	4
11CD	A	D5-E2	~ 1	3.8	4.5	4
11E		D5-D4	~ 2/3	.9	4.0	4
11F	A	D5-D4	1	1.6	2.1	3
11I	C	D5-D4	1/2	.7	2.6	3
17	B	D5-D4	~ 1/2	.6	2.0	3
23A	A	D5-D4	~ 2/3	1.1	2.7	3
30B	C	D5-D4	1/5	3.2	.8	5
44B	B	D5-D4	~ 1	1.0	1.6	3
44C	B	D5-D4	5/6	2.1	6.3	4
44D	A	D4-D4	2/3	1.6	1.3	3
44F	B	D4-D4	1/3	2.1	1.9	3
51A	B	D0-D4	2/3	.8	1.2	3
51C	A	D5-D4	~ 5/8	1.6	1.0	3
51D	B	D5-D4	2/3	1.1	1.8	3
55	A	D5-D4	1	2.7	2.0	3
57A	B	D5-D4	3/4	.8	1.6	3
59A	B	D5-D4	1	3.3	6.4	4
59B	A	D0-D4	2/3	1.3	3.2	3 → 4
			1 (filled ?)	.5		
63	B	D5-D4	1/6 (intense →)	2.9	2.0	3
68B		D5-D4	(if 1, then →)	.8		
			(if 1/10, then →)	8.4	1.6	3
69	A-	D5-D4	(if 1, then →)	1.0		
			(if 1/10, then →)	9.8	1.4	3
70	C	D5-D4	~ 1	.25	1.8	3
77			~ 1	1.5	I(3727) = 3.7	
79	A	D5-D4	(if 1, then →)	3.4*		
			(if 1/4, then →)	5.9	3.9	4
79 (north)	A	D0-D4	~ 1	1.9	1.5	3
83	A	D5-D4	5/8	3.4	4.1	4
91	A	D5-D4	2/3	2.4	2.2	3
92	C	D5-D4	2/3	.65	2.2	3
103	E	D5-D4	~ 1	.65		
105A	A	D5-D4	~ 1	1.5	2.9	3
1131 ABED	A	D4-D4	2/3	1.7	1.9	3
1131i	E	D4-D4	~ 1/2 ?	.4	3.4	4
119	A	D5-D4	~ 1	1.6	1.9	3
120	A	D5-D4	~ 1	2.4	1.2	3
144	A	D5-D4 D4-D4	~ 1 ?	1.7	4.9	4
148C	C	D5-D4	3/4	.8	2.1	3
154A	A	D5-D4	3/4	2.0	1.9	3
158C	B	D5-D4	3/4	1.5	2.8	3
159		D4-D4	5/6	1.7	2.5	3
159A	B	D4-D4 D3-D4	1/4, 1/3	4.4	5.8	4
159C	A	D5-D4	1	1.7	3.2	3 → 4
159D+F	A	D5-D4	5/6	1.7	1.9	3
160		D4-D4	~ 1	3.2	4.4	4
160A		C5-C4	2/3	19.0	4.1	4
160A+D		D5-D4	5/6	4.5	4.4	4
160B+C	A	D5-D4	~ 2/3	1.6	3.8	4
163	B	D5-D4	1	.5	2.0	3
164	B	D5-D4	1	.7	1.8	3
180	A	D5-D4	5/6	1.1	2.4	3

*(1/4 for the most intense blob)

TABLE 5-3

RELATIVE INTENSITIES (Hβ = 10)

Nebula No.	[OIII]	N_1+N_2	Hβ	Helium 4472	Hγ	Hδ	3969	3865	3835	[OII] 3727
5	A	15	B 10		E 1.1	E 2.1	E .9	E 1		B 15
8	A	41	B 10		C 5	D 3.4	E 1.4	E 2.5		B 20
9	C	21	C 10							D 26
11AB	A	40	A 10	C .7	A 4.1	B 1.5	B 1.2	B 2.8		A 16.5
		N_1 N_2								
11B		32 11.5	10							
11C		32 8.6	10							
11CD	A	45	A 10	E .6	B 4	B- 2	C 1.4	B- 3.8		B+ 22
11E		40	10	1.7	5.3	4.9	1.1	5.5	2.3	25
11F	A	21	A 10	.2	C 3.8	D 2.8	E .6	E 1.1		A 30
11I	C	26.5	C 10		C 4.4					C 36
17	B	19.5	B 10		D 3.8	E 1.4				B 35
23A	A	27	A 10		D 3.8	D 3.5	E 1.5	E 4.7		(A) 22
30B	C	8	C 10	D 2.5	D 4.4	D 4.9	E .6	E 1.6		D 10
44B	B-	16	B 10		D+ 2.5	D- 2.4	E .8	E 1.6		A 19
44C	A	63	B 10	E .5	B 5	D 2.1	E 1.3	C- 4.1	1.1	A 21.3
44D	A	13	A 10	E .8	C 5	D 2.8	E 1.8	E 1.2	E .6	A 37
44F	A	19	B 10		D 5	D 1.4	E 1.5	E 1.4		B 34
51A	B	12	B 10		E 3.8	E 1.7				B 35
51C	B	9.7	A 10	E .5	B 3.8	D- 3.1	E 1.5	E 2.5		A 37
51D	B	18	B 10							B 21
55	A	20	A 10	E .2	B 3.9	C 2.25	D 1.5	D 1.6		A 32
57A	B	16	B 10	E 1.1	D 4.4	E- 4.5	E- 4.1			A 51
59A	A	64	B 10	C .7	B 3.8	B 2	C 15	B 2.8		A 13
59B	A	32	A 10	E 1.2	B 5	C 2.8	E .9	D 2.7		A 32
63	B	20	B 10	E 1	C 3.8	D 5.6	E 3	E 2.8		B 31
66A										C 14.5
68B		16	10		C 6.9	D 2.8	E 1.5	E 1.1		A 41
69	B+	14	A- 10		B 4.3	C 4.2	D 2.1	D 2.1		A 43
70	C	18	C 10		D 4.3	E 3.8				B 40.5
77		10								3.7
79	A-	39	A 10		C 3.8	D 2.5	E .6	E 1.2		A 23
79N	A	15	A 10	E .5	C 1.9	E 1.4	E 1.5	E .8		A 35
83		41	A 10	.7	B 4	C 2.1	D- 1.1	D- 1.9	E .6	A 22
91	A	22	A 10	E .7	D 4	D 2.8	E 1.4	E 3.2	E 1.9	A 31
92	B	22	C 10		D 4.5	E 4.2	E 2	E 4		C 19
103			E 10		E 4.6					
105A	A	29	A 10	E .35	C 3.5	D 2.1	E 1.5	E 1.6		A 28
1131 ABED	A	19	A 10		C 3	D 1.4	E .9	E 2.1	E 1	A 29
11311	E	34	E 10		E? 10					D 44
119	A-	19	A 10	E .2	B 3.8	D 2.1	D 1.4	D 3.2		A 27
120	A	12	A 10	.35	B 4.3	C 2.4	C 2.7			A 33
144	A	49	A 10	E .35	C 3.6	D 2.95	D 2	D 5.4		A 23
148C	B	21	C 10		E 4.5	D 5.3				C 28
154A	A	19	A 10	D- .95	C 3.4	C 1.7	C 1.4	D 1.3		A 21
158C	A	28	B 10	E .8	C 4.8	C 3.4	D 1.4	C 2.7	D 1.4	A 25.5
159		25	10	.6	3.1	3.1	1.2	3.5		31.5
159A	A	58	B 10	D .8	C 4.3	C- 3.9	D 1.6	C- 3.2	E .8	A 30
159C	A	32	A 10	D- .5	B 4.1	C 1.7	D .9	D+ 1.4		A 16
159D+F	A	19	A 10	E .2	B 4.3	B 2.5	D 1.1	C 1.6		A 30
160		43.5	10	.8	3.8	1.8	1.5	2.8	.8	14
		N_1 N_2								
160A		30 10.6	10							
160A+D		43.5	10		3.6	2.4	2	2.4		16
160B+C	A	38	A 10	C 1.9	B 4.6	D+ 3.5	E 1.1	D 1.6		A 27
163	B	20	B 10		C- 4.1	E 2	E .8	B 2.2		B 25
164	A	18	B 10	E .35	C 4.4	D 6.2	1.2			B 28
180	A	24	A 10	E .95	B 6.3	B 6	C 1.8	C 3.2		A 31

TABLE 5-4

ELECTRON DENSITIES AND IONIC CONCENTRATIONS FOR T_e = 10,000°K

Nebula No.	Ne	N(OIII)	N(OII)/N(OIII)	Nebula No.	Ne	N(OIII)	N(OII)/N(OIII)
5	8	.39 x 10^{-3}	1.13	79A	40	5.00 x 10^{-3}	.68
8	19	2.55	.56	79E	15.5	.75	2.65
9	4	.27	1.35	83	12	1.51	.61
11AB	17	2.12	.47	83A	36	4.68	.61
11CD	22	3.30	.54	91A+B	25	1.79	1.57
11E	12.5	1.63	.70	92	9	.65	1.01
11F	15.5	1.10	1.57	103	6	-	-
11I	14.5	1.20	1.51	105A	10.6	1.10	1.06
17	12.5	.78	2.00	113ABED	19	1.19	1.71
23A	15.5	1.37	.90	113ii	4	.42	1.44
30B	57	14.4	.14	119	7	.39	1.62
44B	18	.97	1.31	120	20	.80	3.02
44C	28	5.77	.38	144	9	2.43	.52
44D	20	.87	3.10	148C	12.5	.85	1.49
44F	27	1.65	2.02	154A	25	1.57	1.24
51A	29	1.12	3.33	158C	36	3.32	1.03
51C	20	.60	4.32	159	11.6	.91	1.44
51D	7	.37	1.31	159A	40	7.80	.59
55	12.5	.81	1.82	159C	17	1.73	.54
57A	21	1.05	3.55	159D+F	17	1.66	1.71
59A	21	4.21	.22	160	10	1.46	.34
59B	15.5	1.62	1.13	160A	68	8.84	-
63	5.6	.33	1.73	160A+D	34	4.98	.40
63A	40	2.59	1.75	160B+C	22	2.66	.79
68B	11.6, 98	.60, 5.1	2.84	163	8	.50	1.39
69	12.5, 104	.56, 4.72	3.37	164	8	.44	1.75
70	3.7	.23	2.54	180B	9	.69	1.46

TABLE 5-5

ELECTRON DENSITIES AND IONIC CONCENTRATIONS FOR T_e = 15,000°K

Nebula No.	Ne	N(OIII)	N(OII)/N(OIII)	Nebula No.	Ne	N(OIII)	N(OII)/N(OIII)
5	10	.18 x 10^{-3}	.79	79A	5	2.34 x 10^{-3}	.49
8	23	1.15	.40	79E	18	.35	1.85
9	4.5	.12	.97	83	15.5	.72	.43
11AB	20	.97	.32	83A	44	2.24	.43
11CD	26.5	1.46	.38	91A+B	31	.81	1.12
11E	15.5	.72	.50	92	10	.27	.72
11F	18	.50	1.12	103	8	-	-
11I	17	.54	1.06	105A	13.5	.49	.76
17	15.5	.35	1.40	113ABED	23	.53	1.21
23A	20	.63	.65	113ii	51	.21	1.03
30B	70	6.88	.097	119	8	.18	1.13
44B	23	.44	.92	120	24	.37	2.14
44C	34	2.67	.27	144	10	.61	.38
44D	25	.40	2.20	148C	15.5	.38	1.04
44F	33	.77	1.42	154A	31	.69	.88
51A	36	.53	2.34	158C	43	1.50	.72
51C	24	.28	3.04	159	14.5	.40	1.01
51D	8	.14	.92	159A	49	3.47	.41
55	15.5	.35	1.28	159C	20	.78	.38
57A	25	.50	2.50	159D+F	22	.53	1.21
59A	25	.69	.16	160	11.6	.62	.23
59B	18	.74	.79	160A	82	4.32	-
63	6.5	.15	1.22	160A+D	40	2.57	.29
63A	51	1.22	1.22	160B+C	26.5	1.21	.56
68B	14.5, 120	.27, 2.34	2.00	163	9	.22	.99
69	15.5, 127	.25, 2.04	2.38	164	9	.18	1.24
70	4.5	.10	1.80	180B	10	.32	1.03

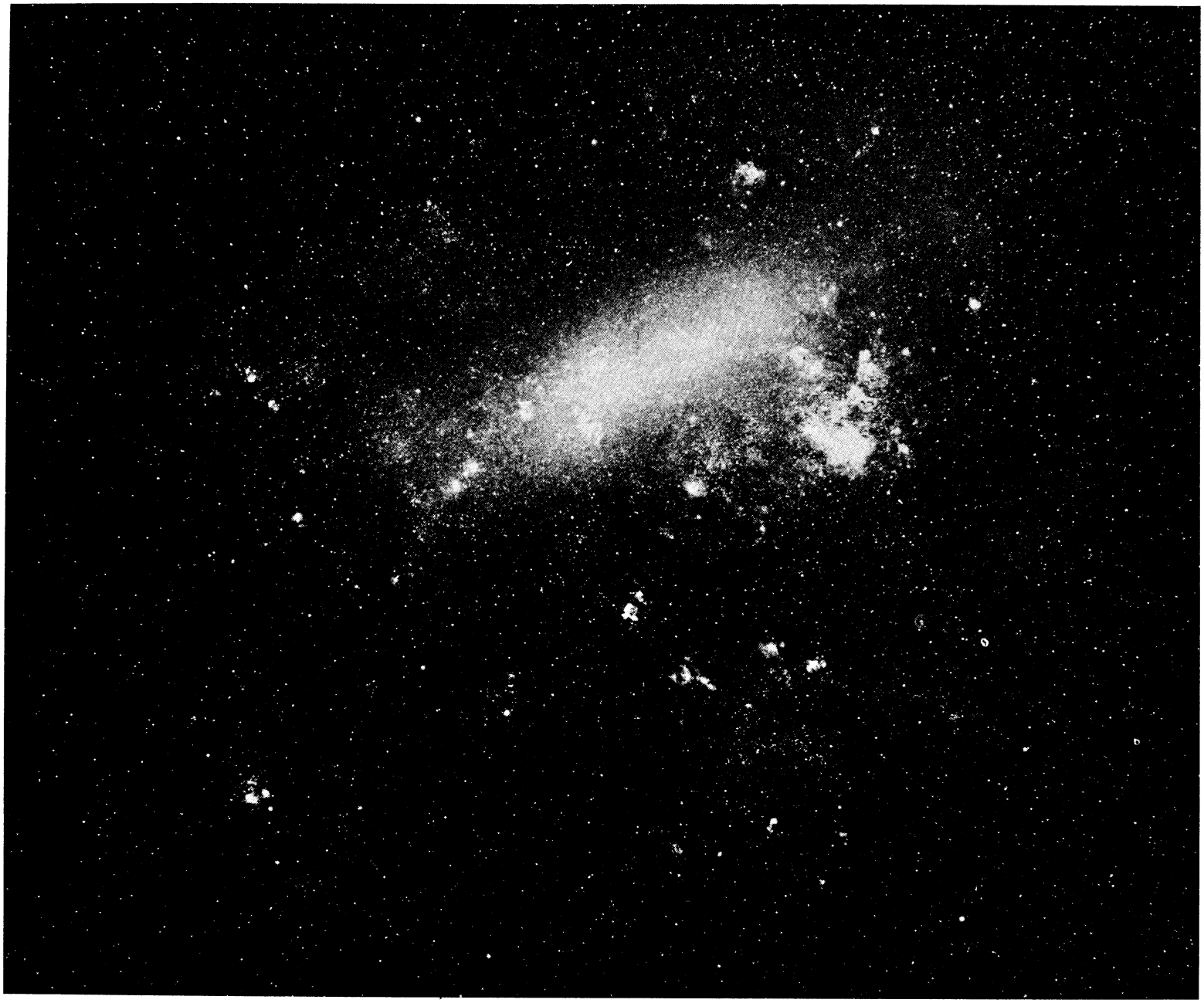

Fig. 5-1. The Large Magellanic Cloud photographed by Karl G. Henize at the Lamont-Hussey Observatory with a 10-inch telescope loaned by Mt. Wilson Observatory. A red plexiglass filter and red-sensitive emulsion were used to record the nebulosities in the red radiation of hydrogen.

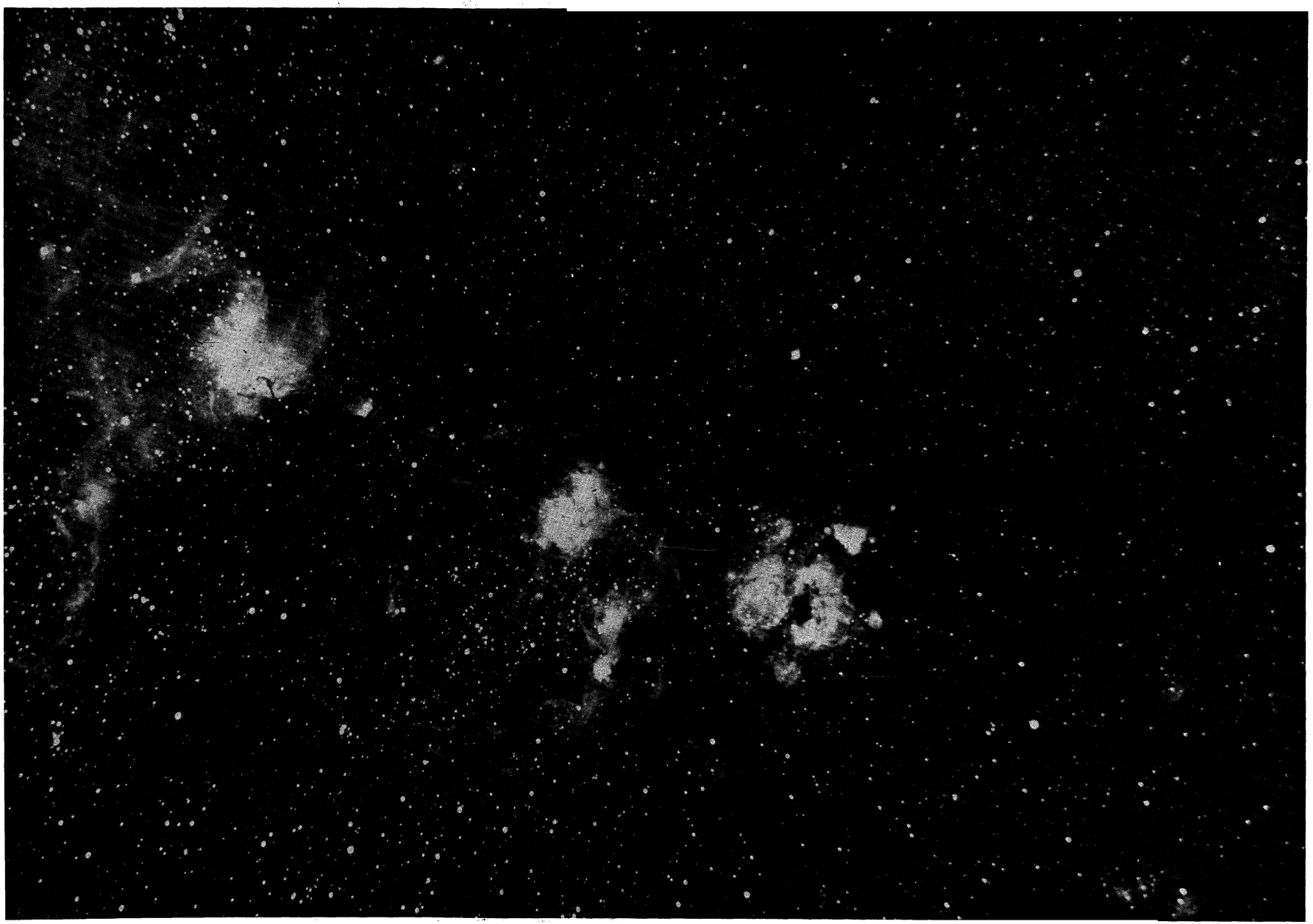

Fig. 5-2. Emission nebulosities in the Large Magellanic Cloud near 30 Doradus. This photograph was obtained with the 74-inch reflector at Mt. Stromlo on Dec. 21, 1960. The photograph shows Henize nebulosities 159 and 160, which include NGC 2077, 2078, 2079, 2080, 2083, 2084, 2085, and 2086. (ORI (red) filter, 103aE emulsion, 60 min exposure.)

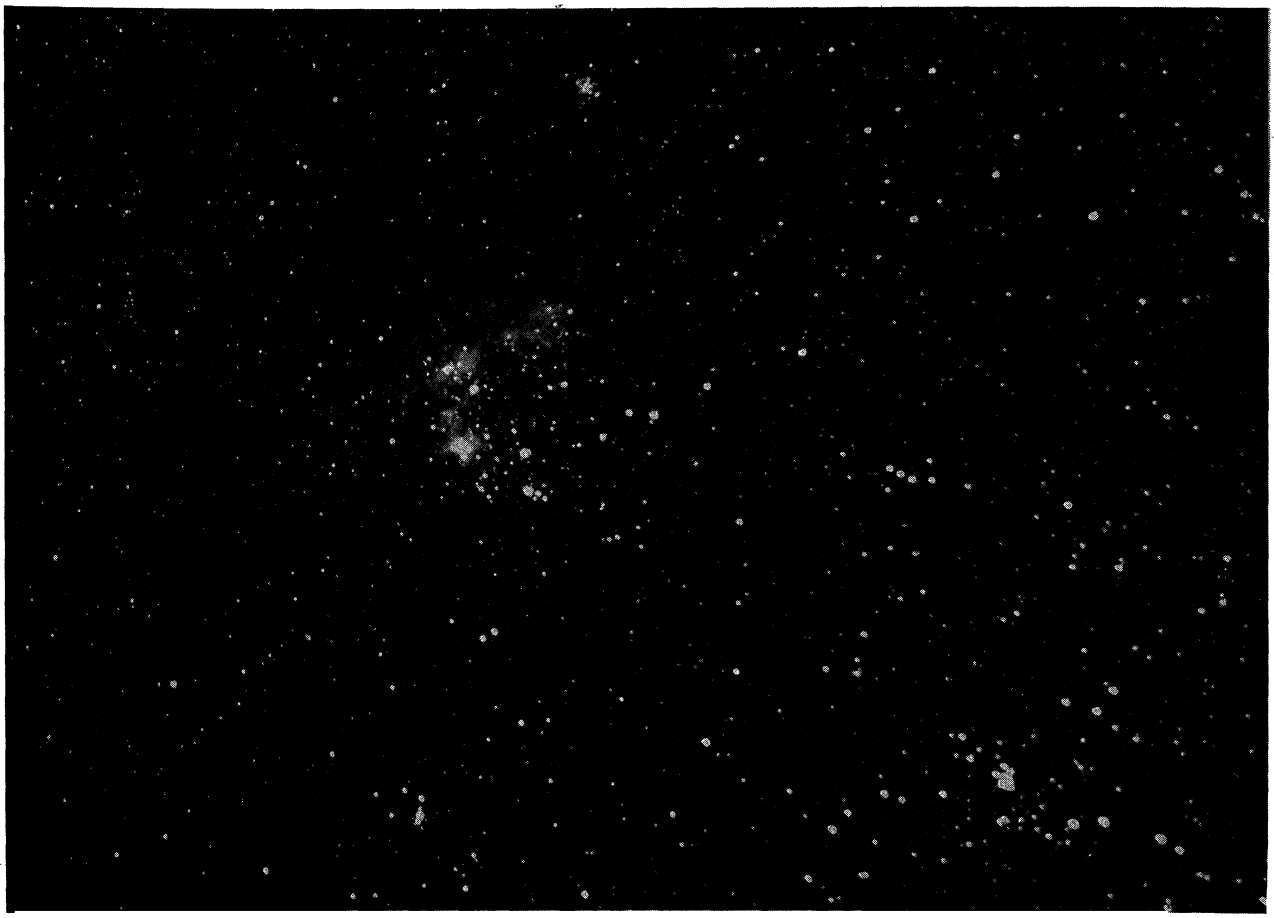

Fig. 5-3. The emission nebulosity Henize 144 in the Large Magellanic Cloud photographed with the 74-inch reflector at Mt. Stromlo. This object includes NGC 1962, NGC 1965, NGC 1966, and NGC 1970. (ORI filter, 103aE emulsion, 60 min exposure.)

Fig. 5-4. The emission nebula near S Doradus photographed with the 74-inch reflector at Mt. Stromlo Observatory December, 1960. (ORI filter, 103aE emulsion, 60 min exposure.)

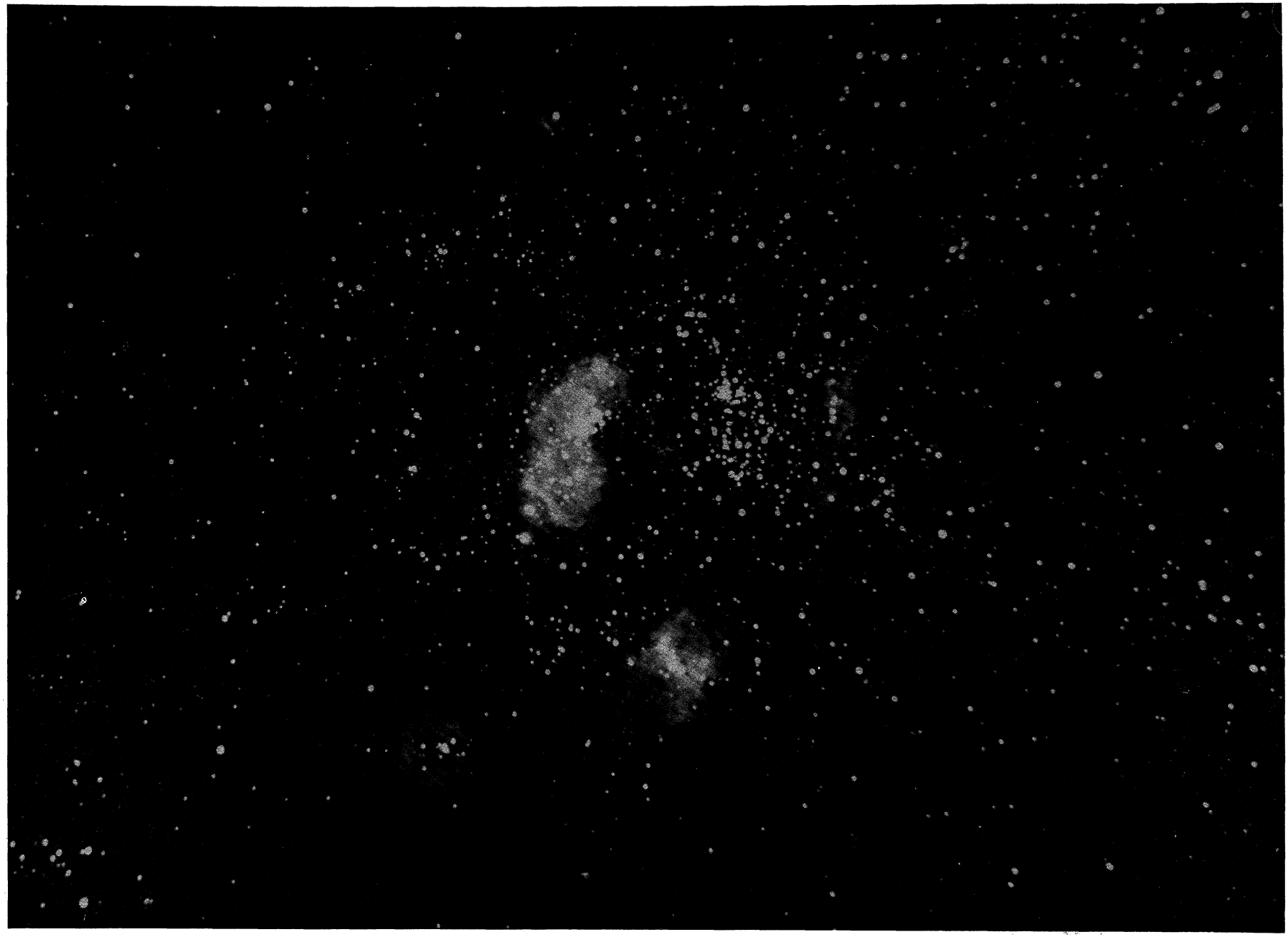

Fig. 5-5. Emission nebulosities, Henize 11, in the Large Magellanic Cloud photographed with 74-inch reflector at Mt. Stromlo. This nebula includes IC 2116, NGC 1769, NGC 1763, IC 2115, NGC 1773, and NGC 1760. (ORI filter, 103aE emulsion, 60 min exposure.)

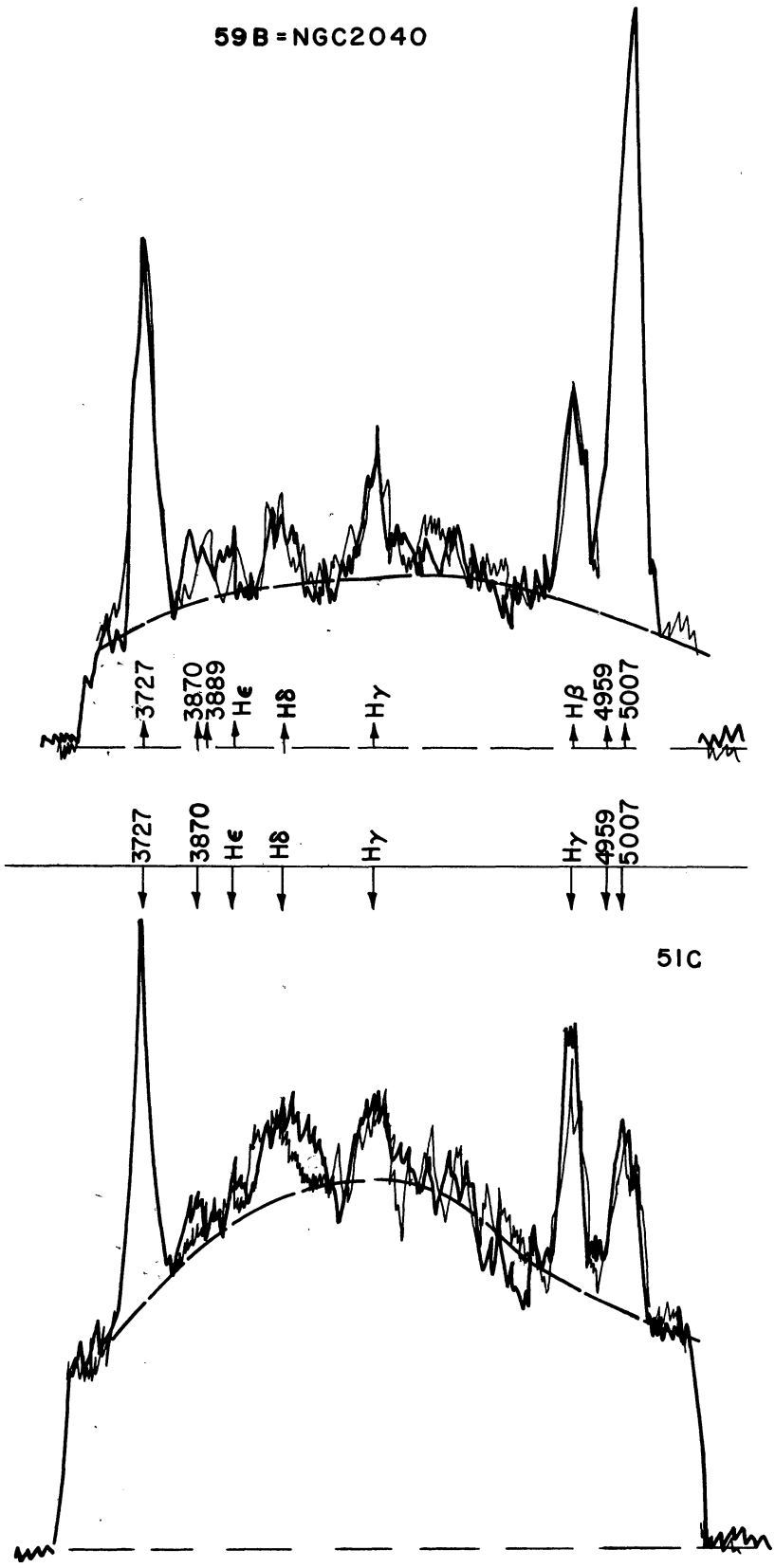

Fig. 5-6. Scans of typical emission nebulosities in the Large Magellanic Cloud.

REFERENCES

1. Henize, K. G. Ap. J. Suppl. 2, 315, 1956.

2. Shapley, H. and Wilson, H.H. Harvard Circular 271, 1924.

3. Johnson, H. Publ. Astron. Soc. Pac. 71, 425, 1959.

4. Doherty, L., Henize, K. G., and L. H. Aller. Ap. J. Suppl. 2, 345, 1956.

5. Ambarzumian, V. A. Zeits f. Astrophysik 6, 107, 1933.

6. Aller, L. H. Gaseous Nebulae, Wiley, New York, 1956.

7. Seaton, M. J. Progress in Physics. 23, 313, 1960.

8. Aller, L. H. Nuclear Transformations, Stellar Interiors and Nebulae, 1954, Ronald Press Co.

9. Burgess. Monthly Notices Roy. Astron. Soc. 118, 488, 1958.

10. Aller, L. H. Ap. J. 120, 401, 1954.

11. Seaton, M. J. and Osterbroch, D. E. Ap. J. 126, 66, 1957.

12. Liller, W., and Aller, L. H. Ap. J. 130, 45, 1959.

SECTION VI

EMISSION NEBULOSITIES IN THE SMALL MAGELLANIC CLOUD

by H. R. Dickel, L. H. Aller, and D. J. Faulkner

The Small Magellanic Cloud (see Fig. 6-1) is considerably farther than its companion although it contains a number of bright stars and clusters. Two of the clusters, NGC 330 and NGC 419, have been described previously. The emission nebulosities are fainter and less conspicuous than those in the LMC. Shapley and Miss Wilson [1] discussed 106 nebulosities which have an average diameter of 8 or 10 Parsecs. Whitney, et al. [2] discussed 152 nebulosities in the SMC, and Lindsay found six small emission nebulosities and possibly a dozen planetaries identified on Schmidt plates secured at the Boyden Station. Henize (Ref. [1] of Section V) listed 90 sets of emission nebulosities, some of which were described as separate units, e.g., 84A, 84B, 84C, and 84D.

The brightest and largest nebula is NGC 346 = Henize 66. It is comparable in size with Gum's nebula—the largest known HII region in our galaxy [3]. The level of excitation of the nebula is slightly higher than that of Orion. The hydrogen/helium ratio in this nebula [4] is found to be exactly the same as in the LMC (Ref. [3] of Section V), our galaxy [5] and M33 [6].

Scans of 12 emission nebulosities in the SMC were secured with the 50-inch and 74-inch reflectors. Table 6-1 gives the relative intensities of the principal lines observed. Column 1 lists the nebula according to the number in Henize's catalogue; Column 2 gives the surface brightness of Hβ in ergs cm^{-2} sec^{-1} $ster^{-1}$; Column 3 gives the number of scans; and the remaining columns give the intensities for various nebular lines of the scale I(Hβ)=10. The quality of each line is also indicated. The most detailed study was carried out for NGC 346, for which the additional intensities were measured (see also Ref. [4]):

λ5007	4959	4363	3889
43.1	16.1	1.0	2

For HeI λ4471, see Ref. [4].

Table 6-2 gives the electron densities for the various emission nebulosities observed in the SMC. Successive columns give the number of the nebulosity, its radius in seconds of arc, the electron density calculated both for temperature 10,000°K and 15,000°K. (The electron temperature of NGC 346 seems to be about 14,000°K.)

The problem of estimating elemental abundances for the ions involves the same difficulties as those previously noted for the LMC. Fewer objects are involved, however, and [NeIII] is observed in only one nebulosity, NGC 346.

The general level of the nebular line intensities and excitation indicates that the abundance ratios of O to H and of Ne to H are probably also about the same as for the LMC and our own galaxy. An intensive spectroscopic study of NGC 346 ought to be carried out to observe weaker lines that may serve to fix the general level of ionization and to supply abundance data. It cannot be

too often emphasized that small abundance differences that may exert a marked influence on stellar structure and therefore on color-magnitude arrays, etc., are very difficult to establish from studies of gaseous nebulae.

SECTION VI:

TABLES, FIGURES, AND REFERENCES

TABLE 6-1

RELATIVE INTENSITIES OF THE NEBULAR LINES OBSERVED IN THE SMALL MAGELLANIC CLOUD

Nebula	$S_{H\beta}$	$\lambda \rightarrow$	N_1+N_2	Hβ	Hγ	Hδ	3969	3865	3835	3727
12A	1.2×10^{-4}	2	A	A	B+	C	D	C		B+
			48	10	4.6	2.5	1.2	3.2		12.5
12B	.32	1	A	C	C	E		D		B
			67	10	7.9	5.2		5.0		15.2
19	.27	1	B→C	C	D	E				B→C
			22	10	3.5	2.6				28.5
36	.58	1	A	B→B-	D-	D			E?	B→C
			45	10	7.1	2.8			2.1	15.4
37	.30	1	A	B	C	D				B
			33	10	7	3.8				16.7
66	2.2	7	A	B	B	C	C	B		B
			62.3	10	4.7	2.5	2.4	3.8		8.4
76	.47	2	A	C	C-D	C-D	D	C		C
			80.7	10	5.0	4.8	2.9	8		10.9
78	.36	1	17	10						
80	.22	1	28.3	10						
83	1.36	4	A	B	B	C	D	C-D		A-B
			35	10	5	2.7	1.2	2.2		14.9
84	1.0	3	A	A	B	C-D	D	D		A
			52	10	5.8	3.1	1.6	5.5?		31.9
90	1.4	1	A	C	D	D	E	D		C
			44	10	2.5	3.1	.7	2.0		12.1

Notes: Neb 12B: 3 additional scans of N_1+N_2; Neb 19: 2 additional scans of N_1+N_2, λ3727; Neb 36: 2 additional scans of 3727, 3 of N_1+N_2; Neb 66: 9 additional scans of N_1+N_2.

TABLE 6-2

ELECTRON DENSITIES IN THE SMALL MAGELLANIC CLOUD

SMC	Θ_n"	$N_\epsilon(T_\epsilon = 15 \times 10^4 °K)$	$N_\epsilon(T_\epsilon = 10^4 °K)$
12A	56	19	15
12B	56	10	8
19	75	8	6
36	75	11	9
37	150	6	5
66	100	19	16
76	100	9	7
78	156	6	5
80	88	6	5
83	90	16	13
84	80	14	12
90	87	16	13

Fig. 6-1. The Small Magellanic Cloud photographed by K. G. Henize with the Mt. Wilson 10-inch telescope at the Lamont-Hussey Observatory of The University of Michigan. A red plexiglas filter and red sensitive emulsion is used.

REFERENCES

1. Shapley, H. and Wilson, H. H. Harvard Observatory Circular 275, 276, 1925.

2. Whitney, C. A., Wade, C. M. and Nail, V. Proc. Nat'l. Acad. Sci. 39, 1168, 1953.

3. Johnson, H. Publ. Astron. Soc. Pac. 73, 20, 1961.

4. Aller, L. H. and Faulkner, D. J. Publ. Astron. Soc. Pac. 74, 219, 1962.

5. Mathis, J. S. Ap. J. 125, 318, 328, 1957.

6. Mathis, J. S. Ap. J. (in press).

SECTION VII

PHOTOGRAPHIC REGION OF THE SPECTRUM OF NGC 7009

by L. H. Aller

From the standpoint of theories of physical processes in gaseous nebulae and nebular compositions, one of the most interesting planetary nebulae is NGC 7009, $\alpha = 21^h02^m6^s$ $\delta = -11°32'$ (1960), sometimes called the "Saturn" nebulae because of its well-developed ansae. Its southern declination makes it a not to favorable object for study. Although NGC 7027 [1] shows a much richer spectrum than does NGC 7009 [2,3], it is a less favorable object for theoretical studies and abundance investigations. The reason appears to be that NGC 7027 is characterized by a filamentary structure which may show a great range in excitation conditions. On the other hand, the structure of NGC 7009 is relatively smooth for a planetary nebula [4] and it seems possible to allow for effects of stratification within the nebula. Whereas the central star of NGC 7027 has never been observed, that of NGC 7009 is well-defined. It seems to show a continuous spectrum with neither emissions nor absorption lines.

A characteristic feature of the spectrum of NGC 7009, noted in the classical investigations of Bowen and Wyse [2] and of Wyse [3], is the great number of permitted lines of OII, CII, NII, and other ions. These arise from recombination and permit one to deduce abundances of a number of ions, e.g., C^{++}, which cannot be studied in other ways. With the development of reliable theories of recombination and subsequent cascade by Seaton and his associate, it will be possible to use these lines to derive ionic abundances and the distribution of atoms among various ionization stages.

Earlier attempts to deduce the chemical composition [5] of NGC 7009 were based on rather limited material. It is hoped that when the present investigation is extended to other spectral regions and improved intensity calibrations are obtained, the problem can be handled in a much more effective manner.

In August, 1961, I was able to secure a graded sequence of spectrograms of NGC 7009 with the Coudé spectrograph of the 100-inch telescope covering the region from λ3100 to λ4900. The plates were calibrated photometrically with a calibrating spectrograph and were traced with the microphotometer at The University of Michigan. Table 7-1 lists the relevant data. The image rotator was used for all observations so that the nebula was held in a fixed position on the slit. In the two-night exposure, care was taken to avoid getting the light of the central star on the slit.

The four plates in Fig. 7-1 show the appearance of the spectrum as photographed on plate 14767. The faint background continuum arises from the nebula. At wavelengths longer than λ3665 it arises from recombinations on the third and higher levels in H; shortward of λ3665 it comes mostly from recombinations on the second level of hydrogen. Most lines are intensified in the region of the bright ring but spurious sky lines denoted as L.A.--due to the light of Los Angeles—extend across the entire field. Some lines, e.g., 4227.49 [FeV] are intensified in spots in the ring; others have a more uniform appearance.

A microphotometric tracing of the spectrum is shown in the twelve strips of Fig. 7-2. Deflection is not strictly proportional to intensity since the characteristic curve of the plate is involved. The tracing shows, however, many of the features that are not too easily seen in the reproduction. The marked rise in intensity at the Balmer limit is clearly shown. The dotted line indicates the estimated position of the background continuum.

First we used the photographic calibration exposures secured in the calibrating spectograph to get the deflection - log I relation. This relation changed slowly with wavelength, so it was necessary to use different curves for different wavelength regions. With the aid of these curves we determined the intensities of the lines on a relative scale. It is not possible to compare lines in different regions of the spectrum because the sensitivity of the plate changes with wavelength, atmosphere extinction varies with wavelength, and the transmission of the optics changes with wavelength. The intensity of the spectrum of the background star changes with wavelength but since its temperature is known approximately, we might expect that it could be used to calibrate the wavelength-dependent effects. Unfortunately this hope is not justified since atmospheric dispersion seriously affects the energy distribution in the stellar image but does not affect the nebula at all.

Photographic calibrations may be carried out by comparing the nebula with a standard star. This procedure has been used for a number of nebula by various observers, but suffers from several difficulties inherent in using photographic photometry in any fundamental way. Another alternative, which has actually been employed, is to use photoelectric photometry. Since a wide slit must be used, care must be exercised in regions of density packed lines as, for example, near the Balmer limit.

In undertaking the calibrations we proceeded as follows. First, the intensities obtained from the three Coudé plates were combined in one master list. The weaker lines appeared only on the two night exposure on which the strong lines were "burned out." Hence, we used the short exposure to get the intensities of the stronger lines and the intermediate exposure to tie together the strong and weak lines with the aid of lines of medium intensity. To secure definitive line intensities in this way, it will be necessary to obtain additional plates, covering the ranges of intermediate and high intensities.

The photoelectric scanning techniques give only the intensities of strong lines and these must be compared with the stronger lines observed photographically to ascertain how the effects of plate sensitivity, atmosphereic transmission, etc., are to be taken into account.

Two series of photoelectric measurements were used for this investigation. One series of observations was secured by Liller and the writer at the Mt. Wilson Observatory in 1956 (see Fig. 7-3). These observations covered the lines from the Balmer limit to longer wavelengths. In order to secure a

calibration for the ultraviolet, Faulkner and the writer observed NGC 7009 with the Michigan scanner on the 74-inch telescope, covering the spectral range λ3100-λ4100. Thus it was possible to obtain a set of photoelectric intensities for all the stronger lines; and by comparing the photographic intensities with them, the effects of atmospheric transmission, plate sensitivity, etc., could be assessed. Nevertheless, the lines intensities in the ultraviolet are still subject to considerable uncertainties. We have no assurance that the atmospheric transmission remains the same from one night to another.

Hence the entire calibration of intensities is to be regarded as tentative. The results are given in Table 7-2. The first column gives the wavelength measured on the Coudé plate 14767, the second column is the identification taken from Miss Moore's Multiplet Table of Astrophysical Interest, and from more recent work by Bowen. The third column gives the multiplet number from Miss Moore's table and the last column gives the tentative intensity.

SECTION VII:

TABLES, FIGURES, AND REFERENCES

TABLE 7-1

DETAILS CONCERNING SPECTROGRAMS SECURED WITH THE COUDÉ SPECTROGRAPH ON THE 100-INCH TELESCOPE

Plate No.	Date	Emulsion	Exposure	Remarks
14763	Aug. 29, 1961	Kodak IIaO	300 min	(1)
14765	Aug. 30, 1961	IIaO baked	459 min	(1)
14767	Aug. 31-Sept. 1, 1961	IIaO baked	906 min	2 nights (2)

(1) Centered on star.
(2) Centered on bright ring, avoiding star.

TABLE 7-2

PHOTOGRAPHIC REGION OF THE SPECTRUM OF NGC 7009

λ	Identification	Multiplet	Tentative I
3121.71	OIII		73.8
3132.87	OIII		678.0
3187.74	HeI		78.7
3203.10	HeII		158.6
3260.98	OIII	8	7.9
3263.43	NeII	15	7.3
3265.46	OIII	8	5.4
3267.3			2.7
3299.36	OIII	3	48.9
3306.60	OII	23	46.4
3305.15	OII	23	2.6
3312.30	OIII	3	108
3334.87	NeII	2	13.7
3340.74	OIII	3	134.7
3342.5	[NeIII]		8.3
3354.92	HeI NeII	8 2	8.1
3367.00	OII	52	4.4
3375.74	OII	52	
3392.78	NeII	7	
3397.90	NeII	36	1.5
3399.80			2.0
3405.74	OIII	15	6.0
3408.13	OIII NeII	15 45	3.2
3411.84	OIV		2.2
3414.8	OIII	15	7.1
3417.00	[NeV]		2.6
3425.57	OIV	3	
3428.70	OIII	15	47.7
3430.55	OIII	15	8.3
3438.35			2.7
3490.32	OIII	13	3.3
3442.00			2.4
3444.00	OIII	15	208.3
3447.59	HeI	7	5.0
3450.78	OIII	25	
3464.21			1.8
3466.04	OIII	25	0.8
3468.44			1.4
3472.00	HeI	44	1.0
3478.95	HeI	43	2.2

TABLE 7-2 (Continued)

λ	Identification	Multiplet	Tentative I
3480.80	NeII	49	
3487.77	HeI	42	0.6
3494.55	OII	70	1.5
3498.70	HeI	40	2.6
3504.23			1.8
3512.51	HeI	38	2.3
3520.40			
3525.38			
3530.58	HeI		5.2
3554.55	HeI		5.0
3563.11			
3568.62	NeII	9	4.4
3570.27			
3574.29	NeII	9	0.9
3578.08			0.6
3580.05			
3583.03			1.2
3587.36	HeI		8.3
3597.91			
3613.70	HeI		6.1
3634.35	HeI		14.1
3657.59	H		0.3
3658.81	H		0.7
3659.28	H		1.1
3660.22	H		1.4
3661.25	H		1.9
3662.28	H		3.4
3664.48	H		6.5
3665.93	H		8.2
3667.52	H		10.5
3669.27	H		10.9
3671.32	H		13.3
3673.61	H		14.7
3676.25	H		16
3679.25	H		17.1
3682.74	H		21.3
3686.86	H		23.8
3691.49	H		28.9
3694.17	NeII		7.7
3697.11	H		35.1
3702.82	OIII		11.7
3703.82	H		41.3
3705.02	He		24.5

TABLE 7-2 (Continued)

λ	Identification	Multiplet	Tentative I
3707.23	OIII		11.4
	OIII		
3709.67	NeII AII		2.6
3711.92	H		44.8
3713.04	NeII		8.4
3714.04	OIII		7.7
3715.15	HeII		10.4
3721.90	H		82.2
3726.01	[OII]		238.7
3728.73	[OII]		112.9
3730.85			.8
3732.60	HeI		3.1
3734.39	H		68.5
3736.62			
3740.24	OII		2.2
3746.37	AII	130	1.0
3750.14	H		85.9
3754.50	OIII	2	18.3
3757.33	OIII	2	11.8
3759.93	OIII	2	54.5
3762.40	SiII	3	3.4
3766.48	NeII	1	2.2
3768.93	HeII		2.9
3770.63	H		120.0
3773.08	SiIV	3	2.4
3774.13	OIII		7.2
3777.16	NeII	1	2.6
3778.65	SIII		2.5
3784.91	HeI		1.3
3791.42	OIII	2	11.8
3796.36	HeII	5	3.6
3797.93	H		151.7
3805.96	HeI		1.8
3811.08	OIII	2	1.2
3813.59	HeII	4	3.9
3819.66	HeI		40.0
3826.93	AII	54	.8
3829.38	MgI	3	1.1
3831.74			1.4
3833.77	HeII		6.8
3835.43	H		237.3
3838.23	HeI		3.3
3839.83	[FeV]		
3851.10	OII		1.9

TABLE 7-2 (Continued)

λ	Identification	Multiplet	Tentative I
3852.90			1.2
3855.90	SiII	1	3.4
3858.04	HeII	4	4.9
3861.52	SiII		4.2
3866.61			1.4
3868.63	[NeIII]		Too Bright
3870.58			5.6
3871.73	CII	18	3.0
3882.38	OIII	12	4.0
3888.79	H He		Too Bright
3891.44	[FeV]		3.8
3895.66	[FeV]		3.2
3905.83			1.3
3907.38	OII	11	1.2
3914.90			1.1
3918.91	CII NII	4 17	1.3
3920.52	CII	4	1.8
3923.51	HeII	4	6.3
3926.56	HeI	58	5.8
3928.87			0.8
3933.19	[FeII]	8	0.9
3935.02			0.9
3944.87	OII	6	1.1
3947.99	CII	32	1.7
3959.94	OII	6	1.3
3960.72			0.9
3964.79	HeI	5	23.6
3967.40	[NeIII]		Too Bright
3970.00	H		Too Bright
3973.16	OII	6	2.0
3976.77			0.5
3979.71			0.7
3982.96	OII	6	0.7
3986.19			0.9
3993.06			1.0
3995.04			0.8
3997.15	[FeIII]		0.6
3998.91			1.3
4001.03			0.5
4003.62	NIII	16	2.3
4009.31	HeI		8.0
4026.15	HeI		74.6

TABLE 7-2 (Continued)

λ	Identification	Multiplet	Tentative I
4035.08	OII	51	2.2
4041.41	OII NII	50 39	4.0
4043.57			1.5
4056.03	CIII	24	0.7
4060.22	OII	97	1.4
4062.91	NeII OII	53 60	1.9
4068.37	[SII]		
4069.96	OII	10	18.8
4072.16	OII	10	15.8
4074.05	OIII	23	2.2
4075.94	[SII] OII		20.8
4080.90	OIII	23	2.6
4081.90			1.0
4083.86	OII	49	4.0
4085.24	OII	10	5.0
4087.19	OII	48	4.9
4089.18	SiIV OII	1 48	10.9
4092.98	OII	10	3.1
4097.25	NIII	1	69.1
4101.67	Hδ		Too Bright
4103.41	OII	20	34.6
4104.90	OII	20	3.7
4107.01	OII	47	2.3
4109.82			1.2
4110.63	OII	20	1.9
4112.55	OII	21	1.3
4115.88	SiIV	1	1.0
4119.52	OII	20	7.7
4120.85	HeI		8.4
4123.55	[FeV]	158	0.9
4125.30			0.9
4128.70			1.9
4132.66	OII	19	3.6
4135.31			1.1
4136.76			0.6
4139.94			1.5
4143.81	HeI		12.8
4146.00			1.4
4150.56	NeII	53	0.7
4153.56	OII	19	5.5

TABLE 7-2 (Continued)

λ	Identification	Multiplet	Tentative I
4155.48	OII	19	3.7
4163.12	[KV]	15	1.1
4169.14	OII	19	2.8
4171.57	NII	43	1.1
4176.75			1.2
4181.15	NII	49	1.5
4185.51	OII	36	2.8
4186.94	CIII		4.5
4189.78	OII	36	3.9
4195.72	NIII	6	2.8
4199.90	HeII	3	16.7
4202.00	AII	8, 124	0.6
4215.80	NIII	6	1.1
	OI	33	
4217.20	NeII	52	1.1
4219.79	NeII	52	2.8
4222.83	OI	33	
4225.07			1.1
4227.44	[FeV]		
4231.61	NeII	52	1.1
4233.83	OI	33	0.7
4237.04	NII	48	2.2
4241.24	NII	47,48	3.3
4245.28			0.8
4248.84			0.8
4250.53	NeII	52	1.1
4253.88	OII	101	3.2
4267.11	CII	6	34.6
4275.57	OII	67	6.5
4276.73	OII	54,67	3.7
4277.74	OII	67	2.7
4272.88			1.1
4281.38	OII	40	0.9
4283.29	OII	54,67	2.4
4285.70	OII	78	2.5
4288.80	OII	54	1.2
4291.61	OII	78	2.0
4294.85	OII	54	3.2
4303.89	OII	54	5.9
4307.33	OII	53	0.8
4309.21	AII	36	1.7
4311.50	CII	28	0.8
4313.95	OII	78	1.2

TABLE 7-2 (Continued)

λ	Identification	Multiplet	Tentative I
4315.36	OII	78	1.2
4317.24	OII	2	4.3
4319.81	OII	2	2.9
4325.83	OII	2	3.1
4327.63	OII	11	2.3
4331.39	OII	11	1.1
4333.01	OII	65	1.6
4337.10	OII	2	1.9
4340.42	Hγ		Too Bright
4344.51	OII	65	2.7
4345.72	OII		4.8
4347.80	OII	16	2.1
4349.46	OII	1	7.1
4351.75	OII	16	1.2
4355.47			0.7
4363.16	[OIII]	15	255.1
4366.97	OII	2	5.1
4369.20	OII	26	1.5
4371.73	OII	76	1.5
4376.67	OII	46	1.6
4379.20	NIII	17	12.4
4387.90	HeI		21.7
4392.00	NeII	57	3.3
4398.02	NeII	56	1.8
4400.91			
4403.51			
4408.31			1.8
4409.42	NeII	57	3.0
4412.95	NeII	55	1.5
4414.94	OII	5	4.0
4416.94	OII	5	3.4
	NeII	61	
4419.98			
4425.43			0.6
4428.50	NeII	61,57	7.5
4431.09	NeII	56	2.4
4432.76	NeII	55	2.1
4434.87			1.1
4437.60	HeI	50	2.5
4439.95	NeII	61	0.9
4442.47	NeII	56	0.3
4446.68	NeII	56	0.9
4448.37	OII	35	1.7

TABLE 7-2 (Continued)

λ	Identification	Multiplet	Tentative I
4453.29			1.0
4456.83	NeII	61	1.3
4459.04			1.3
4464.25			0.9
4465.65	OII	94	1.8
4471.50	HeI		184.4
4478.04	OII	68	1.5
4481.16	MgII	4	1.1
4487.85	OII	104	1.0
4489.70	OII	86	1.3
4483.23			
4491.89	OII	86	2.1
4495.58			
4498.52	AII	136	1.0
4504.40			
4510.98	NIII	3	6.9
4515.08	NIII	3	2.2
4517.32	NIII	3	2.0
4521.07			0.3
4523.65	NIII	3	2.4
4527.82	NIII	3	0.2
4529.7	OIII	15	
4530.32	NII	59	1.5
4531.96			1.9
4534.57	NIII	3	2.7
4541.59	HeII		19.4
4544.80	NIII	12	2.6
4547.34	NIII	3	1.4
4552.54	NII	58	
4557.72			0.9
4562.66	NeII	64	0.8
4564.43	AII	85	1.1
4571.10	MgI	1	3.8
4574.58	SiIII	2	
4588.6			
4590.97	OII	15	2.8
4596.17	OII	15	2.2
4602.1	OII	93	2.3
4609.9	OII	93,92	4.8
4613.30			
4621.07			
4631.10			
4634.16	NIII	2	44.5

TABLE 7-2 (Concluded)

λ	Identification	Multiplet	Tentative I
4638.85	OII	1	1.5
4640.64	NIII	2	83.3
4641.90	NIII	27	25.7
	OII	1	
4647.40	CIII	1	9.1
4649.14	OII	1	24.7
4651.35	CIII		9.8
4658.42			
4661.64	OII	1	8.3
4667.28			
4671.09			
4673.75	OII	1	2.7
4676.26	OII	1	6.7
4683.40			4.9
4685.68	HeII	1	Too intense
4698.27			
4702.00	OII	25,40	63.3
4705.36	OII	25	
4708.56			
4711.34	AIV		142.5
4713.17	HeI		17.1
4714.80			1.7
4740.20			
4782.39			14.0
4805.06			23.5
4861.30	Hβ		
4921.96	HeI		
4958.95			

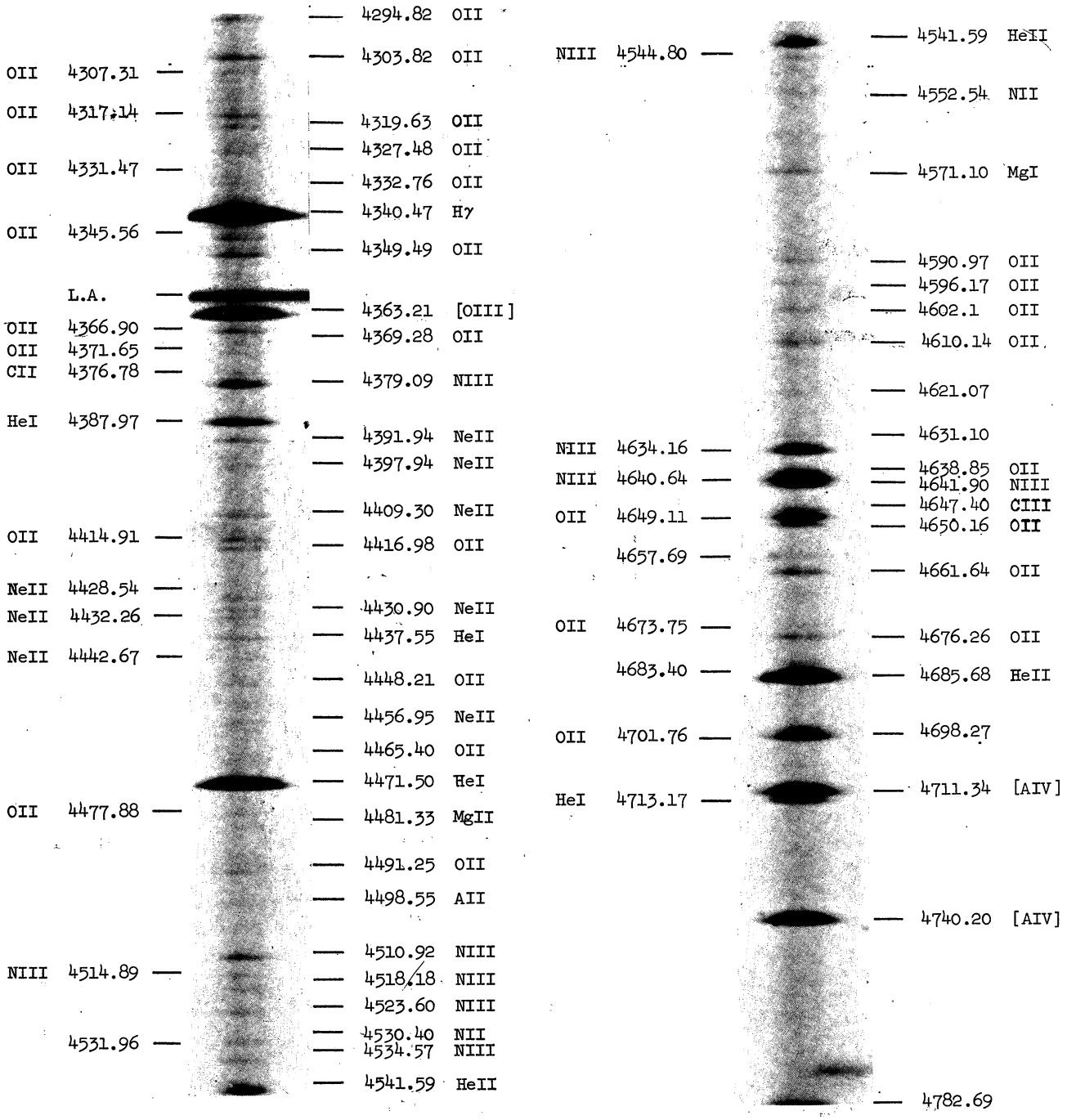

Fig. 7-1. Spectrum of NGC 7009.

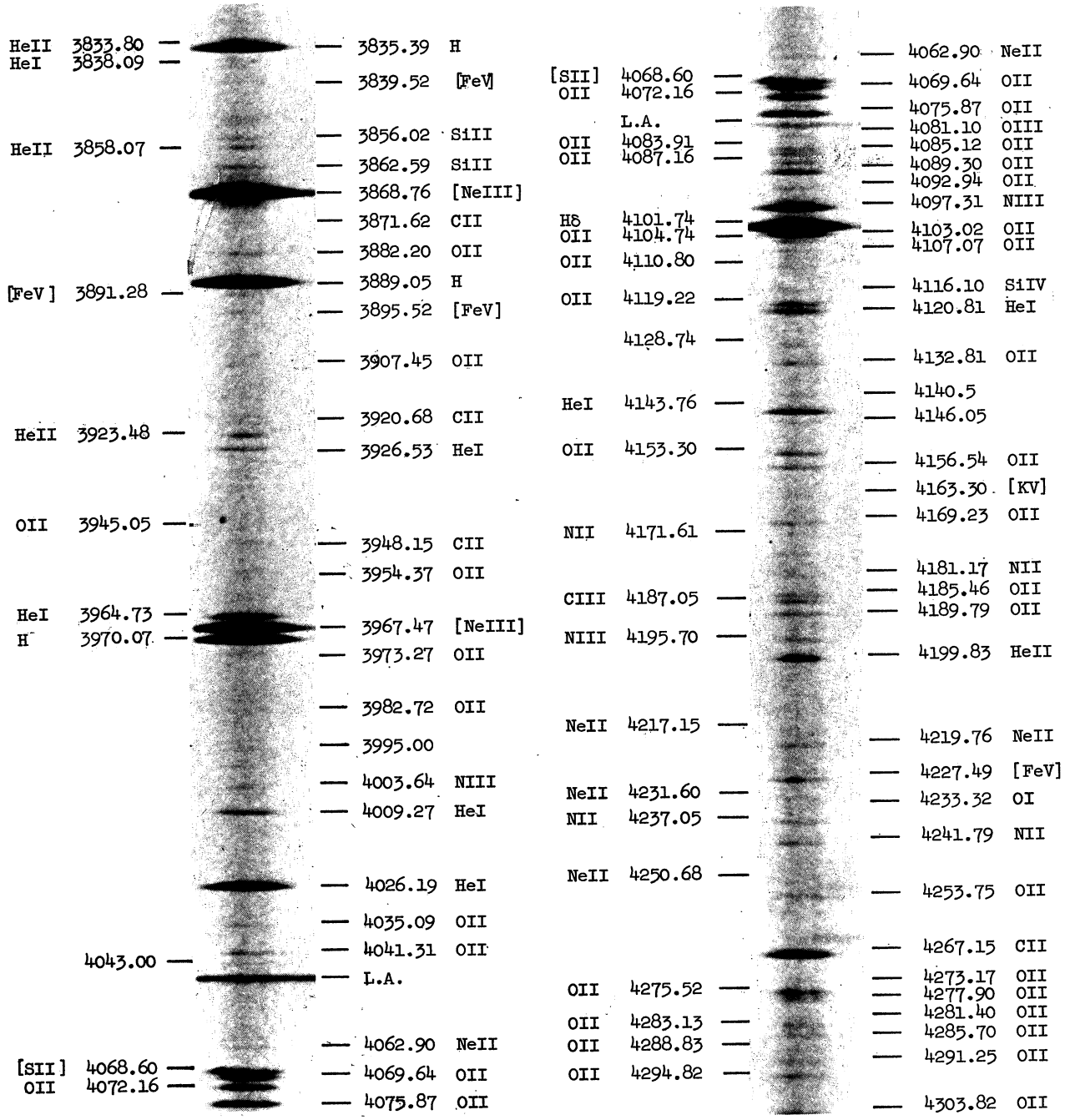

Fig. 7-1. Continued.

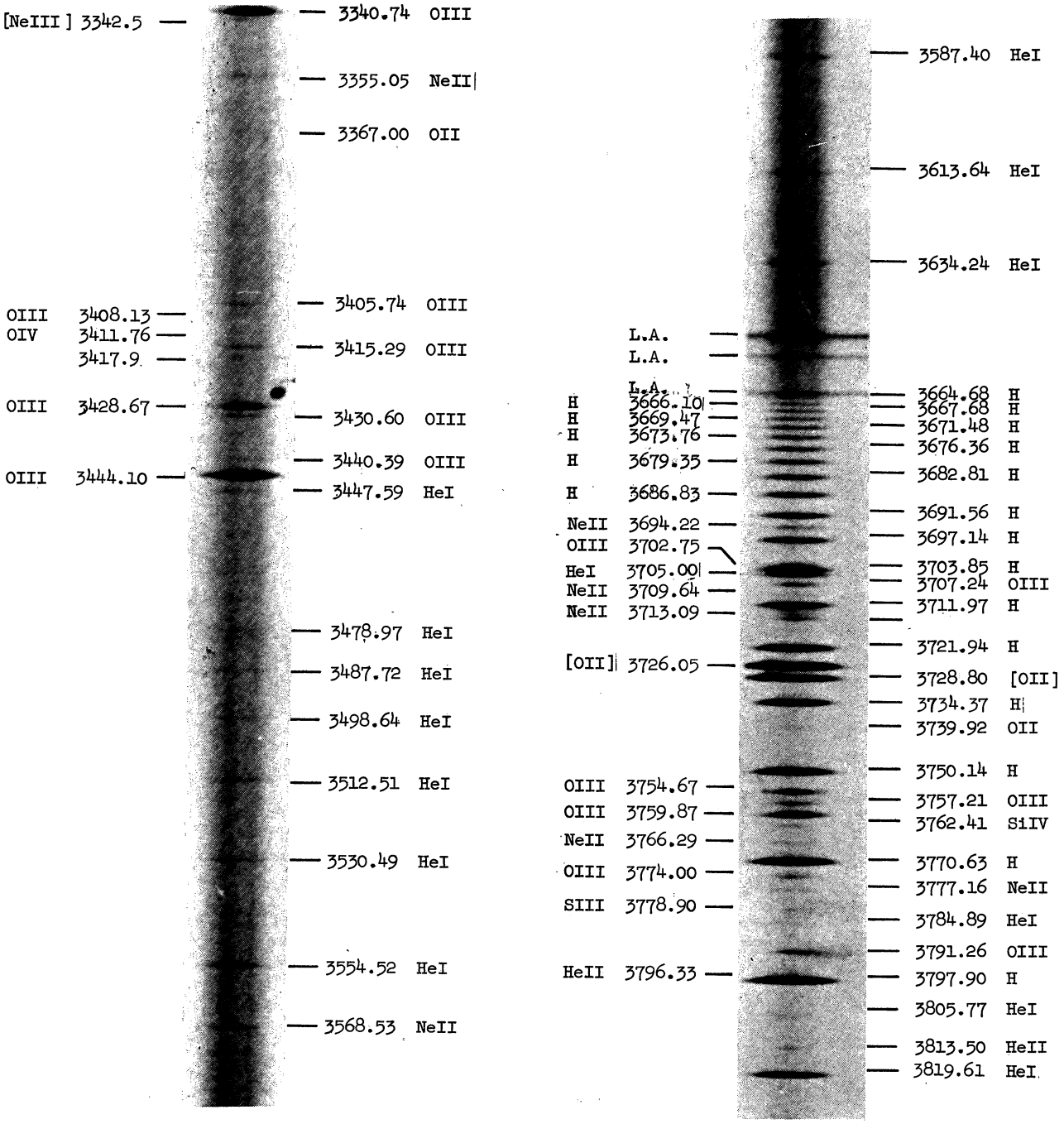

Fig. 7-1. Continued.

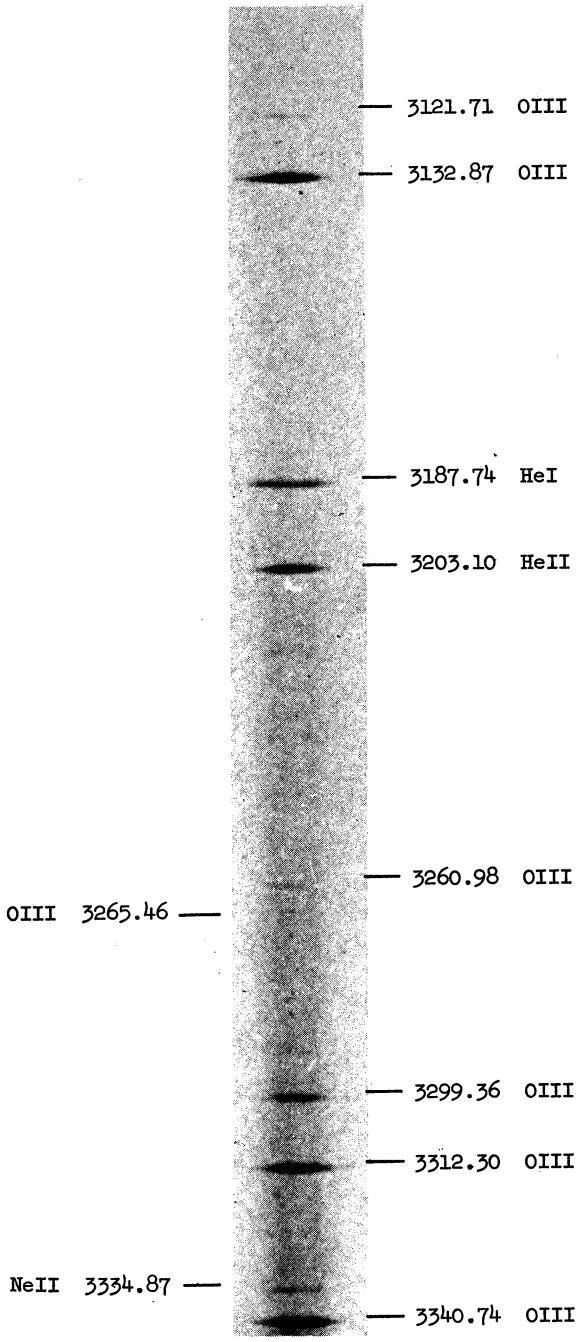

Fig. 7-1. Concluded.

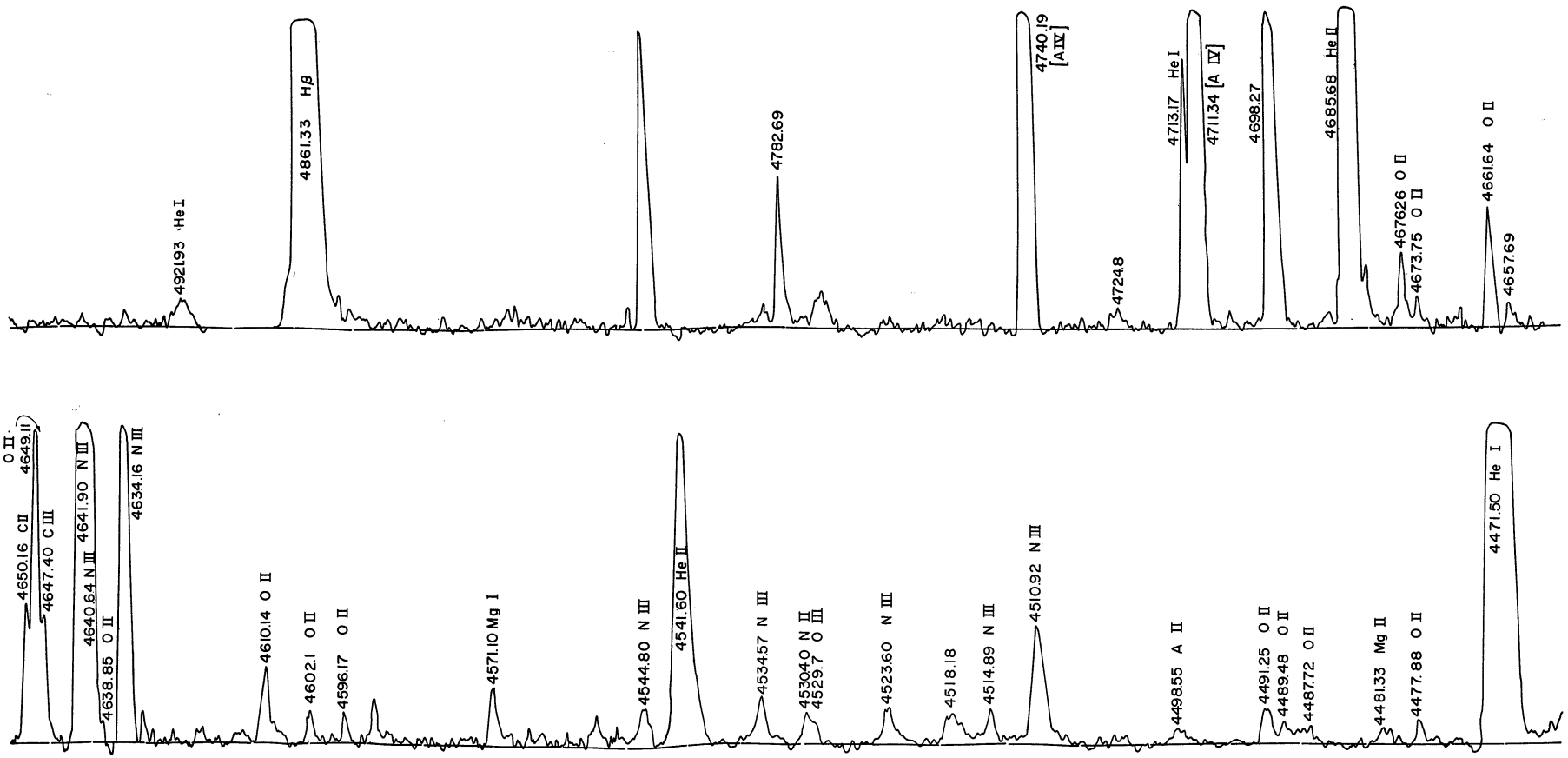

Fig. 7-2. Microphotometric tracing of the spectrum of NGC 7009.

Fig. 7-2. Continued.

Fig. 7-2. Continued.

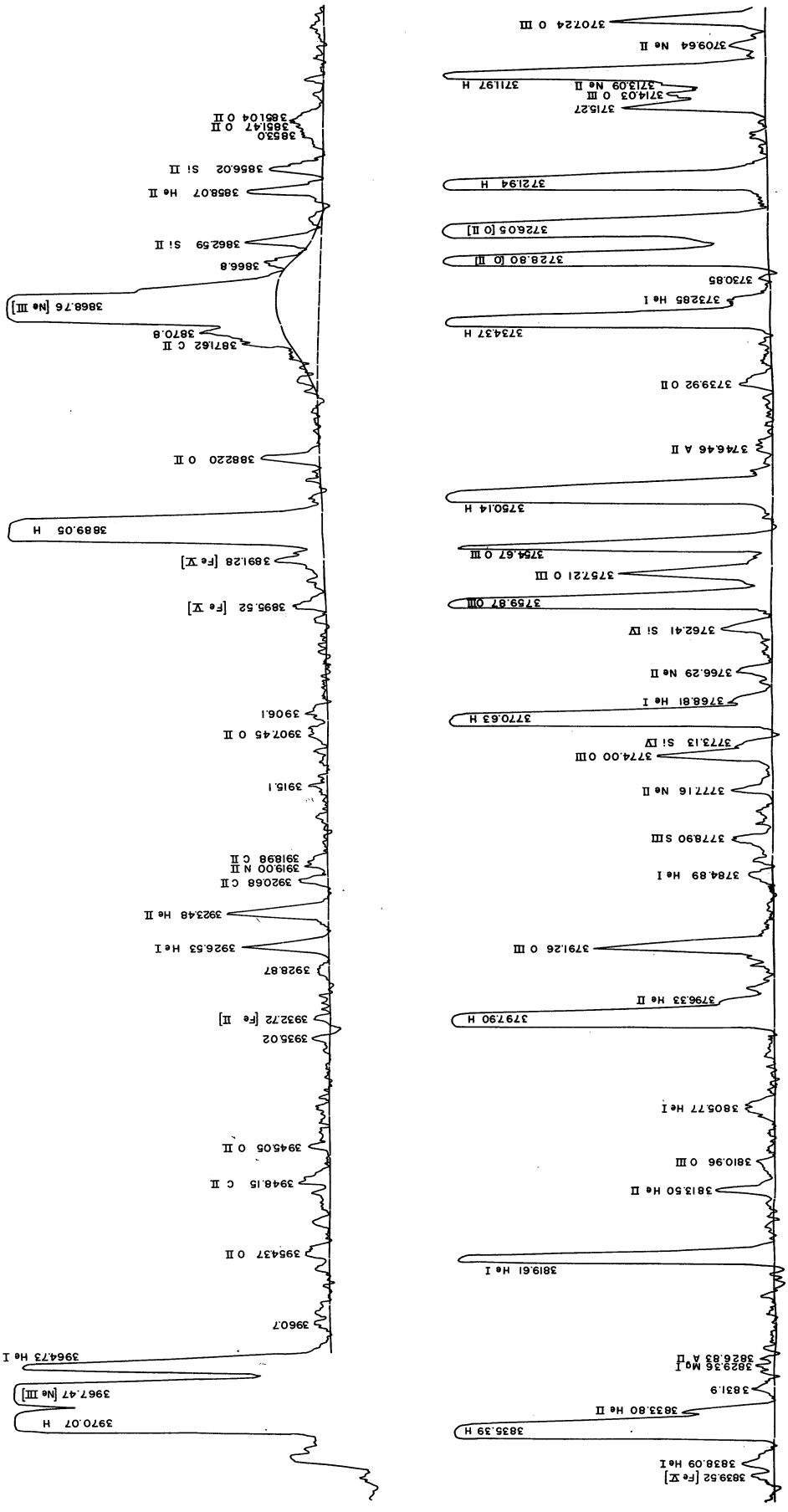

Fig. 7-2. Continued.

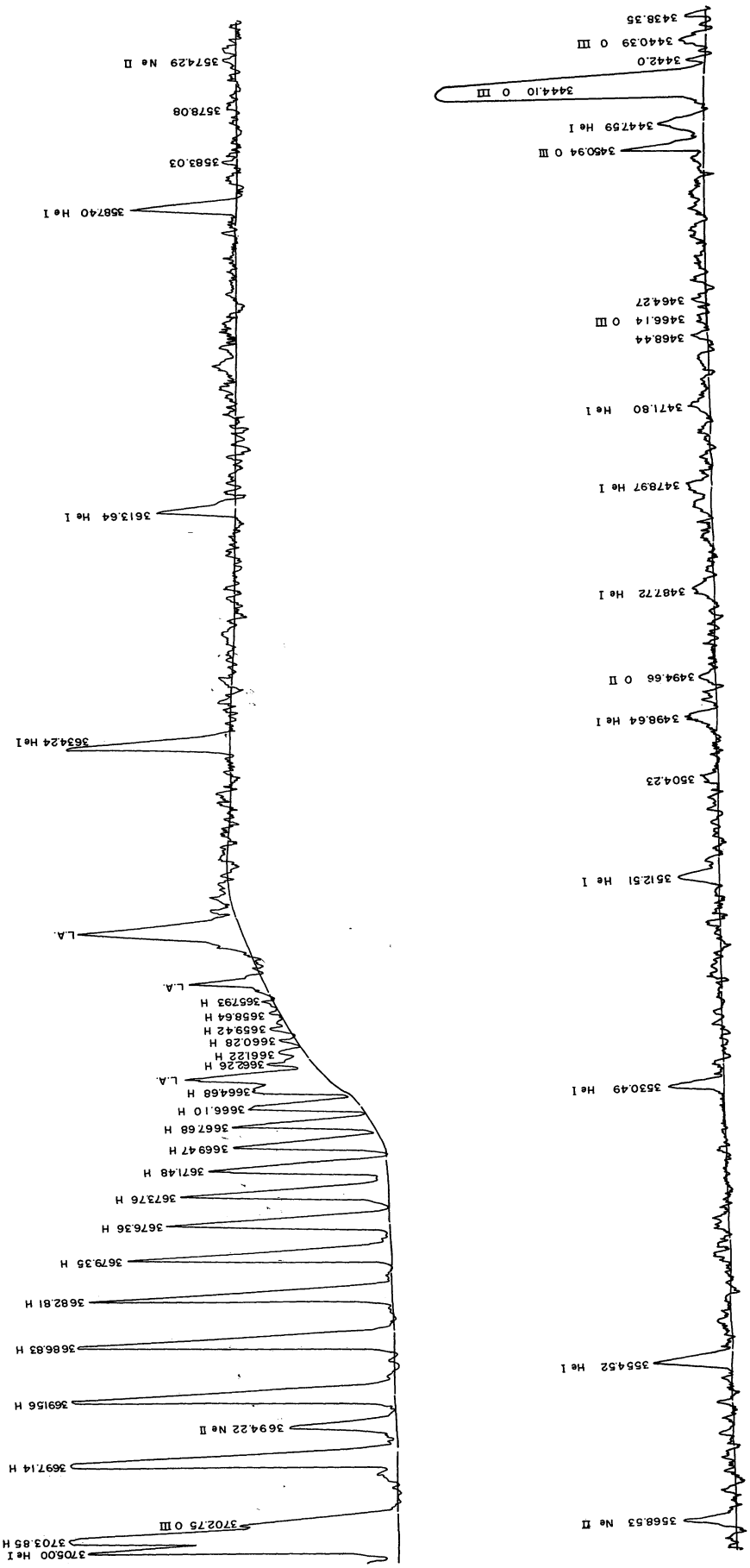

Fig. 7-2. Continued.

Fig. 7-2. Concluded.

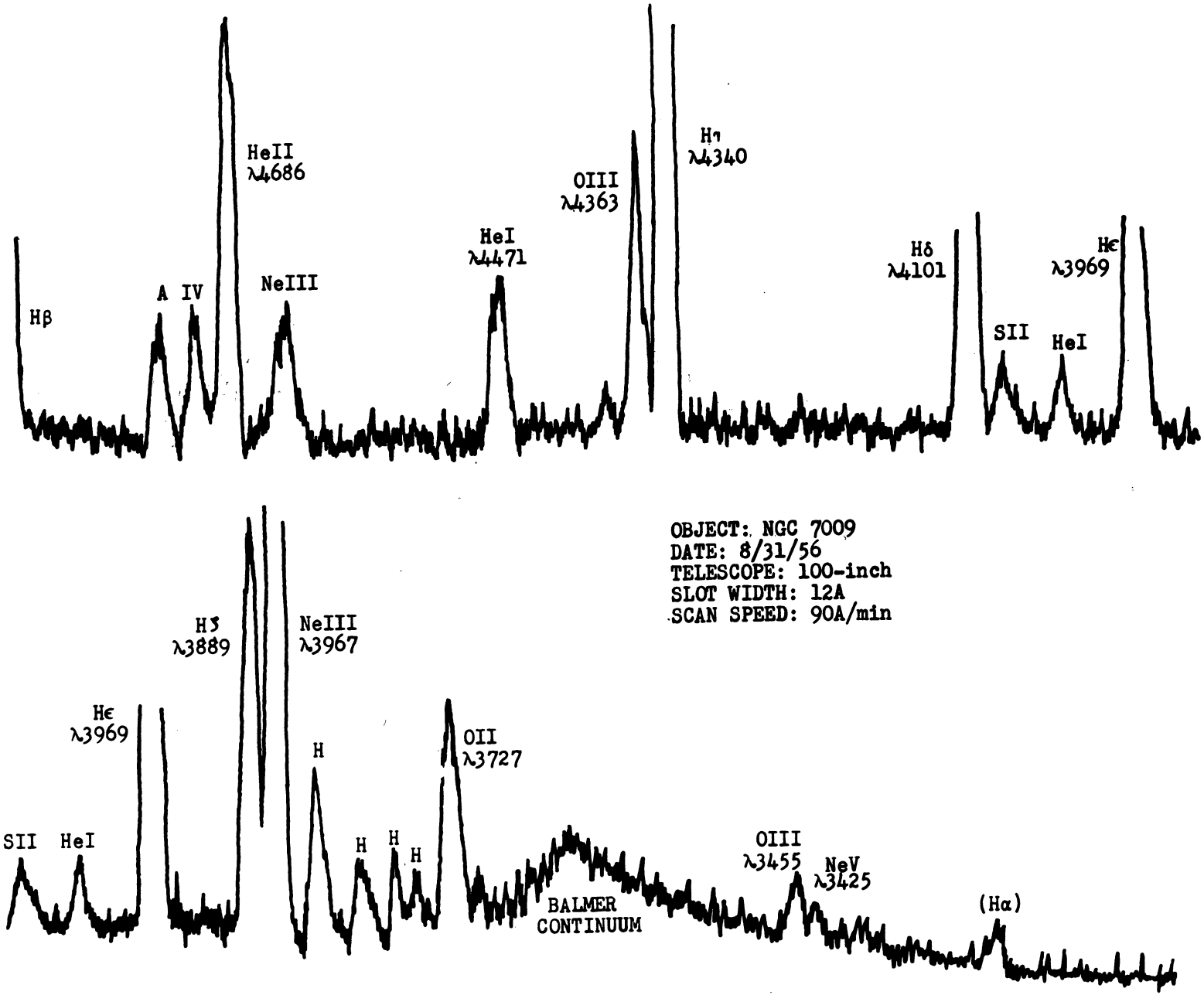

Fig. 7-3. Spectral scan of NGC 7009.

REFERENCES

1. Bowen, I., Minkowski, R., and Aller, L. H. Ap. J., 1955.

2. Bowen, I. S., and Wyse, A. B. Lick Obs. Bull. 19, 1, 1939.

3. Wyse, A. S. Ap. J. 95, 356, 1942.

4. Aller, L. H. Gaseous Nebulae, Wiley, New York, 1956, p. 30.

5. Aller, L. H. Abundances of the Elements Interscience, New York, 1961, p. 71 et seq.

SECTION VIII

REPORT ON RESEARCH CARRIED OUT AT THE UNIVERSITY OF MICHIGAN AND SUPPORTED BY THE U.S.A.F. UNDER CONTRACT NO. AF 49(638)-807

by D. Mugglestone

An extensive and detailed study of the most recent literature in the field of stellar and solar abundances was made—particularly of the literature brought to light and forming the bases of controversial discussion at the recent International Astronomical Union meeting at Berkeley, California. Particular attention was given to (1) considerations of the effects of saturation on the derived abundances of elements from the observed absorption lines, and (2) the very controversial question of the possible deviations from local thermodynamic equilibrium (L.T.E.) in the solar atmosphere.

(1) A paper by Neven, brought to the author's attention at the I.A.U. meeting, severely criticised published material by the author on solar atmospheric abundances. The theoretical background of this criticism was studied and, except in minor matters, was found to be erroneous. A program was initiated to recalculate Neven's results in the case of oxygen and nitrogen (this is nearing completion at the University of Queensland) and to establish numerically the source of Neven's error.

(2) A major controversial topic at the I.A.U. meeting was the question of the applicability of Local Thermodynamic Equilibrium (L.T.E.) to the outer atmospheric layers of the sun. Astrophysicists were strongly divided on the question, as some groups of research workers (notably the Paris group) require strong non-L.T.E. effects to reconcile the solar abundances they derive from weak and strong absorption lines, whereas others (notably the Michigan group) find close agreement between weak and strong lines while still maintaining that L.T.E. applies. It is felt that the situation can be clarified by a study of one element (oxygen has been selected) by theoretically predicting the detailed profile of the absorption lines, not only at the centre of the solar disk but also at various disk positions toward the limb of the sun, and then establishing whether or not non-L.T.E. effects must be invoked to reconcile these predictions with observations. The basic theory necessary to accomplish this objective has been closely studied and completed in detail, and a program has been initiated to utilize high-speed computor techniques to deal with the lengthy and complex calculations necessary for this analysis. Very accurate observational line profiles are necessary and will be obtained by Dr. Edith Müller. The high-dispersion spectrograph of the McMath-Hulbert Solar Observatory (The University of Michigan) will be used and corrections will be made macro-turbulence in the solar atmosphere ("wiggly-line" analysis). The programing will be carried out on the new G.E. 225 computor of the University of Queensland. It is fully expected that the analysis will provide valuable information on the applicability, or non-applicability, of the concept of Local Thermodynamic Equilibrium in the outer layers of the sun.

I would like to express my appreciation for valuable discussions with the Department of Astronomy of The University of Michigan, particularly Professor Aller and Dr. Müller, who gave so freely of their time. I would also like to thank the United States Air Force Office of Scientific Research, whose financial assistance made so profitable a visit possible.

D. Mugglestone
Senior Lecturer in Theoretical Physics
University of Queensland
Brisbane, Australia